

*COMSTAR Satellite*

# COMSAT

---

## Technical Review

Volume 7 Number 1, Spring 1977

# COMSAT TECHNICAL REVIEW

## Volume 7 Number 1, Spring 1977

*Advisory Board* Joseph V. Charyk  
William W. Hagerty  
John V. Harrington  
Sidney Metzger

*Editorial Board* Pier L. Bargellini, Chairman  
Robert D. Briskman  
S. J. Campanella  
William L. Cook  
Jorge C. Fuenzalida  
R. W. Kreutel  
Norman S. Lomas  
Akos G. Revesz  
Robert Strauss  
George R. Welti

*Editorial Staff* Stephen D. Smoke  
MANAGING EDITOR  
Margaret B. Jacocks  
TECHNICAL EDITOR  
Edgar Bolen  
PRODUCTION  
Michael K. Glasby  
CIRCULATION

COMSAT TECHNICAL REVIEW is published twice a year by Communications Satellite Corporation (COMSAT). Subscriptions, which include the two issues published within a calendar year, are: one year, \$7 U.S.; two years, \$12; three years, \$15; single copies, \$5; article reprints, \$1. Make checks payable to COMSAT and address to Treasurer's Office, Communications Satellite Corporation, 950 L'Enfant Plaza, S.W., Washington, D.C. 20024, U.S.A.

© COMMUNICATIONS SATELLITE CORPORATION 1977

vii	FOREWORD	
1	THE COMSTAR PROGRAM	<b>R. D. Briskman</b>
35	THE COMSTAR SATELLITE SYSTEM	<b>G. E. A. Abutaleb, M. C. Kim, K. F. Manning, J. F. Phiel, Jr., AND L. H. Westerlund</b>
85	COMSAT GENERAL SATELLITE TECHNICAL CONTROL NETWORK	<b>W. J. Gribbin AND R. S. Cooperman</b>
103	CENTIMETER WAVE BEACONS FOR THE COMSTAR SATELLITES	<b>L. Pollack</b>
109	CENTIMETER WAVE BEACON TRANSMITTER DESIGN	<b>W. J. Getsinger</b>
129	19- AND 28-GHz IMPATT AMPLIFIERS	<b>M. J. Barrett</b>
153	LOW-JITTER LOCAL OSCILLATOR SOURCE FOR THE COMSTAR BEACON	<b>R. E. Stegens</b>
171	THERMAL AND STRUCTURAL DESIGN ASPECTS OF THE CENTIMETER WAVE BEACON	<b>N. L. Hyman, D. Perlmutter, H. W. Flieger, AND P. R. Schrantz</b>
197	IN-ORBIT TESTING OF COMMUNICATIONS SATELLITES	<b>I. Dostis, C. E. Mahle, V. E. Riginos, AND I. G. Atohoum</b>
227	CARRIER FREQUENCY ASSIGNMENT FOR NONLINEAR REPEATERS	<b>R. J. F. Fang AND W. A. Sandrin</b>
247	A DUAL-POLARIZED 4/6-GHz ADAPTIVE POLARIZATION CONTROL NETWORK	<b>A. E. Williams</b>
263	A DYNAMIC MODEL FOR SATELLITE NONSYNCHRONOUS ALOHA SYSTEMS	<b>A. K. Kaul</b>
291	CTR NOTES	
	SCPC SATELLITE TELEPHONY WITH 4-Dimensionally-Coded QUADRATURE AMPLITUDE MODULATION	<b>G. R. Welti</b> 291
	FIELD TESTS OF 120-CHANNEL HYBRID MODEMS VIA SATELLITE	<b>D. Chakraborty, M. Sugiyama, AND T. Muratani</b> 299
	SUMMARY OF THE INTELSAT V COMMUNICATIONS PERFORMANCE SPECIFICATIONS	<b>J. C. Fuenzalida, P. Rivalan, AND H. J. Weiss</b> 311
327	TRANSLATIONS OF ABSTRACTS	
	FRENCH	327
	SPANISH	334
343	1976 AUTHOR INDEX	

## **Foreword**

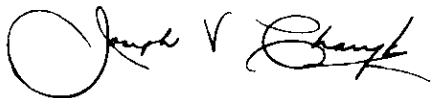
This issue of *COMSAT Technical Review* features papers devoted to the COMSAT GENERAL COMSTAR Program. The papers deal with the various aspects of this United States domestic satellite program, and contain detailed descriptions of the major elements such as the spacecraft and communications subsystems; the tracking, telemetry, and command facilities; the ground stations; and the experimental Centimeter Wave Radio Beacons.

The COMSTAR Program constitutes the only United States domestic satellite communications system which is integrated into the public dial telephone system, providing it with additional capacity, diversity, and flexibility. The entire communications capacity of the COMSTAR satellites is leased to the American Telephone & Telegraph Company and used jointly by AT&T and GSAT, a subsidiary of the General Telephone & Electronics Corporation.

The COMSTAR Program includes two technological developments of considerable importance: the operational use of cross-polarization in satellite communications, a technique which doubles the available spectrum; and the implementation of the first space-qualified, all solid-state 19/29-GHz beacons for propagation measurements.

The success of the COMSTAR Program is due to the cooperative efforts of Hughes Aircraft Company as prime contractor, and the various subcontractors such as General Dynamics, Ford Aerospace & Communications Corporation, COMSAT Labs, and NASA.

I wish to offer my personal thanks to all the people at COMSAT GENERAL and COMSAT Corporations for their dedicated work in this venture, which represents a milestone in the history of communications.



JOSEPH V. CHARYK,  
President  
Communications Satellite Corporation

# ***The COMSTAR program***

R. D. BRISKMAN

(Manuscript received February 23, 1977)

## ***Abstract***

This paper describes the COMSTAR program, including its origin and background engineering development. It defines the major characteristics of the program, implementation aspects, and operational performance. In addition, it addresses certain technical aspects of the communications service, spacecraft, launch vehicles, earth stations, and telemetry, tracking, and command system.

## ***Introduction***

The purpose of this paper is to provide an overall description of the COMSTAR program and to introduce subsequent papers which describe in detail the major program elements. Since these papers describe the characteristics of the program elements in terms of what was done, the major emphasis herein is on why and how it was done.

## ***Origin***

The origin of the COMSTAR program can be traced back to 1966, when the Communications Satellite Corporation (COMSAT), the American

Telephone and Telegraph Company (AT&T),\* Western Union, and other entities filed applications with the Federal Communications Commission (FCC) for authorization to establish domestic satellite communications systems. The effort by COMSAT culminated in a filing with the FCC on April 3, 1967,† proposing a "Pilot Program For Domestic Satellite Communications Services" [1], [2]. Its object was to create a single U.S. domestic communications satellite system serving all authorized users. Although the geosynchronous satellite technical design‡ was different from that of the COMSTAR satellite, and FCC approval of the "Pilot Program" was never obtained, the early exposure to the AT&T transmission requirements proved useful during the conceptual phase of the COMSTAR program.

In early 1970 the FCC adopted the "open entry" policy in regard to domestic satellite systems. The FCC authorized COMSAT in 1972 [3] to provide the space segment for a satellite system to serve AT&T's long-distance domestic communications requirements. This authorization led eventually to the COMSTAR program, which is the subject of this paper.

The communications capacity of the satellite originally proposed for the "Pilot Program" in 1967 would have been inadequate in 1970 in terms of both cost per circuit mile (compared to the improved microwave and cable terrestrial systems such as the L-4 Cable System), and the AT&T communications requirements. Since the original satellite system communications design capacity was severely constrained by limited RF bandwidth, as shown in Figures 1 and 2, the concept of increasing the available bandwidth by cross polarization was investigated [4]. The use of cross polarization would permit the capacity of the satellite system to be almost doubled with only small increases in satellite and earth station complexity.

Several iterations of the original proposal to AT&T concluded in a definitive agreement§ [5] during early 1973. In the course of the approval process [6], AT&T was required to provide satellite communications cover-

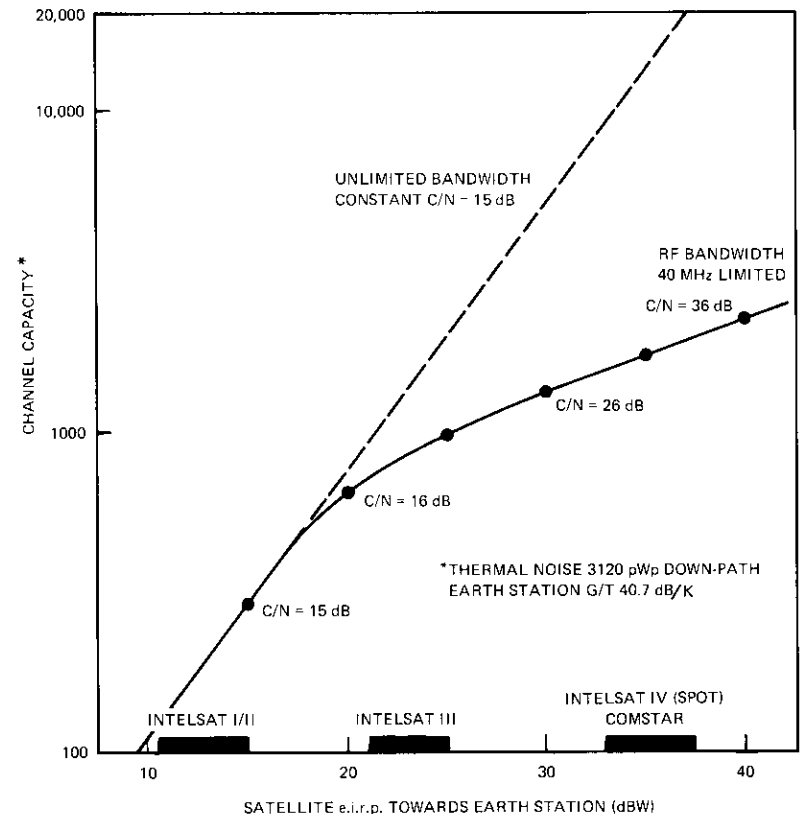


Figure 1. Satellite Transponder Telephone Channel Capacity

age of Alaska, Hawaii, and Puerto Rico as well as the 48 contiguous United States. The agreement and, more importantly, the satellite design were revised to incorporate these coverage areas. The COMSAT GENERAL Corporation (COMSAT GENERAL), a wholly owned subsidiary of COMSAT, was created in February 1973\* to pursue this activity and others.

\*AT&T's communications satellite activities began with TELSTAR I in 1962. In December 1966, AT&T filed with the FCC a domestic satellite proposal entitled "A Space-Earth Integrated Communications System."

†Elements of the technical plan were filed by COMSAT with the FCC on August 1, 1966; detailed technical information was filed on July 26, 1967.

‡The satellite would have provided 12 radio repeaters (transponders) and would have been launched by an Atlas-Agena launch vehicle.

§The first agreement was consummated on October 16, 1970; the second on February 19, 1971 (amended December 28, 1972); and the current one on February 28, 1973 (with four subsequent amendments).

\*The use of these two corporate identifications (*i.e.*, COMSAT and COMSAT GENERAL) throughout this paper is chronologically correct, and the personnel in COMSAT responsible for the COMSTAR program were transferred to COMSAT GENERAL in mid-1973.

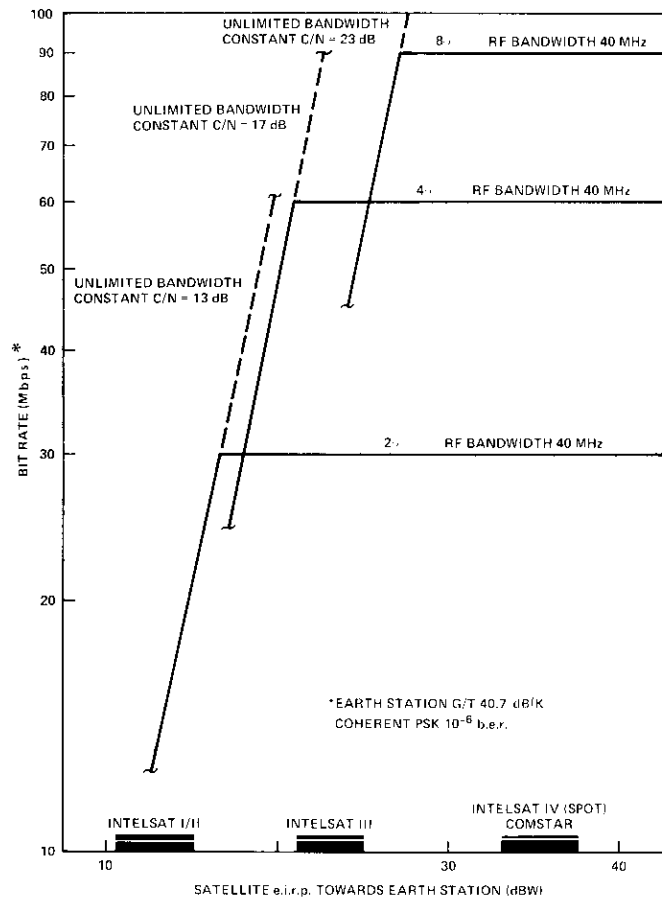


Figure 2. Satellite Transponder Digital Capacity

In 1974 General Telephone and Electronics (GTE) Corporation's subsidiary, the GTE Satellite Corporation (GSAT), petitioned the FCC to allow it to access the COMSAT GENERAL satellites. GSAT is now using the capacity of the COMSTAR satellites jointly with AT&T.

### The Agreement

Certain elements of the agreement between AT&T and COMSAT GENERAL are noteworthy. COMSAT GENERAL is completely responsible for the space

segment, which includes the satellites, launch vehicles, and telemetry, tracking, and command (TT&C) earth stations. AT&T leases all the satellite communications transponder capacity from COMSAT GENERAL. AT&T, together with GSAT, provides all earth segment facilities (e.g., communications earth stations and interconnection of these earth stations with communications switching centers). Communications capacity is now being provided by two satellites, and later a third satellite is planned. The capacity is defined in terms of radio repeater (i.e., transponder) performance characteristics.

The agreement defines the number of transponders required, the derivable communications capacity in terms of individual 4-kHz-wide channels, and the quality of the worst channel. It also stipulates test procedures, standards, and parameter values for determining that the conditions of satellite communications performance have been met.

### Program guidelines

Several program guidelines resulted in important decisions. The most significant was the selection of a conservative spacecraft design based on improvements of the INTELSAT IV/IV-A design [7]–[9]. At the end of 1972, the only geosynchronous commercial communications satellite system with any significant in-orbit history was the INTELSAT system. Other possible satellite design selections were also considered, but all were rejected due to lack of in-orbit qualification and "design inheritance" criteria. The only important COMSTAR design unknown was the cross-polarization isolation, which will be discussed in the following section.

A second guideline stemmed from AT&T's plan to use the satellites to handle communications channels in its switched message toll system (e.g., normal customer dialed telephone and data calls). Such channels are carried terrestrially by radio relays (e.g., TD-2 and TH-3) and coaxial cables (e.g., L-4 and L-5). The guideline provided for a continuity and a quality of service at least meeting or exceeding those of the equivalent terrestrial facilities for route distances of more than several hundred miles. This guideline caused dissimilar redundancy to be added to the spacecraft, particularly in the antenna despun control electronics and in the communications receiver, as will be described more fully in a subsequent paper. It also resulted in a COMSAT GENERAL decision to improve the quality objective cited in the agreement (6,800 pW0p in the worst 4-kHz channel of a reference 1,200-channel FDM/FM baseband) by 25 percent during design, since some of this margin might be lost during implementation.

As discussed in a subsequent paper, both the satellite and the communications earth station measured performance surpassed the original design performance goals.

This same guideline resulted in a design of communications earth stations capable of switching communications without outage during "sun transit." It should be noted that sun transit occurs when the sun appears behind the satellite and consequently is in the earth station antenna's main beam. In this case the sun's noise energy is strong enough to degrade severely the communications performance. Such periods occur once a day for several minutes during two approximately 4-day periods spaced six months apart. During these sun transit periods, the AT&T and GSAT earth stations are capable of switching the communications signals at the affected earth station from one satellite-earth station set to another satellite-earth station set without service interruption.

A third guideline concerned the future use of earth station antennas with smaller diameters so that, if the satellite could be held accurately enough to a specific geosynchronous orbital position, these antennas would require no autotracking capability. This would allow simple, unattended, and inexpensive earth stations to be used. Consequently, the COMSTAR satellites were required to remain within  $\pm 0.1^\circ$  of their assigned geosynchronous orbital positions. This is quite simple in the case of hour angle (apparent east-west motion along the geosynchronous orbit), but requires considerable onboard propulsion capability in the case of inclination (apparent north-south declination motion perpendicular to the geosynchronous orbit). At least 91 kg (200 lb) of onboard fuel (hydrazine) is required to meet this requirement over seven years.

A fourth guideline dealt with the desire to obtain engineering data on propagation at 19 and 28 GHz [10] for application to future generations of satellites. As described in the following papers, this resulted in the design and fabrication of solid-state Beacon transmitters at these frequencies for the COMSTAR satellite.

Some of the basic physical characteristics of the COMSTAR satellite are given in Table 1.

#### Cross polarization

Orthogonally polarized co-frequency-band transmissions had never been employed in communications satellites or earth stations and some concern was evident at Bell Telephone Laboratories when they were initially proposed. Cross polarization had been used on terrestrial radio-relay links (e.g., TD-3), but the microwave antenna beamwidths were

TABLE 1. COMSTAR SATELLITE PHYSICAL CHARACTERISTICS

Launch Vehicle	Atlas-Centaur
Spacecraft Mass	
Launch	1,520 kg (3,350 lb)
In Orbit	810 kg (1,780 lb)
Spacecraft Dimensions	
Solar Drum Diameter	2.4 m (94 in.)
Overall Height	6.1 m (240 in.)
Attitude Stabilization	Gyrostat
Antenna Pointing Tolerances	
East-West	$\pm 0.20^\circ$
North-South	$\pm 0.26^\circ$
Stationkeeping Tolerances	
East-West	$\pm 0.1^\circ$
North-South	$\pm 0.1^\circ$
Primary Power	
Solar Array	600 W after 7 years
Batteries	Full operation during eclipse
Design Life	7 years

narrow, and it was necessary to maintain isolation only over the center portion of the beam. Conversely, for the COMSTAR satellite, the typical satellite antenna beamwidth is wide and asymmetrical ( $3.5^\circ$  by  $7.0^\circ$  elliptical), and isolation must be maintained down to the 4-dB gain contour from peak gain over the 500-MHz bandwidth at both 4 and 6 GHz. There are also many practical constraints on size and methods of construction for satellite antennas so that it is difficult to apply certain cross-polarization techniques. Secondary problems, such as Faraday rotation by the ionosphere and depolarization by rain, must also be noted.

As a result of the decision that the cross-polarization technique must be demonstrated, various tasks were initiated. Approximately two-thirds of this effort, accomplished primarily during 1969-1972, has been previously reported [11]-[13]. Several different techniques were applied and several different antenna design configurations were actually constructed, most of which demonstrated the potential for meeting or exceeding the cross-polarization isolation objective of 33 dB for the satellite antenna alone.

The COMSTAR spacecraft antenna design technique adopted used external polarization gratings, for which several configurations are possible. This selection was influenced by the requirement for a complex satellite antenna feed subsystem, which included multiple feed horns, their combiners, and diplexers. It appeared more difficult at that time (1973) to eliminate all of the unwanted cross-polarization components originating in the complex

of internal feed waveguide plumbing than to remove them by using an external grid or grating. As discussed in a subsequent paper, the spacecraft contractor chose a reflector aperture grating approach. Figure 3 shows

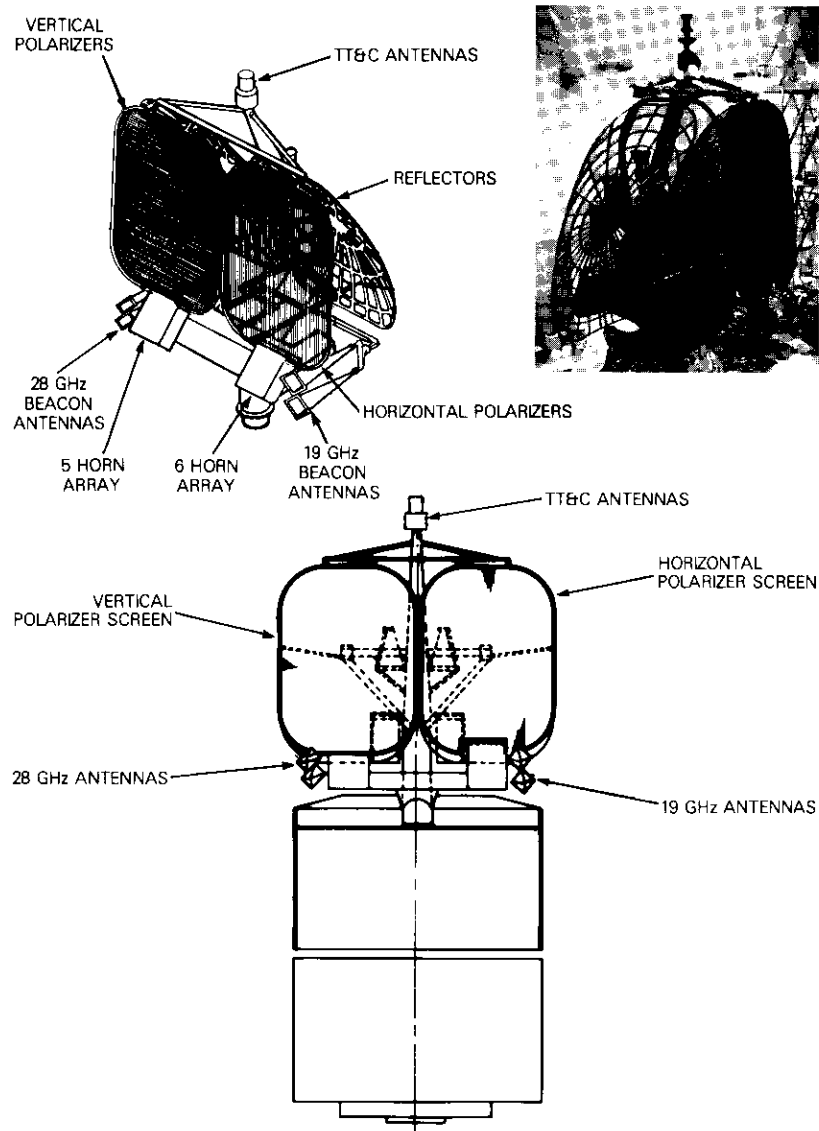


Figure 3. COMSTAR Satellite Antennas

the mechanical construction of the spacecraft, including a photograph and drawing of the COMSTAR satellite antennas. The selection of linear rather than circular cross polarization was based on implementation ease as perceived in 1973. The advantage of linear polarization is that polarization grids or gratings can be employed in the spacecraft design.

AT&T developed an earth station feed capable of correcting non-orthogonal polarized waves [14]. Essentially, the feed components effect three corrections to the transmit and receive waves, as shown in Figure 4. First the feed eliminates the cross-polarized component (ellipticity) of each desired polarization by differential phase shift and attenuates the two polarization vectors for equal amplitude. It then corrects the axis angle so that the two polarization vectors are orthogonal and finally rotates the incoming wave for coincidence with the feed polarization orientation. This last feature, which corrects for such aberrations as rotation of the polarization vectors by the Faraday effect, has been automated using error signals derived from the COMSTAR satellite's 4-GHz beacon emissions. Figure 5 shows the AT&T earth station at Hawley, Pennsylvania.

The cross-polarization isolation is obviously imperfect. To ensure the highest effective carrier-to-interference (C/I) ratio between cross-polarized transmissions, an interstitial radio frequency plan has been chosen for COMSTAR [15], as shown in Figure 6. This basic plan, which has been adopted by all other U.S. and Canadian domestic communications satellites, is constructed to avoid cochannel center frequencies between wide-bandwidth transmissions on each of the two polarizations. Because the highest power spectral densities exist at the carrier center frequencies, the potential for interference would be higher if cochannel or near-cochannel center frequency assignments were used.

#### Satellite antenna pointing

The previously described requirements for almost perfect communications continuity have resulted in an engineering effort to improve further the redundancy, accuracy, and operating modes of the satellite subsystems involved in antenna pointing.\* The most significant result was the provision of a redundant "analog" despun control electronics subsystem in addition to the existing redundant "digital" despun control electronics subsystem. The original subsystem design was predicated on  $\pm 0.35^\circ$  antenna pointing

\*As described subsequently, the antennas are mounted on a platform which is spun equal and opposite to the satellite body. The platform must be accurately pointed at a specific location on the earth's surface to achieve the desired communications coverage.

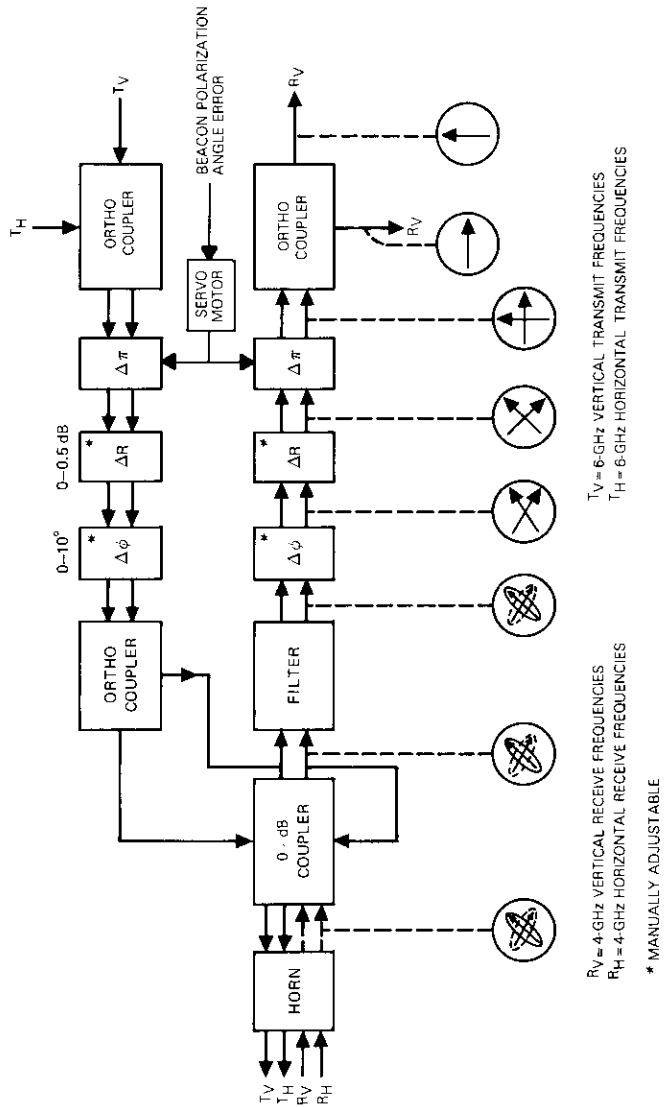


Figure 4. AT&T Earth Station Dual-Polarized Feed System

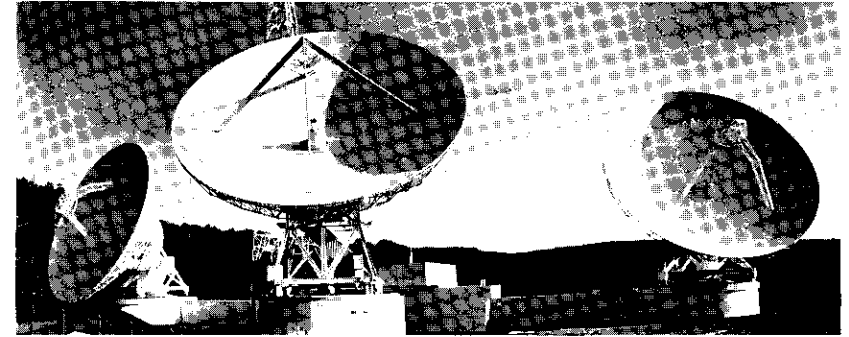


Figure 5. AT&T Earth Station At Hawley, Pennsylvania (Courtesy AT&T)

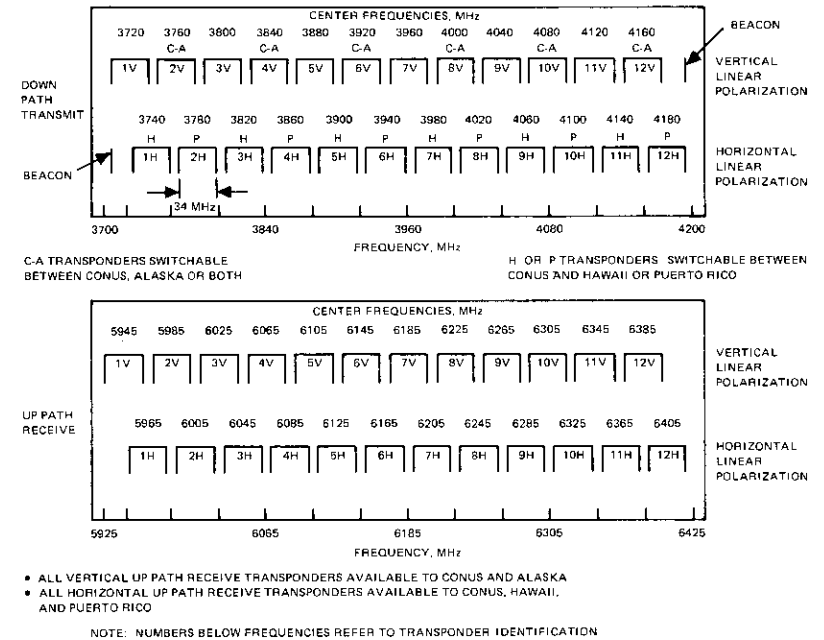


Figure 6. COMSTAR Satellite Radio Frequency and Polarization Plan

error ( $3\sigma$  jitter). The analog subsystem provides  $\leq 0.1^\circ$  pointing error, and the existing digital subsystem has been improved to provide  $\leq 0.2^\circ$  pointing error. These subsystems will be described in more detail subsequently. Other improvements have involved the sensors (three earth sensors and one sun sensor), the processing electronics, and the control loops.

### Communications

Communications aspects are described in detail in a companion paper. The COMSTAR satellites must be flexible to satisfy communications capacity demands many years later. The additional requirement for satellite coverage of Alaska, Hawaii, and Puerto Rico has been mentioned previously. The coverages are shown in Figure 7, where the dotted lines roughly depict a satellite antenna beam which provides simultaneous coverage of both the 48 contiguous United States and Alaska. In the implementation of these coverage requirements, two important design changes were incorporated to achieve high communications flexibility.

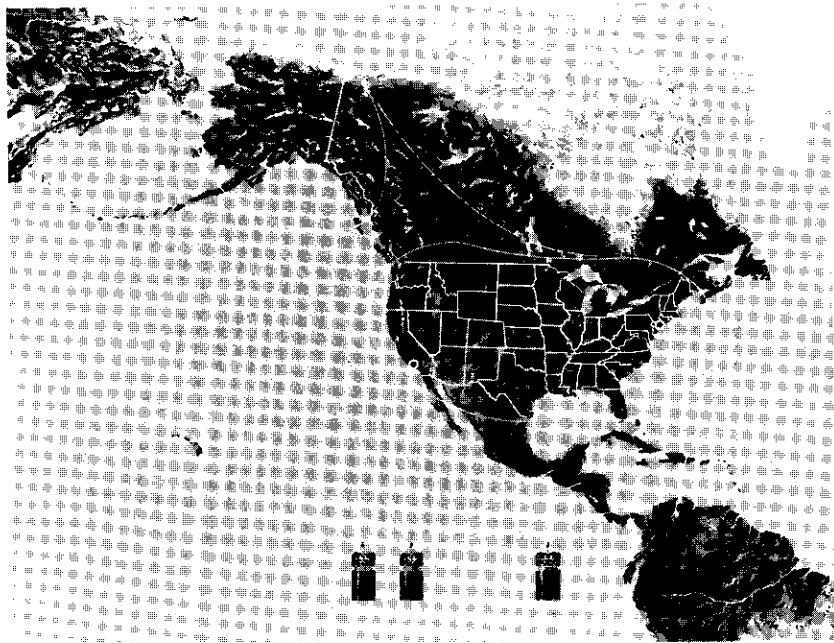


Figure 7. COMSTAR Satellite Communications Coverage Areas

One change was the implementation of a configuration with the greatest possible flexibility for switching the satellite capacity among the five beams (*i.e.*, the 48 contiguous United States, Alaska, Alaska and the 48 contiguous United States, Hawaii, and Puerto Rico). This change was necessary because the initial communications capacity demand among the beams was unknown and would be, in part, determined by future regulatory actions, and because future increases and changes in demand within and between the beams could not be accurately predicted. Figure 8 indicates the achieved flexibility, and Figure 9 is the COMSTAR satellite's communications block diagram, where **S** and **T** indicate the output switching elements. Each **S** switch can be moved between two positions and each **T** switch between three positions by ground command. This switching design is the most flexible implemented to date for domestic use.

The second change was the addition of group-delay equalizers and ground-commanded 4-position attenuators to each transponder in the spacecraft. Originally (circa 1970) it had been expected that single-carrier access would be the primary operational mode, that the earth stations would compensate for the satellite up- and down-link group delay, and that only one earth station size would be employed. Subsequently none of these expectations materialized, and the incorporation of the switched attenuators and equalizers permits transponder access by earth stations of various sizes and by varying numbers of carriers per transponder in an optimized manner. Transponder access can now also be switched rapidly between various earth stations since no significant "re-equalization" is necessary.

Each COMSTAR satellite was designed to provide a *minimum* of 1,200 voice/data channels per transponder into a communications earth station with a G/T of 41.2 dB/K and a worst channel noise performance objective of no more than 6,800 pW0p.\* This transponder capacity objective is equivalent to a capacity of 28,800 channels (14,400 two-way circuits) for each COMSTAR satellite or over 86,000 channels (43,000 two-way circuits) theoretically available for the envisioned 3-satellite system.

The actual performance of the satellites and earth stations, as described in the following paper, is substantially better than the design objectives. It is therefore possible to provide at least 1,500 channels per transponder with an additional DUV (data under voice) 1.544-Mbps digital group placed below the low-frequency end of the 1,500-channel FDM baseband,

\*Baseband-to-baseband between the transmit and receive earth stations including 2,000 pW0p for assumed external interference contributions.

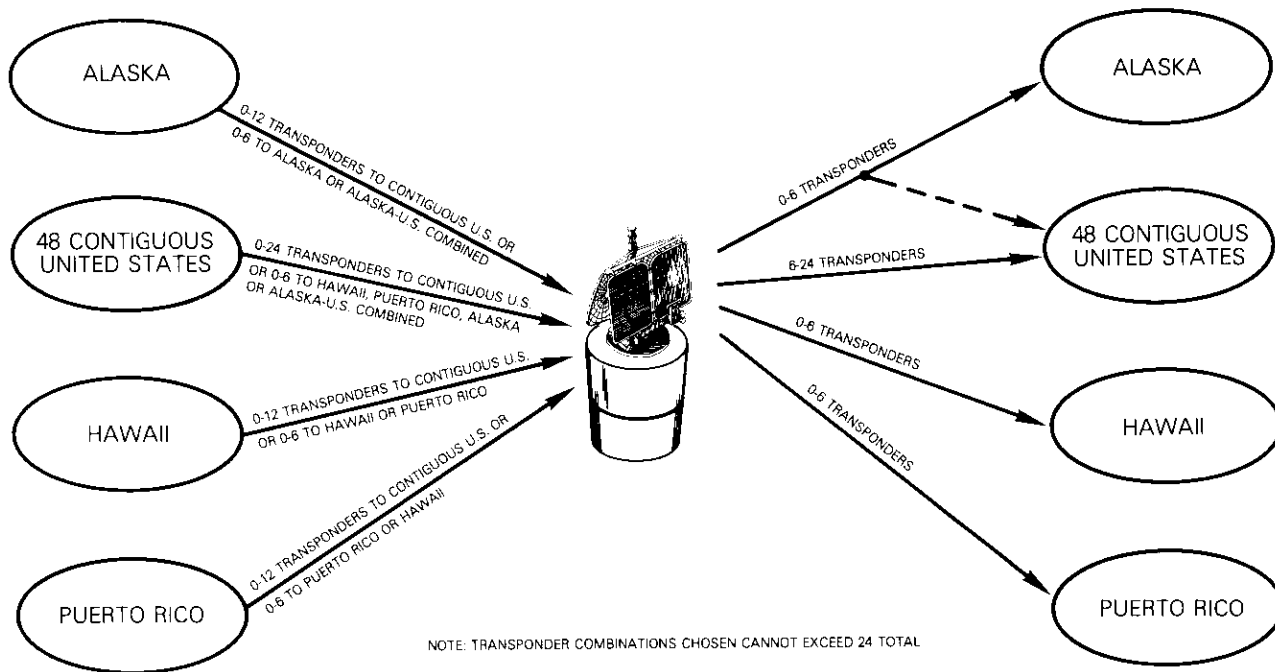


Figure 8. Communications Area Switching Flexibility

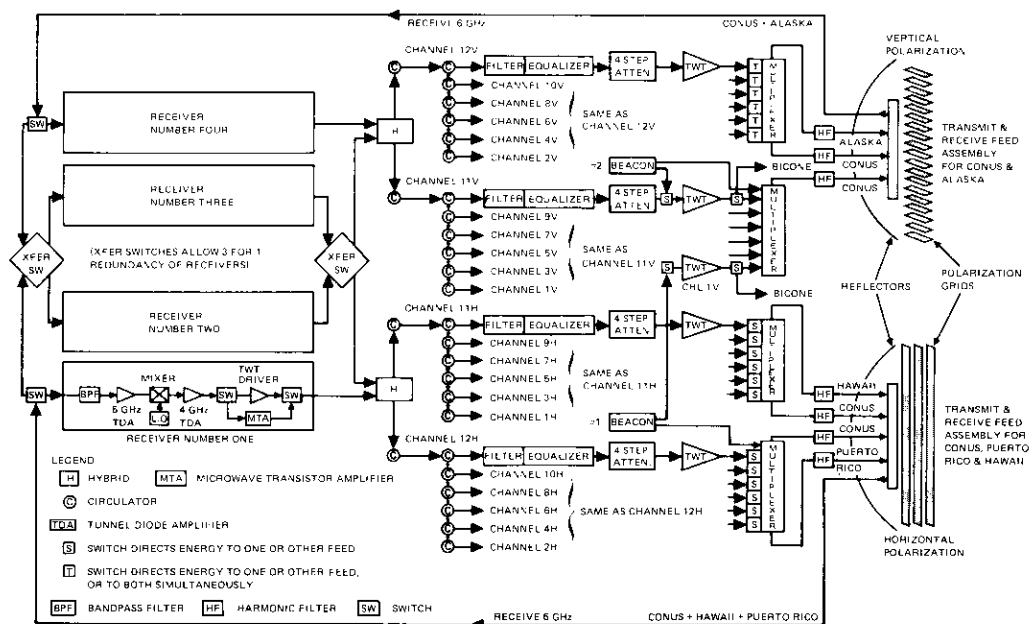


Figure 9. COMSTAR Satellite Communications Subsystem

while fully maintaining the performance quality objective. It is believed that, in practice, a capacity of at least 1,800 channels per transponder, including DUV, can be achieved with satisfactory quality by using companders. This would result in a 3-satellite system theoretical capacity of approximately 130,000 channels (65,000 two-way circuits).

The channels, which are full-time transmission paths, will be initially used primarily for handling telephone conversations. Each channel will obviously handle many individual telephone calls each day so that the satellites are capable of handling several million calls per day. In addition, the capacity of the satellite system can be further increased by using time-assignment speech interpolation (TASI) [16]. Alternatively, the satellite capacity can be more than doubled by using an all-digital transmission configuration incorporating speech processing.

It should be noted that AT&T plans to use one of the three satellites for occasional services, sun transit protection, and outage backup (rather than for full-time services) to obtain the desired high-reliability objective. Consequently, the number of full-time channels in service will be less than that theoretically available.

**Implementation**

The major program elements are the spacecraft, the launch vehicles, the TT&C complex, the communications earth stations, and the terrestrial interconnection facilities. Figure 10 shows the program implementation schedule.

**Spacecraft**

The basic design of the satellite was defined in early 1973 using the guidelines described previously. The specified minimum communications performance characteristics of the satellite are given in Table 2. A contract to build four such spacecraft was awarded to the Hughes Aircraft Company on September 14, 1973. In addition, in October 1973 a separate contract was awarded to COMSAT Laboratories to provide five sets of 19- and 28-GHz radio frequency Beacons. The Beacons, which are described elsewhere in this issue, feature all solid-state transmitters with 1-watt power output, a noteworthy achievement for that time period. Figure 11 is a photograph of the COMSTAR spacecraft despun platform containing the bulk of the communications equipment with antennas removed, and Figure 12 is a photograph of the spinning portion of the spacecraft with the solar cell array panels removed.

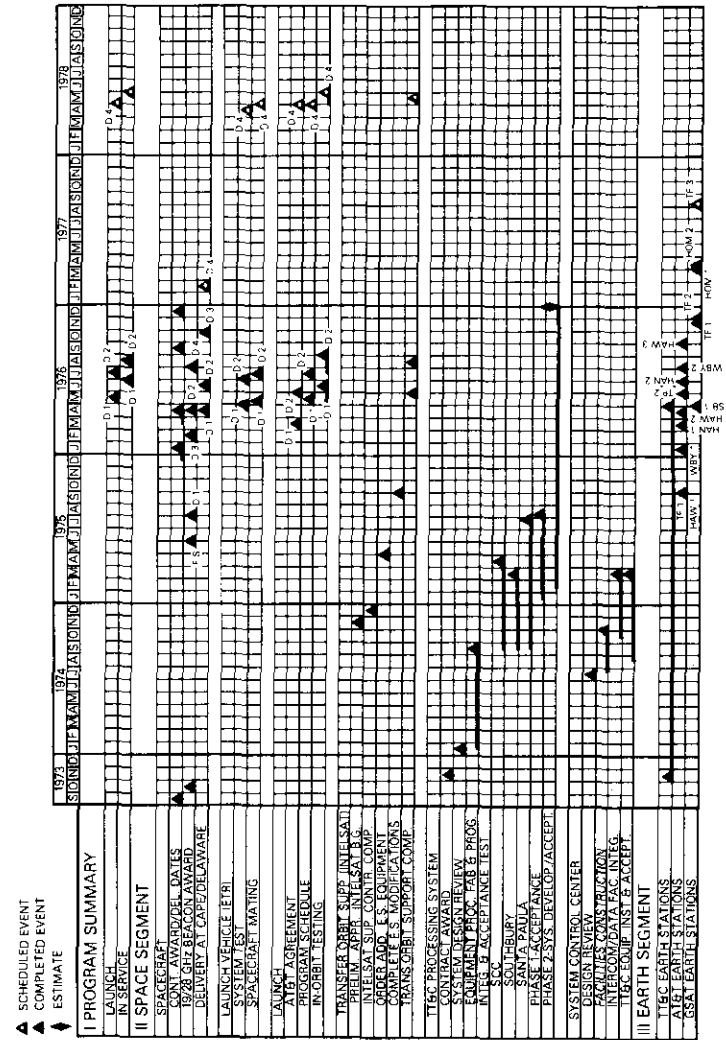


Figure 10. COMSTAR Program Schedule

TABLE 2. COMSTAR SATELLITE MINIMUM COMMUNICATIONS PERFORMANCE CHARACTERISTICS

Antenna Coverage	48 Contiguous United States, Alaska, Hawaii, and Puerto Rico
Polarization	Linear (frequency reuse by horizontal and vertical cross polarization)
Polarization Isolation	33 dB (worst case over coverage area)
Transponders per Satellite	24
Transponder Distribution	
Satellite Receive	12 Contiguous U.S. and Alaska 12 Contiguous U.S., Hawaii, and Puerto Rico
Satellite Transmit	6-24 Contiguous U.S. ≤6 Alaska or Contiguous U.S./Alaska combined ≤6 Hawaii ≤6 Puerto Rico
Satellite Receive Frequency Band	5,925-6,425 MHz
Satellite Transmit Frequency Band	3,700-4,200 MHz
e.i.r.p. per Transponder (at beam edge)	33.0 dBW (31 dBW for Contiguous U.S./Alaska combined)
G/T	-9 dB/K (worst case over coverage area)
Usable RF Bandwidth	34 MHz per transponder

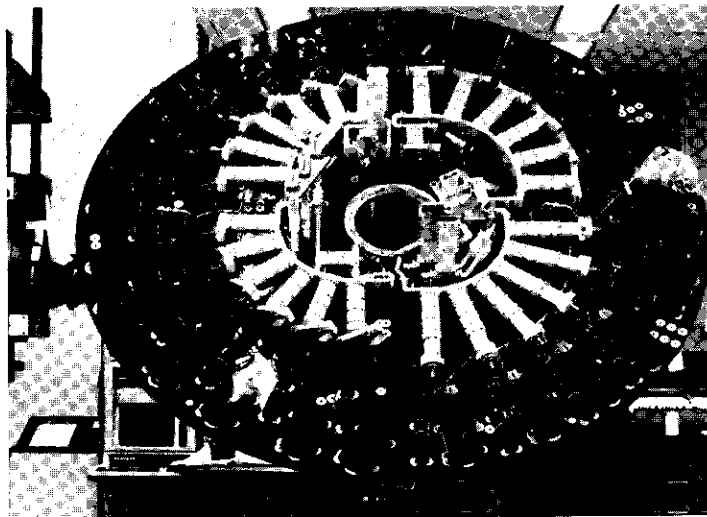


Figure 11. Spacecraft Despun Compartment (Courtesy HAC)

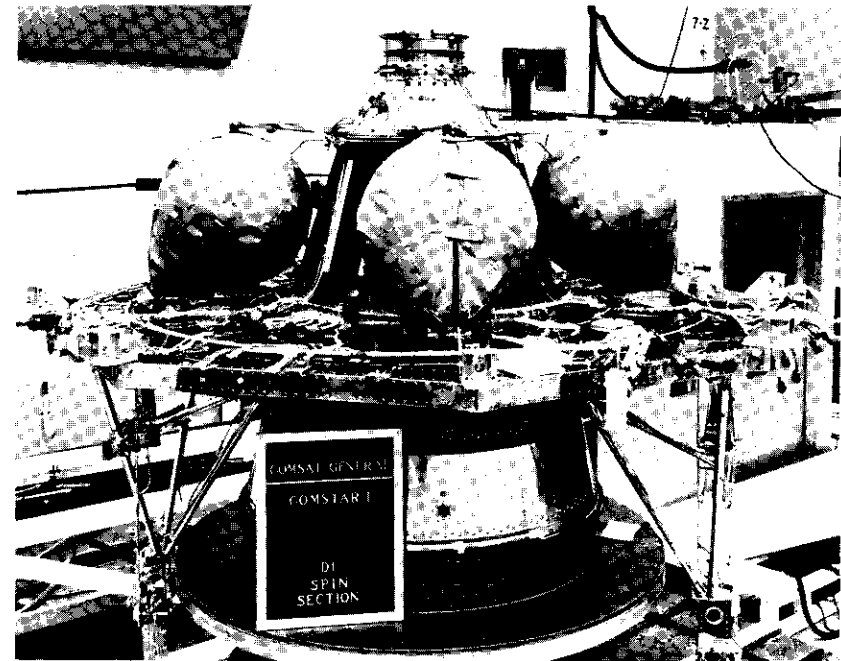


Figure 12. Spacecraft Spinning Section (Courtesy HAC)

#### Launch vehicles

The General Dynamics (Convair Division) Atlas-Centaur launch vehicle [17] is shown in Figure 13. Four of these vehicles with associated launch services were purchased under contract with the National Aeronautics and Space Administration (NASA). No significant design changes in the launch vehicle were necessary since the interface, shroud, and adapter were almost identical to those used to launch INTELSAT IV-A. All launches take place from Cape Canaveral, Florida; the liftoff mass of the spacecraft is approximately 1,520 kg (3,350 lb).

#### TT&C complex

The TT&C complex, described in detail in a companion paper in this issue, consists of two TT&C earth stations, one located in Southbury, Connecticut, and the other in Santa Paula, California, and the System Control Center located in Washington, D.C. These facilities, which are

## CENTAUR STAGE CHARACTERISTICS

LENGTH: 9.84 m

DIAMETER: 3.281 m

GUIDANCE: INERTIAL

PROPULSION: P &amp; W RL10A-3-3

RATED THRUST: 13,160 kg

RATED  $I_{sp}$  (vac): 444 secPROPELLANTS: LO<sub>2</sub> 11,427.68 kgLH<sub>2</sub> 2,219.32 kg

CENTAUR JETTISON: 1,988.8 kg

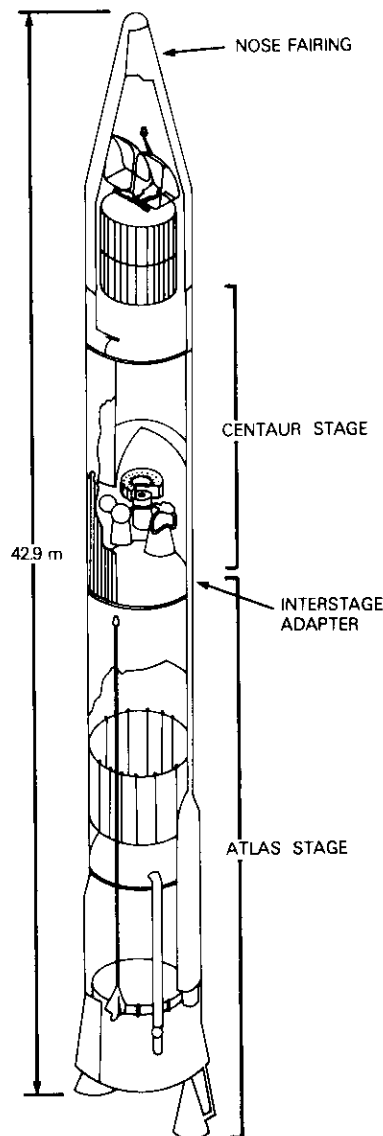


Figure 13. Atlas-Centaur Launch Vehicle

interconnected by leased private line and dial-up communications facilities, are shown in Figure 14. Figure 15 is a photograph of the Santa Paula earth station. The earth station sites were selected in late 1969 for use in the originally proposed domestic satellite systems mentioned previously. These stations are also used in support of the COMSAT GENERAL MARISAT satellite system [18].

The two TT&C earth stations were designed by COMSAT GENERAL during 1973, and a contract for their construction was awarded to Philco-Ford (now Ford Aerospace & Communications Corp.) on November 28, 1973. Table 3 gives their basic characteristics. A contract to construct the special

TABLE 3. CHARACTERISTICS OF COMSAT GENERAL'S SANTA PAULA AND SOUTHBURY EARTH STATIONS

Parameter	Full-Performance Antenna	Limited-Motion Antenna
Antenna Diameter	12.8 m (42 ft)	10.3 m (34 ft)
Type of Antenna Mount	Elevation/azimuth	Hour angle-declination
Azimuth (hour angle) Steerability	$\pm 180^\circ$	$\pm 65^\circ$
Elevation (declination) Steerability	$0^\circ$ to $90^\circ$	$+6^\circ$ to $-19^\circ$
Type of Tracking System	Angle monopulse	Manual
Nominal Antenna Pointing Accuracy (rms)	$0.04^\circ$	$0.1^\circ$
Antenna Tracking Accuracy (rms)	$0.02^\circ$	N/A
Antenna Slew Velocity	$0.1^\circ/s$	$0.1^\circ/s$ (hour angle) $0.03^\circ/s$ (declination)
Feed Polarization Capability	Linear or circular	Linear
Frequency Reuse	Linear only	Linear only
Polarization Isolation (within tracking beamwidth)	$>35$ dB	$>35$ dB
Antenna Gain		
6 GHz	55.8 dB	53.0 dB
4 GHz	52.3 dB	50.0 dB
Receiver Noise Temperature	55 K	55 K
Antenna System G/T at $20^\circ$ Elevation	31.9 dB/K	29.5 dB/K
Transmitter Tube Type	Klystron	Klystron
Rated Transmitter Power	3 kW	3 kW
Maximum Up-Link e.i.r.p. at 6 GHz	88 dBW	85.2 dBW

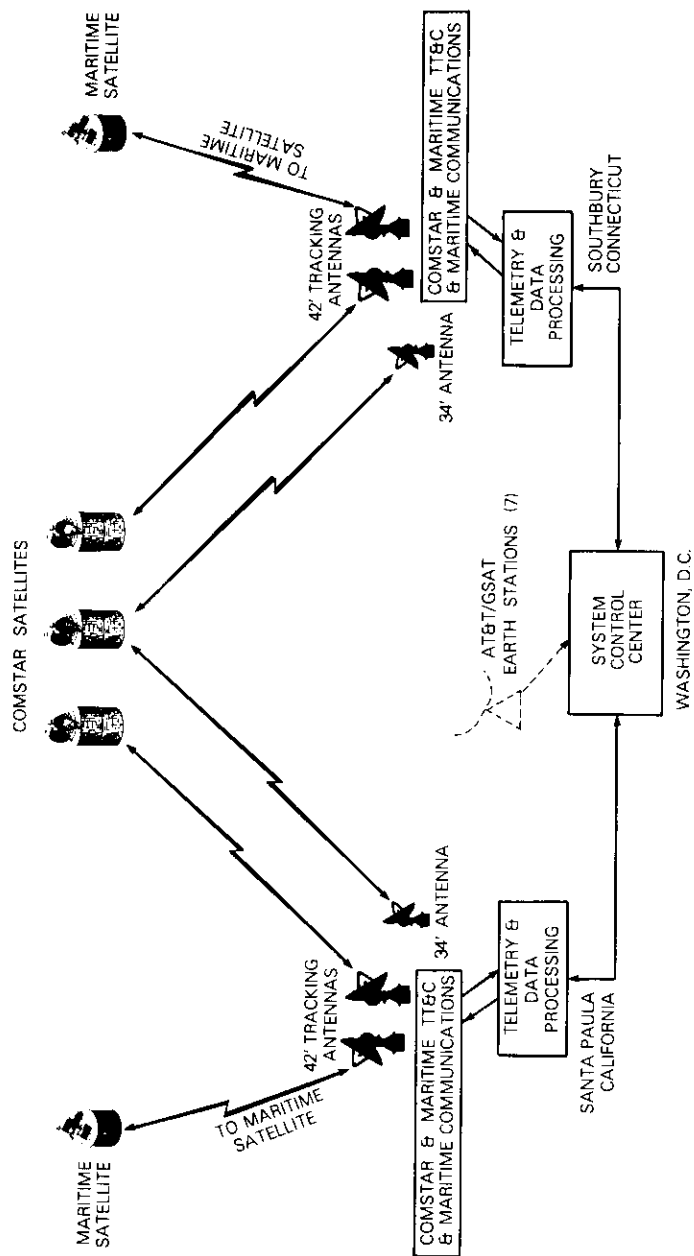


Figure 14. COMSAT GENERAL Facilities

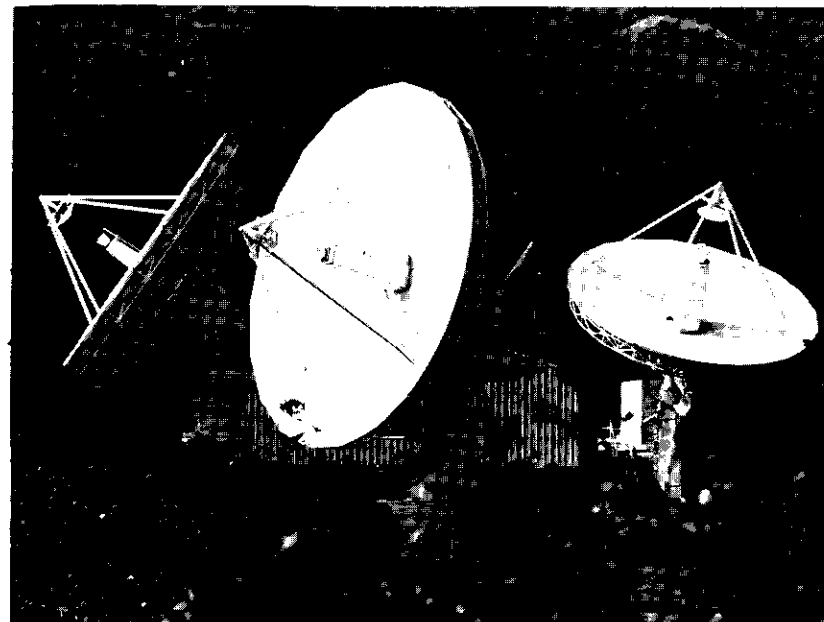


Figure 15. Santa Paula Earth Station

satellite control and processing equipment at the two TT&C earth stations and at the System Control Center was also awarded to COMSAT Laboratories on November 28, 1973. One of the primary features of the TT&C complex is the ability to operate effectively with few personnel. An additional antenna and redundant equipment are provided to ensure high reliability.

#### Communications earth stations and terrestrial interconnect equipment

The communications earth stations and terrestrial interconnect equipment are owned and operated by AT&T and GSAT [19]. Table 4 gives the principal characteristics of the earth stations. The locations of the earth stations in operation or under construction are as follows. The Hawley, Pennsylvania, earth station (AT&T) serves New York City\* and has three

\*These indicate primary geographical cities. Service is provided through the corresponding metropolitan junction offices to other cities and adjoining areas.

antennas 30 meters (98 feet) in diameter. The Triunfo Pass, California, earth station (GSAT) serves Los Angeles\* and will have three 32-meter-diameter (105-ft) antennas. The Three Peaks, California, earth station (AT&T) serves San Francisco\*; the Woodbury, Georgia, earth station (AT&T) serves Atlanta\*; the Hanover, Illinois, earth station (AT&T) serves Chicago\*; the Sunset, Hawaii, earth station (GSAT) serves Honolulu\*; and the Homosassa, Florida, earth station (GSAT) serves Tampa.\* These stations each have two 30- or 32-meter-diameter antennas, although Sunset's second backup antenna is shared and also provides backup for accessing the INTELSAT satellite system.

TABLE 4. CHARACTERISTICS OF AT&T COMMUNICATIONS  
EARTH STATIONS

Antenna Diameter	30 m (98.4 ft)
Type of Antenna Mount	Elevation/azimuth
Azimuth Steerability	$\pm 35^\circ$
Elevation Steerability	$10^\circ$ to $75^\circ$
Type of Tracking System	Step track
Nominal Antenna Pointing Accuracy (rms)	0.032°
Antenna Tracking Accuracy (rms)	0.016°
Antenna Slew Velocity	0.2°/s
Feed Polarization Capability	Linear-frequency reuse
Polarization Isolation (within tracking beamwidth)	>35 dB
Antenna Gain	
6 GHz	62.6 dB
4 GHz	59.5 dB
Receiver Noise Temperature	17 K
Antenna System G/T at 20° Elevation	42 dB/K
Transmitter Tube Type	Klystron/TWT
Rated Transmitter Power	3/1 kW
Maximum Up-Link e.i.r.p. at 6 GHz	94/89.3 dBW

\*These indicate primary geographical cities. Service is provided through the corresponding metropolitan junction offices to other cities and adjoining areas.

### Schedule and status

The AT&T agreement called for a launch schedule objective of 27 months after FCC approval, or March 1976 for COMSTAR D-1 and June 1976 for COMSTAR D-2. The launches occurred in May and July 1976, respectively; the 1- to 2-month slippage for a 2.5-year program is considered quite acceptable in view of the normal quality control problems characteristic of all complex spacecraft programs. The COMSTAR D-3 is currently available for the next scheduled launch in April 1978, and the final spacecraft, COMSTAR D-4 (the on-the-ground spare), is scheduled for completion in February 1977.

The TT&C earth stations and the System Control Center were completed in late 1975 and were first used to support the MARISAT launches [18]. They were well exercised by the May 1976 launch of COMSTAR D-1. The AT&T communications earth stations and interconnection facilities were completed during early 1976 and were operational at the time of the COMSTAR D-1 launch. Initial operation of Triunfo Pass commenced in January 1977 and full operation of Triunfo Pass and Homosassa is scheduled for early 1977.

### Launch and orbit injection

As mentioned previously, the actual launch is performed by NASA for COMSAT GENERAL. After liftoff, the launch vehicle is controlled by the avionics in the second (Centaur) stage. The first (Atlas) stage fires its main engines followed by its sustainer engine and, at end of burning, separates from the Centaur. After separation, the Centaur stage has its "first burn," at the end of which the Centaur is in a parking orbit of approximately 1,800-km (1,100-mile) apogee and 185-km (115-mile) perigee. It burns a second (and final) time as it passes the equator, placing the satellite in a transfer orbit of approximately 35,800-km (22,200-mile) apogee and 550-km (340-mile) perigee. These orbits are shown in Figure 16. After this second firing, the Centaur separates from the satellite and all further operations become the responsibility of COMSAT GENERAL.

COMSAT GENERAL has TT&C earth stations for COMSTAR only in the U.S. To provide worldwide TT&C coverage during the transfer orbits, an agreement with INTELSAT was made whereby TT&C services for COMSTAR would be performed using the TT&C earth stations providing such services to INTELSAT. Five of these earth stations are located in Zamengoe, Cameroon; Fucino, Italy; Paumalu, Hawaii; Carnarvon, Australia; and Andover, Maine.

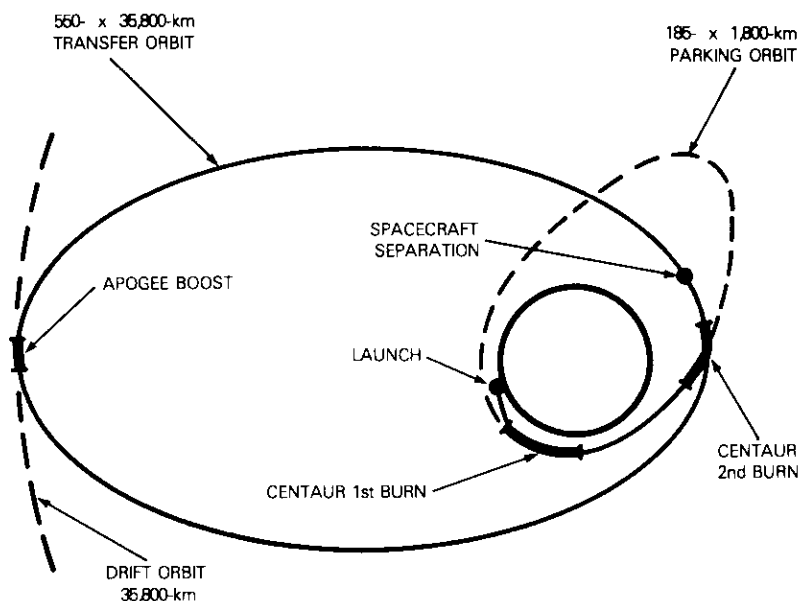


Figure 16. COMSTAR Satellite Parking and Transfer Orbits

The TT&C services are provided from initial satellite acquisition until after the solid apogee kick motor on the COMSTAR satellite is fired to convert the transfer orbit into a near-circular orbit of 35,800 km (22,200 miles). In the COMSTAR program, this firing is accomplished on the fifth transfer orbit apogee. Due to the apogee motor sizing, the apogee motor firing must be followed by a "post-burn" (usually 24 hours later) using hydrazine propellant stored in the satellite to achieve the synchronous orbit. Additionally, a 123-kg (270-lb) load of hydrazine is carried on the satellite for stationkeeping, as described in a companion paper.

The COMSTAR D-1\* was launched from Cape Canaveral on May 13, 1976, at 6:28 PM EDT using pad 36A. The performance of the Atlas-Centaur launch vehicle (AC-38) was perfect. The TT&C earth station at Zamengoe acquired at liftoff plus 28 minutes and Carnarvon acquired at liftoff plus 44 minutes. The satellite communications electronics and the 19- and 28-GHz Beacons were activated soon thereafter. The satellite was functionally checked during transfer orbit, and the apogee motor was fired on May 15 at 6:42 PM EDT when the satellite was at approximately 190°W longitude. This was followed by the post burn on May 16 from 5:50—6:00 PM EDT

\*Officially assigned space object number 1976-042A.

and, a half-hour later, the satellite was reoriented to its operating attitude in a 48-minute maneuver. The near-synchronous orbit (called a "drift orbit") had a 35,850-km (22,276-mile) apogee and a 35,296-km (21,932-mile) perigee with an inclination of 0.12° and a 3.2° per day drift eastward toward its FCC-assigned orbital operating position at 128°W longitude.

With a scheduled 6:04:00.000 liftoff, the COMSTAR D-2\* was launched from pad 36B on Atlas-Centaur vehicle AC-40 on July 22, 1976, at 6:04:00.208 PM EDT. Figure 17 is a photograph of the launch. The sequence and performance were almost identical to those of COMSTAR D-1. Apogee motor firing was at 6:12 PM EDT on July 24. The post burn on July 25 from 5:41—6:15 PM EDT was followed by the reorientation maneuver, which ended at 7:20 PM EDT. The achieved drift orbit had a 35,790-km (22,238-mile) apogee and a 35,450-km (22,027-mile) perigee with an inclination of 0.15° and a 2.7° per day drift eastward toward its FCC-assigned orbital operating position at 95°W longitude.

During the transfer orbit, a comprehensive set of functional and kinematics tests was performed to ascertain satellite survival of the launch and to obtain detailed engineering data on satellite stability in different operating modes. The tests indicated that all systems were functioning properly. As described in a subsequent paper, the satellite is spin-stabilized and operates as a gyrost. However, there are several destabilizing forces; the most significant is fuel slosh in the hydrazine tanks [20]. In the COMSTAR program, although comprehensive computer modeling and limited ground simulator verification were performed to prove satellite stability under all possible operating conditions, in-orbit kinematics testing of the satellite was deemed essential to verify the analytical models. The tests indicated that the dynamic models were correct, and both the mechanical and electronic nutation damping (DANDE) subsystems functioned as predicted.

#### In-orbit testing

Following the orbital synchronization operations, both COMSTAR satellites were subjected to rigorous in-orbit performance tests, as described in a companion paper. These tests were conducted during the three to four weeks while the satellites were drifting from the post-apogee motor firing orbital location of approximately 190°W longitude to their operating locations at 128°W and 95°W longitude, respectively, and during a few days after reaching their operating positions. It should be noted that these tests had to be halted whenever the satellite drifted within a few degrees

\*Officially assigned space object number 1976-073A.

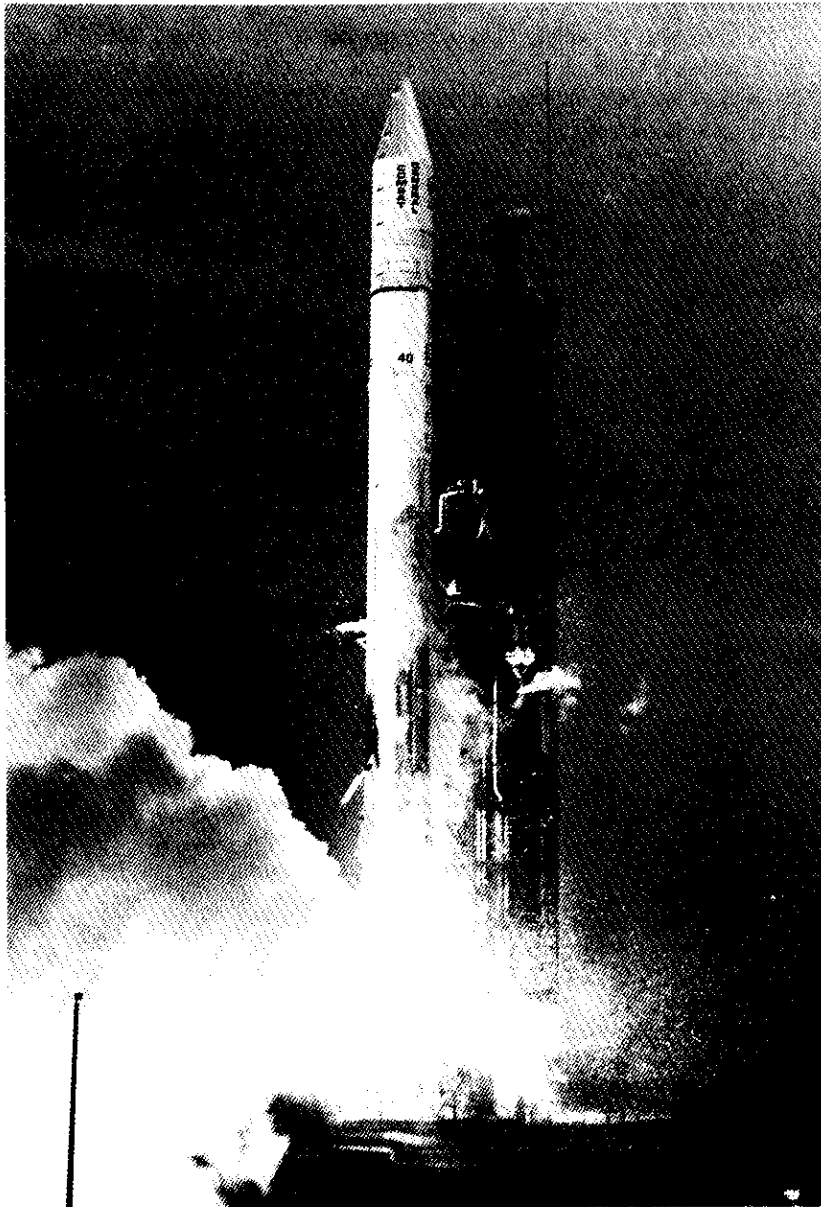


Figure 17. COMSTAR D-2 Satellite Launch

of transit of already operating U.S. and Canadian domestic satellites. During these transit periods, all radio communications receivers on the satellite were turned off to avoid interfering with the operating satellite being passed.

The test sequence starts with a check of the non-communications satellite equipment such as the thermal, power conditioning, antenna pointing, propulsion, command, and telemetry subsystems. This portion of the testing is conducted from the System Control Center in Washington, D.C., with the radio commands sent by and telemetry received from the Santa Paula TT&C earth station. This portion of the testing generally takes two to three days.

The next portion of the sequence, which generally takes two to three weeks, is a performance test of the satellite communications equipment. Table 5 lists the tests and their general order. Accurate in-orbit performance

TABLE 5. LIST OF COMSTAR SATELLITE IN-ORBIT COMMUNICATIONS TESTS

Calibration
Satellite Antenna Patterns
Spin-Ripple
Saturation Flux Densities
Effective Isotropically Radiated Power (e.i.r.p.)
Gain Step Attenuator Settings
Transponder Frequency Response
Antenna Gain/Receiver Noise Temperatures (G/Ts)
Transmitter Turn-on Times
Polarization Isolations

testing is extremely difficult since sophisticated tests and a large number of measurements are required. As an example, 144 sets of measurements are required to determine the e.i.r.p. for all the transponders in every operational mode of a COMSTAR satellite (considering its multiple beams and interbeam switching capabilities) at three radio frequencies. Arrangements were made with COMSAT to perform the in-orbit tests at the Paumalu earth station using an antenna which had been precisely calibrated and configured for such in-orbit performance measurements of INTELSAT satellites, to use an automated performance measuring subsystem developed by COMSAT Laboratories, and to assemble a test team composed of engineers experienced in this technical area.

The communications performance tests are started at Paumalu where the test director is located. He is supported by personnel in the System Control

Center in Washington, D.C. The latter portion of the tests is monitored and then performed in part by the Santa Paula TT&C earth station. The final performance tests, involving cross-polarization performance, are performed only from Santa Paula, since a 12.8-meter (42-foot) diameter antenna at this station has been specially calibrated for such isolation measurements. Table 6 and Figure 18 summarize the results of the antenna cross-polarization isolation measured during acceptance tests.

TABLE 6. TEST RESULTS OF FULL-PERFORMANCE ANTENNA AT SANTA PAULA, CALIFORNIA, EARTH STATION

	Cross-polarization Isolation (dB)					
	Specified		Measured		On-Axis Degradation	
	On Axis	-1-dB Pt	On Axis	-1-dB Pt	Specified C + L*	Measured C + L*
4-GHz Receive Band	35	30	38	37	25	35
6-GHz Transmit Band	35	30	34	29	25	33

\*Special feed which incorporates receive and transmit capability at 1,400-1,500 MHz.

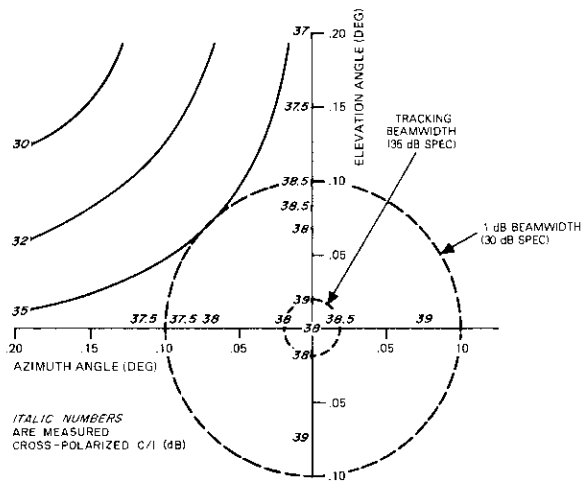


Figure 18. 4-GHz Cross-polarization Performance of Full-Performance Antenna at Santa Paula Earth Station

Table 7 compares specified parameter values with measured data on COMSTAR D-1 and D-2. It should be noted that the measured data for the two satellites were almost identical. The performance data are discussed in more detail in a companion paper. It appears that the performance of the satellites exceeded initial expectations.

TABLE 7. COMSTAR COMMUNICATIONS IN-ORBIT TEST RESULTS

Parameter	Specification	Measured	
		COMSTAR D-1	COMSTAR D-2
e.i.r.p.*	33 dBW	≥ 34 dBW	≥ 34 dBW
Flux Density* (for saturation)	-72.7 dBW/m <sup>2</sup>	≤ -73.7 dBW/m <sup>2</sup>	≤ -73.7 dBW/m <sup>2</sup>
Antenna Patterns	Contiguous U.S., Hawaii, Puerto Rico, and Alaska	Matched prelaunch data	Matched prelaunch data
Cross Polarization*	33 dB	33 dB	33 dB
Frequency Response (transponder)	34-MHz usable bandwidth	34-MHz usable bandwidth	34-MHz usable bandwidth
19/28-GHz Beacons			
19-GHz e.i.r.p.*	23.0 dBW	22.8 dBW	24.0 dBW
28-GHz e.i.r.p.*	23.5 dBW	26.4 dBW	27.0 dBW
1,200-Channel Noise*	6,800 pW0p (objective with 2,000 pW0p of external interference)	≈ 4,000 pW0p	≈ 4,000 pW0p

\* At worst point and frequency anywhere within coverage areas.

These performance tests were followed by a 2-week series of preoperational tests conducted by AT&T from the communications earth stations. The primary communications earth station for these tests was the Hawley, Pennsylvania, earth station. The series concluded with a communications system path "line up" between each pair of AT&T terrestrial communications centers, which encompasses two terrestrial interconnection facilities, two earth stations, and the satellite link. It is difficult to test satellite communications systems accurately in an operational environment. In addition, certain parameters such as satellite antenna patterns are not measured in such preoperational tests. The tests performed by AT&T verified the previously described measurements from Paumalu and Santa Paula.

Tests of the 19/28-GHz Beacons were performed separately from COMSAT Laboratories at Clarksburg, Maryland.

## Operations

COMSAT GENERAL provided AT&T with operational use of COMSTAR D-1 on June 19, 1976, and COMSTAR D-2 on September 9, 1976. Communications service was authorized on July 20, 1976, and actual operations commenced on July 24, 1976.

At the time this paper was prepared (January 1977), COMSTAR D-1 had been in operation for seven months and COMSTAR D-2 for four months. Both satellites have gone through a solar eclipse cycle, which was the first realistic test of the solar cell-battery power subsystem. Performance to date has been exactly as predicted and can be described as excellent. Table 8 shows some satellite parameter values on September 21, 1976, which is the longest eclipse day and consequently reflects the maximum depth of battery discharge. Operation of the TT&C earth stations and the System Control Center has also been excellent.

TABLE 8. COMSTAR SATELLITE STATUS (SEPTEMBER 21, 1976)

Parameter	COMSTAR D-1	COMSTAR D-2
Location (W. longitude)	128.06°	95.05°
Drift	0.001°E	0.019°W
Inclination	0.019°	0.058°
North-South Attitude	0.012°	0.029°
Attitude Drift	0.062°/day	0.063°/day
Total Power	695 W	697 W
Battery Depth of Discharge	47%	51%
Fuel Remaining	277.58 lb	294.25 lb
Spin Speed (rpm)	53.47	53.26

In terms of onboard fuel capacity, solar cell degradation, bearing lubrication, battery capacity, and assigned electronic equipment failure rate data, a COMSTAR satellite lifetime of at least nine years appears probable.

## Acknowledgments

The successful completion of such an extensive program as COMSTAR clearly depends on the competence, dedication, and cooperation of many people who cannot be individually acknowledged. The author would like to take this opportunity to express his gratitude to all.

## References

- [1] Communications Satellite Corporation, Reply Statement to the Federal Communications Commission, March 31, 1967 (received April 3, 1967), Docket 16495.
- [2] R. D. Briskman, "Domestic Communications Services Via Satellites: COMSAT Pilot Program," *Journal of Spacecraft and Rockets*, Vol. 6, No. 7, July 1969, pp. 835-840.
- [3] Federal Communications Commission, "Second Report and Order" (35FCC2d844), adopted June 16, 1972; Memorandum Opinion and Order (38FCC2d655), adopted December 21, 1972, Docket 16495.
- [4] R. D. Briskman, "A Domestic Satellite Design," *IEEE Transactions on Aerospace and Electronic Systems*, AES-7, No. 2, March 1971, pp. 263-268; 1970 International Conference on Communications, San Francisco, California, June 1970.
- [5] Federal Communications Commission, "Application of COMSAT to Construct a System of Domestic Satellite Facilities for Use by AT&T," File No. 10-DSS-P(4)-71, March 1973, Annex I.
- [6] Federal Communications Commission, "(First) Report and Order" (22FCC2d86), adopted March 20, 1970, Docket 16495.
- [7] "The INTELSAT IV Spacecraft," edited by E. T. Jilg, *COMSAT Technical Review*, Vol. 2, No. 2, Fall 1972, pp. 271-389.
- [8] "The INTELSAT IV Communications System," edited by P. L. Bargellini, *COMSAT Technical Review*, Vol. 2, No. 2, Fall 1972, pp. 437-572.
- [9] J. L. Dicks and M. P. Brown, Jr., "INTELSAT IV-A Transmission System Design," *COMSAT Technical Review*, Vol. 5, No. 1, Spring 1975, pp. 73-104.
- [10] D. C. Cox, "Design of the Bell Laboratories 19 and 28 GHz Satellite Beacon Propagation Experiment," IEEE International Conference on Communications, June 1974, *Conference Record*, pp. 27E-1-27E-5.
- [11] R. W. Gruner and W. J. English, "Antenna Design Studies for a U.S. Domestic Satellite," *COMSAT Technical Review*, Vol. 4, No. 2, Fall 1974, pp. 413-447.
- [12] D. F. DiFonzo and R. W. Kreutel, "Communications Satellite Antennas for Frequency Reuse," G-AP International Symposium, September 1971, *Proc.*, pp. 287-289.
- [13] E. J. Wilkinson, "A Dual Polarized Cylindrical Reflector Antenna for Communication Satellites," *Microwave Journal*, Vol. 16, No. 12, December 1973.
- [14] J. L. Fromme, "A Dual-Polarized Antenna System for Satellite Earth Stations," *EASCON 74 Record*, October 1974, p. 394.

- [15] Federal Communications Commission, "Application of COMSAT to Construct a System of Domestic Satellite Facilities and Associated Services for Use by AT&T," October 19, 1970, Annex II, p. A-1 and Figure A-1.
- [16] Bell Telephone Laboratories, *Transmission Systems for Communications*, Revised Fourth Edition, December 1971, pp. 677-684.
- [17] D. J. Shramo, B. R. Foushee, and P. J. O'Leary, "Centaur—A Major Element of the Current Space Transportation System," IAF XXVth Congress, Amsterdam, The Netherlands, September 1974.
- [18] E. J. Martin, "Marisat—A New Commercial Application of Communications Satellite Technology," *Proceedings of the Thirteenth Space Congress*, Canaveral Council of Technical Societies, April 1976, pp. 8-9-8-17.
- [19] Federal Communications Commission, "Application of American Telephone and Telegraph Company for a Domestic Communications Satellite System," March 29, 1973 (amended May 3, 1973), pp. 1-34.
- [20] E. R. Martin, "Experimental Investigations on the Fuel Sloss of Dual-Spin Spacecraft," *COMSAT Technical Review*, Vol. 1, No. 1, Fall 1971, pp. 1-20.



*R. D. Briskman received a B.S.E. from Princeton University and an M.S.E. in electrical engineering from the University of Maryland. Joining COMSAT in 1964, he was initially responsible for command and control activities and later involved with the development and implementation of the INTELSAT global system. He has been responsible since 1967 for the technical planning involved with the provision of domestic communications services via satellites. He is presently Assistant Vice President, Space & Information Systems of COMSAT*

*GENERAL. His responsibilities include the COMSTAR satellite system and the development of earth resources and data collection systems. Prior to COMSAT, he worked for NASA, the Army Security Agency, and IBM. He is a Fellow and officer of the IEEE. He has been President of the Aerospace and Electronic Systems Society, Director of the National Telecommunications Conference, and Chairman of the EASCON Board of Directors. He has been awarded the NASA Apollo Achievement Award and the Army Commendation Medal.*

**Index: system analysis, COMSTAR, domestic satellite communications system**

## ***The COMSTAR satellite system***

G. E. A. ABUTALEB, M. C. KIM, K. F. MANNING,  
J. F. PHIEL, JR., AND L. H. WESTERLUND

(Manuscript received November 29, 1976)

### ***Abstract***

This paper describes, on a broad basis, the COMSAT GENERAL communications satellites, which, in conjunction with the AT&T-GSAT earth segment, form the COMSTAR domestic satellite system. Following a description of the spacecraft and its various subsystems, the communications subsystem is treated in detail and the earth station characteristics are presented to give an overall picture of the system.

The transmission analysis of the COMSTAR satellite system is based on the use of analog FDM/FM with 1,200 1-way voice channels per transponder. In operation it is planned to provide a capacity of more than 1,500 1-way voice channels per transponder. The system is also capable of handling narrowband or wideband data, TV, high-bit-rate digital carriers, and multiple-access modes of FDMA and/or TDMA. The COMSTAR system has been designed with emphasis on high-quality transmission performance, high reliability, and operational flexibility. System performance is presented in terms of specified and measured parameters.

### ***Introduction***

The objective of the COMSTAR system design has been to provide high-quality, high-channel-capacity voice circuits between terrestrial points with additional flexibility to provide other types of service such as multi-point transmission and distribution. The initial formulation of the system

revealed that AT&T's service requirements could not be accommodated by satellites launched with the available Delta vehicles. Therefore, it was decided to use Atlas-Centaur launch vehicles, with the system design directed toward maximizing the transmission capacity by using existing technology in the 4/6-GHz bands.

In view of the required transmission service, the flux density restrictions, the high G/T ratio of the AT&T earth stations, and the satellite e.i.r.p. obtainable when using an Atlas-Centaur, it became clear that the available 500-MHz bandwidth in each of the 4- and 6-GHz bands would become the limiting factor in terms of channel capacity. It was therefore necessary to introduce frequency reuse techniques. Two options were available to accomplish frequency reuse: frequency reuse between alternate U.S. domestic time zones by spatial isolation, or frequency reuse by polarization isolation within a single beam providing U.S. coverage. The use of U.S. time zones was impractical in terms of operational considerations because of the interconnectivity problem; therefore, it was not pursued in detail. The latter approach, which was eventually adopted, constitutes the most salient feature of the COMSTAR program. Although it has been used for many years by microwave communications terrestrial facilities, the concept of frequency reuse by polarization and frequency planning represents the first application by a commercial communications satellite. In particular, the mode of transmission of the COMSTAR system, that of a single carrier per transponder, allows the full benefit of this type of frequency reuse to be realized. With the concept of frequency reuse by polarization isolation, the other building blocks of the system were within the realm of available technology.

The COMSTAR spacecraft communications subsystem contains four operating receivers, two of which are redundant, and 24 non-redundant transponders. Each transponder is characterized by a 34-MHz usable bandwidth and an e.i.r.p. of at least 33 dBW over the contiguous U.S., Alaska, Hawaii, and Puerto Rico. Communications coverage of these areas is produced by two antennas, one for each polarization. Each antenna receives at 6 GHz and transmits at 4 GHz. The AT&T and GTE earth station complex presently has seven earth stations, each having two or three 30-m (98.5-ft) parabolic antennas.

Four COMSTAR satellites have been designed and built to provide continuous operation over a life span of at least seven years. Two of these satellites have been launched and are performing satisfactorily. One of the remaining two satellites will be launched in 1978. Contingent upon

the successful launch of the third satellite, the last one will be kept in storage as a ground spare.

### **Overall spacecraft description**

The COMSTAR spacecraft was derived from the INTELSAT IV and IV-A spacecraft [1], [2]. Major differences are noticeable, primarily in the communications payload. The spacecraft power subsystem closely resembles that of INTELSAT IV, with minor changes in the size of the solar panels and the solar cells themselves. The despun system has also been upgraded to provide more accurate pointing.

The overall spacecraft configuration is shown in Figure 1, and the principal spacecraft elements and their arrangement are shown in Figure 2. Table 1 lists some of the spacecraft characteristics. The two main elements

TABLE 1. SPACECRAFT CHARACTERISTICS

<b>Size</b>	
Solar Panel Diameter	2.38 m (93.75 in.)
Solar Drum Height	2.81 m (111 in.)
Overall Height	6.09 m (239.7 in.)
<b>Weight</b>	
Launch (includes adapter)	1,520 kg (3,350 lb)
On Station (initial)	811 kg (1,787 lb)
<b>Booster</b>	
Apogee Motor	SVM-4A
<b>Electrical Power Subsystem</b>	
	Cylindrical solar array with n-on-p 2-by 6-cm solar cells, 12-mil coverglass
Power, Beginning of Life (equinox)	760 W* at 24.5 V
Power, End of Life (equinox)	610 W* at 24.5 V
Battery Charging	Constant current, three commandable levels
Number of Batteries	2 (24 Ah each), 25 cells/battery
Number of Cells	
Main Array	14,080
Charge Array	2,772
<b>Positioning and Orientation Subsystem</b>	
	Two Redundant Hydrazine Systems
Number of Tanks per System	2
<b>System Construction</b>	
Hydrazine, Propellant, Both Systems (total maximum capacity)	163 kg (360 lb)

\* Includes 54 W for battery charging.

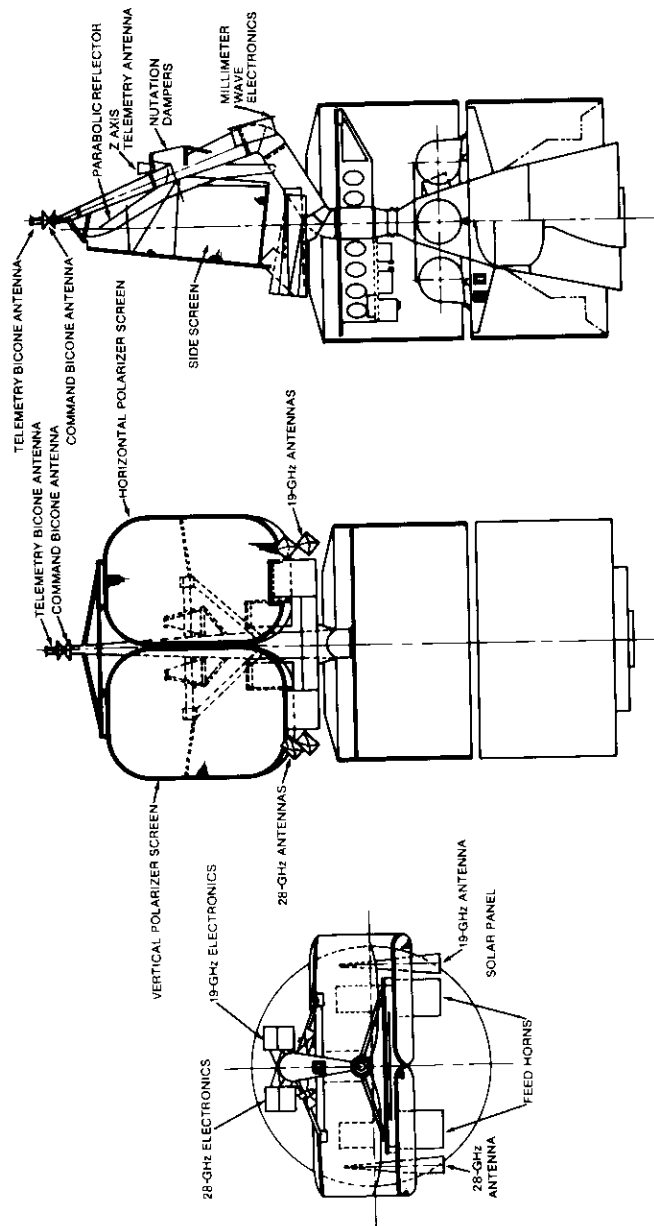


Figure 1. Overall Spacecraft Configuration

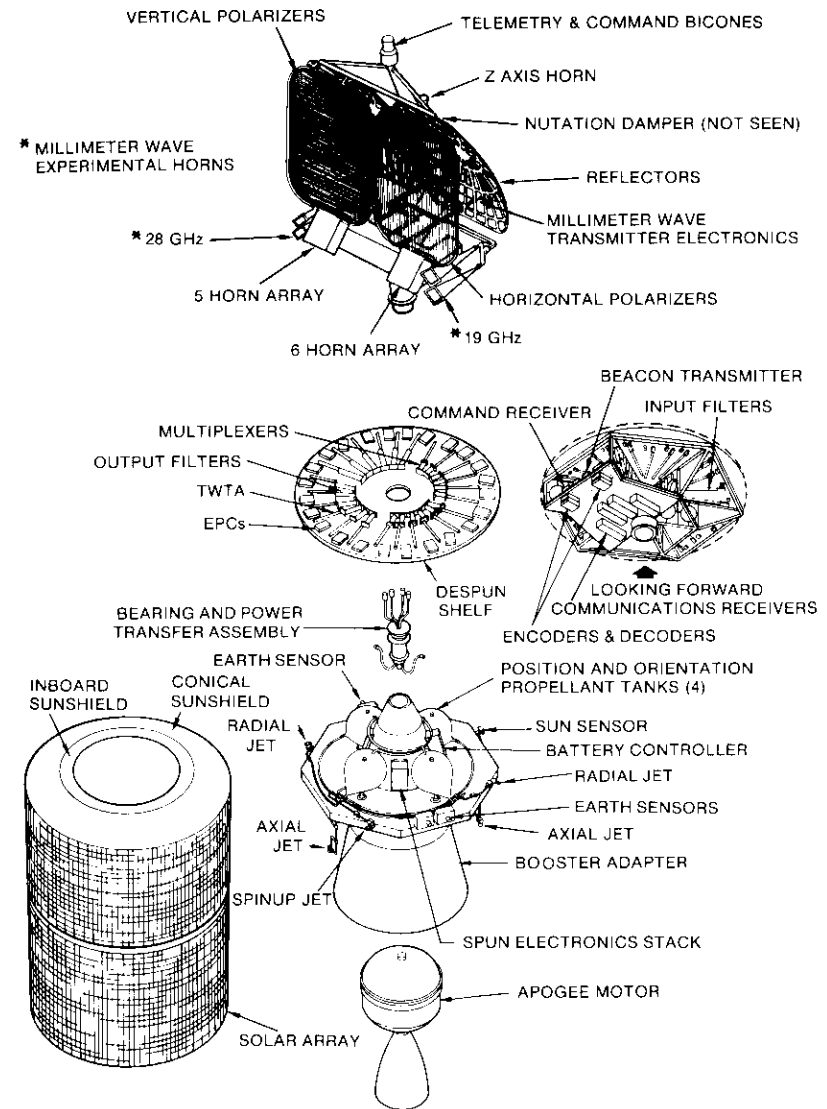


Figure 2. Principal Spacecraft Elements

TABLE 1. SPACECRAFT CHARACTERISTICS (Continued)

Thrusters (two each, axial and radial spin-up jets)	6
Initial Thrust Level	26 N at 207 N/cm <sup>2</sup> (5.85 lb at 300 psi)
Bearing and Power Transfer Assembly	
Outer Diameter	0.14 m (5.51 in.)
Bearings (preloaded)	Two, 90-mm bore, angular contact
Diameter (inner race bore)	0.09 m (3.54 in.)
Lubrication (oil-impregnated retainers)	Hughes coat
Slip Ring (power transfer)	2 redundant paths, 7.5 A each
Material	
Rings (coil silver)	90 percent Ag, 10 percent Cu
Brush (Stackpole SM476)	85 percent Ag, 3 percent C, 12 percent MoS <sub>2</sub>
Rotary Transformer (signal transfer)	2 independent command channels, 2 independent telemetry channels
Despin Control System	Dual loop (position and rate)
Sampled Data System Rate	Once per revolution
Inertial Reference Sensors	3 earth sensors, 2 sun sensors
Rotor Platform Reference Indicator	2 permanent magnet pip coil detectors
Torque Motor	Dual brushless DC
	2.17 N-m (1.6 ft-lb) at 60 rpm and 31.5-V bus
	1.56 N-m (1.15 ft-lb) at 60 rpm and 23.5-V bus
Long-Term Pointing Accuracy	
Maximum North-South Error	±0.28°
Maximum East-West Error	±0.2°
Spin Speed Range	45-75 rpm (45-60 rpm preferred)
Design Spin Speed	53 rpm
Reliability	
Orbital Lifetime Reliability for 18 Out of 24 Operational Repeater Channels Given Successful Injection into Orbit	0.99 (2 mo), 0.7 (7 yr)

are the spinning rotor and the despun earth-oriented platform containing the transponders and antennas. The spinning rotor provides gyroscopic stability to the spacecraft. The rotating interface contains the electric despin motor, rotary transformers, and slip rings for signal paths and power transfer between the two main elements. The rotor contains the propulsion and orientation system, apogee motor, solar panels, and despin control and attitude determination electronics.

The despun portion is dedicated almost entirely to the communications payload. The repeaters are located on the despun shelves, with the communications receivers on the lower shelf. The mast supports the two large 1.27- x 1.78-m (50- x 70-in.) spot-beam antennas and the offset feeds. Polarization screens placed in front of the antennas ensure linear orthogonal electromagnetic waves with high cross-polarization isolation.

The omnidirectional command and telemetry antennas are located at the tip of the mast. A pair of small antennas, mounted external to the communications feed system, provides coverage of the contiguous U.S. for the Centimeter Wave Beacons located on the back of the mast. Also on the back side of the antenna mast, above the Centimeter Wave Beacon package, are two identical eddy current nutation dampers.

The electrical power subsystem located on the rotor includes two cylindrical solar arrays and two sets of nickel-cadmium batteries. The batteries are sized to provide sufficient power to maintain continuous service through eclipses.

The positioning and orientation subsystem is also mounted on the rotor. A pair of redundant radial jets is used to maintain the spacecraft on station. A second pair of axial jets maintains attitude and orbit inclination, and a third pair of jets provides for initial rotor spin-up and maintenance of the desired spin rate throughout the spacecraft life. Thrust is produced by catalytic decomposition of anhydrous hydrazine. The 157.85 kg (348 lb) of hydrazine are loaded into the four propellant tanks. Approximately 13.6 kg (30 lb) of propellant are used in the launch phase, with the remainder expended at a rate of about 17.2 kg (38 lb) per year. A 708.5-kg (1,562-lb) apogee motor, carried in the aft half of the rotor, is utilized to achieve synchronous orbit from transfer orbit.

The spacecraft temperature is controlled passively by selecting the proper ratio of solar energy absorptivity to infrared emissivity for the various external surfaces. Active heaters are provided on certain critical elements such as the apogee motor, and are controlled by command as required.

Spacecraft commanding is accomplished through two cross-strapped command systems. Ninety-five commands are used to control the state of the spacecraft subsystems, while 255 are used for the despun platform. Nearly all of the latter commands are associated with choosing among the multiple operating modes of the communications subsystem. The primary telemetry mode of the spacecraft is accomplished by a PCM system. Real-time FM telemetry is also provided to transmit analog pulses from the attitude sensors and accelerometers for use in attitude determination.

### Despin control subsystem

Figure 3 is a block diagram of the despin control system. The bearing and power transfer assembly (BAPTA), which is thoroughly described in Reference 1 and shown in Figure 4, contains a brushless DC electric motor which produces the necessary torque to overcome friction and keep the antennas pointed toward the earth. The torque is controlled by the despin control electronics (DCE), which consists of two redundant digital despin control electronic (DDCE) units, two analog despin control electronics (ADCE) units, and two redundant motor drivers (Figure 5). Each DCE unit is part of a closed-loop feedback control system. The digital unit is used for all transfer orbit operations and for earth acquisition when on station. After having achieved position lock, the analog unit is updated by ground command, and despin control is switched to the analog unit for steady-state high-resolution on-station platform orientation.

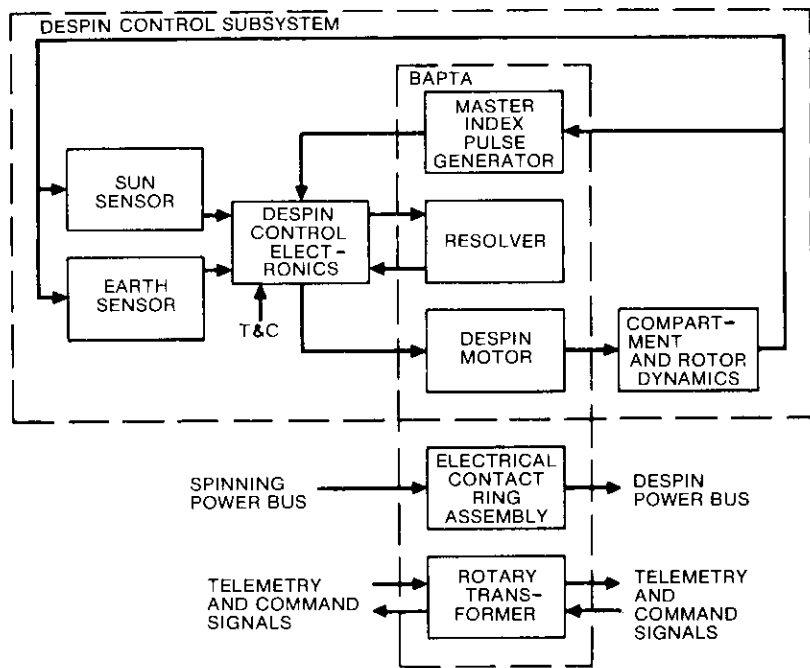


Figure 3. Despin Subsystem

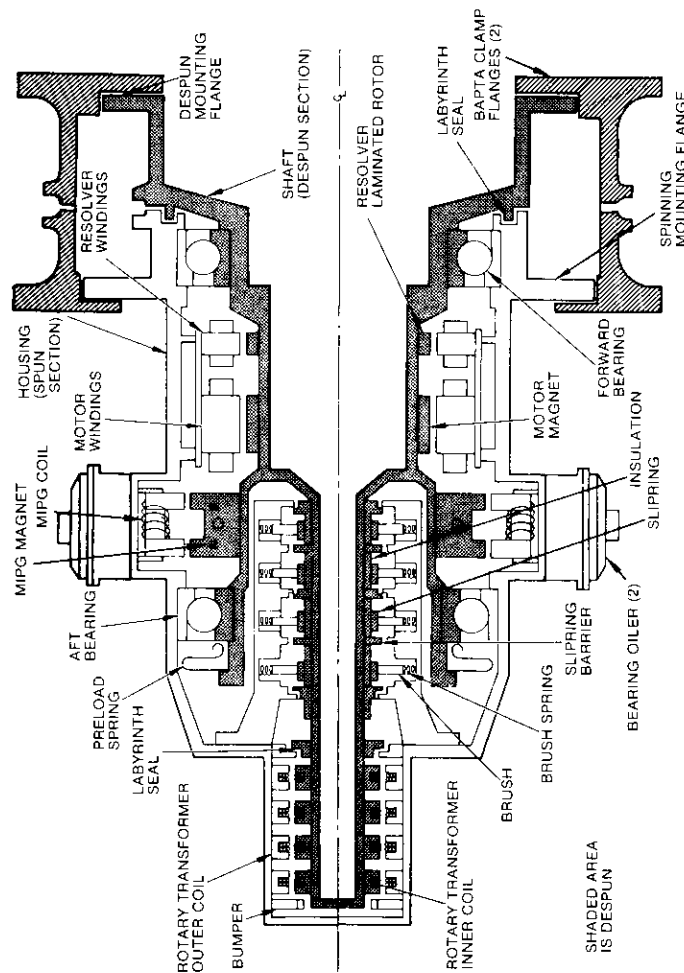


Figure 4. BAPTA

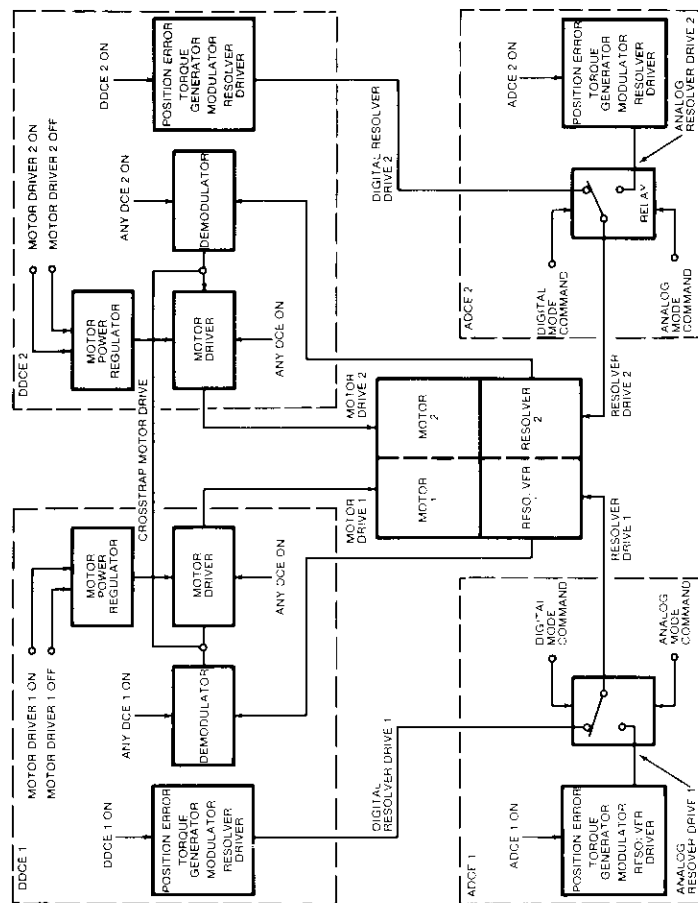


Figure 5. Resolver and Motor Drive

Although the COMSTAR despin subsystem is similar to that of INTELSAT IV, it incorporates the following additional features:

- an analog unit which utilizes earth center finding for despin control;
- an improved earth sensor providing less sensor jitter;
- a digital unit similar to that of INTELSAT IV, but with increased gain and additional interconnect signals to the analog unit.

Since the digital unit is thoroughly described in Reference 1, only the analog unit will be discussed herein.

While the digital unit is capable of using sun sensor, earth sensor leading-edge, or pseudo-earth pulses as its despin reference, the analog unit relies solely on the three leading- and trailing-edge earth sensor pulses. Earth sensor pulses are combined with the platform reference pulse to calculate the position error, as shown in Figure 6. An analog integration, initiated by an earth leading-edge pulse, is reversed by the platform reference pulse and stopped at the earth trailing edge. Since the residual integrator voltage is proportional to the pointing error, a null pointing condition exists if the platform reference pulse is centered exactly between the leading and trailing edges, corresponding to a zero residual integrated voltage. The position error is calculated once per spacecraft revolution. The error signal is summed with a ground commandable position bias voltage used for null offset control, shaped, and added to an integrated friction signal before it is sent to the modulator and resolver driver of the motor shown in Figure 7. The significant design parameters

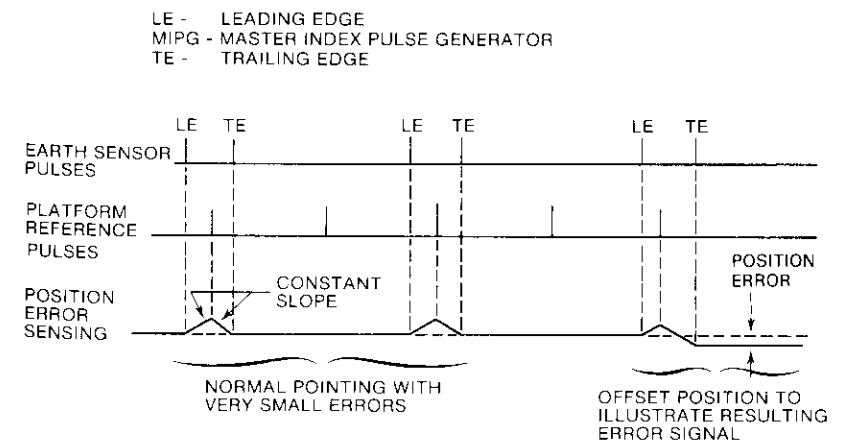


Figure 6. Analog DCE Position Error Derivation

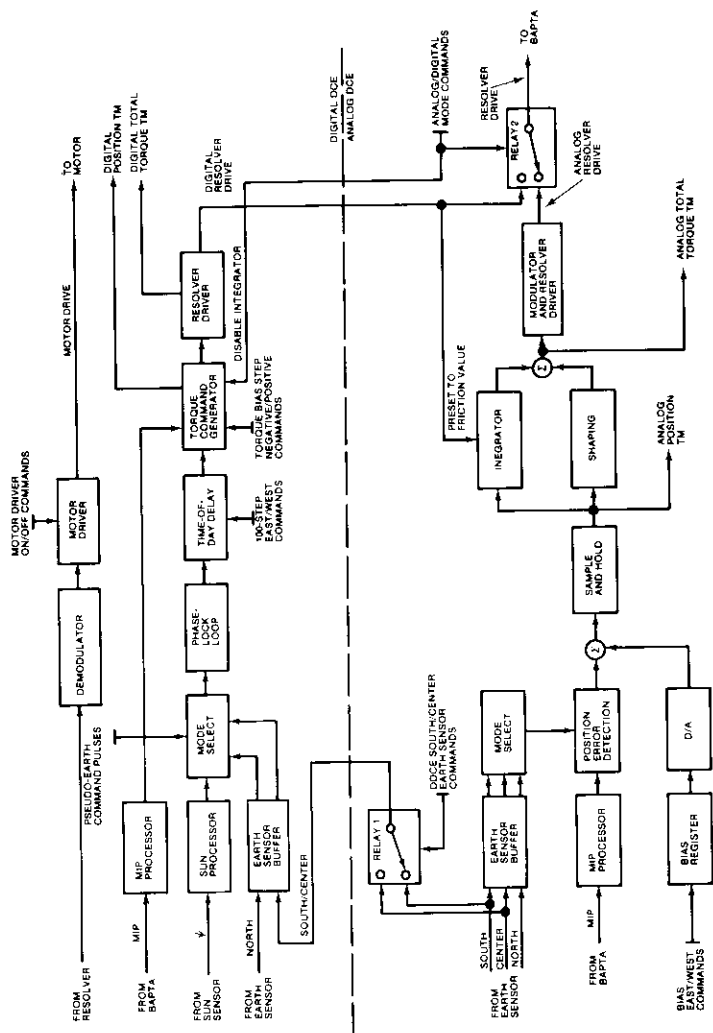


Figure 7. Despin Control Electronics Block Diagram

of the analog unit are shown in Table 2. Although the original design specifications called for a pointing accuracy of  $\pm 0.1^\circ$ , an in-orbit value of  $\pm 0.05^\circ$  has been achieved.

TABLE 2. ANALOG DCE DESIGN PARAMETERS

Performance Characteristics	
Pointing Accuracy (any 1-minute interval), Earth Mode Only	$\pm 0.10^\circ$
Spin Speed Range	50 to 60 rpm
Pointing Bias Capability	$\pm 5.0^\circ$ in $0.03^\circ$ increments
Control Loop Parameters*	
Position Loop	
Gain*	24.4 N-m/rad (18 ft-lb/rad)
Data Rate	Once per revolution
Dynamic Range*	$\pm 2.0^\circ$
Integrator (friction compensation) loop	
Gain*	0.244 N-m/s/rad (0.18 ft-lb/s/rad)
Dynamic Range*	0 to 0.72 N-m (0 to 0.53 ft-lb)
Initial Conditions	Preset to friction value from digital DCE when analog DCE is powered ON

\* These quantities double for 2-motor-driver operation.

**Attitude control subsystem**

Figure 8 is a flow diagram indicating the primary stabilizing and destabilizing paths in the COMSTAR attitude control system. Although fuel

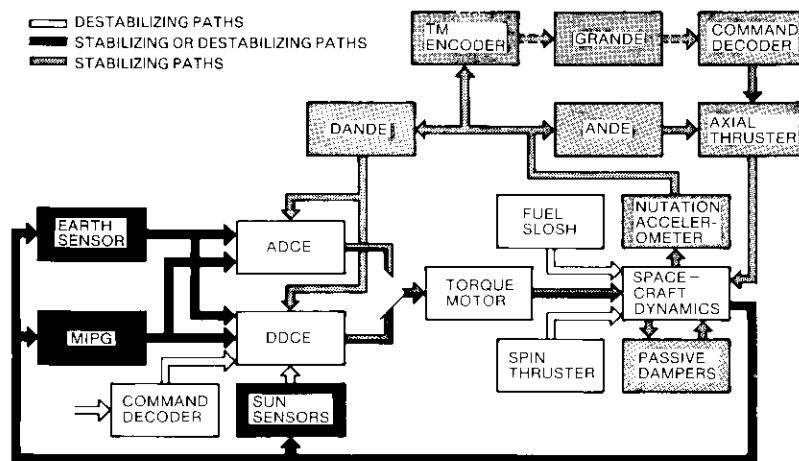


Figure 8. Attitude Control System

slosh remains the primary destabilizing influence, the platform has a large product of inertia which may act as a destabilizing influence by coupling the despin control system to the spacecraft dynamics (kinematic coupling). Kinematic coupling is a function of many parameters, including spacecraft mass properties, despin reference sensor mode, and platform pointing direction.

Under normal conditions, the passive nutation dampers are the primary stabilizing agents on the COMSTAR spacecraft. The active nutation damping equipment (ANDE), which limits the nutation angle in transient or failure modes as on INTELSAT IV, is retained as the automatic onboard system. The ground active nutation damper electronics (GRANDE) is an extension of the spacecraft-borne ANDE, but operates to a lower threshold. It has been incorporated in the COMSTAR system to remedy a trap state (Figure 9) occurring between the minimum sensitivity of the ANDE and the maximum range of the passive nutation dampers. That is, if nutation builds up to an excessive degree, the ANDE must be used to reduce it to the ANDE minimum threshold. The GRANDE is then used to further reduce it to the linear range of the passive dampers. At this point, the passive dampers become effective and reduce the nutation to zero.

The despin active nutation damper electronics (DANDE) is a system implemented for the first time on the COMSTAR spacecraft. Similar to kinematic coupling, it exploits the platform's large product of inertia. In normal operational modes, it potentially provides the strongest stabilizing effect on the spacecraft. As a relatively broadband device, it yields substantial stability margins over a wide range of spin speeds. Figure 10

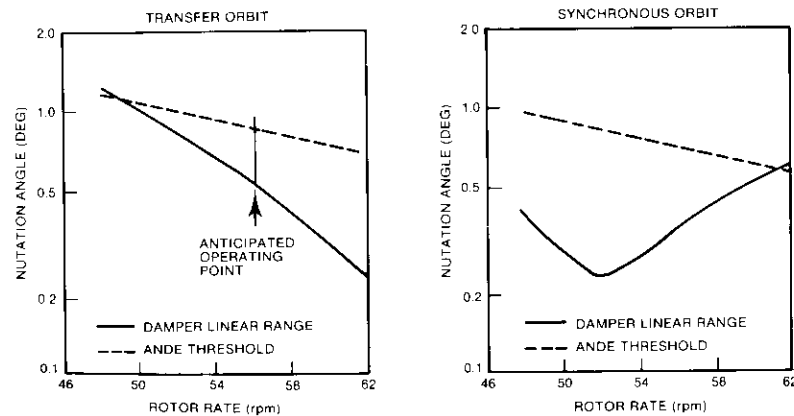


Figure 9. Damper Linear Range and Threshold

shows the damping time constant with and without the DANDE in operation. The passive dampers have been tuned to achieve maximum damping at the expense of effective damping over a large spin range. However, the DANDE achieves damping over most spin rates and results in a stable spacecraft over a very large rotor spin range.

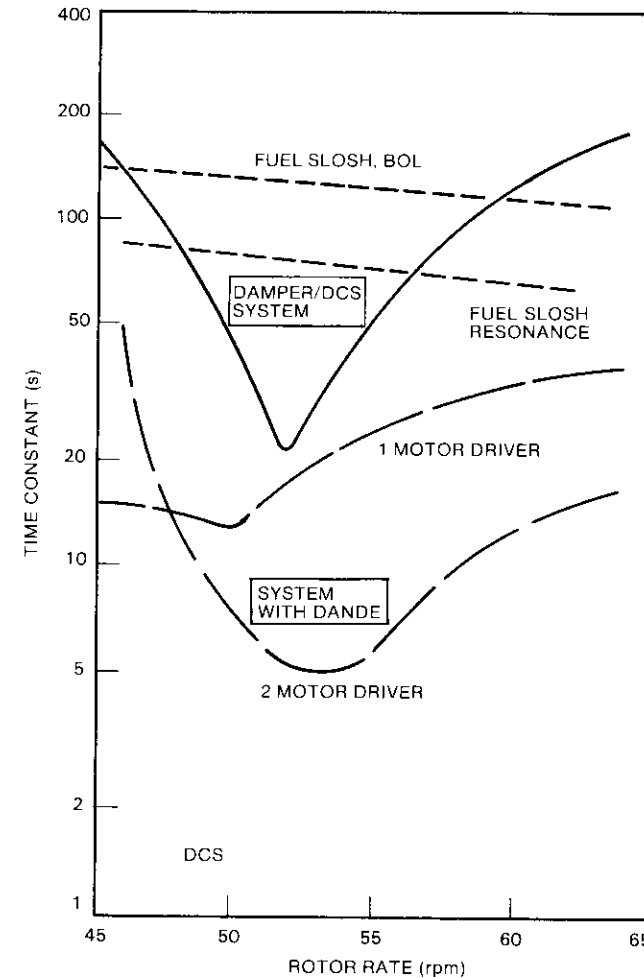


Figure 10. Active and Passive Nutation Damping Characteristics

The despun platform on COMSTAR possesses a relatively large product of inertia; *i.e.*, it is not dynamically balanced. When this body is rotationally accelerated, it reacts with a torque orthogonal to the product of inertia and the rotational acceleration. This torque is exerted on the spinning rotor, causing it to precess. The DANDE operates by sensing nutation via the nutation accelerometer and sending a varying torque to the despun motor phased with respect to the nutation so that the resulting precession of the spin axis reduces the nutation angle.

### Electrical power subsystem

The COMSTAR electrical power levels, indicated in Table 3, are signifi-

TABLE 3. POWER REQUIREMENTS

Load Description	Maximum Bus Current for Bus Voltage in 24.5- to 33.5-V Range (mA)					
	BOL		2 yr		EOL	
	Bus 1	Bus 2	Bus 1	Bus 2	Bus 1	Bus 2
Communications Subsystem						
5-W TWTs (12 at 703.3 mA)	4,220	4,220	4,220	4,220	4,220	4,220
5.5-W TWTs (12 at 766.2 mA)	4,597	4,597	4,597	4,597	4,597	4,597
Communication Receivers (2 at 670 mA)	670	670	670	670	670	670
19/28-GHz Experiment	1,176	1,184	1,170	1,184		
Subtotal	10,663	10,671	10,663	10,671	9,487	9,487
T&C Subsystem	456	221	456	221	456	221
Attitude Control Subsystem	260	900	260	900	260	900
Miscellaneous	225	260	225	260	225	260
Subtotal and Total Battery Load	11,604	12,052	11,604	12,052	10,428	10,868
Equinox Season Maximum Charge Current, 5/3 Array	1,357	1,357	1,268	1,268	1,161	1,164
Total Autumnal Equinox Solar Panel Load	12,961	13,409	12,872	13,320	11,592	12,032

cantly higher than those of the INTELSAT IV and IV-A spacecraft. Consequently, upgraded solar cells and batteries are used on COMSTAR satellites.

The power margins throughout the spacecraft life are shown in Table 4. These margins assume that the Centimeter Wave Beacons will be turned off at the end of two years. However, since that 2-year point has a signifi-

cant margin, the Centimeter Wave experiment will probably be continued through the fourth year of the spacecraft life.

TABLE 4. COMSTAR D-1 SOLAR PANEL POWER MARGINS

	Equinox		Solstice	
	2 Yr	7 Yr	2 Yr	7 Yr
Solar Panel Capability (A)	27.2	25.4	24.3	22.8
Bus Loads (A)	25.2	22.7	23.5	21.1
Margin (%)	+7.9	+11.9	+3.4	+8.1

### Telemetry, tracking, and command subsystem\*

All satellite functions require a command link to control the various states and modes of operation, and a telemetry link to indicate the spacecraft status and performance. These links function together as part of a closed loop with the ground control equipment to supply tracking data (ranging) and provide for synchronous control of satellite attitude. The telemetry, tracking, and command (TT&C) subsystem is located on both sides of the spinning/despun interface. Figure 11 provides an overview of the spacecraft TT&C subsystem.

Since the narrow communications spot-beam antennas are not oriented for transmission to ground during the transfer orbit, the communications transponders cannot be used for ranging as on INTELSAT IV. A switching feature has been incorporated into the TT&C subsystem to allow ranging via the omni antennas. This ranging switch causes the output of command receiver 2 to be rerouted from the decoders to the input of the telemetry Beacon. Ranging tones received by the command receiver are translated and transmitted by one of the telemetry transmitters through the omni antenna. The slant range to the orbiting satellite can then be determined both in transfer orbit and on station by means of a multiple-tone ranging system using a group of four coherent audio frequency signals. The range is calculated by measuring the round trip time of the transmitted signal.

The range measurement is performed by a precision digital phase meter operating in conjunction with a multimode computer-controlled range baseband processor. The processor generates four coherent high-spectral-purity audio tones (35.4 Hz, 283.4 Hz, 3,968 Hz, and 27.777 kHz). The 27.777-kHz tone determines the accuracy of the range measurement,

\*An overall description of the TT&C system is presented in a companion paper in this issue.

while the lower tones provide for removal of ambiguity. In practice, this system achieves a resolution of 10 m at synchronous altitude. The remainder of the TT&C system is essentially identical to that of the INTELSAT IV spacecraft.

The telemetry system utilizes three antennas for transmission of telemetry data. The normal on-station mode is through the contiguous U.S. antenna beams. In addition, the right-hand circularly polarized z-axis antenna transmits in a direction parallel to the spin axis of the spacecraft and can be used in case of unusual spacecraft attitudes. The omni antenna radiates a vertically polarized toroidal beam to be used during transfer orbit operations and to provide redundancy in synchronous orbit. The spacecraft command antenna is a single toroidal beam, dual-mode, bi-conical horn with linear polarization perpendicular to the spin axis.

**Communications subsystem**

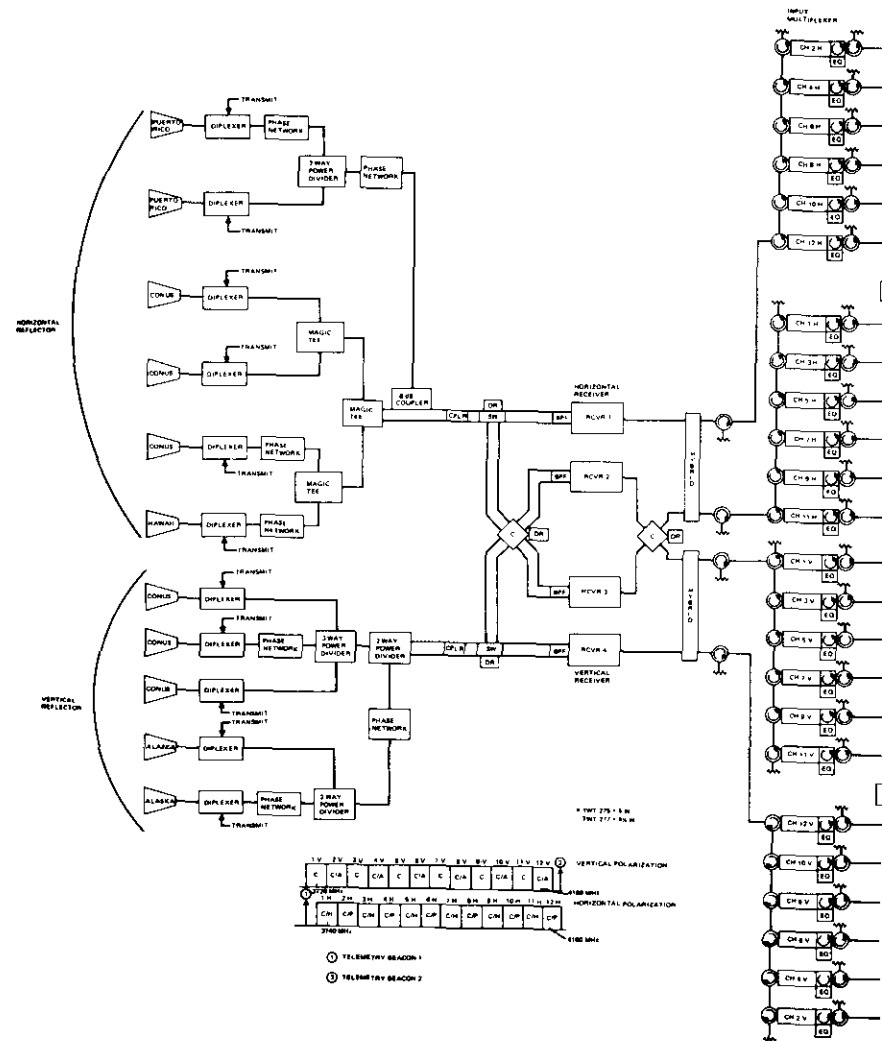
The basic transmission parameters of the COMSTAR satellite system are as follows:

- a. *Type of service:* FDM/FM\* analog voice channels, typically 1,200 channels per transponder, i.e., a total of 14,400 two-way voice circuits.
- b. *Service quality:* Less than 4,800 pW0p for any voice channel (between earth station modems excluding interference noise from terrestrial and adjacent satellites).
- c. *Service coverage:* Contiguous U.S., Alaska, Hawaii, and Puerto Rico.
- d. *Service lifetime:* 7 years.

As mentioned previously, higher channel capacities will be used during the operation of the system.

Figure 12 is the satellite communications subsystem block diagram. Specified coverage areas are shown in Figure 13, and the communications subsystem specifications are listed in Table 5. The service quality indicated above is required by AT&T for its transmissions to the contiguous U.S., Hawaii, Puerto Rico, and Alaska. For combined coverage of Alaska and the contiguous U.S., called the "T-mode," the noise in the worst voice channel must not exceed 6,300 pW0p. These performance specifications must be met when employing a reference earth station whose character-

\*Each transponder is capable of operating in either the TDMA or the FDMA multiple-access mode; mixed-mode operation is also conceivable. However, the agreement between COMSAT GENERAL and AT&T specifies the transmission objectives for the 1,200-channel FDM/FM single-carrier-per-transponder case only.



of ambiguity. In practice, this synchronous altitude. The re- dential to that of the INTELSAT

nas for transmission of telem- s through the contiguous U.S. nd circularly polarized z-axis o the spin axis of the spacecraft aft attitudes. The omni antenna am to be used during transfer cy in synchronous orbit. The toroidal beam, dual-mode, bi- ndicular to the spin axis.

ie COMSTAR satellite system are oice channels, typically 1,200 .4,400 two-way voice circuits. WOp for any voice channel ing interference noise from

Alaska, Hawaii, and Puerto

capacities will be used during

ons subsystem block diagram. re 13, and the communications 5. The service quality indicated ssions to the contiguous U.S., nbined coverage of Alaska and " the noise in the worst voice rese performance specifications earth station whose character-

in either the TDMA or the FDMA is also conceivable. However, the r specifies the transmission objec- rier-per-transponder case only.

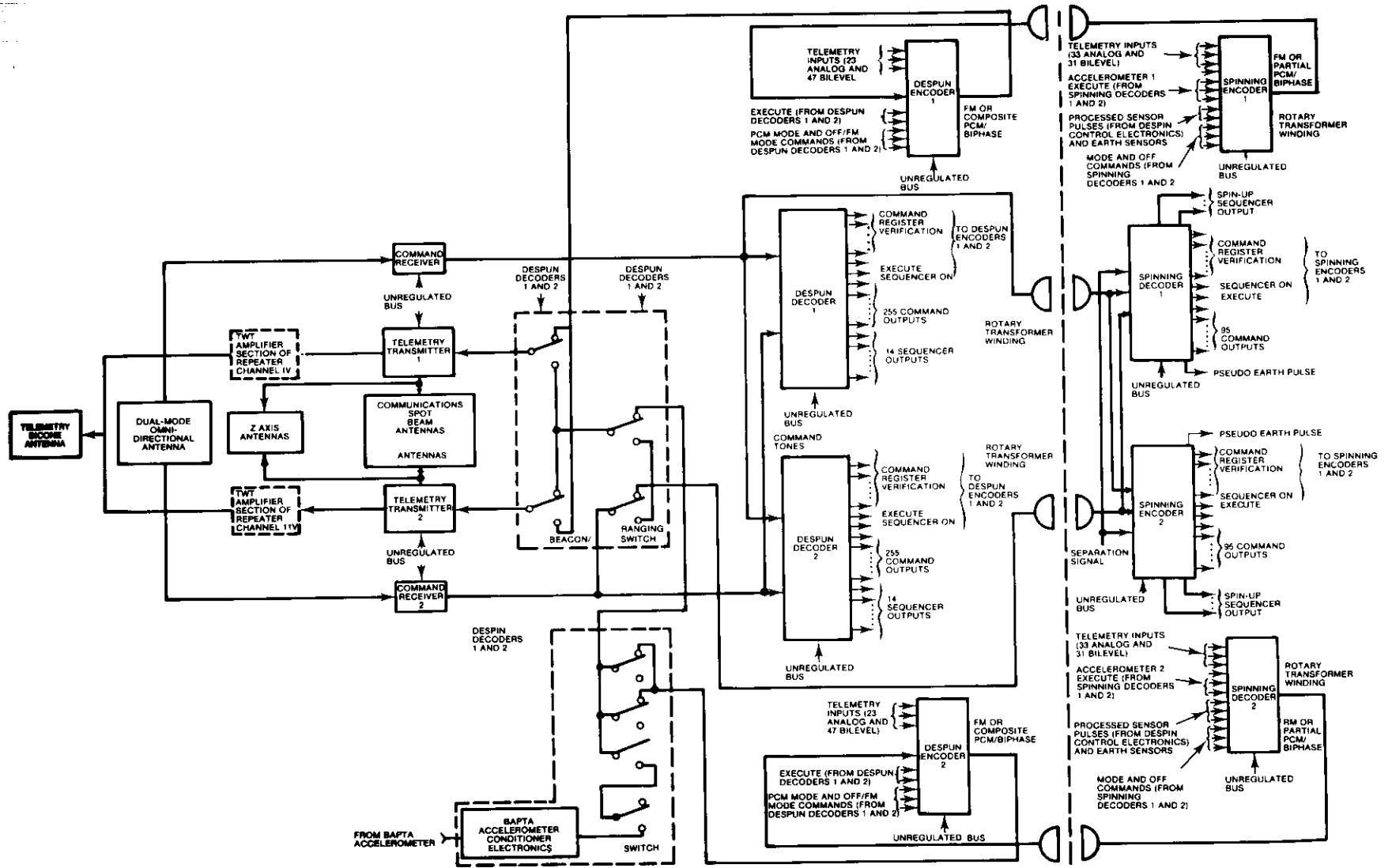


Figure 11. Telemetry, Tracking, and Command Subsystem





TABLE 5. COMMUNICATIONS SUBSYSTEM SPECIFICATIONS (continued)

Receiver Intelligible Crosstalk	$-194 + 20 \log f$ dB ( $f$ = modulating frequency, Hz)
Receiver Intermodulation, 2 Carriers	
Each	
-64.9 dBW/m <sup>2</sup>	C/I = 43 dB
-74.9 dBW/m <sup>2</sup>	C/I = 63 dB
Cross-polarization Discrimination (minimum)	
Contiguous U.S., Hawaii, Alaska, and Puerto Rico	33 dB
Combined Coverage of Contiguous U.S. and Alaska	31 dB
Translation Frequency Tolerance	
1 Month	$\pm 1 \times 10^{-6}$
Lifetime	$\pm 1 \times 10^{-5}$

TABLE 6. SYSTEM COMMUNICATIONS PARAMETERS AND NOISE BUDGET FOR WORST VOICE CHANNEL IN THE 1,200-CHANNEL-PER-CARRIER TRANSMISSION

a. Communications Parameters		
	Specification (edge of coverage)	Measurement (typical) <sup>a</sup>
Satellite G/T (dB/K)	-8.8	-4.5
Saturation Flux Density (dBW/m <sup>2</sup> )	-72.7	-76.1
Satellite e.i.r.p. (dBW)	33	36
Earth Station G/T (dB/K)	41.2	41.8
b. Voice Channel Noise Budget Noise Level (pW0p)		
	Specification (edge of coverage)	Measurement (typical) <sup>a</sup>
Thermal Noise (operating with reference earth station)		
Up-Link	925	720
Down-Link	2,070	927
Intermodulation (satellite receiver)	830	420
Interstitial Interference (satellite and earth station)	160	50
Group Delay/Gain Slope (satellite communications subsystem)	250	70
Total Noise	4,235 <sup>b</sup>	2,187

<sup>a</sup> Transmissions between Three Peaks, California, and Hawley, Pennsylvania.

<sup>b</sup> The AT&T agreement specified an overall noise performance objective of 4,800 pW0p.

The communications subsystem utilizes the 500-MHz bandwidth allocated for fixed satellite communications in the 4- and 6-GHz band. The frequency and polarization plan for the system is shown in Figure 14. Frequency reuse is achieved by virtue of orthogonal linearly polarized beams. The antenna design is capable of maintaining orthogonal linearly polarized signals with cross-polarization isolation of the order of 33 dB for both the up- and down-link over the entire coverage area. The frequency spectrum is divided into 24 RF channels (transponders), 12 vertically polarized and 12 horizontally polarized. Each transponder is 34 MHz wide and the channels of the same polarization are spaced at 40-MHz intervals. The horizontal and vertical transponders are centered on frequencies that are 20 MHz apart (*i.e.*, frequency interleaved) to minimize the amount of interference between orthogonally polarized signals. Signals received by the satellite are translated in frequency by 2,225 MHz and transmitted with the same polarization with which they were received.

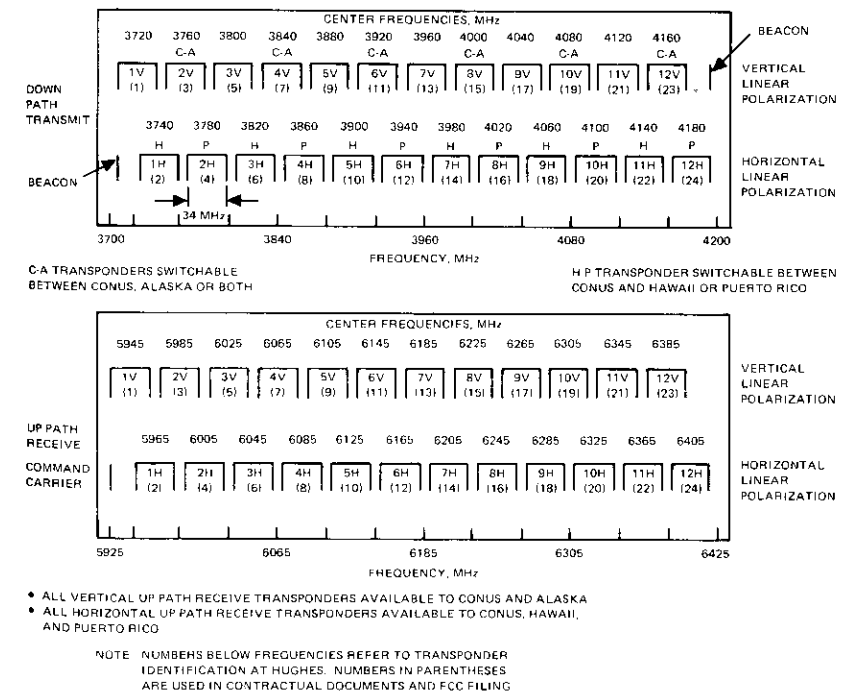


Figure 14. Frequency and Polarization Plan

Vertically polarized channels serve the contiguous U.S. and Alaska; horizontally polarized channels serve the contiguous U.S., Hawaii, and Puerto Rico.

On the down-link, odd-numbered horizontally polarized channels can be switched into either the contiguous U.S. or Hawaii spot beams. Even-numbered horizontally polarized channels can be switched into either the contiguous U.S. or Puerto Rico spot beams. Even-numbered vertically polarized channels can be switched in one of three ways: all power to the contiguous U.S., all power to Alaska, or power divided between Alaska and the contiguous U.S. (combined service mode). Odd-numbered vertically polarized channels serve the contiguous U.S. only.

The receive sensitivity of each of the 24 transponders can be adjusted separately through ground commands which activate switches to insert 6- and 9-dB attenuators in front of the high-level TWTs. Four receive sensitivity levels are obtainable; transmission performance can thus be optimized for the various service modes. The following subsections describe the major units of the communications subsystem.

#### ANTENNAS

The communications antenna assembly consists of two orthogonally polarized, offset, parabolic reflector antennas which receive at 6 GHz and transmit at 4 GHz over a 500-MHz bandwidth. The reflectors, which measure  $1.27 \times 1.78$  m ( $50 \times 70$  in.), have F/D ratios of 0.25. The antennas provide the following performance:

receive gain: 24.5 dBi  
 transmit gain: 27.0 dBi (horizontal polarization)  
                   26.5 dBi (vertical polarization)

cross-polarization isolation: 33 dB (31 dB for T-mode)

Each of the vertical and horizontal polarization feed assemblies consists of a multihorn offset feed array\* and separate feed networks for reception and transmission. These feed horns are configured in conjunction with the reflector to produce shaped spot-beam patterns. Phasing and combining networks of the input/output ports of the feeds ensure that the overlapping portions of the spot beams will combine to provide the required beam coverage.

\*For each polarization the same feed horns are used for transmission and reception.

Due to the feed assembly arrangement, the contiguous U.S. vertical horn array illuminates the reflector less efficiently than the horizontal array. As a result, the vertically polarized antenna provides lower gain over the specified area. Therefore, TWTs used for the vertical channels have slightly higher output power, yielding the same e.i.r.p. for both polarizations.

The reflective surface consists of a fine wire mesh made of gold-plated nickel-chromium alloy woven into a flexible cloth. This configuration permits transparency to photons required to reduce solar radiation pressure which causes attitude drift. Polarization screens made of horizontally and vertically strung parallel conductive strips for vertical and horizontal polarizations, respectively, are mounted in front of the reflectors to reduce the cross-polarized components\* and thereby enhance the antenna polarization purity. The strips, approximately 2.54 cm wide with a spacing of 1.27 cm, are made of fiberglass-reinforced aluminized Kapton held in tension by a spring mechanism at the frame attach points. They are stabilized by fiberglass strings running perpendicular to them. Wanted (*i.e.*, copolarized) signals from the reflector propagate edgewise through the strips. The strips act as a waveguide below cutoff for the cross-polarized components and thereby inhibit these propagations through the screen. Figure 15 shows the polarization screen design.

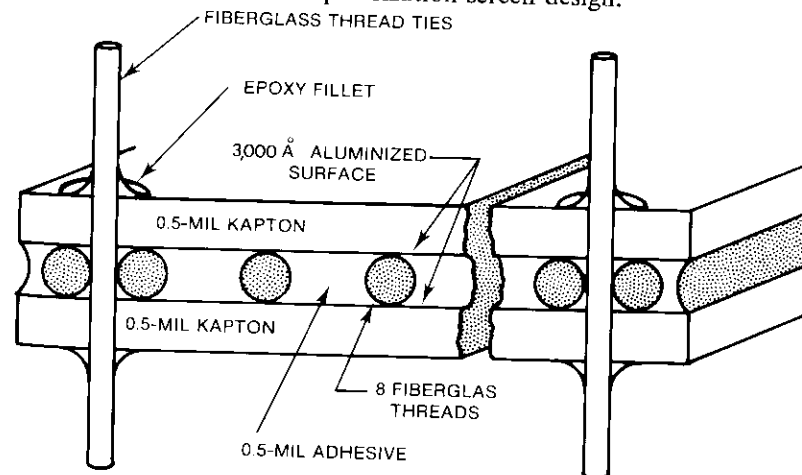


Figure 15. Polarization Screen Design

\*These components are produced by the parabolic reflector curvature, blockage, feed component non-orthogonality, etc.

During the satellite design phase, the wire grid polarization screens were rejected because the best practical wire grid screen would not provide adequate cross-polarization rejection without excessive aperture blockage of the wanted polarization.

#### COMMUNICATIONS RECEIVER

The communications subsystem contains four receivers with associated input and output switches. The switches permit vertically and horizontally polarized received signals to be routed through any two of the four receivers. Vertically or horizontally polarized signals can thus be transmitted through any of three of the four receivers, resulting in augmented system reliability. Figure 16 is a block diagram of the receiver whose performance

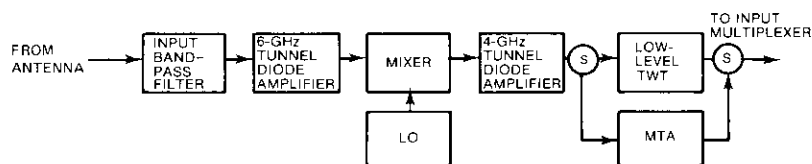


Figure 16. Receiver Block Diagram

characteristics are indicated in Table 7. Signals in the 6-GHz band (5,925 to 6,425 MHz) are translated via a single conversion process to the 4-GHz band (3,700 to 4,200 MHz).

TABLE 7. MAJOR RECEIVER PERFORMANCE CHARACTERISTICS

	Specification	Measurement (typical)
Usable Bandwidth	500 MHz	500 MHz
Noise Figure		
TWTA Mode	—	8 dB*
MTA Mode	—	7 dB*
2-Carrier Third-Order Intermodulation (each carrier at $-64.9$ dBW/m <sup>2</sup> )	43 dB	>43 dB
Intelligible Crosstalk at Top Baseband of 1,200-Channel Carrier	59 dB	75 dB
Receiver Gain	—	$\cong 55$ dB

\* These measured noise figures in conjunction with the receive antenna gain give a G/T better than  $-8.8$  dB.

To augment reliability, a microwave transistor amplifier (MTA) incorporated in each receiver can replace the low-level driver traveling wave tube (TWT) at any time by ground command. When the MTA is used, the receiver sensitivity is approximately 9 dB lower than that which can be achieved when the TWT is used.

#### INPUT MULTIPLEXER

The input multiplexer assembly consists of four 6-channel networks which are used for the even- and odd-numbered horizontal and vertical channels. Figure 17 shows a typical input multiplexer network. Each

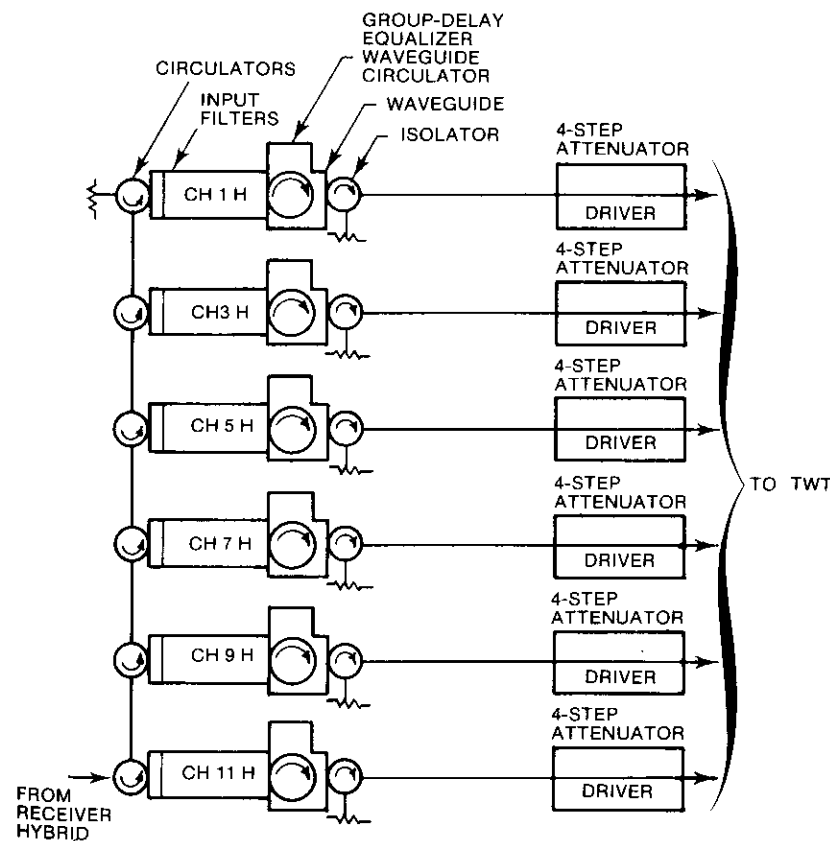


Figure 17. Input Multiplexer

network consists of six 8-section Chebychev bandpass waveguide filters. The output of each filter is coupled to a 2-section reactively terminated group-delay equalizer. All the multiplexer filters and delay equalizers are fabricated from Invar to minimize performance variations with temperature changes.

The filter and delay equalizer assembly is followed by a 4-position switch attenuator which can be commanded to change the gain of the transmission channel. The 4-position attenuator consists of two latching-type circulator switches, with one port of each circulator terminated in a resistive mismatch. The mismatch is such that the return loss from each of the two terminated circulators is 6 and 9 dB, respectively. This arrangement is capable of providing attenuation values of 0, 6, 9, and 15 dB.

The gain slope and out-of-band response of the input multiplexer are given in Table 8. The group-delay specification of the input multiplexer is shown in Figure 18.

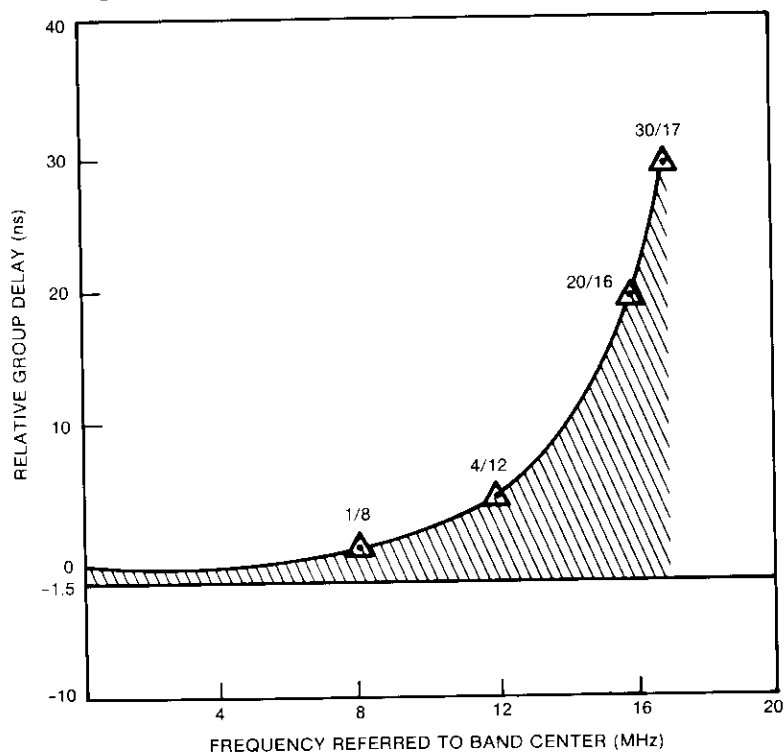


Figure 18. *Input Multiplexer Group-Delay Specifications*

TABLE 8. INPUT MULTIPLEXER GAIN SLOPE AND OUT-OF-BAND RESPONSE

	Specification	Measurement (typical)
	Gain Slope	
Band Center $\pm$ 10 MHz	0.08 dB/MHz	0.04 dB/MHz
Band Center $\pm$ 12 MHz	0.13 dB/MHz	0.05 dB/MHz
Band Center $\pm$ 14 MHz	0.2 dB/MHz	0.06 dB/MHz
Band Center $\pm$ 16 MHz	0.3 dB/MHz	0.06 dB/MHz
	Out-of-Band Response	
Band Center $\pm$ 23 MHz	-15 dB	-15 dB
Band Center $\pm$ 29 MHz	-38 dB	-45 dB
Band Center $\pm$ 40 MHz	-50 dB	

#### HIGH-LEVEL TWT

Twenty-four TWTs are utilized for amplifying the 4-GHz signals. The TWTs used for the horizontal channels have saturated output power levels of 5 W, while those for the vertical channels have saturated output power levels of 5.5 W. Performance characteristics of the high-level TWTs are given in Table 9.

TABLE 9. MAJOR HIGH-LEVEL TWT PERFORMANCE CHARACTERISTICS

	Specification	Measurement
RF Power Output		
275HA TWT		5 W
277H TWT		5.5 W
2-Carrier Third-Order Intermodulation at 10-dB Input Backoff	16 dB	16.5 dB
AM/PM Transfer Coefficients at Saturation	4°/dB	2.5°/dB
Gain (275HA and 277H)	—	$\approx$ 55 dB

#### OUTPUT MULTIPLEXER

The output multiplexer assembly includes all the circuitry from the high-level TWT outputs to the inputs of the transmit antennas. The multiplexer assembly itself includes four output multiplexer networks, each designed to perform a 6-channel summing, and operates with minimum in-band insertion loss. Specified values of the out-of-band response of the

output multiplexer with reference to band center are  $-4$  dB at  $\pm 29$  MHz,  $-15$  dB at  $\pm 40$  MHz, and  $-30$  dB at  $\pm 63$  MHz. The total group-delay specification (including both input and output multiplexers) is shown in Figure 19. Figure 20 shows a typical measurement of the total group delay of the transponder. With this remaining level of group delay, the impact of required group-delay equalization at the earth station is minimized.

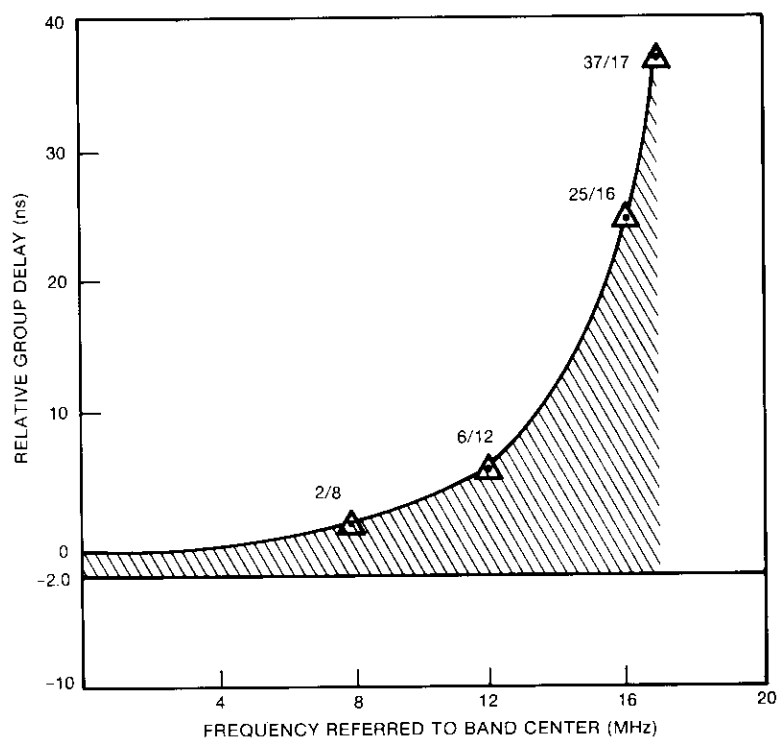


Figure 19. Total Transponder Group Delay

The bandpass directional filters are 4-section Chebychev waveguide filters fabricated from thin wall Invar. Switches are used in conjunction with output filters to provide signal routing to various beams.

Signals from the output manifolds are routed to the antenna transmit feed networks. Harmonic filters and test couplers are included in these waveguide runs.

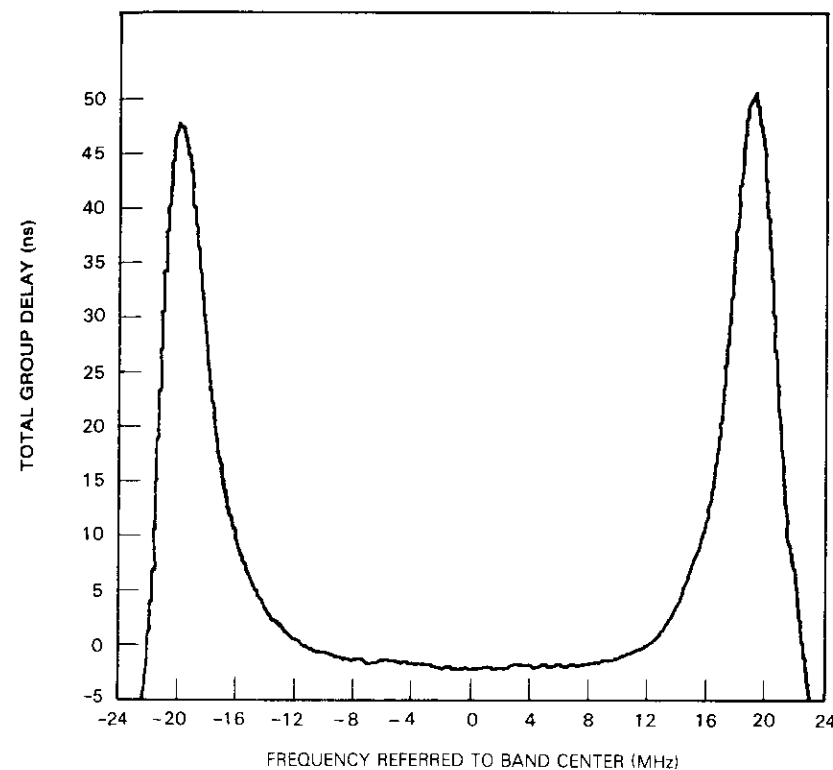


Figure 20. Measured Total Group Delay

### Earth station performance and configuration

The agreement between COMSAT GENERAL Corporation and AT&T states that, to achieve the transmission performance objectives specified for the system, the AT&T earth stations should at least meet the requirements of the reference earth station defined in the agreement. Table 10 gives the performance of the reference earth station as required by the agreement with AT&T. When such earth stations are utilized, the agreement requires that, within the specified service areas, each transponder must be capable of meeting the transmission performance objectives for a transponder capacity of 1,200 high-quality 4-kHz voice-grade channels or a 44.7-Mbps digital data stream.

TABLE 10. REFERENCE EARTH STATION PERFORMANCE<sup>a</sup>

	Transmit
Frequency	5,925–6,425 MHz
Illumination	Properly illuminated for the service area involved
Frequency Stability	1 ppm
Group Delay	Nominal delay distortion of the satellite transponder equalized by delay equalizer <sup>b</sup>
Gain Slope (transmit direction)	0.02 dB/10 MHz over the center 30 MHz
Polarization Isolation (including Faraday rotation and misalignment)	–35 dB
Modulation	1,200 channels or equivalent noise loading with rms modulation index of 0.49, $f_{max}$ of 5.772 MHz, peak modulation index of 1.96, CCIR pre-emphasis, and psophometric weighting
	Receive
Frequency	3,700–4,200 MHz
G/T	41.2 dB relative to 1 K <sup>c</sup>
Polarization Isolation (including Faraday rotation and misalignment)	–35 dB

<sup>a</sup> The earth station will be capable of meeting the indicated parameters in the direction of the satellite.

<sup>b</sup> The reference earth station will be equipped with a delay equalizer. This equalizer shall equalize the nominal delay distortion of the satellite transponder (exclusive of ripple). The nominal group delay shall be equalized to give a residual ripple not to exceed 1 ns peak to peak over the center 20 MHz and 2 ns peak to peak over the center 30 MHz. The ripple period shall not be less than 10 MHz over the center 30 MHz.

<sup>c</sup> This includes both the 7-K noise contribution due to atmospheric absorption and the total receive earth station noise at an antenna elevation angle of 20°.

AT&T presently has four earth stations located at Hawley, Pennsylvania; Three Peaks, California; Hanover, Illinois; and Woodbury, Georgia. The GTE Satellite Corporation, which uses the COMSTAR satellite jointly with AT&T, presently has three earth stations (not described in this paper) located at Sunset, Hawaii; Triunfo Pass, California; and Homosassa, Florida. The AT&T earth station antenna reflector has a diameter of 30 m (98.5 ft). Table 11 gives the specified communications parameters for the earth stations.

The antenna feed subsystem is designed to provide simultaneous reception of two orthogonal linearly polarized signals in the 3.7- to 4.2-GHz band and simultaneous transmission of two orthogonal linearly polarized

TABLE 11. AT&amp;T SPECIFIED EARTH STATION COMMUNICATIONS PARAMETERS

G/T	41.2 dB/K for antenna elevation angle of 20° (includes 7-K atmospheric absorption)
Transmit Net Antenna Gain	≥62.8 dB referred to the input of the feed diplexing and polarization control networks (3-dB beamwidth = 0.12°)
Receive Net Antenna Gain	≥60.4 dB referred to the receiving amplifier input (3-dB beamwidth = 0.18°)
HPA Saturation	3 kW (64.75 dBm)
Transmit Amplitude Response	Gain slope < 0.02 dB/MHz in center 30 MHz of any channel
Transmit Group-Delay Response	
Over Center 20 MHz	1 ns peak to peak
Over Center 30 MHz	2 ns peak to peak (ripple period > 10 MHz)
Receive Group-Delay Response	1 ns peak to peak over ±10 MHz
Transmit Polarization Isolation	–35 dB
Receive Polarization Isolation	–35 dB
LNA Saturation	<0.5-dB gain compression for an input signal level up to –60 dBm (average gain = 60 dB)
LNA Amplitude Linearity	Intermodulation products down >53 dB with two equal-input carriers each at an input level of –64 dBm
LNA Phase Linearity (delay)	
Linear	0.1 ns/MHz
Parabolic	0.03 ns/MHz <sup>2</sup>
Ripple	0.5 ns peak to peak per 40 MHz
Frequency Stability	1 ppm

signals in the 5.925- to 6.425-GHz band. The typical cross-polarization isolation measured at AT&T's earth stations is about 40 dB, well above the design objective of 35 dB. The antenna tracking and control system, which uses the step track technique, maintains the required pointing of the main beam steering axis (azimuth and elevation). Since diurnal variations of Faraday rotation are of sufficient magnitude to cause significant degradation in polarization isolation, polarization tracking for both the receive and transmit polarization angles is also included. Figure 21 shows both pointing and polarization tracking mechanisms. The polarization angle tracking is controlled by a proportional control servomechanism analogous to one axis of an antenna monopulse angle tracking system. The polariza-

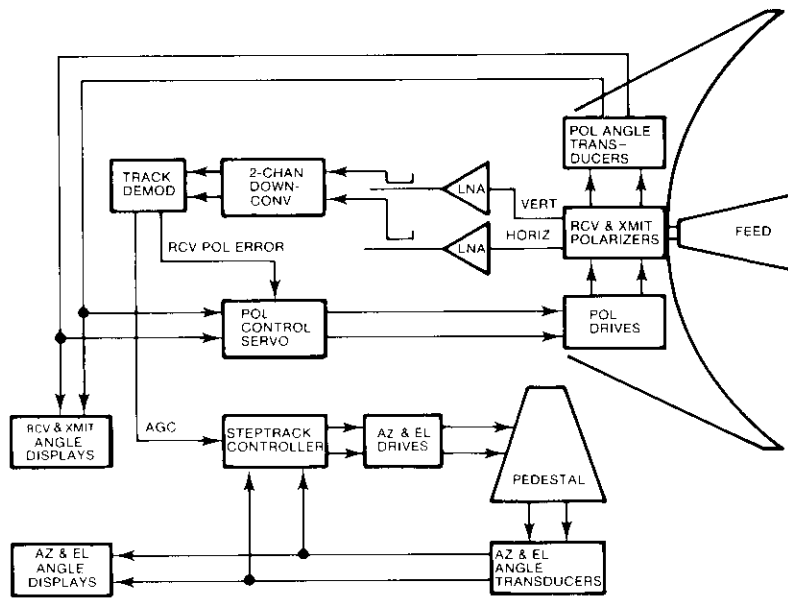


Figure 21. Earth Station Tracking and Control Systems

tion tracking system will track either the vertically polarized COMSTAR Beacon (4.2 GHz) or the horizontally polarized Beacon (3.7 GHz).

The earth station ground communications equipment (GCE), which handles all communications processing between the terrestrial link and the satellite, consists of the transmit and receive GCE shown in Figures 22 and 23, respectively. No baseband multiplexing equipment is included at any of the AT&T earth stations. The incoming and outgoing baseband signals are passed through without reassembly. The transmit GCE includes a deviation converter, up-link equalizers, up-converter, high-power amplifier (HPA), transmit equipment switching, RF combining network, and transmit waveguide system. The deviation converter consists of a frequency demodulator followed by a frequency modulator to change the 0.78-MHz rms frequency deviation used on the terrestrial link for 1,200 channels to the 2.8-MHz rms frequency deviation used on the satellite link. The up-link equalizers compensate for the group delay of the HPAs and satellite input filters, and any cumulative group-delay or amplitude distortion of the transmit GCE.

The receive GCE includes a low-noise amplifier (LNA), receive waveguide

system, RF dividing network, down-converter, down-link equalizer, deviation converter, and receive equipment switching. The down-link equalizers equalize the group delay of the satellite output filters and any cumulative group delay or amplitude distortion in the receive GCE.

The earth stations are provided with power switching capability so that the traffic can be transferred from one antenna to another (for example, during sun transit periods) with minimum outage.

### Transmission analysis and system performance

Analytical system modeling and actual laboratory simulation have been performed to verify that the COMSTAR satellite system design is optimized to meet the performance objectives for up- and down-link thermal noise, satellite receiver intermodulation, adjacent (overlapping) channel interference in both up- and down-links, multipath transmission noise, and noise from group-delay ripple and gain slope in the satellite and earth station.

#### Selection of optimum transponder gain step for the 1,200-channel carrier transmission

The carrier-to-intermodulation (C/I) ratio specified for the satellite receiver is 43 dB when the satellite is illuminated by two carriers each at a level of  $-64.9$  dBW/m<sup>2</sup>. When the receiver is accessed by 12 equal carriers, this corresponds to a top baseband channel noise of approximately 800 pW0p for the 1,200-channel FDM/FM carrier located in the center of the 500-MHz band. At this input level the receiver can be considered to be operating in a mode which is approximately linear (*i.e.*, a 1-dB change in input level results in a 2-dB change in the intermodulation noise level).

The up-link\* and receiver intermodulation noise are plotted in Figure 24 vs the up-link saturation flux density at the satellite receive antenna. The sum of the two values shows that the optimum saturation flux density lies in the region of  $-73$  to  $-75$  dBW/m<sup>2</sup>.

#### Worst carrier-to-intermodulation ratio for any 1,200-channel carrier due to the satellite wideband receiver

The agreement with AT&T requires that the C/I ratio shall be greater than 36 dB in any channel when 12 carriers, each at a level of  $-72.7$

\*A satellite G/T of  $-8.8$  dB/K (manufacturer's specification) has been used for calculating the up-link noise.

dBW/m<sup>2</sup>, illuminate the satellite. The manufacturer's specifications for the satellite are based on a C/I ratio of 43 dB when two carriers, each at a level of -64.9 dBW/m<sup>2</sup>, illuminate the satellite. The total C/I in transponders 6 and 7 (for 12 carriers illuminating the satellite) is 36.6 dB when the manufacturer's specifications are met. Figure 25 shows the intermodulation noise power spectrum within the 500-MHz bandwidth of the receiver when twelve 1,200-channel FDM/FM carriers, each at a level of -72.7 dBW/m<sup>2</sup>, are transmitted through the receiver.

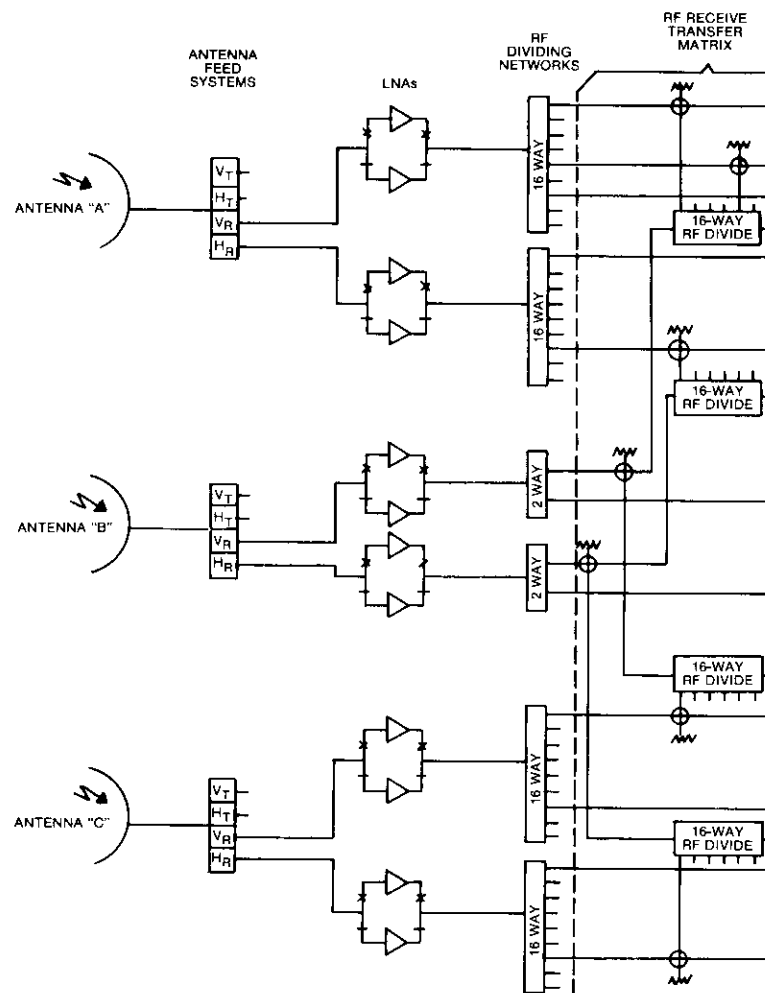
#### Worst channel within the baseband of a 1,200-channel carrier due to all thermal and receive intermodulation noise

The effect of the satellite receiver intermodulation on the performance of the voice channel in a 1,200-channel FDM/FM carrier varies with the location of the voice channel within the baseband. For example, the noise level in the top baseband channel is about 800 pW0p, while that in a channel located at a baseband frequency that is 0.6 of the top baseband frequency is about 1,000 pW0p. With respect to thermal noise on FM carriers, the top baseband channel is the worst. The sum of channel thermal noise plus intermodulation noise is plotted in Figure 26, which indicates that the worst channel is located at a frequency which is about 0.7 of the top baseband frequency. Since the sum curve is approximately flat in the top portion of the baseband, the top baseband channel can still be considered to be the worst channel; hence, all previous noise breakdown budgets have been given for the top baseband channel.

#### Multipath effect for adjacent transponders

The effects of multipath on transponder gain and group delay were calculated for different relative gains of adjacent transponders. Figures 27 and 28 give an example of the gain and group-delay changes resulting from the multipath effect for relative adjacent transponder gains of 6 dB and relative phase differences from 0° to 360° in steps of 45°. With the intrinsic group-delay response equalized, the channel noise resulting from multipath under these changes was found to be negligible for the 1,200-channel transmission case. However, as the channel capacity is increased, the effect of multipath will result in increased intermodulation noise.

\*This may be caused by different levels of the transmitted carriers, different transponder gain settings, or compression of small signals, and different signal path lengths through the wanted and adjacent transponders.



NOTE  
1. THIS FACILITY MAY INCLUDE AN IF ENTRANCE CABLE.

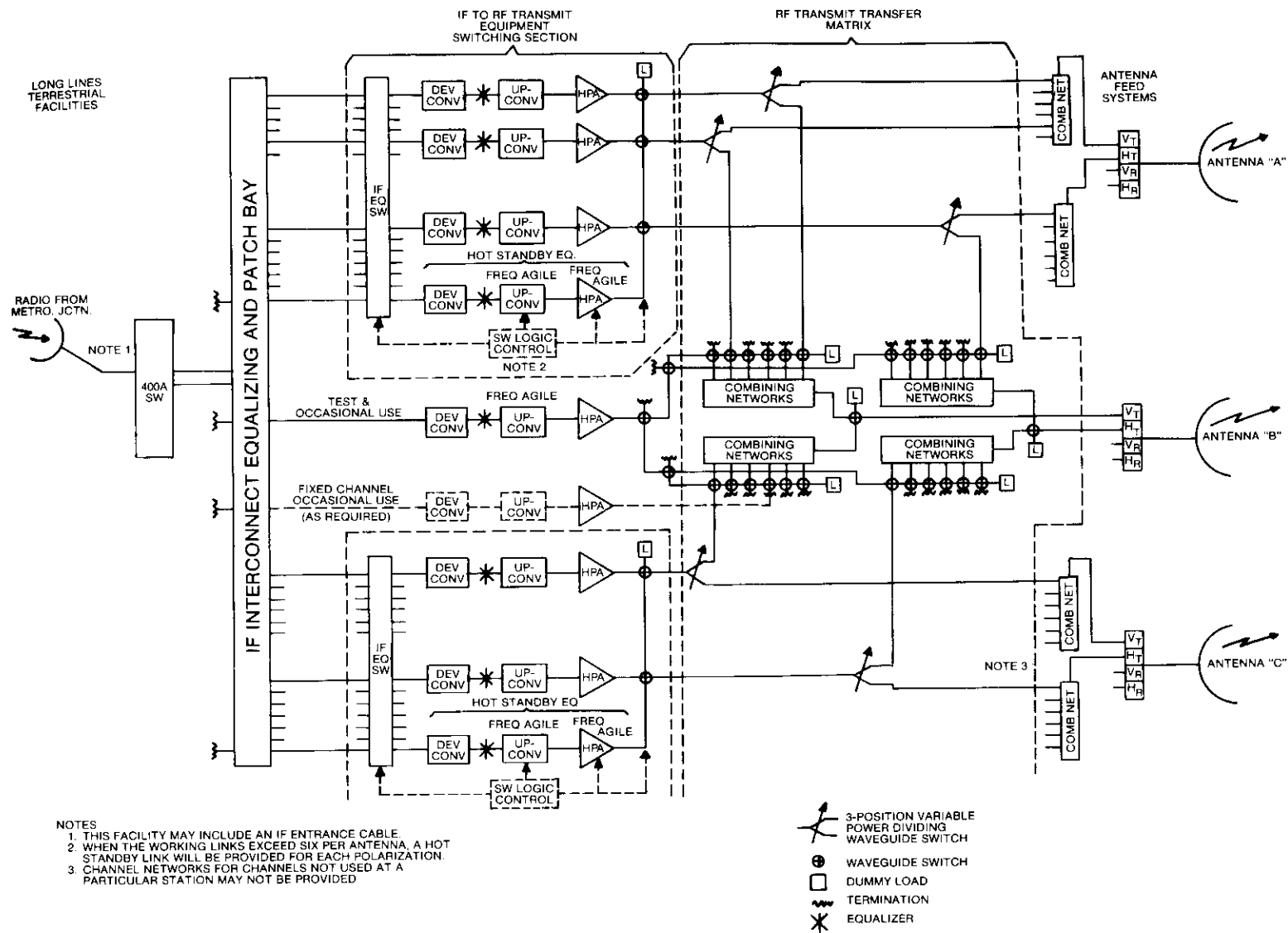


Figure 22. Transmit GCE

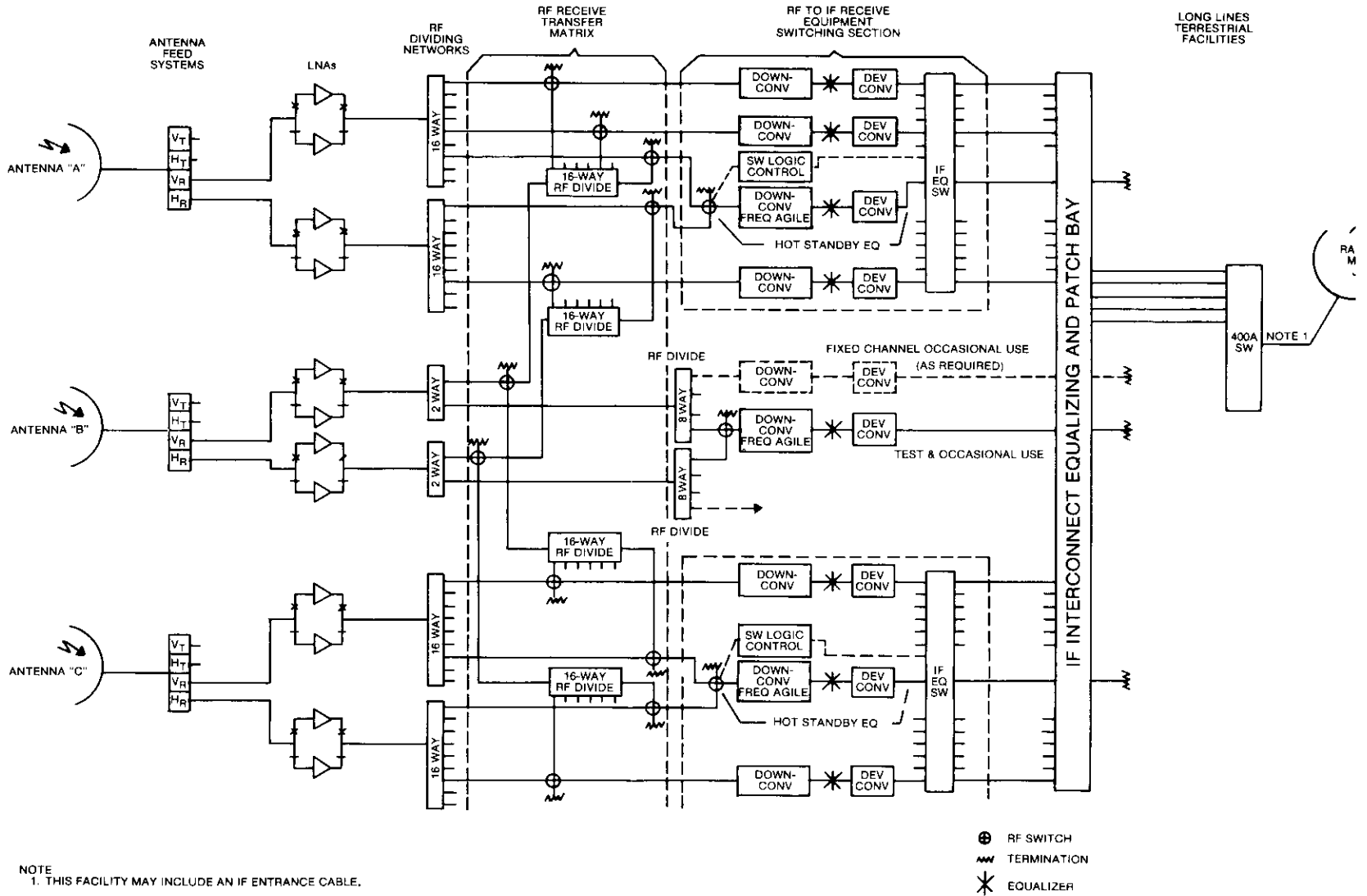


Figure 23. Receive GCE

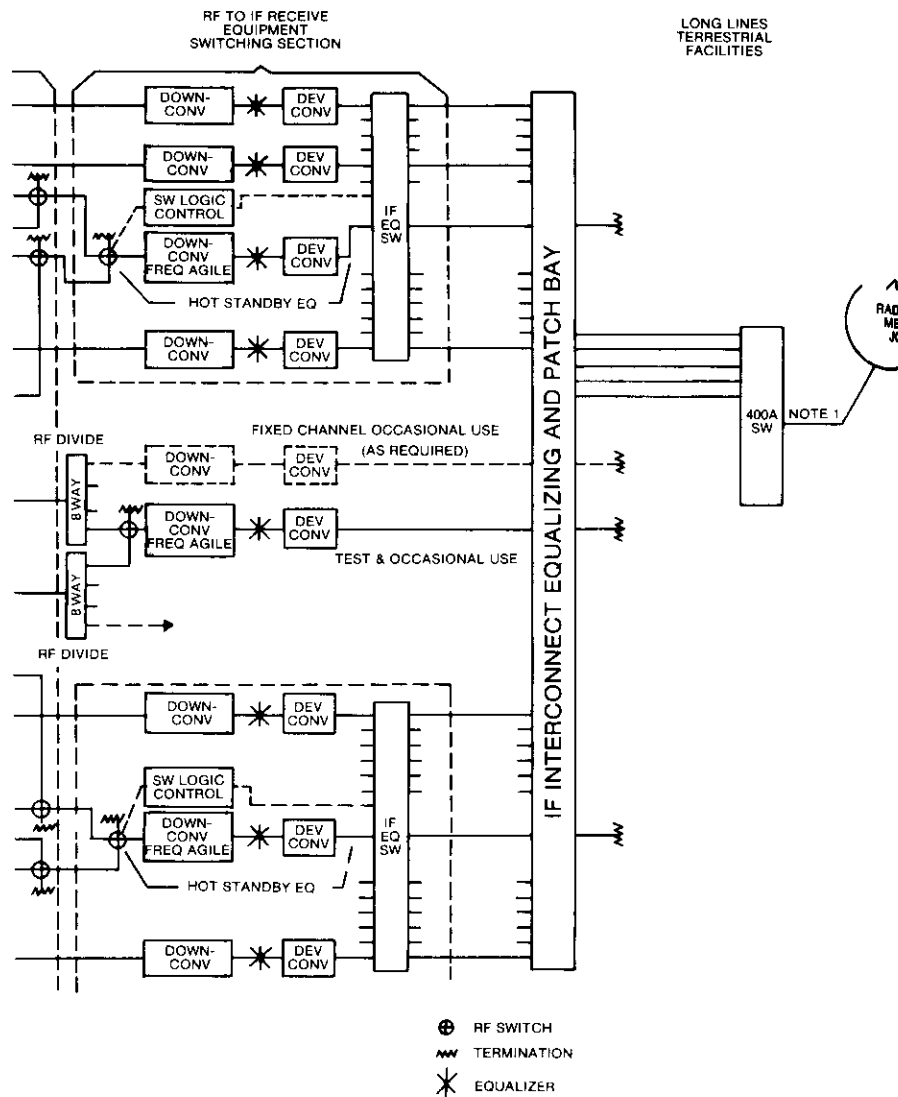


Figure 23. Receive GCE

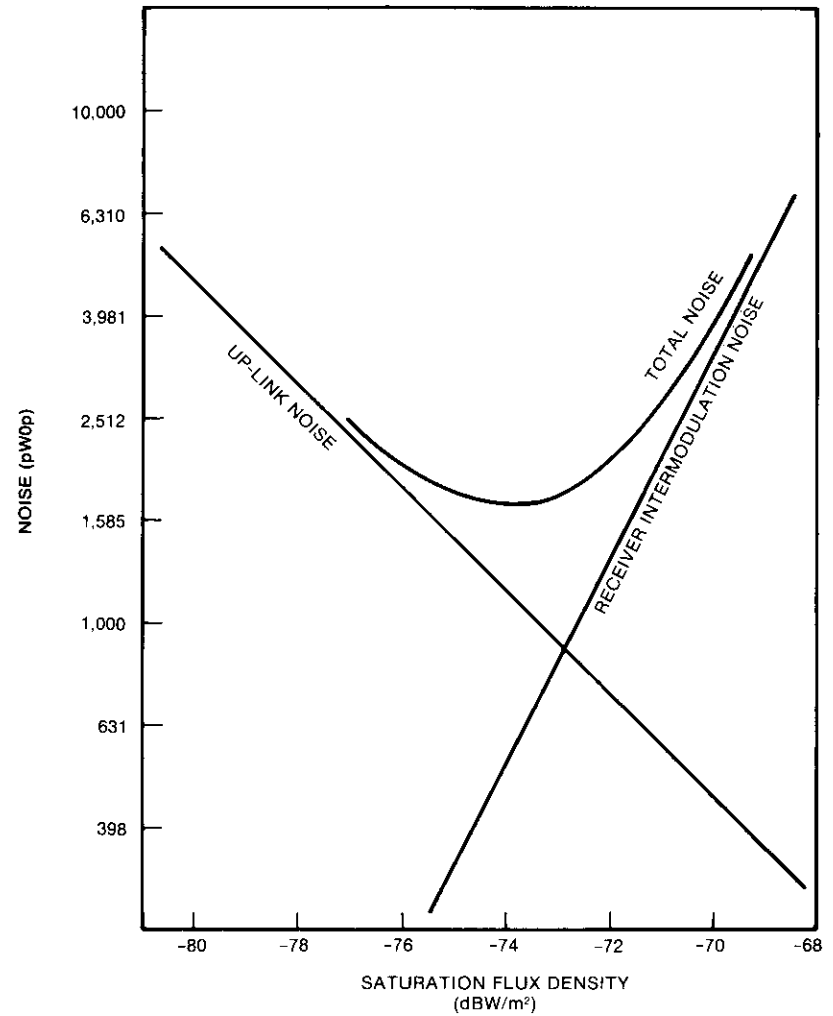


Figure 24. Up-Link and Receiver Intermodulation Noise

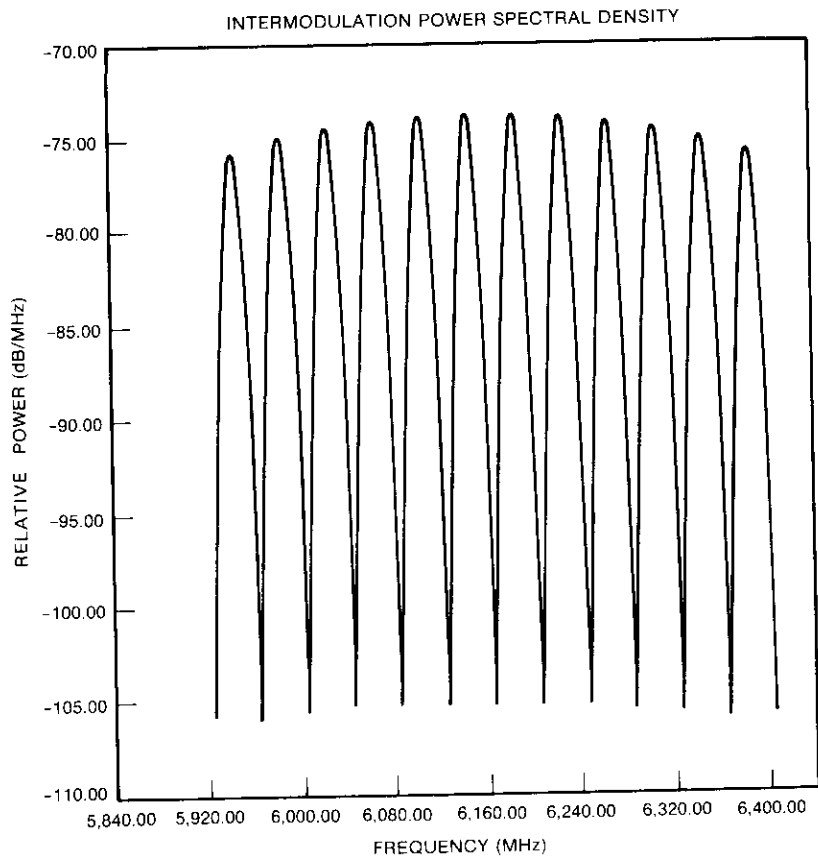


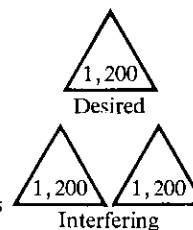
Figure 25. Intermodulation Noise Power Spectrum

**Interference noise due to the interstitial transponder**

Interference noise due to the cross-polarized interstitial RF channels was calculated as less than 200 pW0p. Table 12 shows the details of the calculation and the final results for the case in which a 1,200-channel FDM/FM carrier is transmitted in each of the interfering and interfered with transponders.

TABLE 12. INTERSTITIAL INTERFERENCE <sup>a</sup>  
(Reference Earth Station/Satellite Specification) <sup>b</sup>

Up-Link			Down-Link			Total C/I	NPR with One Carrier Interfering, C/I = 0 dB (K factor)	Interstitial Interference with Two Carriers Interfering (pW0p)
C/I <sub>es</sub>	C/I <sub>sat</sub>	C/I <sub>top</sub>	C/I <sub>es</sub>	C/I <sub>sat</sub>	C/I <sub>down</sub>			
35 <sup>c</sup>	33	27.9	35 <sup>c</sup>	33	27.9	24.9	26.5	165



<sup>c</sup> The carrier arrangement is

The normalized carrier separation,  $f_s/f_{top}$ , is 3.47 and the level difference is 0 dB.

<sup>b</sup> The actual C/I achieved due to cross polarization was substantially better than the specification values shown in the table.

<sup>c</sup> Includes Faraday rotation and misalignment.

**Noise impairment due to antenna subreflector echo**

Earth station antenna subreflector echo, which had been noticed in other satellite systems, is caused by the part of the transmitted energy which is reflected back from the subreflector into the feed horn. This undesired reflection can be further divided into a component that propagates along the feed and waveguide of the earth station and another component that is reflected once again toward the subreflector along with the desired signal. Noise resulting from this phenomenon was measured using the 12.8-m (42-ft) full-performance antenna at the COMSAT GENERAL earth station at Santa Paula. A fault locator (Scientific Atlanta model 1691) was used for measuring the return loss of the test setup. Figure 29 shows the subreflector echo test setup.

The noise due to the subreflector echo was measured to be about 200 pW0p in the top baseband of a 1,200-channel FDM/FM carrier. AT&T, having recognized this problem, implemented "spoiler" plates, which minimize the reflected energy to the feed horn from the subreflector, thereby reducing the noise to a negligible level.

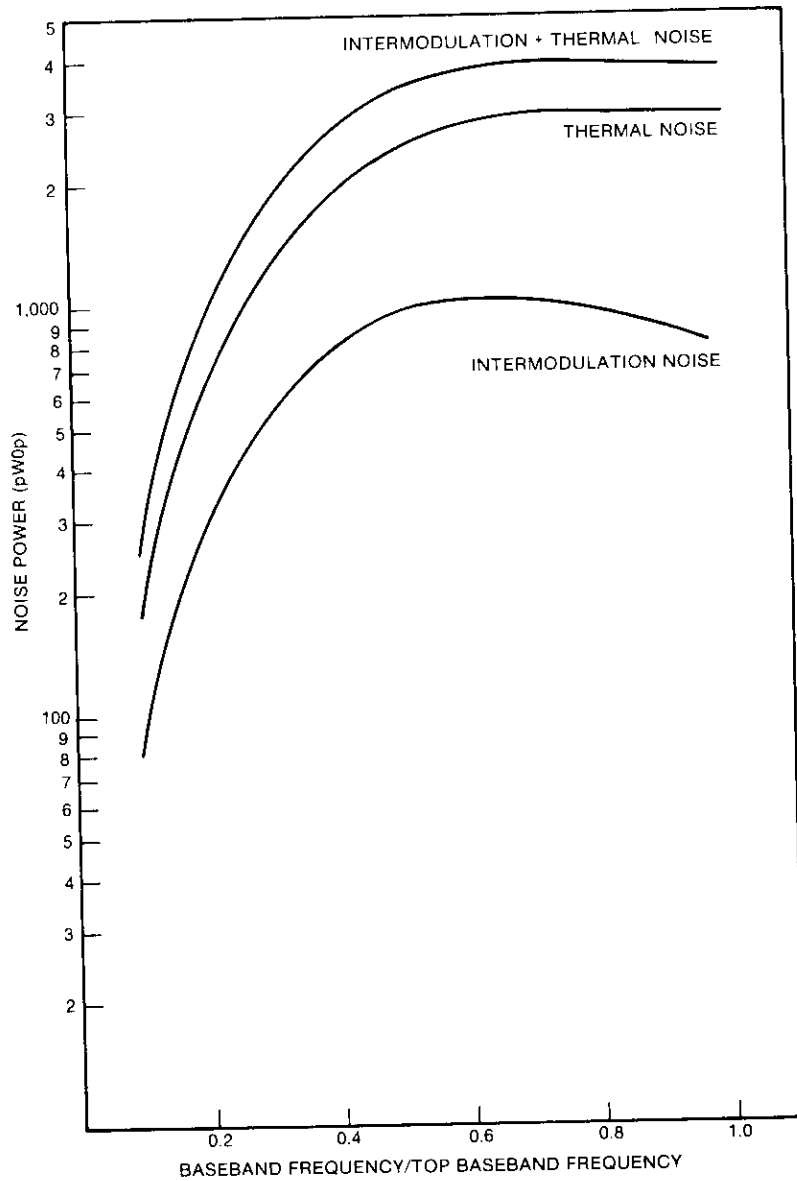


Figure 26. Thermal Noise and Receiver Intermodulation Noise vs Normalized Baseband Slot

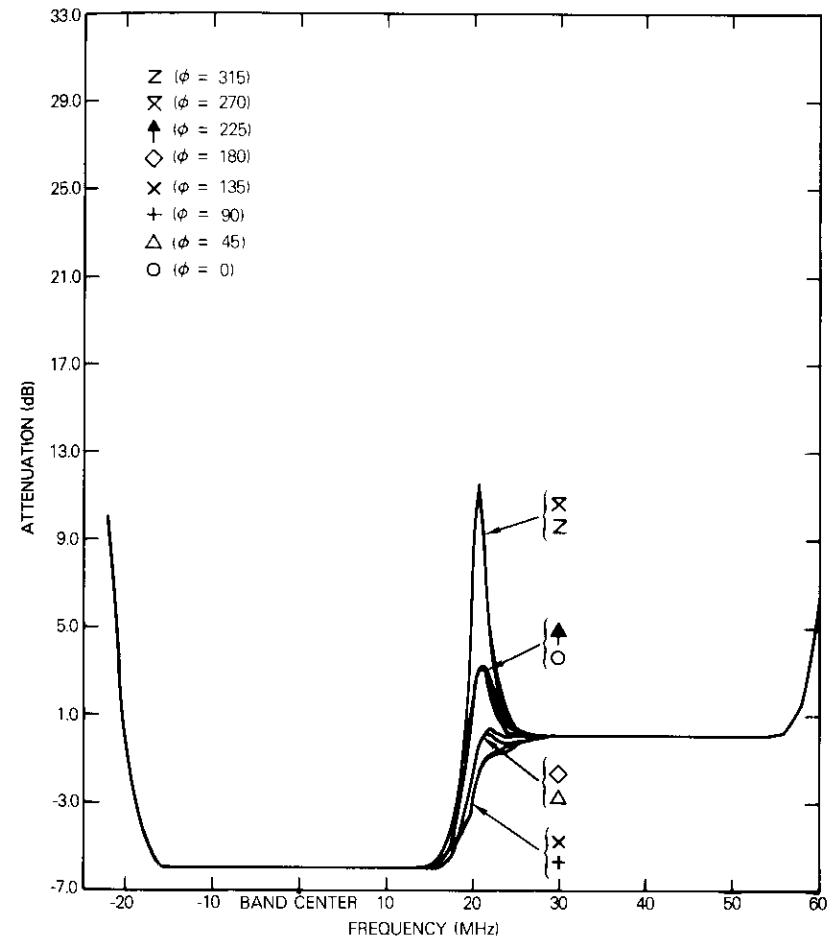


Figure 27. Attenuation vs Frequency

#### Measurements of communications parameters

Communications parameters of the COMSTAR satellites measured in the prelaunch tests at the manufacturer's plant showed that the communications system performance exceeds the specifications. During in-orbit tests [4] at Paumalu, Hawaii, major communications parameters such as e.i.r.p., saturation flux density, translation frequency, attenuator gain

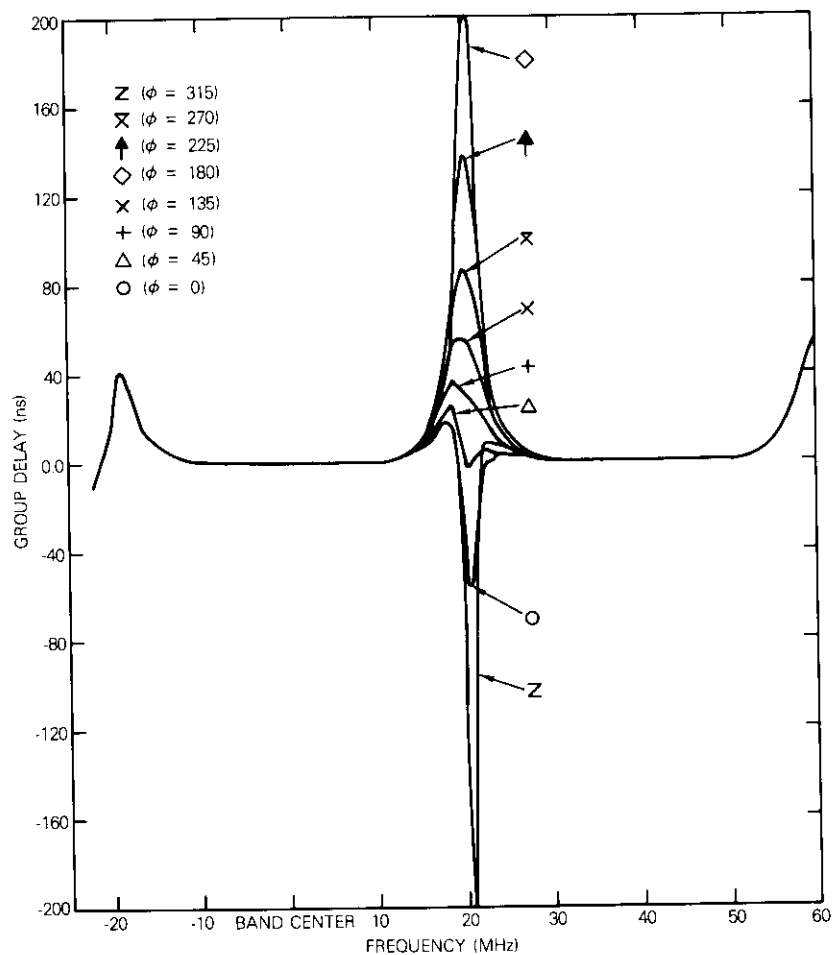


Figure 28. Group Delay vs Frequency

step, cross-polarization isolation, frequency response, and TWT transfer characteristics were measured. Contours of e.i.r.p., saturation flux density, and cross-polarization isolation from prelaunch and in-orbit tests are shown in Figures 30-32. The in-orbit measurements indicated that no

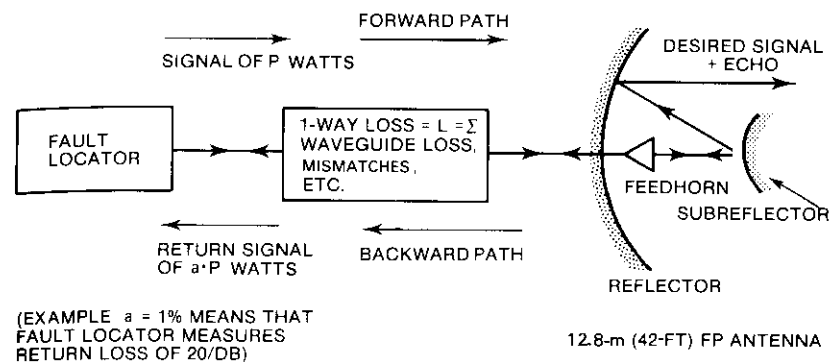


Figure 29. Subreflector Echo Test Setup

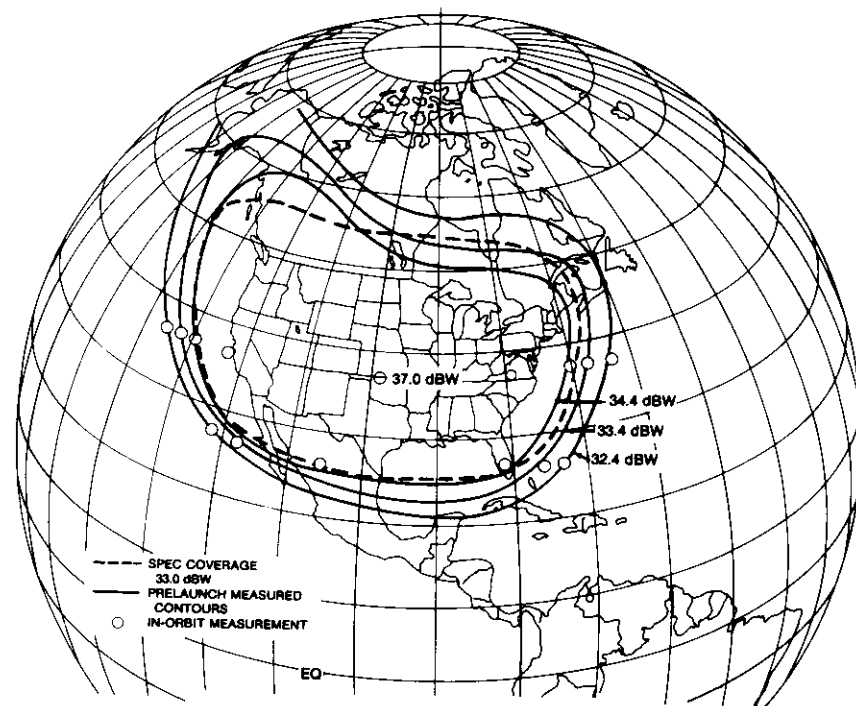


Figure 30. e.i.r.p. Contours for the Contiguous U.S.

**SATURATION FLUX DENSITY  
G/T CONTOURS FOR VERTICAL POLARIZATION**

CHANNEL IV  
SATELLITE LOCATION = 128°W

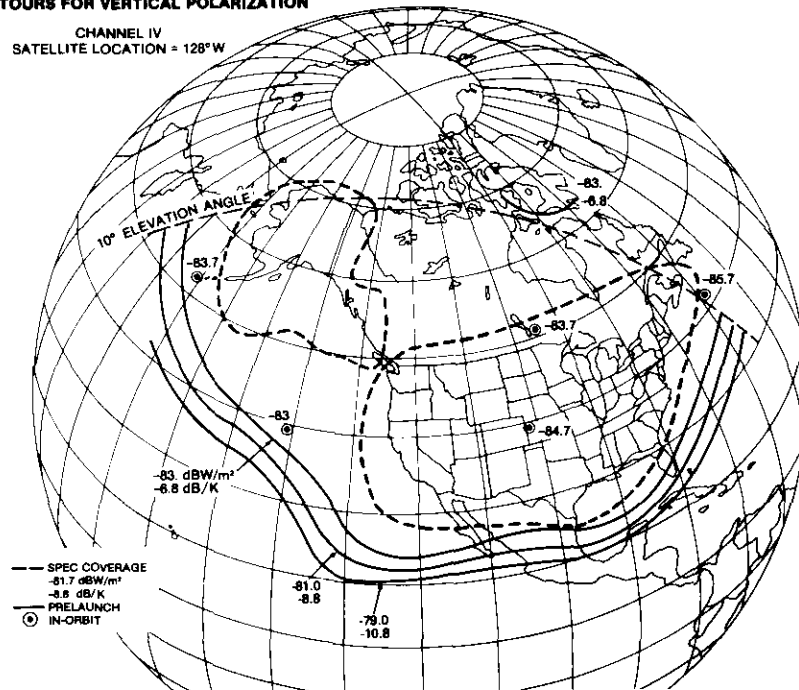


Figure 31. Saturation Flux Density

changes from the prelaunch tests had occurred and that all the communications subsystems function satisfactorily. Subsequent measurements of the COMSTAR communications parameters by AT&T during the acceptance test confirmed that all parameters exceed those specified by the agreement.

**References**

- [1] "The INTELSAT IV Spacecraft," edited by E. T. Jilg, *COMSAT Technical Review* Vol. 2, No. 2, Fall 1972, pp. 271-389.
- [2] "The INTELSAT IV Communications System," edited by P. L. Bargellini, *COMSAT Technical Review*, Vol. 2, No. 2, Fall 1972, pp. 437-572.
- [3] J. L. Dicks and M. P. Brown, Jr., "INTELSAT IV-A Transmission System Design," *COMSAT Technical Review*, Vol. 5, No. 1, Spring 1975, pp. 73-104.
- [4] I. Dostis et al., "In-Orbit Testing of Communications Satellites," *COMSAT Technical Review*, Vol. 7, No. 1, Spring 1977, pp. 197-226.

**CROSS-POLARIZATION ISOLATION  
CONUS HORIZONTAL  
PUERTO RICO  
HAWAII**

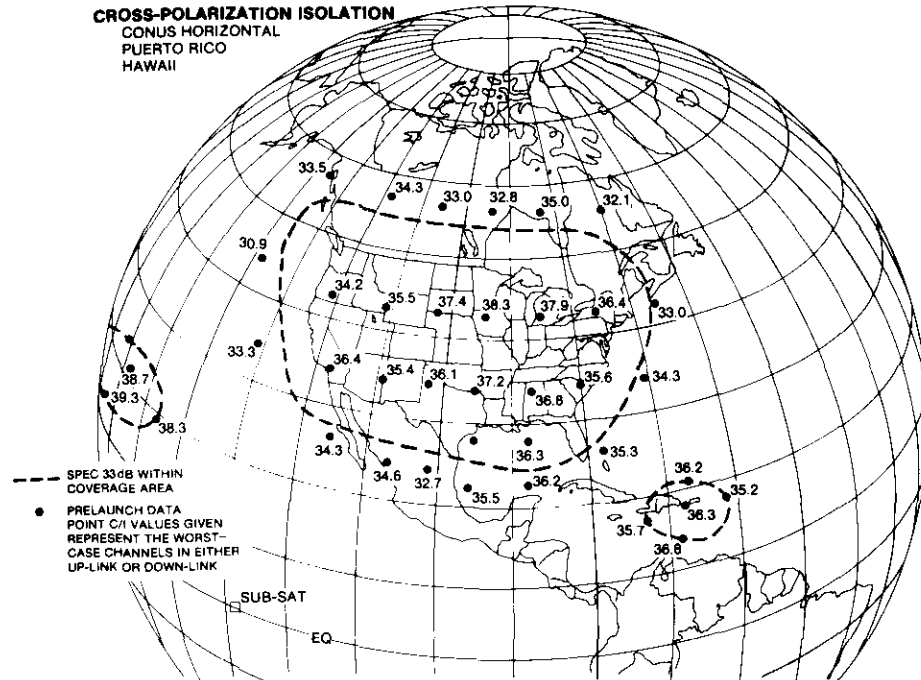


Figure 32. Cross-polarization Isolation



Goma E. A. Abutaleb received a B.Sc. from Cairo University, Egypt, and an M.S. Degree from The George Washington University, Washington, D.C., both in electrical engineering, communications. His experience includes thirteen years with the Egyptian Telecommunications Organization, about five years with INTELSAT, and about six years with COMSAT/COMSAT GENERAL. He is currently Manager of the Transmission Systems Department, Space and Information Systems, COMSAT GENERAL Corporation.



*Myong C. Kim received a B.S. in electronic engineering from Seoul National University in 1964, and M.S. and Ph.D. degrees in electrical engineering from the University of Maryland in 1969 and 1972. From 1973 to 1975 he was a senior staff member at Operations Research Inc. (Silver Spring, Md.), where he worked on satellite communications system. Since 1975 he has been working on the COMSTAR program as a System Design Engineer in the Space and Information Systems of COMSAT GENERAL Corporation.*

*Kenneth F. Manning received a B.S. degree from the University of Southampton, England, and an M.S. degree from McGill University, Canada. Since joining COMSAT in 1967, he has been involved with the system design of INTELSAT III and IV and the U.S. domestic satellite systems. Prior to joining COMSAT, he was involved with the development of attitude control systems for low-altitude orbit satellites.*



*John F. Phiel, Jr. received B.S.E.E. and M.S.E.E. degrees from Drexel University in 1963 and 1965, respectively. From 1965 to 1967 he was with the U.S. Army SATCOM Agency, where he worked on the Initial Defense Communications Satellite Program. Since joining COMSAT in 1967, he has been involved in transmission system engineering and earth station implementation. He is currently a Senior Communication Engineer in the Space and Information System Office of COMSAT GENERAL Corporation. In this capacity, he is engaged in the technical aspects of studies of new business activities and COMSTAR communications performance analysis.*

*L. H. Westerlund received a B.A. in physics (1964) and a Ph.D. in space science (1968) from Rice University. Joining COMSAT Labs in 1968, he became a member of the Space Physics Branch of the Physics Laboratory and later a member of the Propagation Branch of the Transmissions Systems Laboratory. He became Assistant Project Manager for the COMSAT ATS-F Propagation Experiment in 1971. In 1973, he joined COMSAT GENERAL as the Senior Space Segment Engineer for the COMSTAR Program. He is presently the Manager of Engineering in the Space and Information Systems Office, where he is responsible for the implementation of the COMSTAR Space Segment and the 19/28-GHz Beacon experiment.*



## ***COMSAT General satellite technical control network***

W. J. GRIBBIN AND R. S. COOPERMAN

(Manuscript received October 14, 1976)

### ***Abstract***

COMSAT GENERAL has established a satellite command and control system which will soon extend worldwide to meet the ground control requirements of its domestic (COMSTAR) and maritime (MARISAT) satellite systems. This paper discusses the requirements for and the technical characteristics of the earth stations, processing equipment, System Control Center, computer facilities, and communications links which comprise the system. Telemetry data management and reduction philosophies are also addressed.

### ***Introduction***

In-orbit operation of the COMSTAR and MARISAT commercial communications satellite systems requires the support of a terrestrial command and monitoring system. The simultaneous development of these two satellite systems by COMSAT GENERAL presented a unique opportunity to design an entirely new integrated ground support system which would provide cost savings for both programs through economy of scale and reduced manning. The system design combined features learned from 10 years of operating INTELSAT satellites with new technology such as automatic switching and minicomputers [1]-[3].

The operational COMSAT GENERAL satellite control network [4], [5] con-

sists of two earth stations, one located at Southbury, Connecticut, and one located at Santa Paula, California, and a System Control Center (scc) located in Washington, D.C. The system is initially designed to support a network of five satellites with the capability of expanding to eight. The initial space segment comprises two MARISAT satellites, one serving the Atlantic and the other serving the Pacific, and three domestic (COMSTAR) satellites capable of serving the contiguous U.S., Hawaii, Puerto Rico, and Alaska. A third earth station is currently under test at Fucino, Italy, to support a third MARISAT for Indian Ocean Service.

The system is configured for centralized operation, with the scc monitoring the status of and exercising direct control over both the ground and the space segment. For satellite control in the event that communication with the scc is lost, each earth station is capable of fully autonomous operation.

### **Design requirements**

The satellite technical control network was designed to satisfy the following basic requirements:

- a. continuous collection and monitoring of all satellite telemetry data,
- b. collection and processing of ranging and angle tracking data to determine satellite orbits,
- c. transmission of commands to the satellites,
- d. remote control of the earth station configuration from the scc,
- e. increased space segment reliability via backup operational modes and equipment.

Extensive operational experience at COMSAT and an analysis of user needs led to the formulation of network design criteria which satisfy these requirements in a technically efficient and cost-effective manner:

- a. a centralized control center having a close interface with personnel knowledgeable of satellite subsystems;
- b. continuous real-time and historical data readily available for routine operational monitoring, failure analysis, and long-term engineering analyses;
- c. command monitoring and verification at several levels in the system before transmission and execution;
- d. minimal switching response time in the event of critical failure;
- e. angle tracking and ranging information available to the COMSAT

- IBM 360/65 computer for spacecraft orbit and attitude determination;
- f. antenna pointing data available from the COMSAT IBM 360/65 computer to the satellite users including the tracking, telemetry and command (TT&C) earth stations;
- g. a System Control Center which can process data from the INTELSAT TT&C earth stations in support of launch operations;
- h. minimum cost and maximum reliability for a successful commercial venture.

### **System overview**

Full-time acquisition of telemetry data from each satellite requires, as a minimum, a dedicated antenna for each satellite. The additional use of these antennas for orbit determination requires that they be capable of accurate tracking performance and hence incurs increased costs. Experience has indicated that equally accurate orbit determination may be accomplished with a diversity ranging system in which the orbit determination software utilizes satellite range measurements from two widely separated locations in lieu of angle tracking data. It has therefore been decided to deploy two limited-motion (non-autotrack) antennas in the system, one at each domestic site, in lieu of a fifth autotracking antenna. The resulting antenna configuration increases system reliability through antenna redundancy (six antennas for five spacecraft), standardizes the equipment deployment at each site, and results in a system with increased capabilities at a lower cost. The overall system configuration is shown in Figure 1.

Telemetry data are acquired from each satellite and transmitted to the scc, where they are limit checked and stored for use in failure or historical trend analysis. Other telemetry data such as real-time sensor pulses and the analog accelerometer signal are required only occasionally and are available as needed.

To ensure correct commanding of the satellite, commands are echoed back to the scc from the earth station and from the satellite via telemetry. This provides two levels of verification with additional checking via software in the control center processor. Ranging is initiated in the same manner as commanding at the scc, and time-annotated ranging and angle tracking data are transmitted back to the scc and the COMSAT IBM 360/65 computer facility. Antenna pointing data are generated at the IBM 360/65 computer after orbit determination and transmitted to the earth stations and satellite user facilities as required.

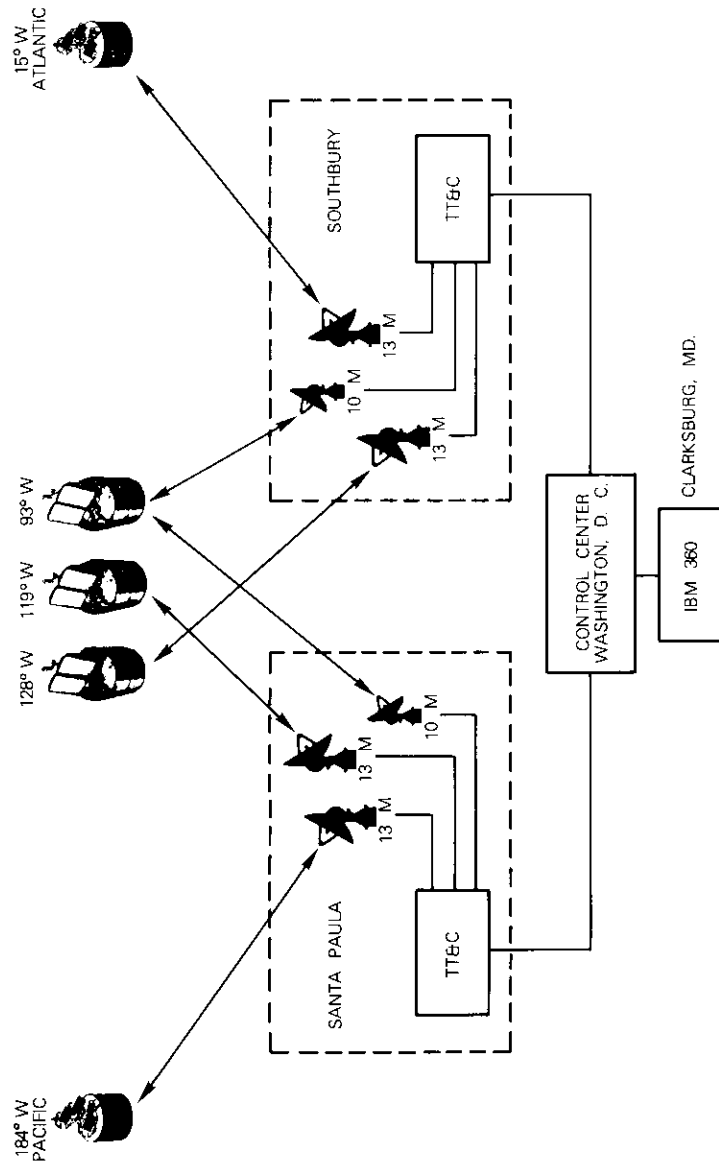


Figure 1. Overall Spacecraft Technical Control Network

**Earth stations**

Two earth stations were constructed, one at Southbury, Connecticut (104 km north of New York City), and one at Santa Paula, California (128 km north of Los Angeles). These locations provide an orbital arc coverage of 8°W to 186°W longitude. The principal elements of each earth station are a control building (see Figure 2) connected via cable/waveguide runs to two 12.8-m (42-ft) full-motion antenna (G/T = 31.9 dB/K at 4 GHz) and a 10.4-m (34-ft) limited-motion antenna (G/T = 29.5 dB/K at 4 GHz). Each antenna is capable of transmitting commands and ranging at 6 GHz and receiving satellite telemetry at 4 GHz.

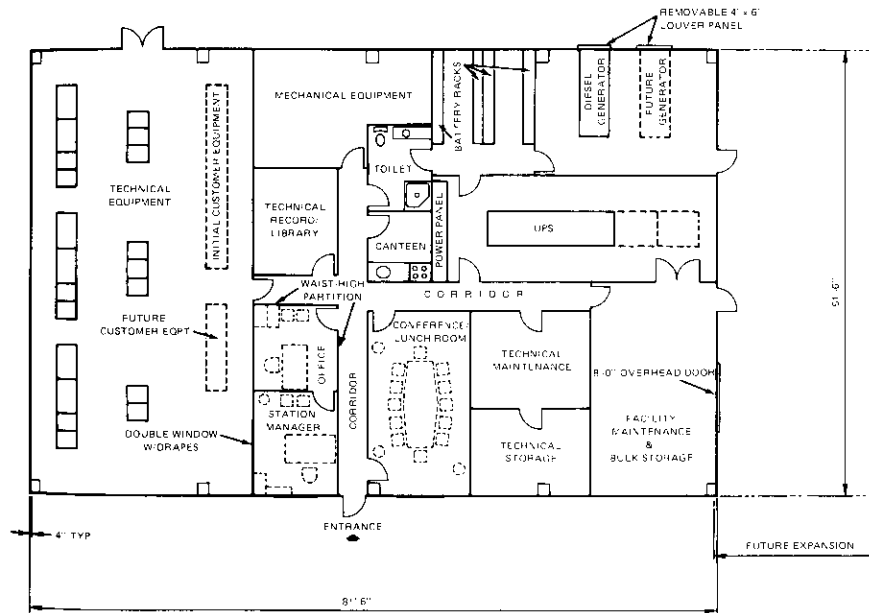


Figure 2. Equipment Arrangement, COMSAT General Control Building

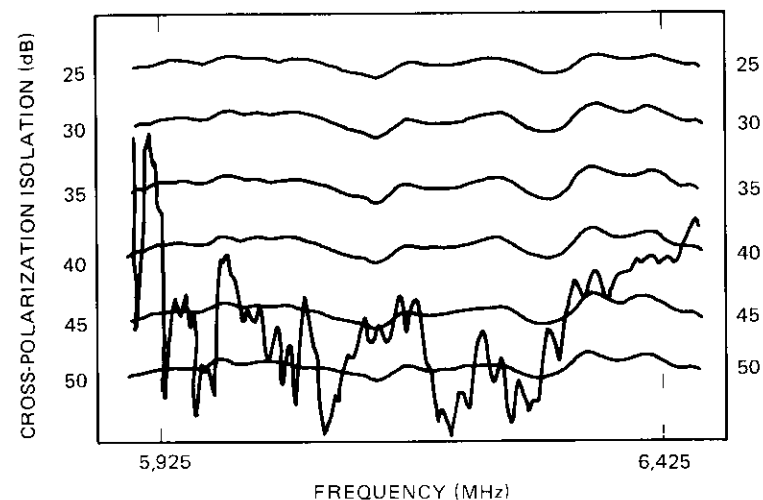
One of the 12.8-m antenna systems includes a feed capable of operating in a dual orthogonal linear polarization (frequency reuse) or circular polarization mode with monopulse tracking capability in either mode. This antenna can serve either the COMSTAR or MARISAT satellites. The second 12.8-m full-motion antenna includes a circularly polarized feed with monopulse tracking capability and is dedicated to the MARISAT

satellite system. This antenna, which is also used to provide communications with the MARISAT satellite at 4/6 GHz, receives L-band communications transmissions from MARISAT. The angle tracking accuracy of the 12.8-m antenna exceeds  $0.020^\circ$  rms. The 10.4-m non-autotracking antenna, intended for use with the COMSTAR satellites, provides linear polarization (frequency reuse) capability only. The antenna subsystem for each configuration includes a non-tilting and environmentally controlled equipment room for easy and quick in-service maintenance.

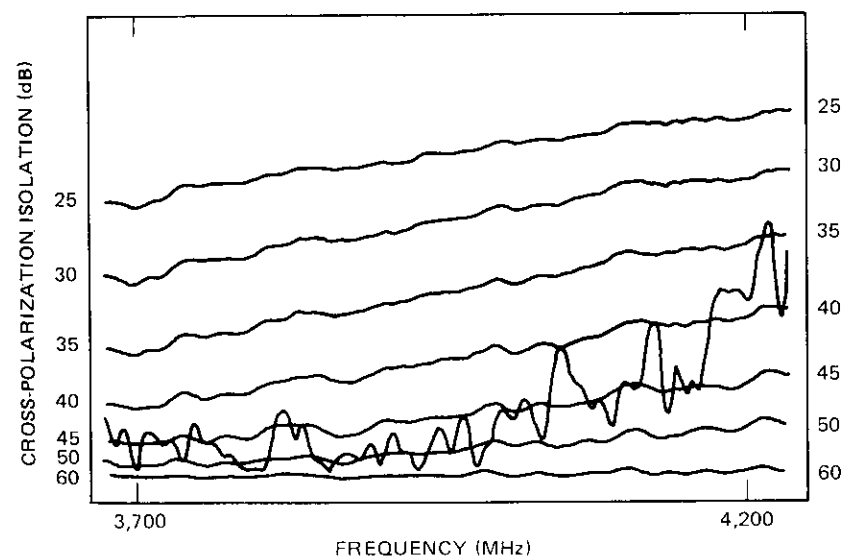
The receiver subsystem consists of the low-noise amplifiers (LNAs), interfacility links, down-converters, and tracking receiver equipment. The LNAs are located in the environmentally controlled elevated equipment rooms and are connected to the down-converters in the control building via interfacility coaxial cable runs. Each LNA consists of a 2-stage, uncooled, ultra-low-noise parametric amplifier followed by a transistor amplifier to provide the required 60-dB gain. The operating bandwidth of the LNA is a minimum of 500 MHz at the 1-dB points, and the noise temperature of the on-line unit does not exceed 55 K anywhere in the 500-MHz receive band. The down-converters may be tuned to convert any frequency within the 3.7- to 4.2-GHz band to 70 MHz by selecting the desired local oscillator frequency.

The transmit subsystem, which consists of the up-converters and the high-power amplifiers (HPAs), is located in the central control building with waveguide runs to each antenna. Patching facilities permit the 70-MHz IF signal from the spacecraft command and ranging equipment to be interfaced to the up-converters. The HPAs are 3-kW klystrons which result in a maximum e.i.r.p. of 85 dBW. A unique RF switching arrangement has been included to permit the output of any HPA to be routed to any antenna. The RF characteristics of each earth station are summarized in Table 1.

The dual-polarized feed subsystem processes two orthogonal linearly polarized signals in the 3.7- to 4.2- and 5.925- to 6.425-GHz bands. The worst-case cross-polarization isolation is better than 34 dB on-axis and 29 dB within the 1-dB beam contour (Figure 3). In addition, the feed is capable of handling circularly polarized signals and has single-channel monopulse tracking. The corrugated horn radiator provides circularly symmetric frequency-invariant patterns for optimum use of the high-efficiency reflector optics. Behind the horn are two  $TE_{21}$  mode couplers to derive the tracking error signal, an orthomode junction to separate the 4- and 6-GHz signals, servo-driven  $90^\circ$  and  $180^\circ$  polarizers in each band to process the diverse polarizations and varied orientations, and standard



a. Typical Transmit Band Cross-polarization Isolation Data



b. Typical Receive Band Swept Cross-polarization Isolation Data

Figure 3. Antenna/Feed Combined Cross-polarization Performance (secondary data for  $0^\circ$  polarization)

TABLE 1. EARTH STATION RF CHARACTERISTICS

Characteristic	MARISAT	Full Performance	Limited Motion
Antenna Diameter (m)	12.8	12.8	10.4
G/T (dB/K)	31.9	31.9	29.5
LNA Temperature (K)	55	55	55
Transmit Gain (dB)	55.8	55.8	53.0
Transmitter Power (W)	3	3	3
Transmit Beamwidth (deg)	0.28	0.28	0.32
Frequency Range (GHz)			
Transmit	5.925-6.425	5.925-6.425	5.925-6.425
Receive	3.700-4.200	3.700-4.200	3.700-4.200
Feed			
Type	Cassegrain	Cassegrain	Cassegrain
Polarization	Circular	Dual linear/ cross or circular	Dual linear/ cross polarization
Control Modes	Manual, programmed, autotrack	Manual, programmed, autotrack	Manual

orthomode transducers to separate the two polarizations in each band.

The electric power system at each earth station receives 3-phase, 60-Hz public utility power at 480/277 V and distributes it to the station at 480/277 and 208/120 V. An uninterruptible power system (UPS) provides battery power for the critical loads during momentary power outages and includes a diesel-engine-driven generator to carry the station load during extended utility outages.

#### Earth station TT&C equipment

The TT&C processing equipment (Figure 4) at each earth station performs the following functions:

- a. antenna pointing,
- b. angle tracking,
- c. ranging,
- d. telemetry acquisition,
- e. command.

#### ANTENNA POINTING/ANGLE TRACKING

Three modes of antenna pointing are provided: manual, program, and autotrack. In the manual mode, earth station operators enter required angle data via a thumbwheel entry system. Program tracking provides a

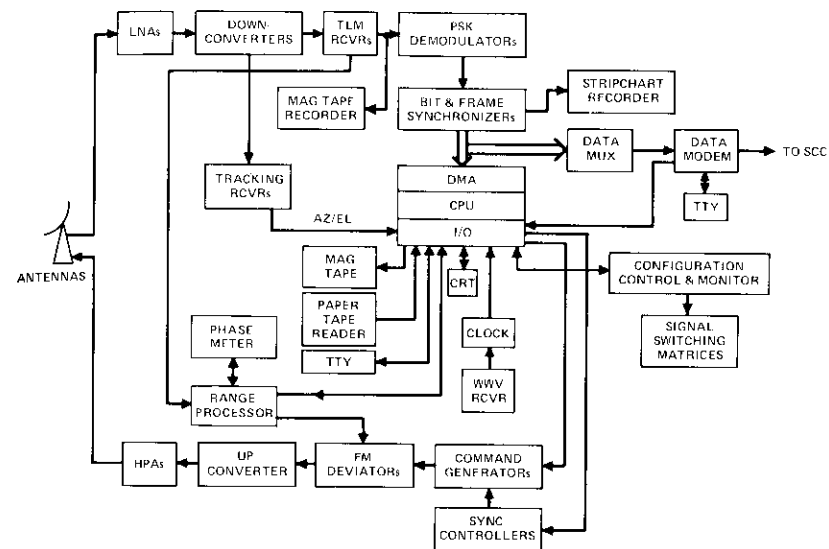


Figure 4. Earth Station Simplified Functional Block Diagram

means of pointing the antenna under local processor control using pointing parameters generated by the COMSAT IBM 360/65 computer facility located at COMSAT Laboratories, Clarksburg, Maryland. The monopulse tracking system permits closed-loop autotracking capability. Antenna axis angular positions (azimuth and elevation) are stored in the earth station processor for subsequent transmission to the IBM 360/65 computer facility for satellite ephemeris generation.

#### RANGING

The slant range to the satellite in transfer orbit and on station is determined by a multimode computer-controlled ranging system. The ranging system generates four coherent high-spectral-purity tones (35.4, 283.4, 3,968, and 27,777 Hz) which frequency modulate a carrier transmitted to the satellite at 6 GHz. The phase difference between the transmitted and received tones is measured by a precision phase meter. The measurements are normalized to eliminate satellite-induced phase changes, resulting in a phase shift measurement directly proportional to the distance of the satellite from the earth station antenna. The lower frequency tones resolve measurement ambiguity in the succeeding higher frequency tone,

which measures the range to within 10 m. A range calibrator, which loops back the ranging signals within the earth station, is used to calculate the portion of the phase difference contributed by the earth station equipment.

#### TELEMETRY ACQUISITION

Telemetry data are transmitted from the satellite on two 4-GHz tracking Beacon carriers. The 4-GHz tracking Beacon signal is received and processed by each earth station antenna subsystem to provide a down-converted RF output signal at 70 MHz. Standard commercial telemetry receivers demodulate the phase modulated carriers (unity modulation index), producing outputs of a 14.5-kHz FM subcarrier, a 32-kHz PCM/PSK subcarrier, or a 93-kHz FM subcarrier.

The 14.5-kHz subcarrier may be modulated either by analog satellite nutation accelerometer data or by analog pulse satellite attitude information signals (earth sensor, sun sensor, and antenna position pulses). The synchronous controller (described subsequently) uses satellite attitude information to execute commands in synchronism with the satellite spin period. A real-time FM digitizer converts the attitude sensor analog pulse information to digital form for computer entry to measure satellite platform pointing and sensor performance parameters and to provide a backup for the onboard satellite attitude pulse measurement equipment.

The 93-kHz subcarrier provides an FM signal derived from an accelerometer located on the spacecraft despin bearing and power transfer assembly (BAPTA). This signal is demodulated by an IRIG channel F discriminator.

The 32-kHz subcarrier, which contains 1-kilobit PCM telemetry data, is demodulated, resulting in a 1-kbps NRZ-M signal which is fed to a multichannel synchronizer/buffer. The multichannel synchronizer/buffer is a completely modularized unit that contains eight channelized bit synchronizers, frame synchronizers, data buffer, and a central CPU interface stage.

Received telemetry signals and time code data may be recorded on a standard IRIG tape recorder for subsequent playback.

#### COMMAND

Commands may be initiated and transmitted to the satellite by either the earth station or the System Control Center. In the normal operating mode, command messages are entered via an interactive keyboard entry system at the SCC and transmitted via the interfacility data link to the earth

station computer. Error correcting/detecting block coding is used in this transmission to prevent data transmission errors. Command messages are logged in the earth station computer and forwarded to the command generator. The command generator in turn encodes the message into a serial RZ FSK baseband which is frequency modulated on a 70-MHz intermediate carrier and then up-converted to a 6-GHz carrier for transmission to the satellite.

Satellite attitude control and velocity control require synchronization of satellite jet firing with the spacecraft spin rate and angle of roll. This is accomplished by using a synchronous controller which derives spacecraft spin and attitude information from the telemetered data to provide synchronization (timing) information to the command generator.

#### EARTH STATION SOFTWARE

The earth station software provides the control and processing which allows the equipment described in the preceding subsections to operate as an integrated system. This software, which is structured as shown in Figure 5, performs the following functions:

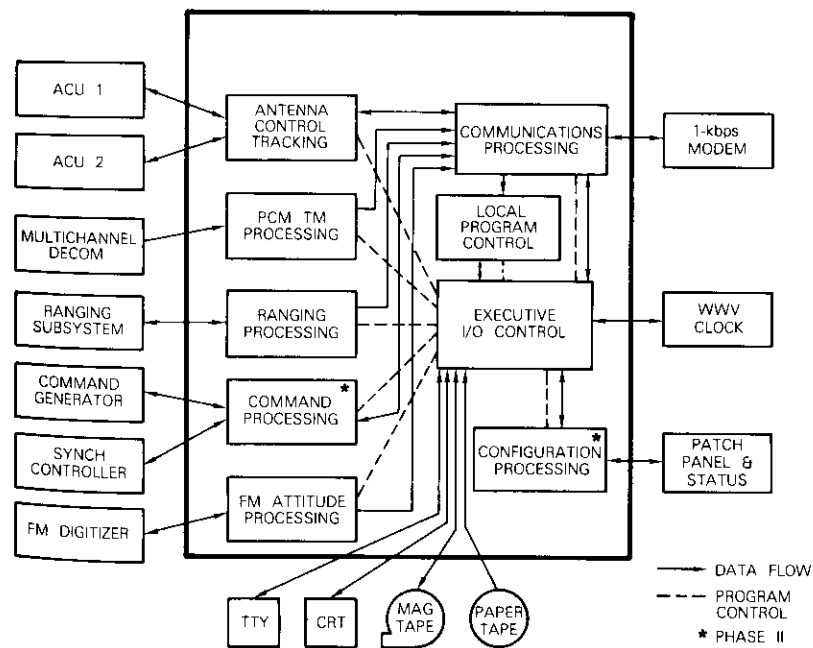


Figure 5. Earth Station Software

*a. TELEMETRY PROCESSING.* The telemetry data are received from the multichannel synchronizer/buffer, time annotated, limit checked, and displayed on the station CRT.

*b. ANGLE TRACKING AND RANGING PROCESSING.* Azimuth, elevation, and slant range measurements are time annotated and stored for transmission to an IBM 360/65 in a PCM-compatible format.

*c. ANTENNA POINTING CONTROL PROCESSING.* Antenna pointing data are stored by the processor on digital magnetic tape. When programmed antenna control is required, the software retrieves the pointing data and transmits them to the antenna control console.

*d. FM ATTITUDE DATA PROCESSING.* The FM attitude data are received from the FM digitizer and transmitted in real time to an IBM 360/65 for statistical processing of sensor and platform pointing data.

*e. STATION CONFIGURATION CONTROL AND MONITORING PROCESSING.* Baseband, IF, and RF switch settings are monitored and the status is formatted for transmission to the SCC. The switches may be controlled from the local CRT keyboard or TTY and from the SCC via the earth station-SCC data link. Alarms are generated upon detection of earth station anomalies.

*f. REMOTE COMMAND AND RANGING PROCESSING.* The command generator and ranging subsystem can be controlled from the SCC via the SCC-earth station data link. Local control is available via the earth station CRT keyboard or TTY.

The data communications processor employed at the earth station is a memory-expanded Hewlett-Packard 9600A Basic Control System (BCS). It consists of an HP 2100S microprogrammable system computer equipped with 32,000 words of 16-bit core memory, two direct memory access (DMA) channels, a teleprinter communications channel, floating point hardware, a time base generator, and selected peripherals (high-speed paper tape reader, teleprinter, magnetic tape transport, and miscellaneous input/output cards).

### System control center

The SCC, shown in Figure 6, serves as the centralized point of control for the COMSAT GENERAL satellite command and control network. Occupying approximately 110 m<sup>2</sup>, it is located in the COMSAT GENERAL building in Washington, D.C.

The SCC performs the following general functions:

*a.* real-time display and limit checking of all significant satellite

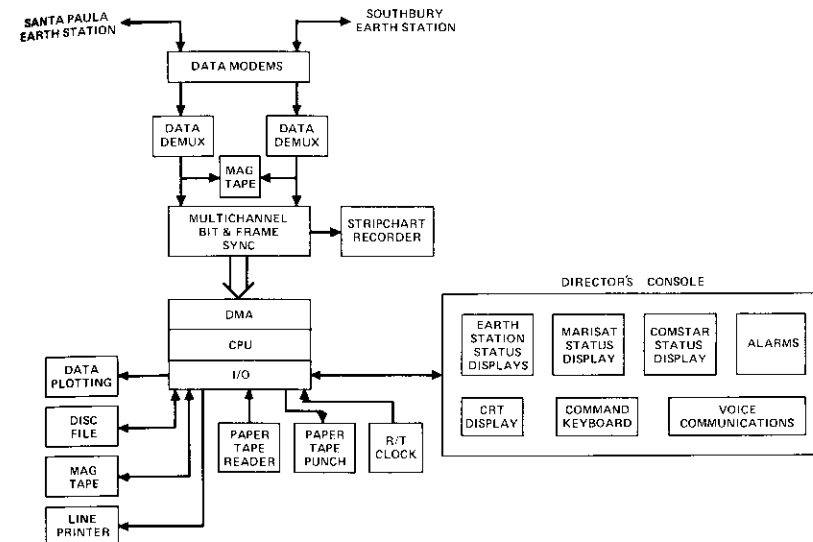


Figure 6. System Control Center Simplified Functional Block Diagram

telemetry data and generation of alarms for out-of-limit parameter values;

*b.* storage and analysis of satellite telemetry data and earth station status;

*c.* initiation and control of earth station configuration and command operations to the satellite;

*d.* interface to the IBM 360/65 for satellite attitude, ranging, angle tracking, and historical telemetry.

### Telemetry signal processing

In the normal mode of operation, telemetry data received from the remotely located TT&C earth stations enter the SCC processor via a multichannel bit and frame synchronizer. The processor assimilates the data and produces a real-time CRT display of the network status. Coupled with the display is a CRT with a data keyboard which allows the operator to query the processor for detailed system information. The main CRT display is located in a director's console (Figure 7), which is the central monitoring and control point of the network. This console also contains time displays and voice communications equipment.

All telemetry data coming into the SCC are recorded by an analog

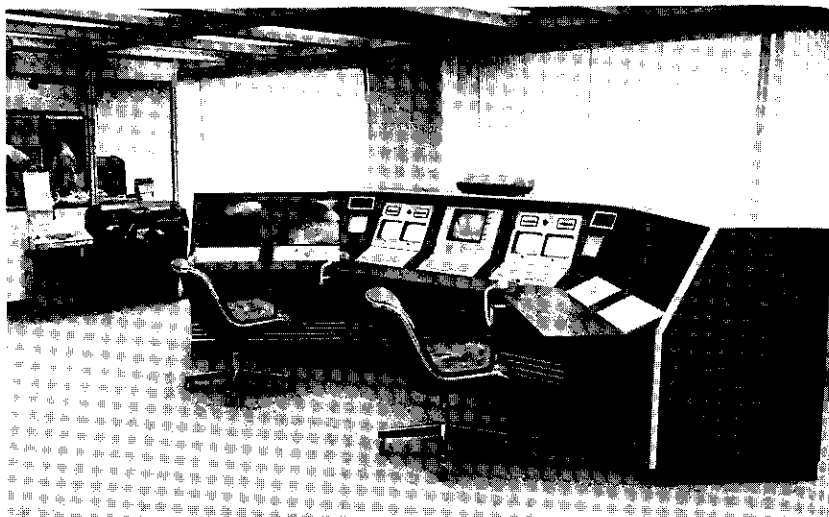


Figure 7. System Control Center Director's Console

magnetic tape recorder which provides a complete record of satellite performance for failure analysis. Associated with the tape recorder is a tape search unit which allows data to be located within a selected time period. Time is placed on the tape by the SCC time code generator, which also provides parallel time data to the CPU and a time annotation reference to the analog stripchart recorder.

A multichannel digital-to-analog converter produces continuous voltage based on selected telemetry channels to drive an 8-channel stripchart recorder.

#### Remote station control and configuration monitoring

Highly centralized system operation from the SCC is achieved through maximum automation of routine TT&C functions. A system design goal was a normal 1-man-per-shift TT&C staffing level at each earth station and the SCC. To achieve this objective, all up-link (command or range) and down-link (telemetry) station equipment can be remotely configured from the SCC. Antenna status data from the earth station up- and down-link annunciator panels are transmitted to and displayed in the SCC.

#### System control center software

The SCC software (Figure 8) processes telemetry data and presents them to the satellite controller in a usable format for operation and analysis. The principal functions of the software are as follows:

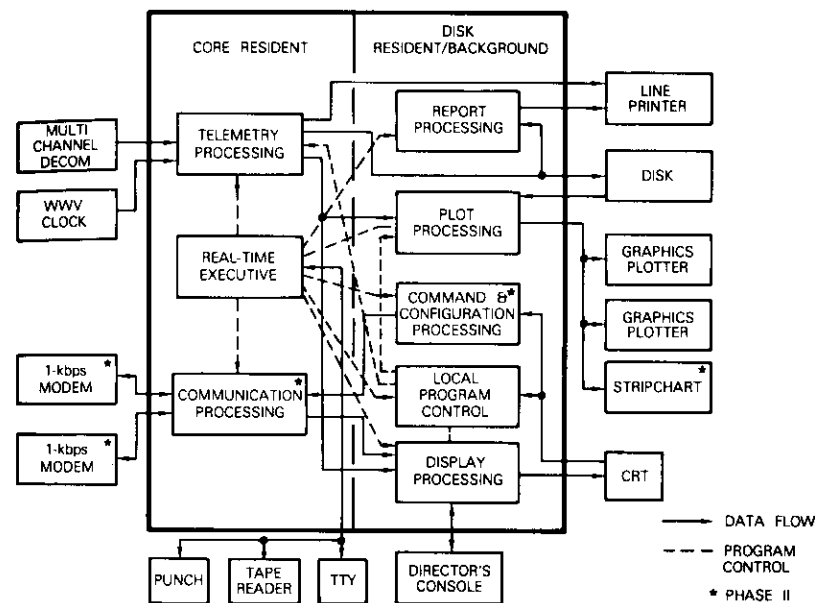


Figure 8. System Control Center Software

a. **TELEMETRY PROCESSING.** Telemetry data received from the multichannel synchronizer/data buffer are limit checked against previously established limits, time annotated, and displayed on a CRT. The data are sorted by satellite and stored on disk at 15-minute intervals for archival record purposes.

b. **COMMAND DISPLAY PROCESSING.** All satellite commands are displayed via CRT and logged on the printer as the command sequence is implemented and on the disk for record purposes.

c. **PLOTTING.** Selected telemetry channels can be plotted on two graphic plotters.

d. **COMMAND PROCESSING.** Commands are entered via the CRT keyboard and formatted for transmission to the TT&C station commanding the satellite.

e. STATION CONFIGURATION PROCESSING. Station monitoring configuration processing permits monitoring and control of the earth station configuration. Commands are entered via keyboard for transmission to the earth station processor. Earth station anomalies will cause an alarm to be activated in the SCC.

f. SUMMARY REPORTS. Daily summary reports are generated for each satellite being monitored. These reports include out-of-limits conditions with time out/time in, command executions, statistical summaries of the telemetry data, and status and command.

g. OPERATOR CONTROL. Operator control of the system is provided by commands which are entered via either the teletype or CRT keyboard. The operator can start and stop processes; change the source and format of displayed data, the sampling rates of data, and the telemetry limit values; command the satellite; and control the TT&C station configuration. The latter two controls are transmitted to the station via the SCC-earth station data link.

The SCC software was developed to run under the HP RTE III and File Manager (FMGR) operating system. The RTE III system schedules programs for execution so that several programs may be run simultaneously and handles input/output and interrupts. Programs communicate through a common data area and are executed in a 3-level hierarchy (*i.e.*, real-time core resident, real-time disk resident, and background), hence giving the most time-dependent functions a higher priority.

The real-time core-resident programs are always in the processor memory and have the highest priority for execution. These programs input each frame of telemetry data, check the data for command executes and out-of-limits conditions, and pass them to other routines via the common area. Unusual conditions detected in the telemetry data are placed in an event table in the common area.

The real-time disk-resident portion of the HP 21MX system performs functions which must be done in real time, but do not require monitoring of every frame of PCM data. Record files and plotter and printer outputs are constructed as the various programs operate on the data. The data interface between the core-resident portion of the program is the common area. These programs are kept on disk, read into memory, and executed as needed. Hence, several programs can share memory and the functions can be performed simultaneously. The background programs provide off-line (non-real-time) file maintenance and report generation.

The processor employed in the SCC is a memory-expanded (64K) Hewlett-Packard 9600E Real-Time Executive (III) System equipped with

digital magnetic tape recorder, disk memory, line printer, and dual graphics plotters.

### Conclusion

The system has been installed and is currently in full operation supporting in-orbit MARISAT and COMSTAR satellites. The basic system approach and the resultant design criteria have proven to be viable. The system was placed on-line in support of the new satellites with no major problems and only a minimum of minor defects. System operation was established prior to the first MARISAT launch and actual control over the satellites accomplished in a smooth transitional period. The successful operation of this system clearly demonstrates that centralized network control combining the advantages of automatic data processing with minimal simplified manual intervention can be implemented in a cost-effective manner.

### References

- [1] G. Quaglione, "Design Considerations of the Installation at Fucino for Telemetry and Telecontrol of INTELSAT Satellites," *Journal of the British Interplanetary Society*, Vol. 23, 1970, pp. 137-158.
- [2] R. S. Cooperman, "Centralized Command and Control for INTELSAT IV," 8th International Symposium on Space Technology and Science, Tokyo, Japan, August 1969.
- [3] A. McCaskill et al., "Launch and Orbital Injection of INTELSAT IV Satellites," *COMSAT Technical Review*, Vol. 2, No. 1, Fall 1972, pp. 391-432.
- [4] A. J. E. VanHover and W. J. Gribbin, "Design of a Ground Control System to Operate Domestic and Maritime Satellites," AIAA 5th Communications Satellite Systems Conference, Los Angeles, California, April 1974.
- [5] R. S. Cooperman, H. L. Parker and R. W. Wallace, "Terrestrial TT&C Data Processing for the COMSTAR and MARISAT Systems," *ITC Proceedings*, October 1975, Vol. 11, pp. 137-147.



*Walter J. Gribbin received a B.S. degree in electronic engineering from Catholic University in 1964, and an M.B.A. from American University in 1973. Prior to joining COMSAT, he was a senior space systems engineer with the General Electric Spacecraft Department, where he was engaged in the design and implementation of ground control systems for body-stabilized spacecraft. He joined COMSAT in 1968 and was the project manager for the design and implementation of the COMSAT GENERAL ground segment.*

*Richard S. Cooperman received a B.E.E. from the City College of New York in 1961 and an M.S.E.E. from The George Washington University in 1967. Prior to joining COMSAT, he was a senior member of the technical staff of Johns Hopkins University's Applied Physics Laboratory, where he was responsible for the design and development of several satellite-borne data processing systems. As Manager of the Control Electronics Department of the Spacecraft Laboratory, he is presently responsible for directing research and development in terrestrial command/control systems and satellite-borne signal processing. In addition, he is project manager for the TT&C data processing system. He is a member of Eta Kappa Nu.*



**Index:** COMSTAR, Beacon, measurement, transmitter, centimeter wave, experimental design

## **Centimeter Wave Beacons for the COMSTAR satellites**

L. POLLACK

(Manuscript received December 2, 1976)

### **Abstract**

Two Centimeter Wave Beacons are carried on each COMSTAR satellite. These Beacons provide modulated signals at 19.04 and 28.56 GHz to enable direct measurement of the following quantities versus atmospheric moisture on a space-to-earth path: attenuation as a function of frequency, depolarization, and phase variations between the 19- and 28-GHz carriers and between the sidebands at  $\pm 264.4$  or  $\pm 528.9$  MHz of the 28-GHz carrier.

The achievement of a low-power-consuming lightweight transmitter design, which uses the early-life excess power available from the solar cells on the satellite, permits an experiment lifetime of more than two years. This paper describes the experiment and spacecraft requirements which have led to the designs described in detail in companion papers in this issue and others to follow.

### **Introduction**

Future satellite systems requiring wide bandwidths to achieve large communications capacities may use the 17.7- to 21.2- and 27.5- to 31-GHz bands assigned to fixed commercial satellite systems. Although the expected rain attenuation in the eastern U.S. is known to exceed 15-18 dB and 27-30 dB at 19 and 30 GHz, respectively, for 0.1 percent of the time, more precise knowledge of the extent, distribution, and duration of

the atmospheric and rain effects is needed to design economical new satellite systems. Hence, the American Telephone and Telegraph Company (AT&T) has established an agreement with COMSAT GENERAL Corporation to include Centimeter Wave Beacons in the COMSTAR satellites [1]. These Beacons provide a direct measurement of the following propagation effects on a space-to-earth path:

a. RAIN AND CLOUD ATTENUATION. Vertical polarization at 19 and 28 GHz and horizontal polarization at 19 GHz with greater than 35-dB range.

b. DEPOLARIZATION BY RAIN AND CLOUDS. Vertical and horizontal polarization at 19 GHz and vertical polarization at 28 GHz.

c. DIFFERENTIAL PHASE. 19 to 28 GHz as well as the sidebands at  $\pm 264.4$  or  $\pm 528.9$  MHz with respect to the 28-GHz carrier.

The satellites are maintained in geosynchronous orbit position to within  $\pm 0.1^\circ$  and approximately  $\pm 0.2^\circ$  in attitude so that each propagation path is stable. After three COMSTAR satellites are deployed, each earth station will be able to measure three paths at different elevation angles.

COMSAT GENERAL Corporation determined that the transmitters could be accommodated if the primary power and weight were less than 70 W and 13.6 kg (30 lb), respectively. With the propagation performance objectives [2] determined by Bell Telephone Laboratories and COMSAT GENERAL, COMSAT Labs proposed an all-solid-state design that would meet the satellite specifications and reliability requirements.

### Transmitter Requirements

The microwave power and frequency stability requirements are based on achieving a signal attenuation dynamic range greater than 35 dB with a nominal link budget shown in Table 1. Detailed performance data given in Reference 3 indicate a power margin of 1 dB and a frequency jitter bandwidth 10 dB less than the objectives.

### Implementation

Detailed knowledge of the particular components required for the experiment was available from previous COMSAT research and development programs for use in making the basic implementation choices for the Beacons. Measurements of the local oscillator source used in the ATS-F COMSAT Propagation Experiment transponder [4] ensured that the frequency stability required of the COMSTAR Beacons could be met with

TABLE 1. PROPAGATION PATH NOMINAL QUANTITIES <sup>a</sup>

	19.04-GHz Carrier	28.56-GHz Carrier	28-GHz Sidebands
<i>Satellite</i>			
Beacon Output Power (dBm)	27	28	21
Waveguide Loss (dB)	0.5	1	1
Atmospheric Absorption (dB)	1	1.5	1.5
Satellite Antenna Gain toward Clarksburg (dB)	29.4	29.4	29.4
e.i.r.p. (dBm)	54.9	54.9	47.9
Distance Loss (dB)	210	213.5	213.5
<i>Receiver</i>			
16-ft Antenna Gain (dB)	55.2 <sup>b</sup>	58.8 <sup>b</sup>	58.8
System Temperature (K)	630	2,500	2,500
Receiver Noise, 10-Hz Bandwidth (dBm)	-160.6	-154.6	-154.6
Received Signal (dBm)	-99.9	-99.8	-106.8
50-Percent Duty Cycle (dB)	-3	—	—
Loss in Modulation Sidebands (dB)	-3	—	—
Carrier-to-Noise Ratio (dB)	54.7	54.8	48.8

<sup>a</sup> For COMSTAR D1 satellite at 128°W longitude.

<sup>b</sup> Includes waveguide and filter loss.

a somewhat improved version of the crystal-controlled source used in that transponder. Thus, the design was based on a relatively simple and light-weight frequency source as described in Reference 5. The multiplier stages up to the final doublers were based on the ATS-F transponder designs, and the final doublers were based on a previously initiated corporate research project.

Traveling wave tubes and IMPATT\* diodes were considered as output amplifier alternatives. Separate traveling wave tube amplifiers for the 19- and 28-GHz frequencies would have exceeded the weight and power limits. Although an available single tube could amplify all the signals while accommodating the power limitation, the provision of a redundant unit would have resulted in excessive weight.

Fortunately, work at COMSAT Labs and elsewhere [6] on silicon IMPATT diode amplifiers provided an approach that accommodated all of the specifications. The amplifiers that were finally designed and used are described in Reference 7. In view of the absence of space qualification and experience with the devices, an extensive reliability, quality assurance, and life testing program was conducted on the 19- and 28-GHz IMPATT

\* IMPact Avalanche Transit Time.

diodes. As a result of this aspect of the program, a mean time to failure greater than  $4 \times 10^6$  device hours has been projected, as will be described in a future paper. Finally, the packaged units had to fit on a spacecraft with a seasoned design so that the electrical, structural, and thermal aspects of the communications payload and the antenna radiation properties would be undisturbed. The accomplishment of this objective is described in Reference 8.

### In-orbit performance

Two sets of Beacons have been operating in space since mid May and late July 1976. In each case, in-orbit performance, measured as soon as the satellites were in view of the calibrated receiving terminal at Clarksburg, was well within the specifications. Unlike measurements of the many satellites operating at lower frequencies, accurate measurements were possible only on clear cloudless days. The results of measurements made on COMSTAR satellites D1 and D2 are listed in Table 2.

TABLE 2. IN-ORBIT MEASUREMENTS

Parameter	Satellite	
	D1	D2
Average <sup>a</sup> Power Output (dBm)		
19 GHz Vertical	25.4	24.7
19 GHz Horizontal	25.9	24.8
28.6 GHz	29.9	30.6
28.824 GHz	22.9	20.5
28.296 GHz	23.8	21.5
Frequency <sup>b</sup>		
19-GHz Carrier <sup>c</sup> (MHz)	19,040.0205	19,039.9789
28-GHz Carrier (MHz)	28,560.0308	28,559.9685
Vertical/Horizontal Switching Rate <sup>d</sup> (kHz)	1.0000	1.0000
Polarization Isolation at Beam Edge for Worst Frequency (dB)	>32	>32

<sup>a</sup> Power variation during daily temperature cycle was <0.2 dB at 19 GHz and <0.3 dB at 28 GHz.

<sup>b</sup> "A" chain driver.

<sup>c</sup> Frequency variation during daily temperature cycle was  $\pm 4$  Hz.

<sup>d</sup> Frequency variation was  $\pm 0.1$  Hz.

Operation in orbit has resulted in over 5,700 hours\* of continuous propagation data indicating the value of a highly stable platform and RF source for accumulating propagation statistics.

### Conclusion

The experiment is currently providing the first space experience with wideband 1-W IMPATT diode amplifiers operating in the 20- and 30-GHz bands, four coherent signals of precisely known power and frequency, a wideband phase modulated set of signals at 28 GHz, and orthogonal polarization with greater than 32-dB isolation at 19 GHz.

### Acknowledgments

Many individuals have contributed to the success of the Beacon project. Although they are too numerous to list here, all these people at COMSAT Labs are to be recognized for their dedication. In particular, Mr. William Getsinger, the project manager, and Mr. Jeffrey Rubin, the assistant project manager, are acknowledged for their efforts in successfully carrying the effort to fruition.

### References

- [1] R. Briskman, "The COMSTAR Program," *COMSAT Technical Review*, Vol. 7, No. 1, Spring 1977, pp. 1-34.
- [2] R. Briskman, R. F. Latter, and E. E. Muller, "19/28 GHz Radio Propagation Research," *IEEE Transactions on Aerospace and Electronic Systems*, AES-10, No. 4, July 1974, pp. 535-536.
- [3] W. Getsinger, "Centimeter Wave Beacon Transmitter Design," *COMSAT Technical Review*, Vol. 7, No. 1, Spring 1977, pp. 109-128.
- [4] "The ATS-F COMSAT Propagation Experiment Transponder," A. L. Berman, editor, *COMSAT Technical Review*, Vol. 3, No. 2, Fall 1973, pp. 341-373.
- [5] R. Stegens, "Low-Jitter Local Oscillator Source for the COMSTAR Beacon Experiment," *COMSAT Technical Review*, Vol. 7, No. 1, Spring 1977, pp. 153-169.
- [6] Gupta Madhu-Sudan, "Large Signal Equivalent Circuit for IMPATT Diode Characterization And Its Application To Amplifiers," *IEEE Transactions on Microwave Theory And Techniques*, Special Issue on Solid State Microwave Amplifiers, MTT-21, No. 11, November 1973, pp. 689-693.

\* As of February 1, 1977.

- [7] M. Barrett, "19- and 28-GHz IMPATT Amplifiers," *COMSAT Technical Review*, Vol. 7, No. 1, Spring 1977, pp. 129-136.
- [8] N. Hyman et al., "Structural And Thermal Design Aspects of the Centimeter Wave Beacon," *COMSAT Technical Review*, Vol. 7, No. 1, Spring 1977, pp. 171-196.



*Louis Pollack, with COMSAT Laboratories since 1967, is Assistant Director-Technical, responsible for the technical direction of the Spacecraft, Communications Processing, Microwave, Applied Sciences, and Transmission System Laboratories. For 23 years he was with the ITT Federal Laboratory, where his last position was Director, Transmission System Operations, concerned with design and development of space communications equipment and other microwave transmission equipment.*

*He received his B.E.E. degree from the C.C.N.Y. in 1953, and is a Fellow of the IEEE, associate member of the National Society of Professional Engineers, and member of the AIAA and Sigma XI.*

Index: IMPATT amplifier, Beacon, transmitter, design criteria

## **Centimeter Wave Beacon transmitter design**

W. J. GETSINGER

(Manuscript received October 15, 1976)

### **Abstract**

The Centimeter Wave Beacon consists of separately packaged, all-solid-state, space-borne transmitters, one delivering about 0.6 W at 19.04 GHz and the other delivering about 1.0 W at 28.56 GHz. Signals for both transmitters are derived from the same redundant crystal oscillator. IMPATT amplifiers are used at the 19- and 28-GHz outputs.

The 19.04-GHz signal is switched at a 1.0-kHz rate between two output flanges for transmission to orthogonally polarized antennas. The 28.56-GHz carrier is sinusoidally phase modulated at 264.4 or 528.9 MHz with an index of about 0.9.

This paper describes the circuit configurations of the two transmitters, the performance achieved by the electronic assemblies comprising the Beacon, and the operating modes and overall performance of the Beacon itself. In addition, it presents the testing requirements for space qualification at all levels of integration.

### **Introduction**

The technical challenge of the Centimeter Wave Beacon project was to design and build five\* highly reliable, highly stable, satellite-borne

\* Designated FS (flight spare), F1, F2, F3, and F4.

transmitters delivering 0.6 and 1 W, respectively, in the 19- and 29-GHz satellite communications bands. The Beacons were to be mounted externally on the spacecraft antenna mast; thus, they needed self-contained thermal and radiation control. In addition, to enhance reliability, minimize weight, and achieve long life, it was decided that the Beacon electronics should be all solid state, including the output amplifiers.

Each Centimeter Wave Beacon system consists of two containers, subsequently referred to as components, mounted on either side of the COMSTAR satellite antenna reflector support mast at the elbow. One component holds the redundant signal generation circuits and the multipliers, power conditioner, and final amplifier for the 19-GHz signal, while the other holds the multipliers, power conditioner, and final amplifiers for the 29-GHz signal.

The two components are interconnected by a multiwire cable for telemetry and command and two semirigid coaxial cables for delivering sub-carrier and modulation frequencies from the 19-GHz component to the 28-GHz component. Figure 1 is an external view of the two components and cables.

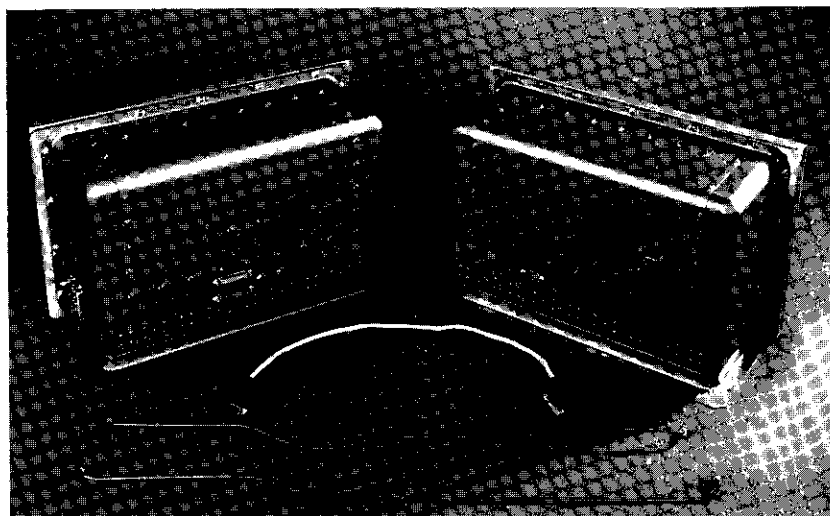


Figure 1. External View of 19- and 28-GHz Components and Cables

With only minor exceptions, the assemblies comprising a complete Beacon system—the power circuits, telemetry and command circuits, signal generation circuits, VHF multipliers and amplifiers, and microwave

assemblies—were developed at COMSAT Laboratories, as were the mechanical structures and thermal control hardware.

This paper describes the overall design of the Beacon transmitters and their component parts, the basic physical structure, thermal considerations, and the tests and techniques employed to ensure space qualification.

### Physical structure

The following basic physical requirements were imposed by COMSAT GENERAL in coordination with the spacecraft manufacturer:

- a. the Beacon must be packaged in two components to be mounted on either side of the mast;
- b. the total weight must be less than 30 lb (13.6 kg);
- c. the total DC power must be less than 70 W, to be taken approximately equally from two separate spacecraft buses.

The weight requirements dictated aluminum construction, not only for the containers but for the waveguide assemblies and chassis within. The external environment and the 70 W to be dumped required a minimum thermal radiator area of 170 in<sup>2</sup> (0.109 m<sup>2</sup>) for each component.

Because of the requirement for approximately equal DC power levels, the 28-GHz IMPATT amplifier and its power conditioner were placed in one component and the 19-GHz IMPATT amplifier, its power conditioner, and the frequency source in the other. The six IMPATT modules of the 28-GHz amplifier were spread over the mounting surface to avoid excessive concentrations of heat in one area.

A thermal analysis indicated that the diurnal temperature variations of the assemblies inside the containers could be held to no more than about 35°C, centered at about 20°C while operating, but that loss of power could cause the temperature to drop to the cryogenic range. To allow the Beacon to be turned off without risking damage from extremely low temperature, it was decided to incorporate simple electrical heaters in each component. Thus, external constraints strongly affected the physical design of the Beacon. A more detailed discussion of the mechanical and thermal design, and photographs of the external appearance and mounting of the Beacon are provided in a companion paper [1] in this issue.

### Signal characteristics

The Beacon signal characteristics which were specified in conjunction with the end user, Bell Telephone Laboratories, further defined the Beacon electronics design. These signal specifications are listed in Table 1.

TABLE 1. BEACON SIGNAL CHARACTERISTICS

Parameter	Center Frequency (GHz)	
	19.040	28.560
Long-Term Frequency Stability	$< \pm 1.0$ ppm, -10°C to 35°C	$< \pm 1.0$ ppm, -10°C to 35°C
Frequency Jitter	90% of power in 100-Hz band	90% of power in 150-Hz band
Modulation	Output switched between 2 ports at 1.0-kHz rate	264.4 MHz (FS, F1, and F3) or 528.9 MHz (F2 and F4); phase modulation index of approximately 0.9
Switching Time (ns)	$< 10$	
Switching Frequency Stability, Medium Term	$< 1$ part per $10^7$ over 10 minutes	
Min Power (dBm)	27 (both ports)	28 (carrier), 21 (sidebands)
RF Power Stability per Year (dB)	$\pm 0.5$	$\pm 0.5$

A high-frequency (fifth overtone) crystal oscillator with a frequency of 132.222 MHz was chosen for the source. A vhf crystal was used to reduce the number of multiplications needed to reach the output frequency and hence minimize multiplier circuitry and output phase noise. Therefore, carrier and modulation frequencies are coherent.

A special effort was made to minimize source phase jitter [2] because jitter limits the minimum signal which can be received. The jitter bandwidth achieved was better than the specification by an order of magnitude.

### Beacon circuits

In Figure 2, which is a simplified block diagram, the 28-GHz transmitter chain and its power conditioner are above the dashed line. Below the line are the signal sources, the 19-GHz multiplier and amplifier chain, and their power conditioners.

### 19-GHz component

#### SOLID-STATE SOURCE CHAIN

The crystal oscillator and doubler constitute the solid-state source. The crystal is stabilized against temperature change by a barium titanate

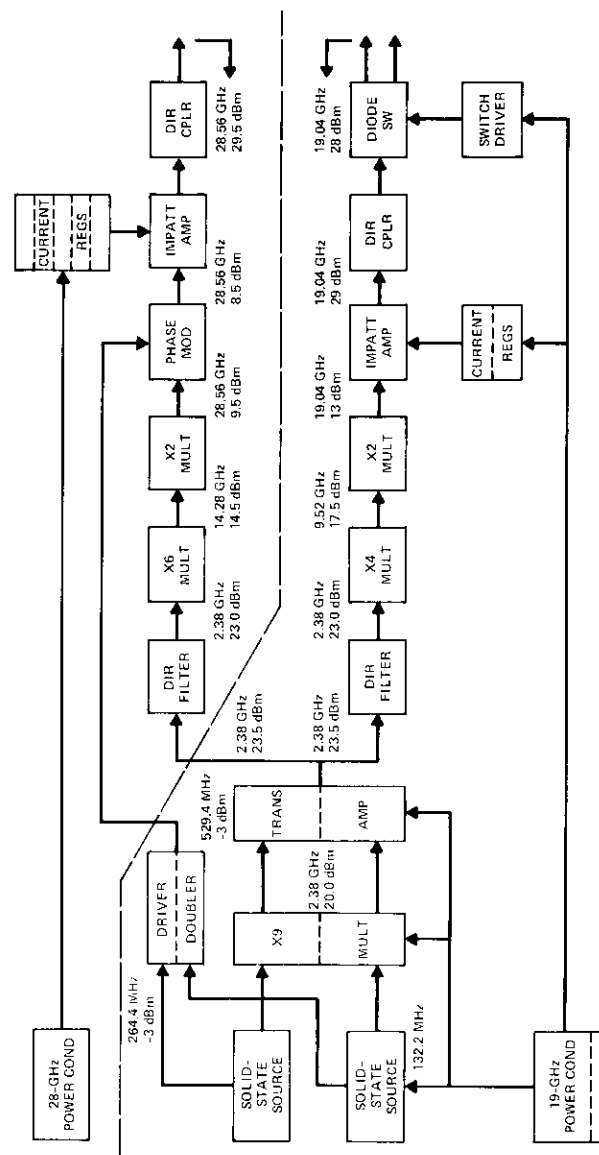


Figure 2. Beacon Block Diagram

thermistor, which is attached to the crystal can and maintains the crystal temperature to within  $\pm 4^\circ\text{C}$  at  $45^\circ\text{C}$  over the ambient range of  $-10^\circ\text{C}$  to  $40^\circ\text{C}$ . The oscillator is followed by a transistor doubler, which delivers 17.5 dBm at 264.444 MHz. The doubler is not only part of the signal multiplier chain, but it also isolates the oscillator from the following circuitry and provides output at the correct frequency for the driver of the phase modulator of the 28-GHz signal. Additional information on the design and performance of the solid-state source is available in a companion paper [2].

The signal path continues from the solid-state source to a  $\times 9$  transistor multiplier delivering 20 dBm at 2.38 GHz, and then passes through a power amplifier to provide 26.5 dBm at 2.38 GHz. The transistor multiplier which has gain maintains the signal at a reasonably constant level despite the high order of multiplication.

The operating and redundant units of each of these assemblies are packaged together to minimize weight. The two 2.38-GHz power amplifiers are connected to two ports of a 3-dB hybrid; one of the output arms of the hybrid leads to the 19-GHz multiplier chain, and the other leads to the 28-GHz multiplier chain. Thus, either amplifier powers both multiplier chains without RF switching. The DC switching is arranged so that only one source chain can operate at a time. The 2.380-GHz frequency is both a multiple of the oscillator frequency common to 19.040 and 28.560 GHz, and the largest such frequency at which efficient transistor power gain can be achieved. Figure 3 is a photograph of the 19-GHz component.

#### 19.04-GHz MICROWAVE CHAIN

Proceeding along the chain that culminates in the 19-GHz output, the signal passes through a directional filter and then a  $\times 4$  multiplier followed by a varactor doubler to deliver 13 dBm at 19.04 GHz. The directional filter, which employs two directional couplers on a ring resonator, is made on a 1- x 1-in. alumina substrate. Its purpose is to provide a matched load to both the 2.38-GHz amplifier and the  $\times 4$  multiplier outside the operating frequency range, thus controlling any out-of-band interaction between the two assemblies. The  $\times 4$  multiplier uses a silicon step recovery diode, and the doubler uses a gallium arsenide varactor. An isolator is included between the multipliers to ensure stability. A single  $\times 8$  multiplier was not used because silicon step recovery diodes have a transition time that is too long for efficient harmonic content above about 15 GHz;

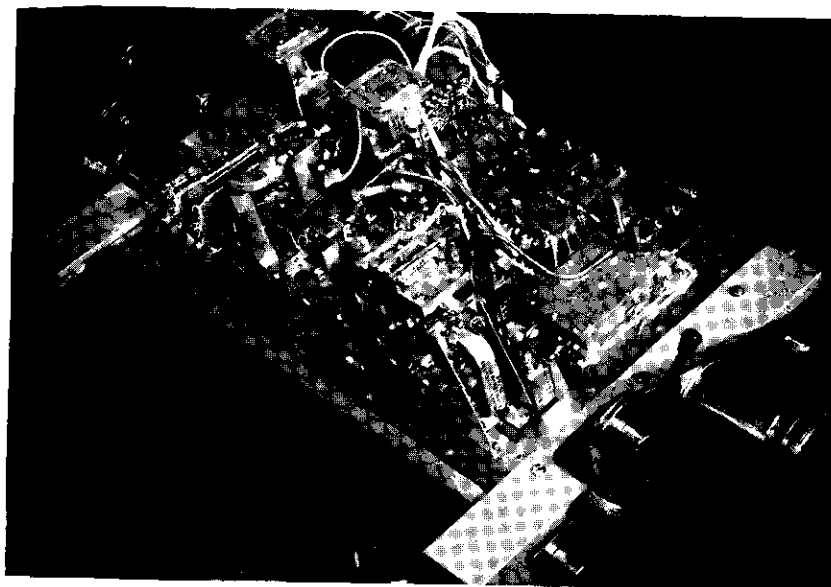


Figure 3. 19-GHz Component

multiplication using varactors without forward charge storage is more efficient above that frequency.

#### 19-GHz IMPATT AMPLIFIER

The signal at 19.04 GHz is used to drive the IMPATT amplifier, which consists of two circulator-coupled stages. The first stage has 10-dB gain, and the second 6-dB gain, giving an output power of 29 dBm.

IMPATT amplifiers were selected because they provide reasonable DC-to-RF conversion efficiency. Through screening and testing techniques, the IMPATT diodes used in the 19-GHz amplifiers were found to have a mean time to failure of the order of 500,000 years at the operating temperature levels. These silicon diodes (N<sup>+</sup>NP) are mounted on a diamond heat sink to achieve a thermal resistance of less than  $14^\circ\text{C}/\text{W}$ . Typical output stage operation is about 180 mA and 48 V, giving an average operating temperature of about  $145^\circ\text{C}$ ; added RF power is about 650 mW, for an efficiency of about 7.5 percent.

The IMPATT stages are energized by DC current regulators that provide a bias source whose impedance is greater than 100 ohms from DC to over

100 MHz. The high impedance is necessary to prevent tuning-induced oscillations and burnout.

Isolators are used before and after the amplifier and between stages to prevent interaction between stages. Each stage dissipates about 7.5 to 8 W, which is removed through the baseplate on which the stages are mounted.

A 30-dB crossguide coupler with Schottky barrier diode detector measures the signal level for telemetry. The signal is switched at a 1-kHz rate between two output waveguides. On the spacecraft, these output waveguides connect to antennas which radiate the signal in orthogonal polarizations. The switch has two PIN diodes in each output arm. A loss of less than 1 dB is incurred in the switch so that the peak level delivered to each output flange is a nominal 28 dBm. Switch isolation is greater than 40 dB.

The switch driver uses a temperature-compensated crystal to set the 1.0-kHz switching rate. The frequency drift is held to a specification of less than 1 part in  $10^7$  over 10 minutes or  $3^\circ\text{C}$  so that the precise energized polarization will be known at a receiving station even after a 10-minute fade. Switching from one waveguide to the other occurs in about 4  $\mu\text{s}$ . The switch driver circuitry is arranged so that failure of the 1-kHz oscillator will cause all the 19-GHz power to be delivered to one of the two output waveguides.

#### MODULATOR DRIVER/DOUBLER

Figure 2 also shows an additional path from the solid-state source to the driver/doubler. This unit accepts 264 MHz from the solid-state source, amplifies it, and sends it to the 28-GHz component, where it drives the phase modulator. For Beacon flight models F2 and F4 a transistor doubler follows the driver to raise the modulation frequency to 529 MHz.

Redundant driver/doublers are connected for mutually exclusive operation with the redundant source chains. RF switching is avoided by connecting the output of the two driver/doublers to a 3-dB hybrid whose third port leads to a connector for delivery to the 28-GHz component. The fourth port of the hybrid goes to a connector in the side of the 19-GHz container for external test purposes. This connector is normally mated to a matched termination.

The driver/doubler can deliver about 15 dBm to the hybrid. In addition, a negative DC bias of about 1 V is generated in the driver/doubler and carried on the center conductor of the interconnection cable to the phase modulator diode in the 28-GHz component.

#### 19-GHZ POWER CONDITIONER

The 19-GHz power conditioner, consisting of four independent solid-state power supplies, a heater control and sequencing circuit, and the Beacon telemetry and command processing circuit, provides DC power at the proper voltages to the solid-state sources, the telemetry circuits, the 19-GHz IMPATT amplifier, and 19-GHz switch driver. It operates at approximately constant input power over the spacecraft unregulated bus voltage range of 24.5 to 48 VDC. It receives eight command signals from the spacecraft command system and provides five analog telemetry data channels and four status indicator outputs to the spacecraft telemetry system.

The telemetry power supply, which provides 160 mW of +12- and -21-VDC power to the telemetry processing circuits, consists of a voltage regulator and a hybrid circuit DC/DC converter. This supply is energized when either solid-state source or either storage heater is activated.

Regulated 24-, 17-, and -3-VDC power is provided by each of two supplies associated with the redundant solid-state sources. These voltages are used by the solid-state source, crystal heater and  $\times 9$  multiplier, and 2.38-GHz transistor amplifier, respectively. The supplies consist of voltage regulators which provide regulated 24-VDC power and also operate a DC/DC converter. The regulators have an efficiency of 81 percent at 24.5-VDC input and draw 275 mA from the bus.

The main power switch routes the unregulated bus voltage to either the heater control switch or the IMPATT supply by means of a relay. The power switch DC line is fused to protect other spacecraft bus usages.

The IMPATT supply is a chain of cooperating circuits, some of which have multiple functions. Within the IMPATT supply, the low-level regulator is a high-efficiency switching regulator which supplies 16 VDC to another circuit, the bias and drive converter. The bias and drive converter contains a DC/DC converter that provides 5 VDC for internal logic,  $\pm 10$ -VDC bias for the IMPATT current regulators, and a square-wave drive for the next circuit, the pulse width modulated (PWM) regulator/converter. The PWM regulator/converter converts unregulated bus voltage to a regulated 54 VDC to supply current to the IMPATT diodes. A feedback control loop modulates the pulse width to regulate the output voltage to within  $\pm 1$  percent for bus voltage from 24 to 48 V. The IMPATT supply operates at an overall efficiency greater than 84 percent.

Six paralleled resistive heaters are included in the 19-GHz component to maintain the component above  $-20^\circ\text{C}$  when the Beacon is otherwise

inoperative. The resistors provide a total power of 15 W of heat at the minimum bus voltage of 24.5 V.

### 28-GHz component

The multiplier chain that leads to the 28.56-GHz output is shown above the dashed line in Figure 2. This chain receives a 23.5-dBm CW signal at 2.38 GHz from the 19-GHz component via an interconnecting semirigid cable. Another semirigid cable carries the modulation signal from the 19-GHz component to the 28-GHz component. A conventional wiring cable conveys telemetry and command signals between the two components. Prime power for the 28-GHz chain power conditioner is taken from a spacecraft bus which is different from that used for the 19-GHz component. Figure 4 is a photograph of the 28-GHz component.

#### 28-GHz MICROWAVE CHAIN

The 2.38-GHz signal input to the 28-GHz component passes through a directional filter, is multiplied to 14.28 GHz by an  $\times 6$  step recovery diode multiplier, and is then doubled to 28.560 GHz. The directional filter is identical to that in the 19-GHz component. The  $\times 6$  multiplier is similar to the  $\times 4$  used in the 19-GHz component; remarks concerning diode frequency limitation for the  $\times 4$  multiplier apply to the  $\times 6$  multiplier as well. The doubler to 28.56 GHz, which is similar in concept to the doubler to 19 GHz, also employs a gallium arsenide varactor. The doubler delivers 9.5 dBm at 28.560 GHz to the phase modulator.

The phase modulator [3] consists of a varactor mounted across a waveguide which terminates one port of a 3-port circulator. The varactor is biased and driven at the modulation frequency from the 19-GHz component. A 50-ohm matching circuit is mounted in the modulation line at the phase modulator. Its purpose is to dampen oscillations or other reactive detuning effects which might occur at the modulation frequency or its harmonics because both the input impedance to the varactor and the output impedance of the modulation driver are mostly reactive.

The phase modulator delivers a spectrum centered at 28.56 GHz with a total power of about 7.5 dBm to the IMPATT amplifier. The first-order sideband-to-carrier ratio was set at about  $-6$  dB, an index of about 0.9, so that the carrier was at a level of about 5.75 dBm and the first-order sidebands at about  $-0.25$  dBm.

The 28-GHz IMPATT amplifier [4] has three stages; the first has about 10-dB gain, and the second and third each have about 6-dB gain. The first and second stages are circulator coupled, but the third has an arrange-

ment of four hybrid couplers that divide the input power for amplification by four IMPATT amplifier modules, and then combine the amplified signals to form a single output. The total output power is nominally 29.5 dBm, but actual Beacon systems tended to deliver about 1 dB more.

P+PN (complementary) IMPATT diodes used in FS (D1 COMSTAR satellite) and F1 Beacons required a negative operating voltage. The diodes used in F2, F3 (D2 COMSTAR satellite), and F4 were of the N+NP type (conventional) using positive operating voltage. Both types of diodes provided added RF power greater than 250 mW. The former structures exhibited slightly greater efficiency (7.5 vs 6.5 percent), but the latter diodes had diamond heat sinks which allowed them to operate at lower temperature with greater reliability.

The general design of the current regulators for the 28-GHz IMPATT diodes was the same as that used for the 19-GHz IMPATT amplifiers, with voltages, currents, and polarities appropriate to the type of diode being used.

The six 28-GHz IMPATT diode amplifier modules dissipated about 3.5 W each. As indicated in Figure 4, which shows the disposition of assemblies

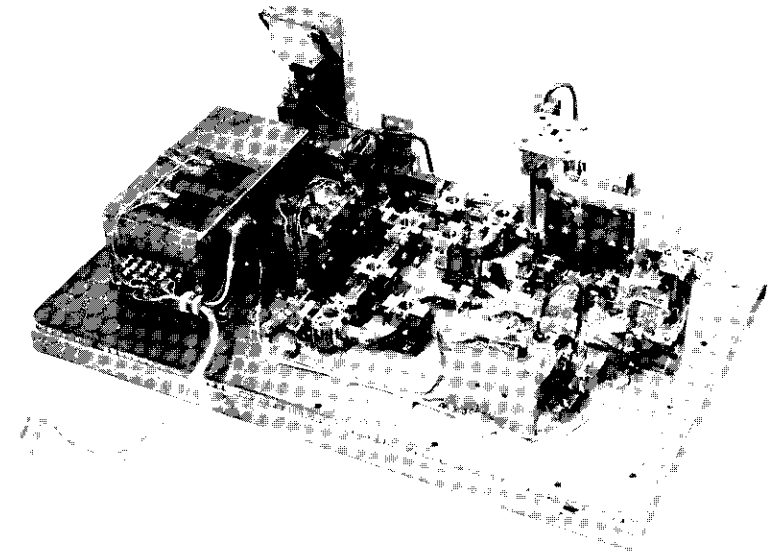


Figure 4. 28-GHz Component

in the 28-GHz component, they were widely spaced on the component mounting surface to avoid heat concentrations.

For amplifiers modulated at 264.444 MHz, the output carrier-to-sideband ratio was found to be about 1 dB lower than that at the input. This difference required no special accommodation on FS, F1, and F3. On the amplifiers (F2 and F4) modulated at 528.889 MHz, however, the output sideband-to-carrier ratio was about 4 dB low until it was corrected with a spectrum conditioner. Analysis showed that the loss of sideband level was a necessary concomitant of IMPATT amplification due to differential phase distortion between spectral components. The spectrum conditioner, a passive device, appropriately predistorts the relative spectral phases to allow the output sideband-to-carrier ratio to be the same as that at the input.

Similar to the 19-GHz signal, a 30-dB crossguide coupler and Schottky barrier diode are employed to measure the RF output power level for telemetry.

#### 28-GHZ POWER CONDITIONER

The 28-GHz power conditioner provides power at three regulated voltage levels to the three dual current regulator units which feed the 28-GHz IMPATT diodes, and switches unregulated power to the heaters in the 28-GHz box. It accepts unregulated DC power from the spacecraft bus at voltages of +24.5 to +48 VDC.

The unit has six sections: a command processing logic block, an input power switch, a heater control switch, a low-level regulator, a bias and drive converter, and a PWM regulator/converter. The command processing logic interfaces with the command lines from the 19-GHz power conditioner to provide proper sequencing of heater and power converter turn-on and turn-off.

The power switch routes power to either the heater control switch or the IMPATT supply by means of a relay. The relay is latched into the heater position by the "all OFF" command. The unregulated spacecraft bus is protected by a fuse.

The low-level regulator is a self-starting, high-efficiency switching regulator. It supplies regulated +16-VDC power to the bias and drive converter. The bias and drive converter contains a driven DC/DC converter which provides +5-VDC power for various internal logic functions, square-wave drive to the PWM regulator/converter, and +10-VDC bias power to the dual current regulators.

The PWM regulator/converter converts the unregulated bus voltages to a regulated voltage level to supply current to the IMPATT diodes. A feedback control loop containing discrete and integrated circuits modulates the pulse width to regulate the output voltage for bus voltage variations of +24 to +48 V. This supply operates with an overall efficiency of 86 percent or more over the full +24- to +48-V bus voltage range.

The 28-GHz component includes seven film heaters of the type used for the 19-GHz component heater. About 15 W of heat are provided at the minimum bus voltage of 25.4 VDC. These heaters will hold the minimum temperature inside the 28-GHz component to about  $-20^{\circ}\text{C}$ .

#### Commands and telemetry

The command hardware is designed into the power conditioners. Commands are activated as part of the normal spacecraft command system using 40-ms command pulses of  $-10 \pm 3$  V. Protection is provided against false command pulses and open or short circuits on the command line and its return. Beacon commands available to the spacecraft operator are listed in Table 2.

TABLE 2. BEACON COMMANDS

Launch Sequence ON
Source Chain A ON/Source Chain B OFF
Source Chain B ON/Source Chain A OFF
19-GHz Amplifier ON/19-GHz Component Heater OFF
19-GHz Component Heater ON/19-GHz Amplifier OFF
28-GHz Amplifier ON/28-GHz Component Heater OFF
28-GHz Component Heater ON/28-GHz Amplifier OFF
All OFF

The launch sequence is a single command that turns on source chain A and 19- and 28-GHz amplifiers, thus activating the Beacon for full operation. All OFF removes all power to the Beacon except that needed to allow a subsequent command to take effect. The telemetry circuits are activated when either source is on or either heater is on. Telemetry is off when the all OFF command is in effect. Telemetered information is listed in Table 3.

Conventional PN junction Schottky barrier microwave detector diodes are used in the coupler-detectors to monitor RF power levels. Temperatures are monitored with thermistor bridge circuits. These outputs are converted in the power conditioners to give about 5 V at the maximum levels.

TABLE 3. TELEMETERED INFORMATION

19-GHz RF Power Level
28-GHz RF Power Level
19-GHz Solid-State Source Temperature
19-GHz IMPATT Amplifier Temperature
28-GHz IMPATT Amplifier Temperature

Four status bits, listed in Table 4, give the spacecraft operator timely information about the operational condition of the Beacon.

TABLE 4. STATUS BITS

Source A ON
Source B ON
19-GHz Component Heater ON
28-GHz Component Heater ON

**Test set**

Three test sets, designed to simulate the spacecraft bus, telemetry, and command circuits, were built. Each test set allows the bus voltage to both Beacon components to be varied from below the level at which the low-voltage cutout circuits in the power conditioners turn the Beacons off (about 20 V) to the maximum voltage expected from the spacecraft (48 V). (This latter value will occur only briefly as the spacecraft emerges from eclipse.) The nominal bus voltage is about 30 V. Bus voltage and current to each Beacon component are monitored by meters on the test set.

All commands can be sent from the test set from either of two encoders, and Beacon response to false commands can be tested by adjusting command pulse magnitude and duration. The test set monitors telemetry voltages produced by the Beacon components using digital readout meters. Status bits are displayed by four small red lamps.

**Beacon system performance**

Typical Beacon performance statistics are summarized in Table 5. The Beacon oscillators passed a go/no go jitter test in which it was observed that at least 90 percent of the oscillator signal power referred to 19 GHz was transmitted through a 10-Hz filter. The 19.04-GHz signal received from the D1 COMSTAR satellite and the signal from a similar oscillator

located in the laboratory were tracked with a phase-locked loop having 0.5-Hz bandwidth. Long-term signal frequency stability is primarily a function of temperature. The diurnal variation is typically about half the allowed variation of  $\pm 1$  part per million, which is about 19 kHz at 19 GHz and 28 kHz at 28 GHz. The daily temperature variation of the 1.0-kHz switching frequency was also observed to be about one part per million.

TABLE 5. CENTIMETER WAVE BEACON PERFORMANCE VALUES

Parameter	Component		
	19.04-GHz	28.5-GHz	Both
Weight (lb)	15.5	11.0	26.5
DC Power at 30 V (W)	33.6	33.6	67.2
Bus Range (V)			24.5-48
Low-Voltage Cut-Off	17.8-20.6	19.5-20.5	
Generated Line Noise, 10 Hz to 100 kHz			<50 mV into 5 $\Omega$
Radio Frequency (GHz)	19.040	28.560	
RF Stability			
Long Term			1 part in 10 <sup>6</sup> (-10°C < T < 35°C)
Short Term			90% of power in 10-Hz band referred to 19 GHz
19-GHz Output Switch- ing Frequency	1.00 kHz		
Switching Frequency			
Medium-Term	<1 part in 10 <sup>7</sup> over 10		
Stability	min		
Long-Term Stability	1 part in 10 <sup>6</sup> (-10°C < T < 35°C)		
Switching Time (ns)	<10		
Switch Isolation (dB)	40		
Spurious Output (-dBc)		>40	>40
RF Output Power (dBm)	28 (total, both out- puts)	30.5 total	
RF Output Power (dBm)			
Carrier		29	
Sidebands		22	
Power Stability, 0°C-40°C (dB)	<1.0	<1.0	
EMI levels, (dBW in 4 kHz), 3.7-6.5 GHz	<-140	<-140	

Figure 5 shows the measured 19.04-GHz output power vs temperature for the F3 Beacon (D2 COMSTAR). The data were taken during a thermal vacuum test of the entire Beacon. Figure 6 shows the telemetered 19.04-GHz output power of the same Beacon for two days in the space environment.

Figure 7 shows thermal vacuum test measurements of output power for the 28.560-GHz carrier and its two sidebands for the FS Beacon (D1 COMSTAR). The telemetered total 28.560-GHz spectrum power of the same Beacon for five days in the space environment is shown in Figure 8.

### Space qualification testing

The mechanical, thermal, electrical, and microwave assemblies were, for the most part, designed and developed at COMSAT Laboratories specifically for application to the Centimeter Wave Beacon. The solid-state source,  $\times 9$  multiplier, and step recovery diode multipliers were upgraded versions of similar assemblies developed for use in a centimeter wave transponder flown on the ATS-6 satellite [5], [6]. The engineering models were subjected to thermal, vacuum, and mechanical vibration tests in the operating condition while critical performance factors were observed.

An engineering model of the complete Beacon system was constructed from the engineering model assemblies, tested electrically and thermally, and used to test for and correct any interaction problems with assemblies.

The first Beacon manufactured was a prototype made to flight standards and subsequently denoted flight spare. High-reliability parts were used throughout. All electrical and microwave assemblies were tested live under thermal vacuum and mechanical vibration conditions. All assembly work on flight units, both assemblies and components, was done in a clean room.

On completion of each Beacon system, the two components were given individual vibration tests while operating and connected to the other component, which was also operating. Later, certain of the components were also given temperature experience in vacuum. The thermal vacuum test began with a cold soak at  $-50^{\circ}\text{C}$ , turn-on at  $-20^{\circ}\text{C}$ , and then two or more days of thermal cycling simulation in real time in the expected space environment (nominal variation about  $35^{\circ}\text{C}$ ) with temperature extended by  $5^{\circ}\text{C}$  at the warmest and coolest times. For the prototype an additional  $5^{\circ}\text{C}$  at extremes was used. The prototype was also subjected to a more rigorous vibration regime. Beacon performance was monitored continuously during the three to five days of thermal vacuum testing.

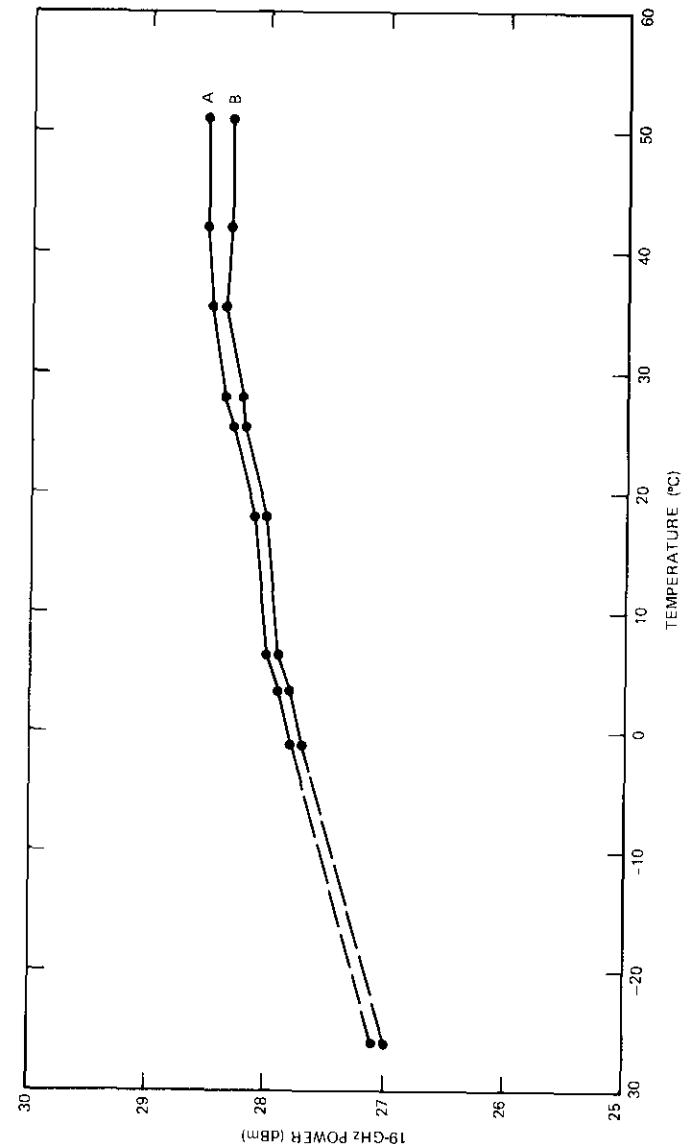


Figure 5. 19-GHz Output (F3) with Temperature

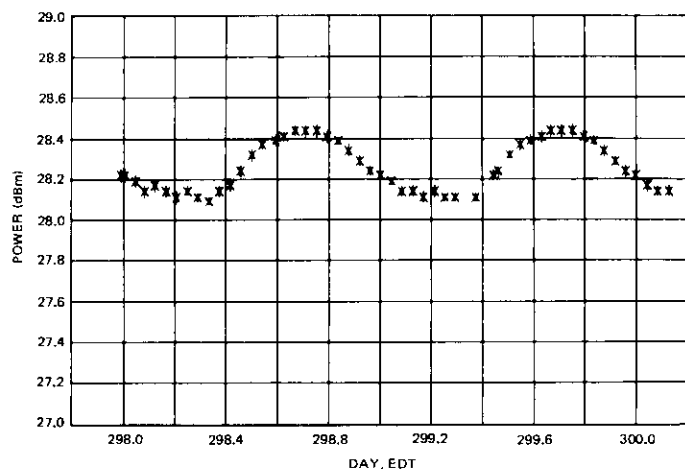


Figure 6. Beacon F3 19-GHz Power vs Time

Performance characterization tests were run before and after all environmental tests. Discrepancies were corrected and the test repeated. Any mechanical change in a completed component was followed by revibration.

The final environmental test was a thermal vacuum test for the complete Beacon system run in COMSAT Labs' large liquid-nitrogen-cooled thermal vacuum chamber. Sunlight was simulated by quartz rod infrared lamps.

Early in the program mechanical/thermal models of the components had been vibrated and run in the large thermal vacuum chamber to verify and correct mechanical and thermal calculations.

### Conclusion

This paper has discussed the basic electrical features of the Centimeter Wave Beacon, as well as the testing procedures used in development and manufacturing to ensure reliable, space-qualified hardware. At the time this paper was written, two of the five Beacons manufactured were in orbit operating on COMSTAR D1 and D2 communications satellites.

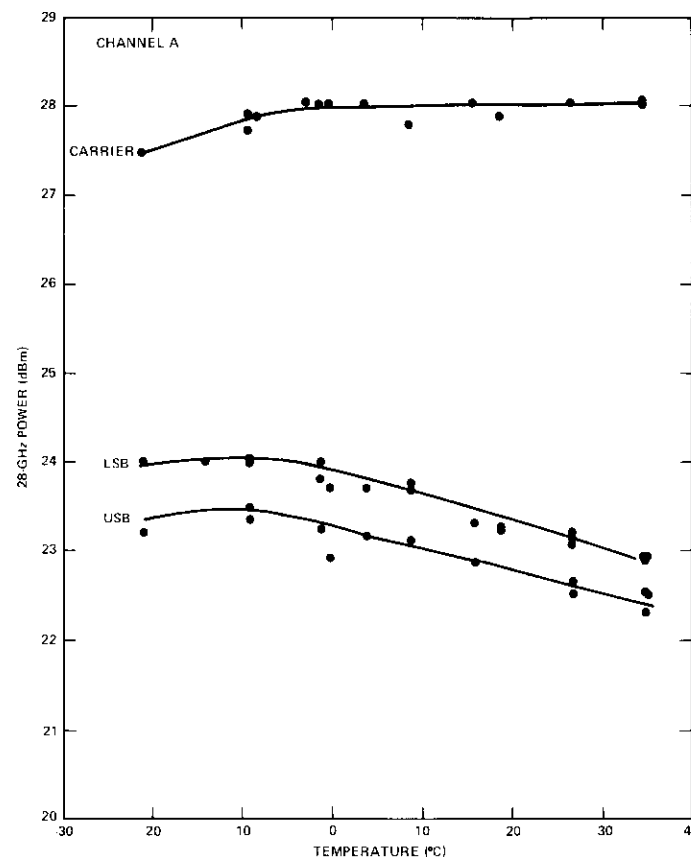


Figure 7. 28-GHz Output Power (FS) with Temperature

### References

- [1] N. Hyman et al., "Thermal Structural Design Aspects of the Centimeter Wave Beacon," *COMSAT Technical Review*, Vol. 7, No. 1, Spring 1977, pp. 171-196.
- [2] R. E. Stegens, "Low-Jitter Local Oscillator Source for the COMSTAR Beacon," *COMSAT Technical Review*, Vol. 7, No. 1, Spring 1977, pp. 153-169.

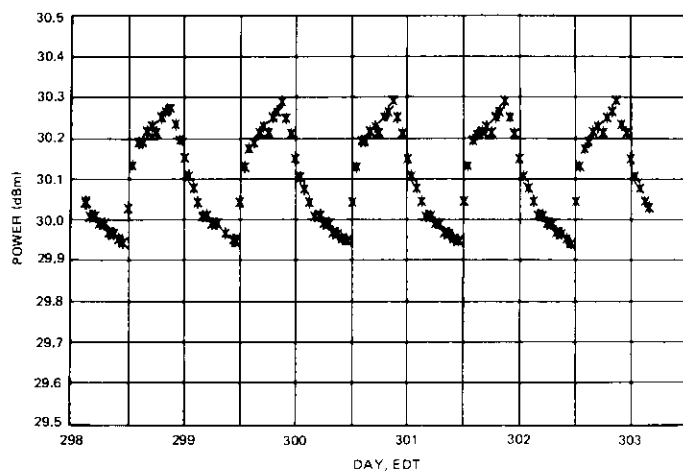


Figure 8. Beacon FS 28-GHz Power vs Time

- [3] Y. S. Lee, "28-GHz Varactor Continuous Phase Modulator," *COMSAT Technical Review*, Vol. 5, No. 2, Fall 1975, pp. 329-354.
- [4] M. Barrett, "19- and 28-GHz IMPATT Amplifiers," *COMSAT Technical Review*, Vol. 7, No. 1, Spring 1977, pp. 129-152.
- [5] L. Westerlund, J. L. Levatich, and A. Buige, "The ATS-F COMSAT Millimeter Wave Propagation Experiment," *COMSAT Technical Review*, Vol. 3, No. 2, Fall 1973, pp. 323-340.
- [6] "The ATS-F COMSAT Propagation Experiment Transponder," edited by A. Berman, *COMSAT Technical Review*, Vol. 3, No. 2, Fall 1973, pp. 341-374.



William J. Getsinger received a B.S.E.E. from the University of Connecticut in 1949 and an M.S.E.E. and the degree of Engineer in Electrical Engineering from Stanford University in 1959 and 1961, respectively. Since 1950 he has worked on microwave components at Technicraft Laboratories, the Westinghouse Electric Company, Stanford Research Institute, and M.I.T. Lincoln Laboratories. In 1969 he joined COMSAT Laboratories, where he is presently Manager of the Microwave Circuits Department.

Index: IMPATT amplifiers, power measurement, beacon, amplifier diodes

## 19- and 28-GHz IMPATT Amplifiers

M. J. BARRETT

(Manuscript received September 29, 1976)

### Abstract

The output RF power for the 19- and 28-GHz Beacons is produced by solid-state IMPATT diode amplifiers. The 19-GHz amplifier is driven by a cw signal at a power level of 13 dBm. The amplifier has two stages, each containing a single diode. The first stage has a gain of 11.3 dB and operates below saturation, while the second operates at saturation with 4.7-dB gain. The amplifier output power is 29 dBm and the overall gain is 16 dB. The total DC power consumption of the amplifier diodes is approximately 16 W.

The 28-GHz amplifier is required to amplify a phase modulated signal of approximately 1-GHz maximum bandwidth. With an input power level of 8.5 dBm, three cascaded IMPATT diode stages provide 21 dB of gain. The input stage, containing one diode, provides 9-dB gain. The second stage, operating close to saturation, has approximately 6 dB of gain. The output stage, also with 6-dB gain, combines the power of four diodes to provide an almost saturated output power of 29.5 dBm. The total DC power consumption of the six IMPATT diodes is approximately 20 W.

### Introduction

The final output power for both 19- and 28-GHz Beacon transmitters is provided by IMPATT diode amplifiers. IMPATT diodes have been used as microwave power amplifiers over a wide frequency range [1]-[3]. The conditions required for high-power operation at optimum efficiency have

been described [4], [5], as have methods of combining multiple diodes to obtain higher power levels [6], [7]. If due attention is paid to the particular characteristics of IMPATT diodes [8]–[11], reliable and stable amplifiers may be designed.

Gain and output power specifications have dictated the use of multi-stage amplifiers. While the 19-GHz amplifier has been realized using two stages, each containing one diode, the 28-GHz amplifier requires three stages. The third or output stage combines the power of four individual amplifier modules to achieve the required performance. Both amplifiers have been built using rectangular waveguide as the basic microwave transmission medium. Waveguide ferrite circulators and isolators provide interstage coupling and isolation. An array of four 3-dB hybrid couplers is used as a power splitter and combiner in the output stage of the 28-GHz amplifier. DC bias to the diodes is provided by current regulators, which are in turn supplied by DC-to-DC converters operating off the spacecraft power bus.

The amplifiers have been qualified for spacecraft use by testing in an operating condition through 3-axis vibration and separately over a  $-30^{\circ}\text{C}$  to  $+55^{\circ}\text{C}$  temperature range in a thermal vacuum chamber.

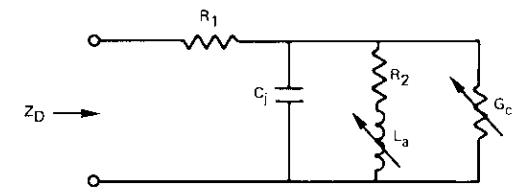
### IMPATT diode amplifier characteristics

IMPATT diodes are useful as the active elements in microwave amplifiers because under suitable conditions of DC bias they exhibit negative resistance which can be available over a frequency range of about one octave. The center frequency depends on controllable parameters of the semiconductor junction.

Negative resistance is exhibited when the diode is reverse biased into the avalanche region. In this region the diode acts as an almost constant voltage device so that a current-regulated supply is required to bias it. Similar to all negative resistance devices, the negative resistance exhibited by IMPATT diodes is nonlinear. In an amplifier this results in gain compression and eventually saturation with increasing drive level.

Figure 1 is a widely accepted equivalent circuit for an unpackaged IMPATT diode. It contains two nonlinear elements, one resistive and one reactive. When the diode is connected to a suitable generator impedance to operate as an amplifier, variation of the diode negative conductance,  $G_c$ , results in gain variation, and variation of the avalanche inductance,  $L_a$ , results in frequency tuning. Both  $G_c$  and  $L_a$  are functions of bias current and RF voltage. Increasing bias current increases the gain and the gain center frequency, while increasing the RF power level has the opposite effect.

Increasing the RF power also increases the bandwidth of the amplifier.



- $R_1$  = SERIES LOSS RESISTANCE
- $R_2$  = SHUNT LOSS RESISTANCE
- $C_j$  = JUNCTION CAPACITANCE
- $L_a$  = AVALANCHE INDUCTANCE
- $G_c$  = CHIP NEGATIVE CONDUCTANCE
- $Z_D$  = DIODE IMPEDANCE AT CHIP TERMINALS  
=  $R_D + jX_D$

Figure 1. Equivalent Circuit of Unpackaged IMPATT Diode

The gain of such a negative resistance amplifier is conveniently determined at the frequency of interest in terms of the diode junction series equivalent impedance  $Z_D = R_D + jX_D$  shown in Figure 1. If this impedance is connected to a generator impedance  $Z_G = R_G + jX_G$ , then the maximum gain occurs when  $X_G = -X_D$  and is given by

$$G(\text{dB}) = 20 \log \left( \frac{R_D - R_G}{R_D + R_G} \right) \quad (1)$$

provided that  $R_G > |R_D|$ .

Before the design and performance of the individual 19- and 28-GHz amplifiers are considered, it is useful to discuss the features of the basic amplifier module. The amplifier module, which is a single-port reflection amplifier containing a single IMPATT diode, is a basic building block of both amplifiers. While the detailed design of the modules and the diode types are different for the two frequencies, the design approach is the same.

Because of DC power limitations and thermal considerations, it is important that the amplifier be designed to operate at the highest practical DC-to-RF efficiency,  $\eta$ , where

$$\eta = \frac{\text{RF output power from amplifier}}{\text{DC input power to amplifier}}$$

High efficiency results when the amplifier diodes operate at the power levels at which both gain and output power levels vary nonlinearly with input power. In this high-efficiency region circuit adjustments permit tradeoffs between output power and gain. Since both amplifiers have multiple stages, careful design is required to tailor the power and gain levels of each module to its application within the amplifier. Since

$$P_o = P_i + P_{add} \quad (2)$$

where  $P_o$  = output RF power

$P_i$  = input RF power

$P_{add}$  = RF power added by the diode

the diode gain is

$$G = \frac{P_o}{P_i} = 1 + \frac{P_{add}}{P_i} \quad (3)$$

Clearly, from equations (2) and (3), both output power and gain increase as  $P_{add}$  increases.

If a suitable model for the diode RF voltage vs current relationship is assumed, it is found theoretically and confirmed experimentally that  $P_{add}$  is a function of circuit parameters, diode parameters, and the RF signal level at the IMPATT device. Further, the variation of  $P_{add}$  with the RF signal is nonlinear.

Theoretically, the maximum value of added power,  $P_{AM}$ , is equal to  $P_{OSC}$ , the oscillator power of the device. In practice, the maximum obtainable added power is usually about 1 dB less than  $P_{OSC}$ . For a given DC power to the diode, maximum conversion efficiency is achieved when  $P_{add} = P_{AM}$ . For this condition, it is desirable to determine the gain and output power which are obtained. If the gain at maximum efficiency,  $G_M$ , is defined as

$$G_M = \frac{P_i + P_{AM}}{P_i} \quad (4)$$

and the normalized output power is defined as

$$P_N = \frac{P_o}{P_{AM}} \quad (5)$$

then, from equations (2), (4), and (5),

$$P_N = \frac{G_M}{G_M - 1} \quad (6)$$

Equation (6) is plotted as curve *ABC* in Figure 2, which shows that for a maximum efficiency amplifier stage there is a tradeoff between gain and output power.

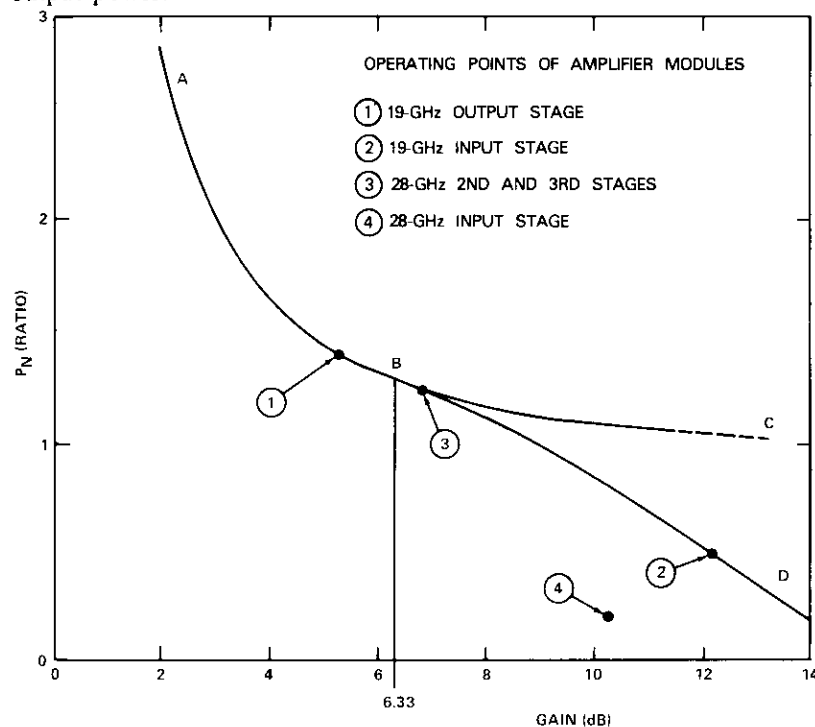


Figure 2. Normalized Output Power vs Gain for Lossless Amplifier Stage

Once the relationship between output power and gain of the desired maximum efficiency amplifier stage has been determined, it is necessary to find the conditions which will permit operation at a selected point on curve *ABC* in Figure 2. It can be shown [5] that there is a relationship be-

tween the small signal gain,  $G_S$ , and  $G_M$ , given by

$$G_S = \left( \frac{3\sqrt{G_M} - 1}{3 - \sqrt{G_M}} \right)^2 \quad (7)$$

This relationship, shown in Figure 3, is useful in designing and building high-power stages. Since the diode small signal parameters are readily measured, it is a relatively straightforward procedure to design and build a module with a given small signal gain by using equation (1).

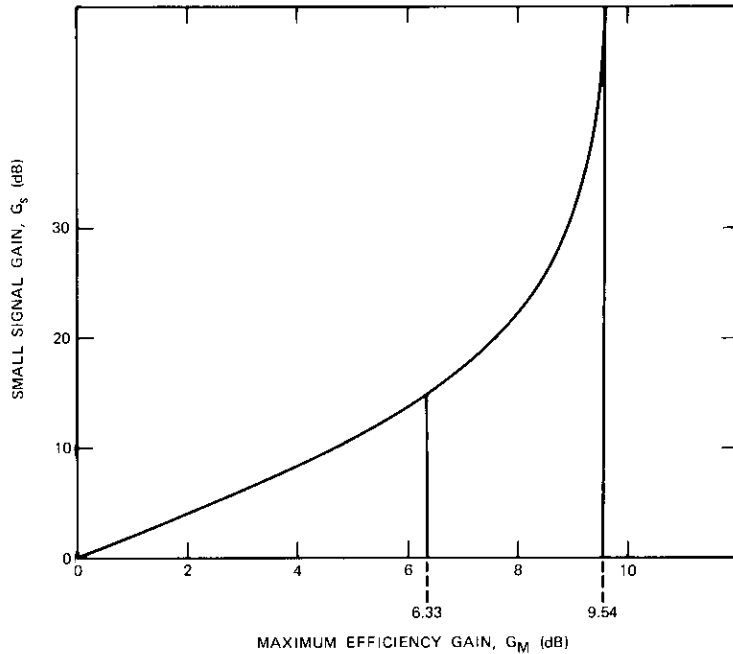


Figure 3. Small Signal Gain vs Gain at Maximum Efficiency

As shown by equation (7), definition of the small signal gain also determines the gain at maximum efficiency, and equation (6) determines the power levels. Operation at maximum efficiency is then obtained by increasing the RF drive to the module to the level given by  $P_N/G_M$ .

Because of the variation of the avalanche inductance,  $L_A$ , with RF drive, there is a shift of the frequency of peak gain as the RF drive is changed.

As an example, Figure 4 shows the swept gain vs frequency response of a single-stage amplifier at three different RF drive levels. The relationship between small signal gain and maximum efficiency gain of a particular module given by equation (7) is maintained approximately provided that the gains are measured at the peak of the gain vs frequency response.

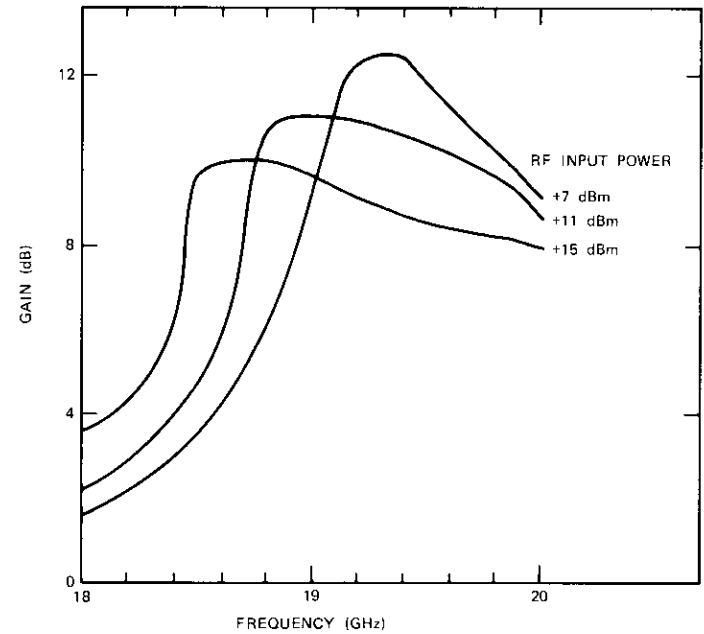


Figure 4. Gain vs Frequency for Single-Stage IMPATT Amplifier at Three Input Power Levels

Figure 3 shows that, for  $G_M \geq 9.5$  dB,  $G_S = \infty$ ; i.e., the module will oscillate when it is undriven even though it will be stable at sufficiently high drive levels. This locked oscillator mode of operation was considered undesirable for this application because failure of the amplifier RF drive would result in undesired RF radiation from the Beacon at an uncontrolled frequency. To ensure an adequate margin of stability under such zero drive conditions, the small signal gain was limited to  $G_S \leq 15$  dB. From Figure 3 it can be seen that if operation at maximum efficiency is required the gain is thus limited to  $G_M \leq 6.3$  dB.

Stable maximum efficiency amplifiers can be designed to operate at any

point between *A* and *B* on the curve of Figure 2. At maximum efficiency, gains above 6.3 dB are impossible without violating the condition that the small signal gain,  $G_s$ , be less than or equal to 15 dB. However, stage gains above 6.3 dB can be realized if the requirement for maximum efficiency is relaxed.

If the gain and efficiency of an amplifier with fixed small signal gain (e.g., 15 dB) are determined as functions of RF drive (by solving the appropriate nonlinear equation), it is found that as the gain drops from 15 to 6.3 dB the efficiency rises from zero to its maximum value. Thus, within the constraint of a fixed small signal gain there exists a trade-off between large signal gain and efficiency, and also between large signal gain and output power. The relationship between large signal gain and normalized output power of such an amplifier is plotted in Figure 2 as curve *BD*.

The composite curve *ABD* in Figure 2 represents the locus of points of stage gain vs stage output power under the double constraint of operating at the highest possible efficiency while maintaining  $G_s \leq 15$  dB for adequate stability. This curve is applicable as a performance envelope for single-stage IMPATT diode amplifiers or for any diode whose RF voltage-current relationship may be represented by the same mathematical model [5]. It is used to determine the basic high-power module properties that are realizable and consequently the combination of modules which can be used to meet the amplifier specifications. In principle, amplifier modules can be made to operate at any point on the curve *ABD*. With a reduction in efficiency, modules can also operate at any point under the curve. The operating points of the four different module designs of the 19- and 28-GHz amplifiers, to be discussed later, are plotted in Figure 2, points 1 through 4.

### DC power supplies

IMPATT diodes are operated beyond their reverse breakdown point where they are almost constant voltage devices with current variation. Accordingly, current-regulated supplies are needed. Six regulators, one to a diode, are packaged in pairs. For the three different diode types used in the amplifiers, the current regulators had to provide 80–200 mA at voltages of 36–48 V.

A significant feature of the regulators is that their output impedance should be controlled at frequencies from DC up  $\approx 100$  MHz, and in fact the impedance has been measured up to several hundred megahertz. If

the impedance is not maintained at a sufficiently high level over a sufficient frequency range, bias circuit oscillations can destroy the IMPATT diode [8]. The impedance of the regulators is controlled by active devices up to approximately 30 kHz. Beyond that frequency a passive LR filter maintains the impedance level. Figure 5 is a plot of output impedance vs frequency.

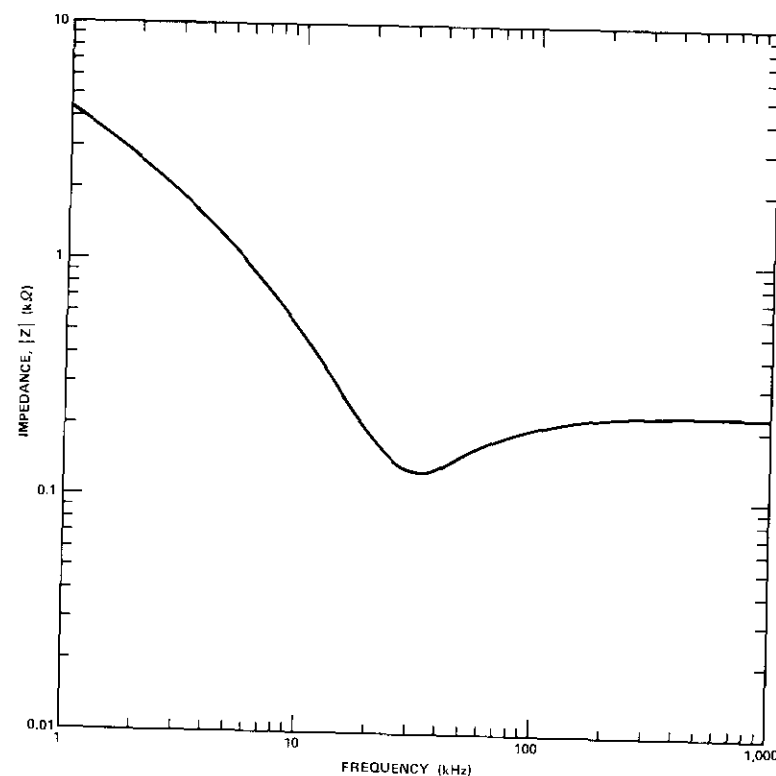


Figure 5. Current Regulator Output Impedance vs Frequency

Both  $P^+PN^-$  and  $N^+NP^-$  type IMPATT diodes have been used in the program, although each amplifier contains diodes of only one type. To accommodate the two diode polarities, two current regulator designs have been used.

Three supply voltages are required for the regulators. They are provided by a switching-type power conditioner which converts the unregulated spacecraft bus DC voltage of 24.5–48 V to the three required regulated

voltages. The power conditioner operates at approximately 85 percent efficiency.

### 19-GHz amplifier

The 19-GHz amplifier is shown in Figure 6. Figure 7 is a block diagram which also indicates the power and gain levels in the amplifier.

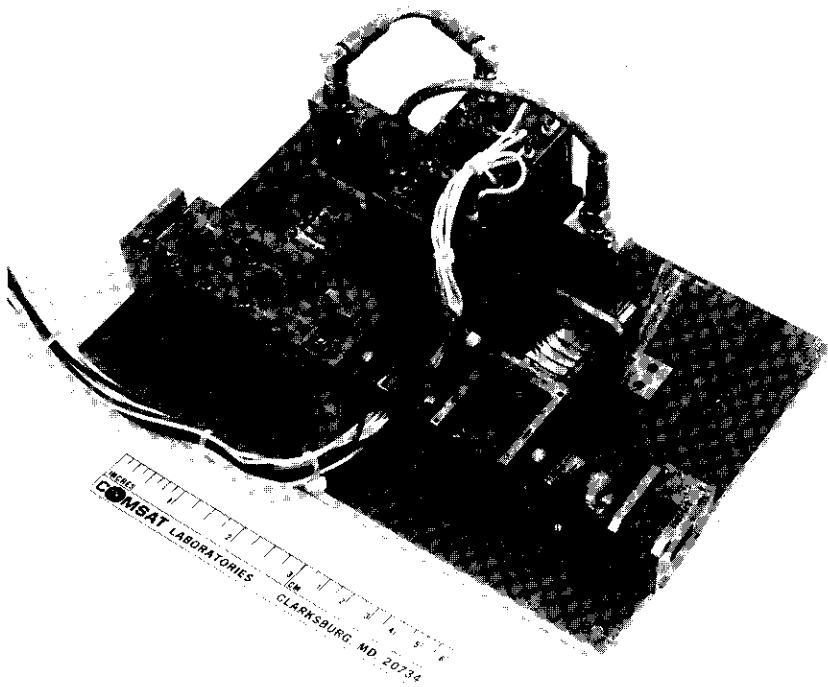


Figure 6. View of 19-GHz Amplifier

The amplifier is a 2-stage circulator-coupled design. It has 16-dB nominal gain at a center frequency of 19.04 GHz and an input RF level of +13 dBm. The two IMPATT diodes are mounted in 1-port reflection amplifier modules which are coupled to the full height WR51 waveguide of the ferrite circulators by 7-section stepped impedance transformers. Two of the circulators convert the 1-port reflection amplifier modules to 2-port transmission amplifiers, while the remaining three provide input, inter-

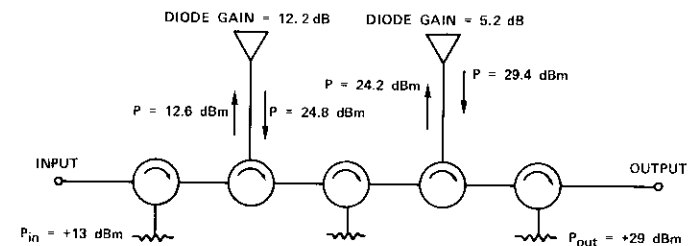
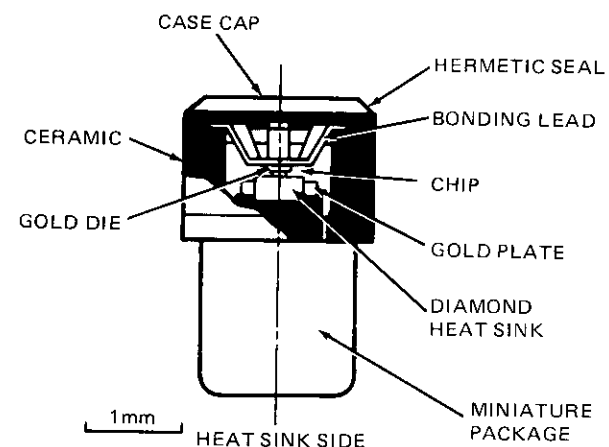


Figure 7. 19-GHz Amplifier

stage, and output isolation. Regulated DC biasing power to the diodes is provided by a dual current regulator which permits individual adjustment of the current to each diode.

### IMPATT diodes

The diodes used in the 19-GHz amplifier are of single-drift silicon  $N^+ NP$  construction purchased from Nippon Electric Company to a rigorous control specification. As shown in Figure 8, the diode chips are mounted on a diamond heat sink and encapsulated in a protective package.



MFG: NEC  
TYPE: 1ST18UR

Figure 8. 19-GHz Diode

At the operating bias of approximately 48 V and 180 mA, the diodes have an added power capability of approximately 610 mW. The diode thermal impedance is approximately 12°C/W so that in operation the maximum junction operating temperature is approximately 160°C. At this temperature the diode mean time to failure (MTTF) is predicted to be approximately 10<sup>9</sup> hours, which is sufficient to satisfy the reliability requirements of the diodes.

#### Module power and gain levels

The specified output power of the 19-GHz amplifier is 29 dBm. To allow for circuit losses, the required second stage diode output power is 29.4 dBm. With an added power capability of 610 mW or 27.85 dBm,

$$P_N = 1.55 \text{ dB}$$

$$= 1.43 \text{ ratio}$$

Therefore, the output stage diode gain is 5.23 dB, as shown by point 1 in Figure 2. For the input stage,

$$P_N = -3.08 \text{ dB}$$

$$= 0.492 \text{ ratio}$$

Therefore, the input stage diode gain is 12.17 dB, as shown by point 2 in Figure 2.

#### Module design

Figure 9 is a cross section of a 19-GHz amplifier module and transformer. The diode is soldered into the diode mount, which is held in place with a retainer nut. This method of mounting ensures that the thermal impedance between diode and heat sink, which is the Beacon baseplate, is minimized. In fact, the thermal impedance outside the diode package is negligible compared to the thermal impedance between the diode chip and diode package, *i.e.*, the impedance inside the package.

The low-pass filter is terminated in an Eccosorb load. The cutoff frequency of the filter is 12 GHz, *i.e.*, the frequency at which the waveguide is approaching cutoff ( $f_c \approx 11.6$  GHz) and the waveguide return loss is beginning to deteriorate. Hence the low-pass filter and waveguide act as a diplexer and together present a resistive load over all frequencies of

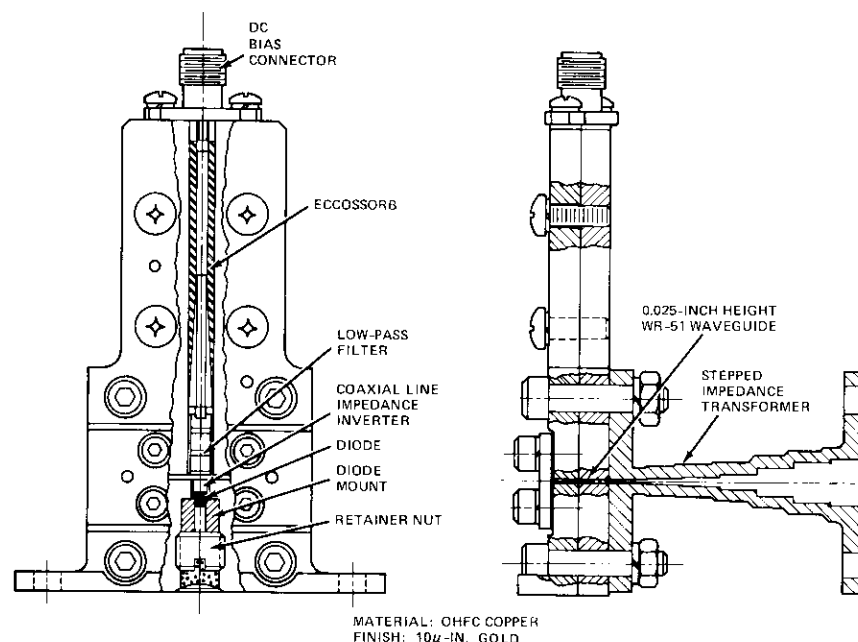


Figure 9. 19-GHz IMPATT Module Construction

interest. In particular, the low-pass filter presents a matched load at 9.5 GHz, *i.e.*, the first subharmonic of the signal frequency, to ensure freedom from subharmonic oscillations.

The diode impedance,  $Z_D$ , seen at the diode package terminals is a function of frequency, DC bias level, and RF voltage across the diode junction. At the levels used in the amplifier, this impedance is of the order of

$$Z_D = R_D + jX_D$$

$$\approx -1 + j4$$

For the desired gain, the generator impedance

$$Z_G = R_G + jX_G$$

seen from the diode terminals must have a real part,  $R_G$ , in accordance with equation (1) and an imaginary part equal to  $-X_D$  at the center fre-

quency. Thus,  $R_G$  is approximately  $+2\Omega$  to  $+5\Omega$  and  $X_G$  is approximately  $-4\Omega$ .

From the definition of waveguide characteristic impedance which is consistent with the impedance of a post shunting the guide [12], the full height WR51 waveguide impedance is approximately  $475\Omega$  at 19.04 GHz. The 3-section stepped height impedance transformer produces a broadband impedance match to the  $\approx 46\Omega$  characteristic of the 0.025-inch reduced height guide. The transformation to the desired  $2\Omega$  to  $5\Omega$  impedance level at the diode terminals is provided by the coaxial line impedance inverter section immediately above the diode. Module performance has been experimentally optimized by adjusting the characteristic impedance of the coaxial line.

#### Amplifier performance

The swept frequency response of a 19-GHz amplifier at three levels of RF drive is shown in Figure 10.

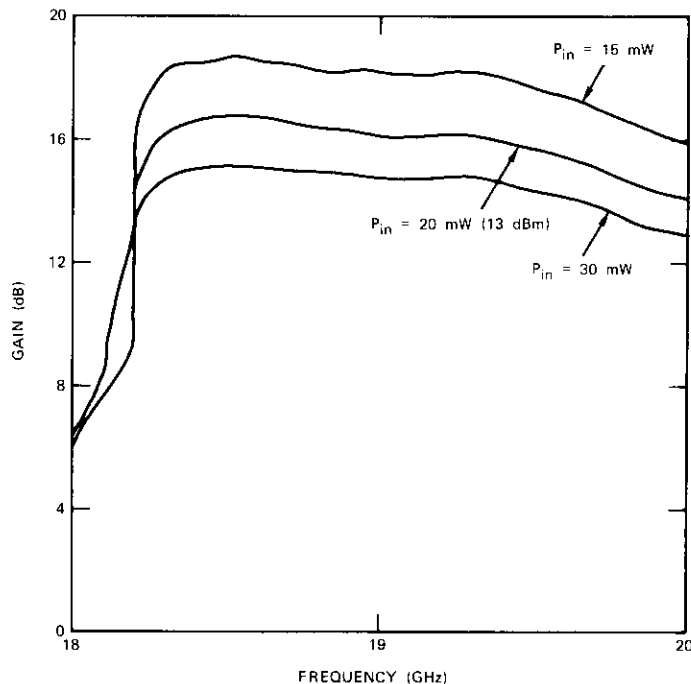


Figure 10. Gain vs Frequency of 19-GHz IMPATT Amplifier at Three Input Power Levels

#### 28-GHz amplifier

The 28-GHz amplifiers are constructed of WR28 waveguide using IMPATT diodes as the active RF devices. Each amplifier uses six diodes and three stages. Each diode is housed in a separate 1-port reflection amplifier module. The first and second stages utilize one diode each and are circulator coupled. The third stage combines the output power of four diodes.

Figure 11 is a view of a complete amplifier. Two amplifier types were

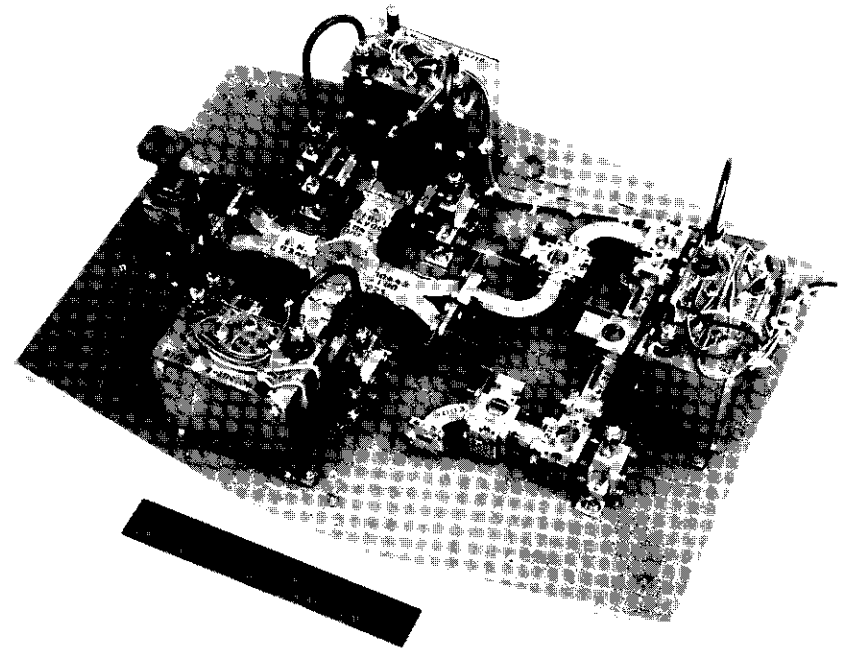


Figure 11. Complete 28-GHz Amplifier

produced. Both were required to amplify phase modulated signals, but for three of the five amplifiers the signal consisted of a carrier at 28.56 GHz plus a pair of sidebands separated by  $\pm 264$  MHz (narrowband), while in the remaining two amplifiers the sidebands were separated by  $\pm 529$  MHz (wideband). In both narrowband and wideband cases, the sidebands were each 7 dB below the carrier. The nominal output signal spectra are shown in Figure 12.

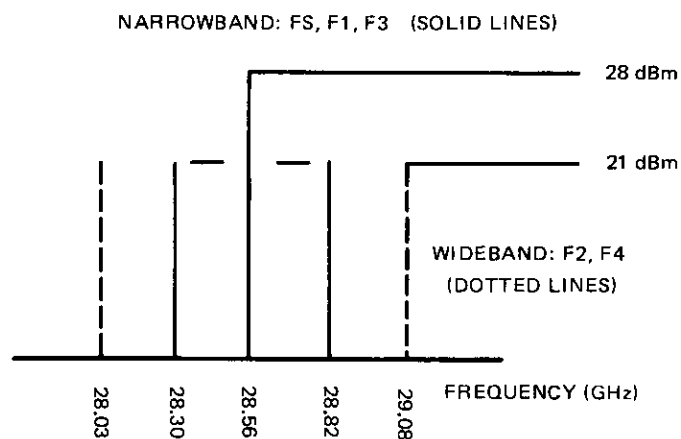


Figure 12. Output Signal Spectra: Design Specification for 28-GHz Amplifier

The total RF input power was approximately +8 dBm, and the total output power was approximately 30 dBm. Silicon IMPATT diodes from two different sources were used in the program. For the first two narrowband amplifiers, RCA diodes (P<sup>+</sup>PN) were used, while on the third narrowband amplifier and both wideband amplifiers, NEC diodes (N<sup>+</sup>NP) were utilized. The wideband and narrowband amplifiers were identical in basic design, but for wideband operation a spectrum "conditioner" was placed between the first and second stages to correct the wideband phase response and preserve the desired sideband levels.

The required amplifier gain was approximately 22 dB, and the required output power was 29.5 dBm. The amplifier configuration needed to achieve these values is shown in Figure 13. The first two stages are circulator-coupled single-diode stages cascaded in series, with interstage isolators to ensure stability. The third stage comprises four single diode modules coupled by a 3-dB hybrid network to operate in parallel. The network operates by dividing the input signal at A into four equal parts for amplification in the modules. The four amplified signals are then recombined at B. For the hybrid network to operate properly, equal phase lengths must be realized in the four signal paths. This was achieved by measuring the phase lengths of the four paths in the hybrid network and the reflection phases of the four modules. Appropriate phase-correcting shims were then inserted between the hybrid amplifier ports and the stepped wave-

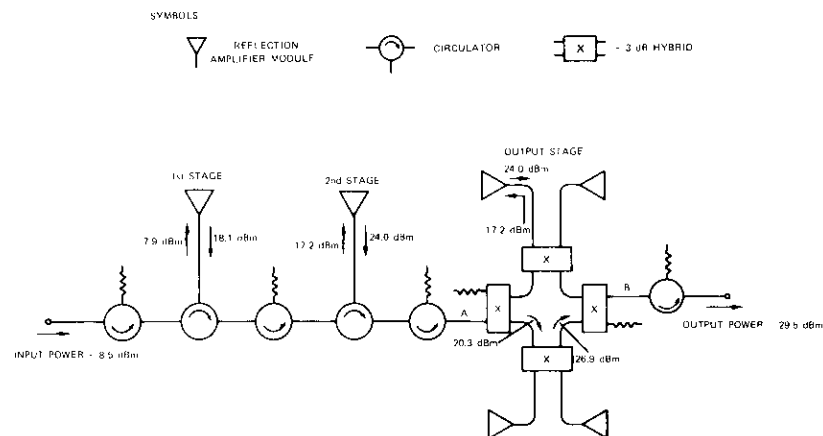


Figure 13. Schematic of 28-GHz IMPATT Amplifier

guide transformer. The phase length inequalities were generally less than 30°. If uncorrected, this would reduce the output power by 0.3 dB.

#### IMPATT diodes

The RCA diodes used on the earlier amplifiers, which were of silicon complementary P<sup>+</sup>PN construction mounted on a copper heat sink, required a negative bias voltage. The NEC diodes were also silicon but of conventional N<sup>+</sup>NP construction; thus, they required a positive bias voltage. These diodes were mounted on diamond heat sinks. Comparative data for the two manufacturers are given in Table I.

TABLE I. COMPARATIVE DATA FOR 28-GHZ DIODES

Manufacturer	RCA	NEC
Diode Material	Si	Si
Construction Type	P <sup>+</sup> PN	N <sup>+</sup> NP
Heat Sink Material	Cu	Diamond
Operating Voltage (V)	-38±2	+37±1
Operating Current (mA)	70-100	94-105
Efficiency (%)	7.4-9.4	6.1-7.2

Because of the different polarities, voltages, and currents, different current regulators were required for the two diode types. Both diodes were supplied in the same package. Figure 14 is a cross section of an NEC diode.

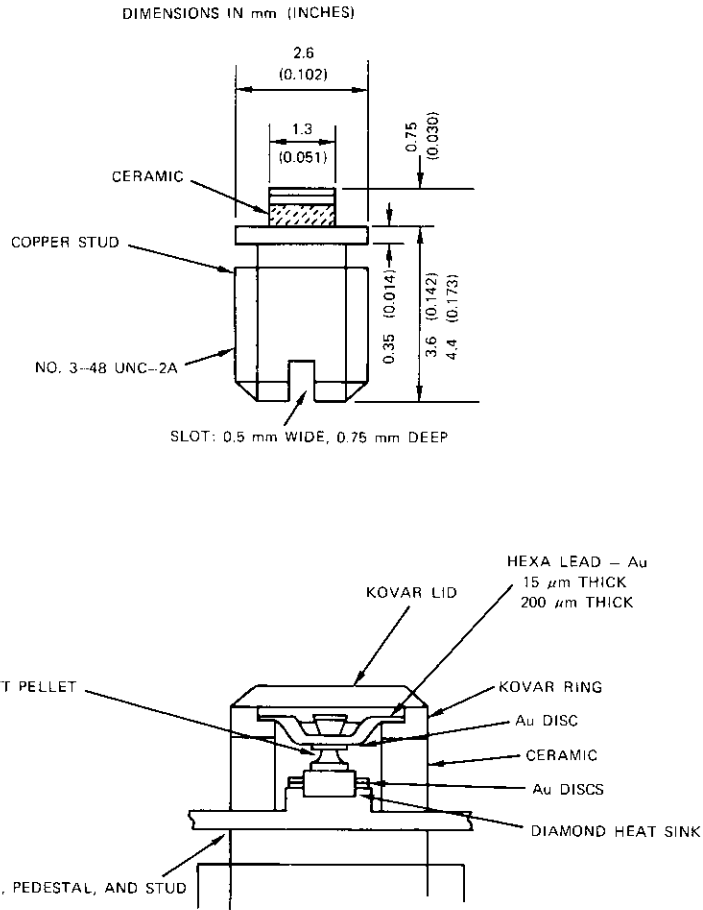


Figure 14. NEC 28-GHz Diode

The diode junction operating temperature has a major effect on the MTF of the diode, and thus on the reliability of the amplifier. The relevant data, derived from measurements made by both COMSAT Laboratories and the diode manufacturers, are shown in Table 2.

TABLE 2. THERMAL PROPERTIES OF 28-GHZ DIODES

Diode Supplier	Thermal Impedance (°C/W)	Maximum Junction Operating Temperature (°C)	Predicted MTF (hr)
RCA	45-50	200	$2 \times 10^6$
NEC	25-30	135	$10^{12}$

**Module power and gain levels**

Available 28-GHz diodes had an oscillator power capability of approximately 250 mW. For a required amplifier output power of 1 W, Figure 2 and the arguments leading up to it indicate that the output stage requires the combination of several diodes to obtain the output power with useful gain. The output stage was made using four diode modules and the power splitting/combining network of hybrids.

Initial experiments showed that the maximum added power,  $P_{AM}$ , obtainable from the diodes was 200 mW. Using this value and allowing for circuit losses yields

$$P_o \approx 24 \text{ dBm} = 250 \text{ mW}$$

$$\therefore P_N = 1.25 \text{ ratio}$$

$$\therefore G_M \approx 6.8 \text{ dB (from Figure 2)}$$

for each diode of the output stage. A fifth module of exactly the same nominal performance may then be used as a driver stage for the output stage. The operating point of the five diode modules of the second and third stages is shown as point 3 in Figure 2.

The input stage of the amplifier requires higher gain, but less than maximum added power. It therefore operates at less than maximum efficiency but with a diode gain of 10.5 dB as shown at point 4 in Figure 2. The small signal gain of all the stages is nominally < 15 dB to ensure stability.

Many actual flight diodes exceeded their specifications, yielding added power levels up to 300 mW. Consequently, flight amplifier output power levels of up to 30.5 dBm have been obtained.

**Module design**

Figure 15 is a diagram of a complete module. To provide 6- to 10-dB gain, the generator impedance,  $Z_G$ , seen by the diode junction must be

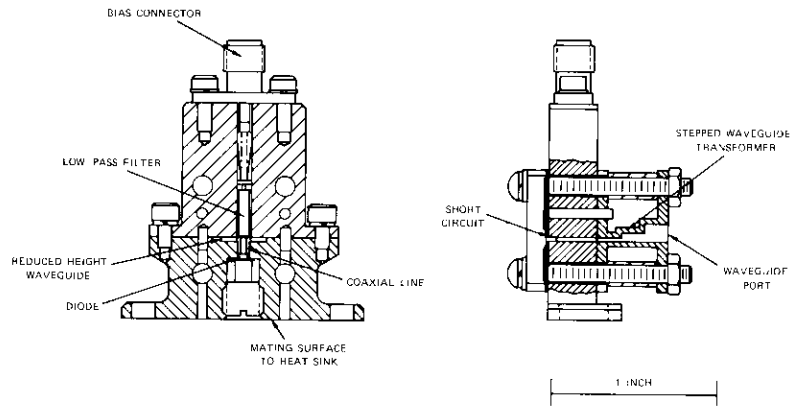


Figure 15. 28-GHz Amplifier Module

approximately  $2\Omega$ – $3\Omega$ . The transformation between the  $Z_0$  of the waveguide, which is  $560\Omega$  at 28.56 GHz, and the generator impedance of  $2\Omega$ – $3\Omega$  is accomplished in three steps. A 3-step waveguide transformer reduces the WR28 waveguide height from 0.140 to 0.020 inch and the characteristic impedance from  $560\Omega$  to  $80\Omega$ . A series reactance (provided by the low-pass filter) and a shunt susceptance (provided by the back short) then provide a variable transformation of real part impedance to the range of  $72\Omega$  to  $33\Omega$ . Finally, a quarter-wave coaxial section of  $10\Omega$  to  $14\Omega$  characteristic impedance reduces the impedance to the  $2\Omega$  to  $3\Omega$  level required at the diode junction terminals.

Because of the variation of characteristics from diode to diode, four mechanical tuning adjustments are provided. The coaxial section length can be varied ( $\pm 0.010$  inch) by selecting from mounts machined to different dimensions. This variable primarily adjusts the center frequency of the response.

The coaxial section center diameter can be varied by selecting parts over a range of  $\pm 0.002$  inch and primarily adjusts the module gain. The length of the bottom section of the low-pass filter is adjustable (with shims) over a range of  $\pm 0.005$  inch and the backshort position over a range of  $\pm 0.030$  inch. These two adjustments provide some fine tuning of gain, frequency, and bandwidth. Finally, the diode bias current is variable and affects the gain and center frequency of the amplitude-frequency response.

### Amplifier performance

The IMPATT amplifiers are required to amplify a phase modulated signal. Signal spectra corresponding to the narrowband (FS, F1, and F3) and wideband (F2 and F4) amplifier specifications are shown in Figure 12.

It was observed in the FS, F1, and F3 narrowband amplifiers that the 28-GHz output signal spectrum from the Beacon was changed only slightly from the output spectrum of the modulator. However, when the F2 and F4 wideband amplifiers were tested with the wideband phase modulated signal, severe and unacceptable compression (3–7 dB) of the sideband-to-carrier ratio was observed. Analysis and investigation demonstrated that the response of the amplifier modules is sensitive to the relative phase of the input signal sidebands and carrier. Further, each module can change the relative phase of the sidebands and carrier of the signal passing through it.

Theoretical work, followed by experimentation, showed that these effects can be corrected by using phase vs frequency predistortion. This is achieved by an iris-coupled single-port waveguide cavity which is converted to a 2-port device by a circulator. The relative phase of carrier and sidebands is adjusted by cavity tuning. The circulator and cavity combination is located in the amplifier between the first and second stages. Suitable location and adjustment of the conditioner permit the amplifier output sideband-to-carrier ratio to be adjusted to achieve linear phase operation. Further modifications for these amplifiers include adjusting the first stage module backshort position to achieve sideband balance, and as required, adjusting the circulator to module distance on the first stage to compensate for temperature variations which affect the output spectral balance.

Figure 16 shows the swept frequency response of a wideband (F2) amplifier. Figure 17 shows the variation of the carrier and sideband levels of the same wideband amplifier (F2) as a function of temperature when driven by the Beacon driver chain.

### Acknowledgments

The 19-GHz amplifier was designed and developed by Mr. R. Sicotte. The theory and design of the spectrum conditioner used on the wideband 28-GHz amplifier were developed by Mr. W. Getsinger, who also provided valuable technical guidance throughout this project. The author is grateful to these gentlemen for their technical help.

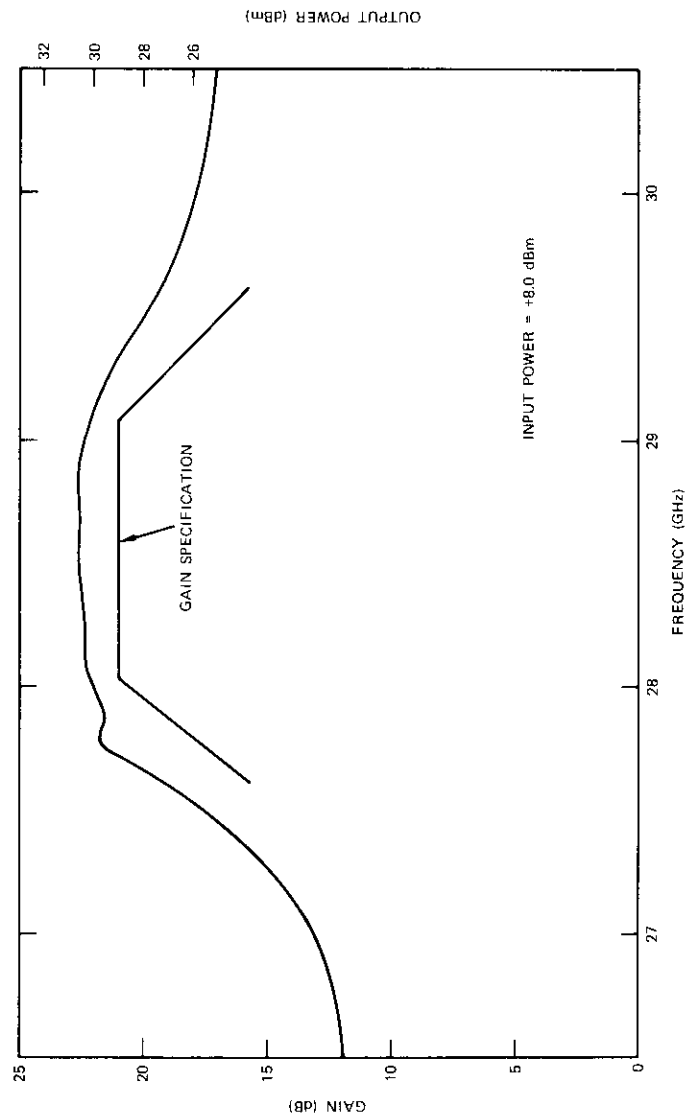


Figure 16. Gain and Output Power vs Frequency of Wideband Amplifier

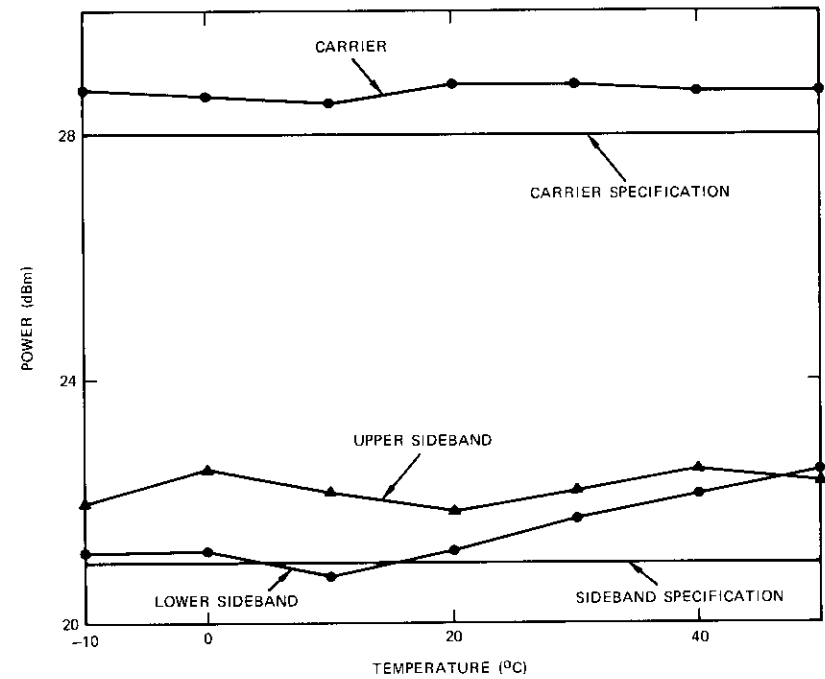


Figure 17. Carrier and Sideband Power Levels vs Temperature (actual performance of F2 amplifier)

## References

- [1] *IEEE Transactions on Microwave Theory and Techniques*, MTT-21, No. 11, November 1973.
- [2] "Microwave Power Generation and Amplification Using Impatt Diodes," Hewlett Packard Application Note 935.
- [3] R. E. Lee, U. H. Gysel, and D. Parker, "High Power C-band Multiple Impatt Diode Amplifiers," *IEEE Transactions on Microwave Theory and Techniques*, MTT-24, No. 5, May 1976, p. 249.
- [4] M. E. Hines, "Negative Resistance Diode Power Amplification," *IEEE Transactions on Electron Devices*, ED-17, No. 1, January 1970, p. 1.
- [5] Chong W. Lee, "High Power Negative Resistance Amplifiers," *Microwave Journal*, February 1972, p. 29.
- [6] H. J. Kuno, D. L. English, and R. S. Ying, "High Power Millimeter Wave Impatt Amplifiers," *ISSCC Proceedings*, Philadelphia, Pennsylvania, February 1973, p. 50.

- [7] R. S. Harp and H. L. Stover, "Power Combining of X-band Impatt Circuit Modules," *ISSCC Proceedings*, Philadelphia, Pennsylvania, February 1977, p. 118.
- [8] C. A. Brackett, "The Elimination of Tuning Induced Burnout and Bias-Circuit Oscillations in Impatt Oscillators," *Bell System Technical Journal*, Vol. 52, No. 3, March 1973, p. 271.
- [9] Hilding M. Olson, "Thermal Runaway of Impatt Diodes," *IEEE Transactions on Electron Devices*, ED-22, No. 4, April 1975, p. 165.
- [10] "Factors Affecting Silicon Impatt Diode Reliability and Safe Operation," Hewlett Packard Application Note 959-1.
- [11] Bertil Hansson, "Hysteresis Effects in Microwave Amplifiers and Phase Locked Oscillators Caused by Amplitude Dependent Susceptance," *IEEE Transactions on Microwave Theory and Techniques*, MTT-21, No. 11, November 1973, p. 739.
- [12] W. J. Getsinger, "The Packaged and Mounted Diode as a Microwave Circuit," *IEEE Transactions on Microwave Theory and Techniques*, MTT-14, No. 2, February 1966, p. 58.



Michael J. Barrett received B.Sc. and Ph.D. degrees from London University. After coming to the U.S. in 1964, he was employed by Raytheon Company and by Sylvania Semiconductor Division, where he designed ferrite devices and microwave semiconductor components. In 1972 he became a member of the technical staff of the Microwave Circuits Department of the Microwave Laboratory at COMSAT Laboratories, where he has worked on solid-state components for advanced transmission systems and performed studies for

future millimeter wave satellite communications systems.

**Index:** IMPATT amplifiers, beacon, oscillator, in-orbit test, COMSTAR

## **Low-jitter local oscillator source for the COMSTAR Beacon**

R. E. STEGENS

(Manuscript received September 29, 1976)

### **Abstract**

This paper describes the approaches used to achieve high short-term frequency stability in the Beacon local oscillator sources which drive the 19- and 28-GHz IMPATT amplifiers and the 264-MHz phase modulator. In addition, the techniques which permit direct measurement in the frequency domain of the Beacon's extremely small RF line width (5 Hz at 19 GHz) are discussed. Finally, features which have made it possible to achieve efficiency, unconditional freedom from circuit instabilities, and a frequency/temperature dependence of less than four parts per  $10^{-8}/^{\circ}\text{C}$  are presented. In-orbit measurements have confirmed that the Beacons produce an RF line width of less than 5 Hz at 19 GHz.

### **System requirements**

Plans for reception of the 19.04- and 28.56-GHz Beacon signals with small-bandwidth phase-locking loops required that a high priority be assigned to achieving low-frequency jitter and a low-frequency slew rate caused by satellite temperature variation. The required frequency jitter was to be such that 90 percent of the RF power would be contained within a 100-Hz bandwidth at 19.04 GHz, and the frequency/temperature dependence would be less than  $\pm 1$  ppm over a daily spacecraft temperature variation of  $-10^{\circ}\text{C}$  to  $+35^{\circ}\text{C}$ . At 28.56 GHz, a maximum line width of 150 Hz was specified.

Because these specifications imposed limits upon spacecraft prime power, size, and weight, the design of each part of the local oscillator (LO) chain had to meet stringent requirements. In terms of reliability, each assembly of the LO chain was designed to operate for the full seven years for which the COMSTAR is intended to be useful. In addition, a fully redundant LO chain was incorporated into each Beacon; either available LO chain could be selected by ground command. Weight and volume savings were realized by constructing the operating and redundant assemblies in a single chassis so that common walls might be utilized.

A further challenge was the requirement for spurious outputs below  $-40$  dBc at both 19.04 and 28.56 GHz. Therefore, very strict spectral purity requirements were imposed on the lower frequency stages. The desired performance was obtained with filtering and saturated amplifiers capable of suppressing spurious components.

### Design approach

Figure 1 is the block diagram around which the Beacon LO was designed. Full redundancy was provided, including the DC power conditioners (not shown). Power amplification was used at the output frequency (2.38 GHz) to reduce DC power consumption; switching between sources was accomplished simply by turning on or off the appropriate power supplies by ground command.

The solid-state source contains transistor crystal oscillator, buffer amplifier, frequency doubler, and power amplifier stages. The quartz crystal is heated to approximately  $45^{\circ}\text{C}$  by a self-regulating barium titanate element. The solid-state source provides two 264-MHz outputs: one at  $+17$  dBm to drive the  $\times 9$  multiplier, and one at  $+2$  dBm to provide coherent phase modulation of the 28.56-GHz signal.

The  $\times 9$  multiplier, which consists of two high-level transistor frequency triplers in cascade, includes a coaxial cavity resonator which suppresses spurious output frequencies. This multiplier exhibits an overall gain of 3 dB, an RF-to-DC (RF/DC) efficiency of 8 percent, and very good stability with variations in power level, frequency, and supply voltage.

Following the  $\times 9$  multiplier, a class B transistor amplifier in MIC form provides 8-dB gain with an RF/DC efficiency of 33 percent. This amplifier is operated at a saturated output level, which stabilizes the 2.38-GHz level despite drive level variations and further suppresses low-level spurious frequencies generated by the  $\times 9$  multiplier. Two outputs are provided by an MIC quadrature hybrid so that ultimate outputs at 19.04 and 28.56

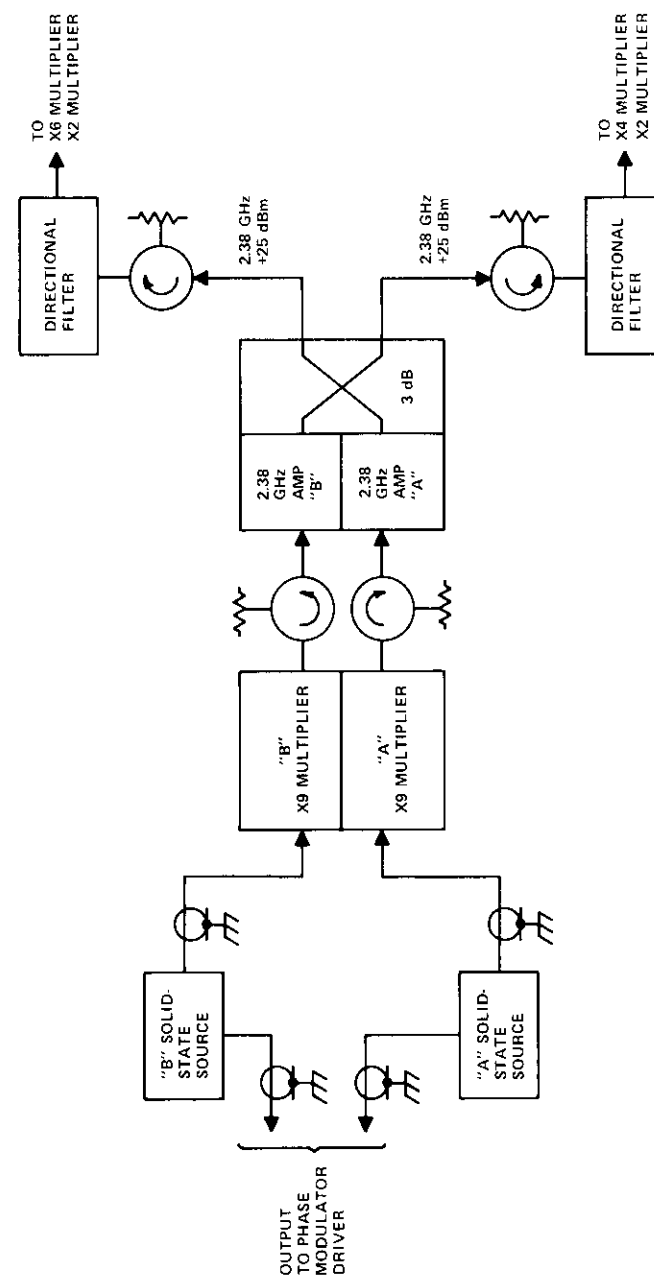


Figure 1. Beacon Local Oscillator Block Diagram

GHz are derived from the same source. The overall RF/DC efficiency of the LO chain was 15 percent as measured at the 2.38-GHz amplifier outputs.

Microwave integrated circuit ring resonators precede each step recovery diode frequency multiplier, providing a well-matched source impedance at virtually all frequencies. This guarantees stability of the step recovery diode multipliers despite highly reactive loads which appear at the circulator outputs at some frequencies.

### Solid-state source

The solid-state source design was based upon that used in the ATS-6 COMSAT Propagation Experiment, with the oscillator section altered to improve both short-term frequency stability and temperature sensitivity characteristics.

Figure 2 is a schematic diagram for the oscillator, which ultimately determines the short-term and temperature stability of the entire Beacon. Although short-term stability has been investigated in References 1-4, it will be of interest to discuss specific approaches which led to the attainment of a "quiet" oscillator. Critical items to the realization of minimal frequency jitter are an absolutely stable DC supply, a very high Q resonator element, and an active device with low  $1/f$  and phase noise.

The DC supply for the oscillator is regulated at two levels, the spacecraft 24-V supply and the 12.8-V level, by low-current, low-noise, temperature-compensated Zener diodes. Two levels of filtering are used to minimize low-frequency voltage jitter on the oscillator; DC supply jitter is commonly produced by Zener voltage regulating diodes which operate in the avalanche breakdown region.

The oscillator circuit utilizes a grounded-base bipolar transistor with a quartz crystal providing series-resonant, in-phase feedback between emitter and collector. The AT-cut fifth overtone quartz crystal has a loaded Q greater than 100,000 [5].

A 2N2857 transistor was chosen for its low noise figure at the frequency of oscillation (3 dB), high  $F_T$  (1.6 GHz), and low  $1/f$  noise. The low noise figure and high  $F_T$  minimize phase jitter which results from time-varying parameters within the device, primarily transit time and collector base capacitance. The  $1/f$  noise, which contributes strongly to phase jitter below 10 Hz, is caused by surface recombination of minority carriers in the base area [6]-[9]. Because  $1/f$  noise is proportional to emitter current, the oscillator was designed to operate at an emitter current of 0.5 mA.

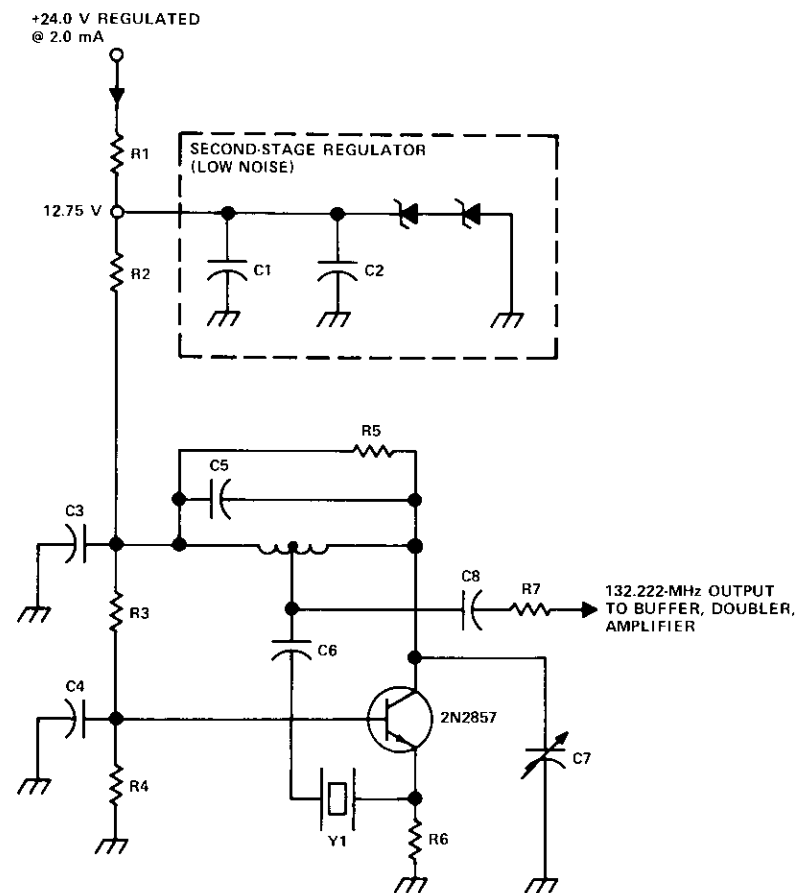


Figure 2. Oscillator Section of the Solid-State Source

A simple temperature regulator was designed to maintain crystal temperature within  $48^{\circ}\text{C} \pm 4^{\circ}\text{C}$  and thus meet the temperature stability requirement of  $\pm 1$  ppm over the ambient range of  $-10^{\circ}\text{C}$  to  $+35^{\circ}\text{C}$ . It consists of a barium titanate resistive element having an exponential resistance-temperature characteristic (Figure 3). Mounted to the TO5 crystal case, this element is operated directly from the 24-VDC supply. Figure 4 shows computed and observed heater current and crystal temperature as functions of ambient temperature. Figure 5 demonstrates the effectiveness of this simple approach in improving the oscillator's tem-

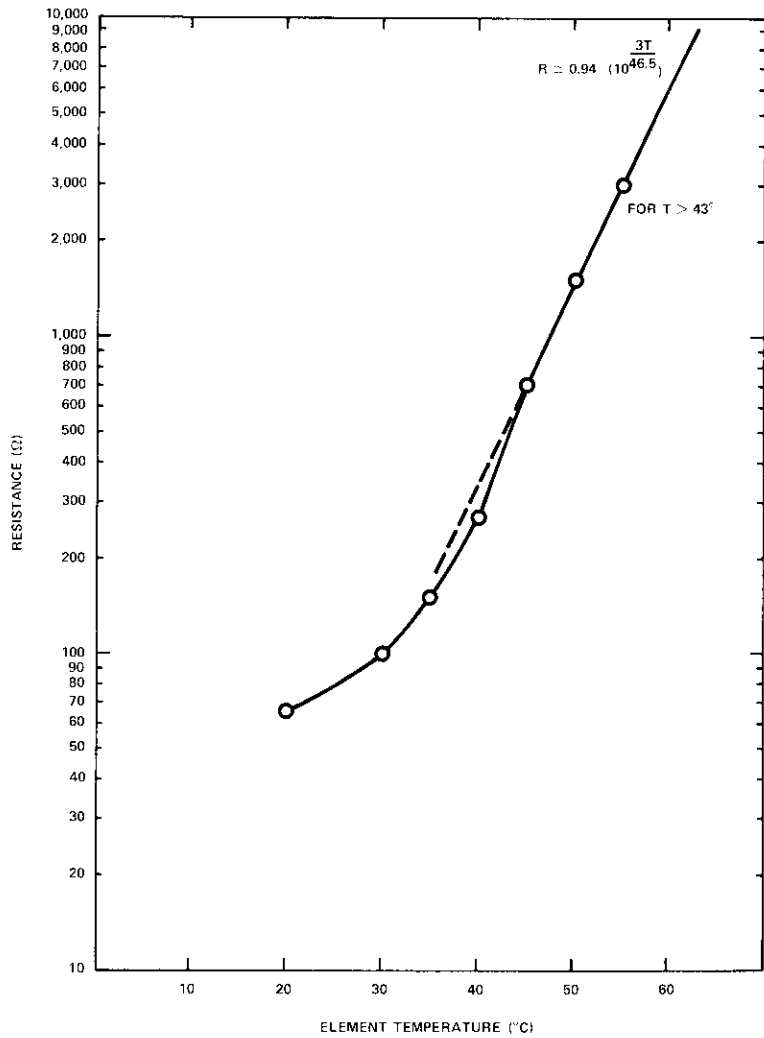


Figure 3. Resistance of the Barium Titanate Heating Element vs Temperature (measured)

perature stability. Each solid-state source, constructed in a light, thin-walled aluminum chassis with components and wiring foamed in place for increased strength, weighs 100 g.

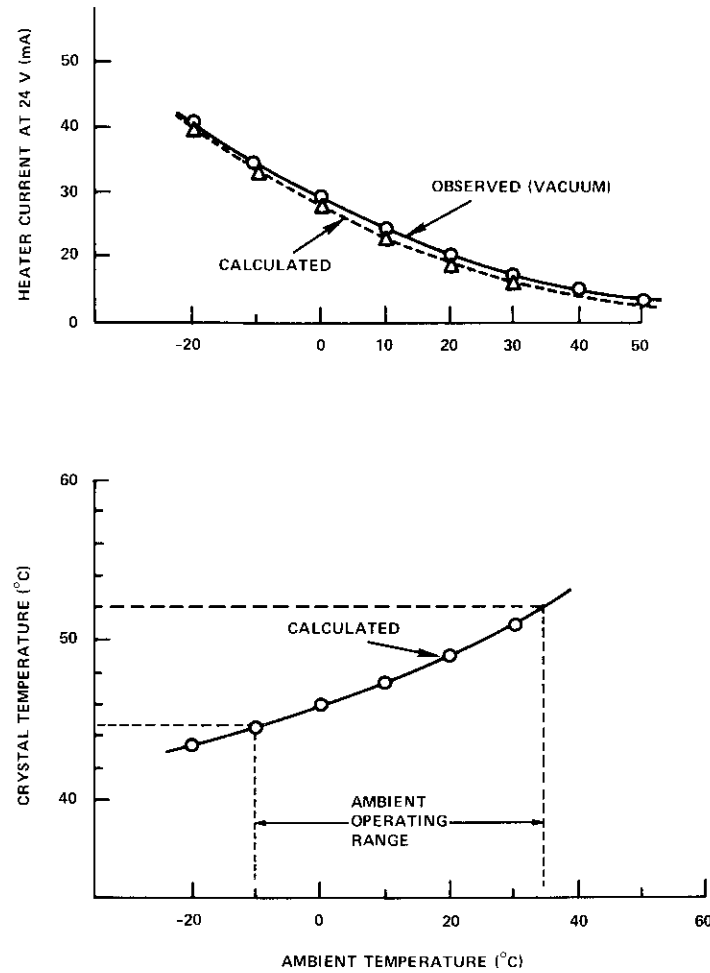


Figure 4. Heater Current and Crystal Temperature (calculated results assume a thermal resistance of 70°C/W between crystal/heater assembly and ambient)

**×9 multiplier**

The design of the ×9 multiplier, shown schematically in Figure 6, is the result of an effort to maximize the stability and overall RF/DC efficiency of the LO chain. Maximum circuit stability results from operating the transistors in the class C frequency multiplier mode rather than utilizing

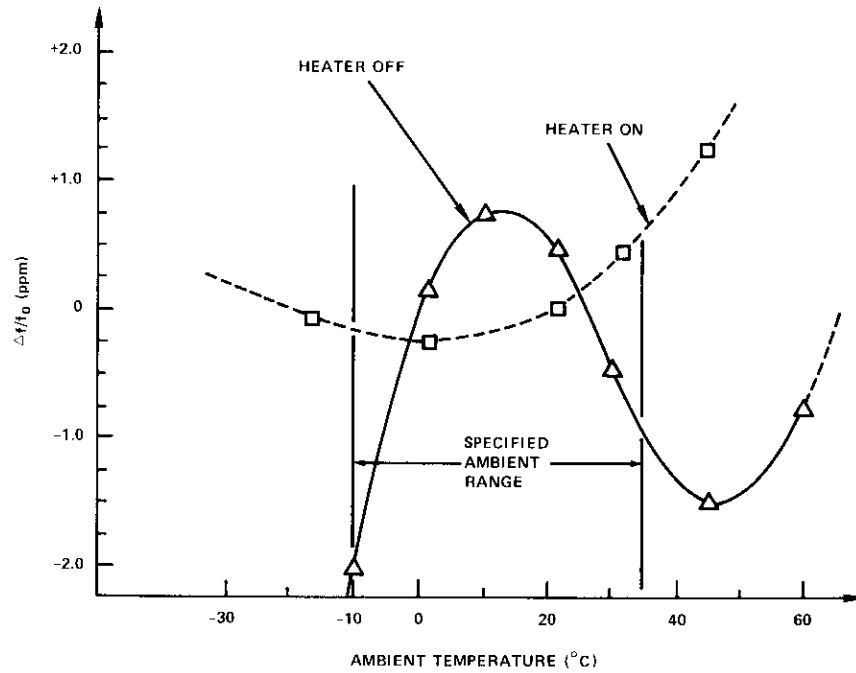


Figure 5. Observed Temperature/Frequency Dependence of a Beacon Solid-State Source Indicating the Effectiveness of a Barium Titanate Temperature Regulator

the nonlinear collector-base output capacitance as a varactor multiplier [10]. In the class C mode, the emitter-base current is forced to be non-sinusoidal by selecting bias conditions so that the conduction angle is approximately  $(360/n)^\circ$ , where  $n$  is the order of multiplication. Amplification then occurs at the output frequency, and filtering reduces the level of spurious outputs.

Two class C triplers in cascade are used with lumped element input and interstage networks at 264 and 792 MHz. The output matching/filtering network consists of a coaxial cavity resonator with a loaded Q of 200. This resonator and the interstage network suppress nearby spurious outputs by 40 dB. Reliability is ensured by utilizing high-level devices ( $P_{DISS} = 10 \text{ W}$ ) in this low-level application.

Figure 7 shows the construction techniques used in the  $\times 9$  multiplier redundant pair. The total weight of the assembly is 150 g; after tuning,

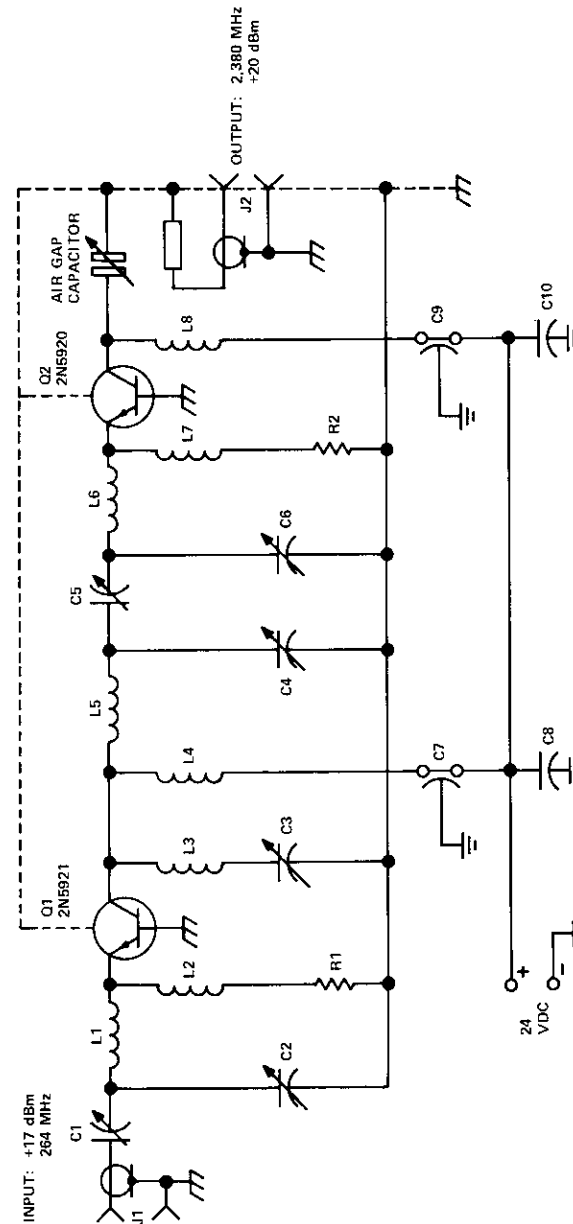


Figure 6.  $\times 9$  Multiplier Schematic Diagram

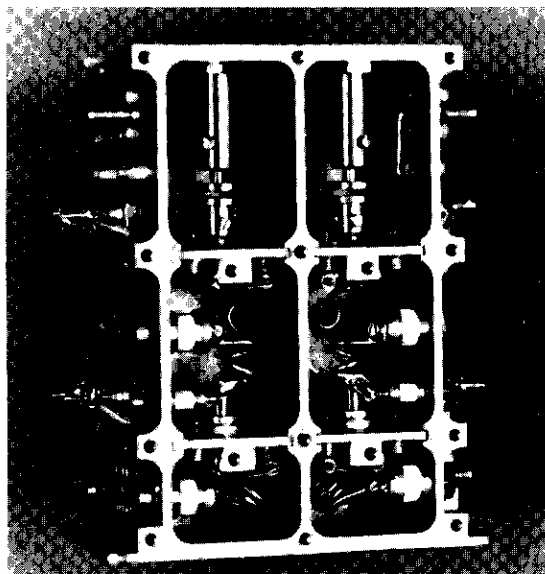


Figure 7.  $\times 9$  Multiplier Redundant Pair

the inner compartments are foamed with an open-cell polyurethane material to reduce vibration stresses.

### 2.38-GHz amplifier design

The 2.38-GHz amplifier was designed as a class B saturated transistor stage to maximize stage efficiency, gain, and dynamic range. Operation with slight forward bias (class B rather than class C) improved the gain and dynamic range, allowing a larger input power margin before the output drops. Hence, overall chain reliability was improved, and output variations with temperature changes were reduced.

Efficiency was maximized by using an MIC output network design in which multiples of the output frequency are reactively terminated. Because of the high conversion efficiency, the device can be operated at a junction temperature of 130°C maximum (for an ambient temperature of 50°C) to ensure reliability.

Two identical amplifiers and a branch-line hybrid are etched on a TFE-glass MIC board and mounted in an aluminum enclosure. The total weight is 167 g. Figure 8 is a schematic diagram and Figure 9 presents performance data for a typical 2.38-GHz amplifier/hybrid combination.

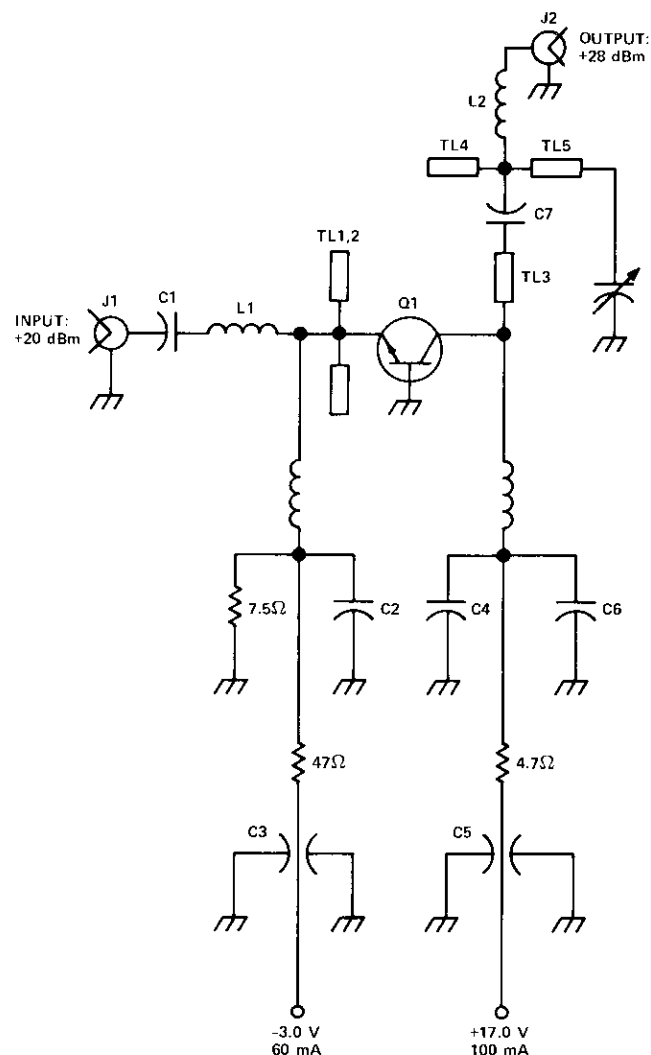


Figure 8. Class B Power Amplifier Schematic Diagram (elements TL1-TL5 are microstrip transmission lines)

### Integration and Tests

As a first step in the process of spacecraft integration and test, the three units comprising the Beacon LO were individually tested to ensure that

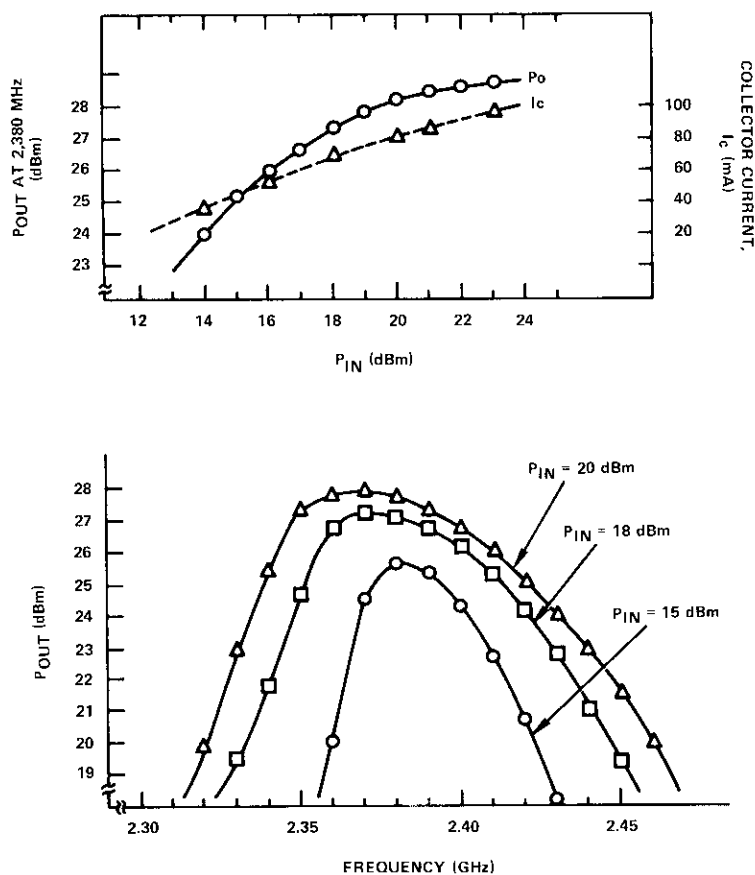


Figure 9. Measured Performance of the 2.38-GHz Amplifier

ample performance margins were available to meet the Beacon requirements. Before integration each unit underwent a separate thermal vacuum operating test over the range of  $-50^{\circ}\text{C}$  to  $+50^{\circ}\text{C}$  and a live vibration test. The assemblies were then sequentially integrated into the Beacon baseplate, with complete room temperature operating tests run as each assembly was added. This procedure ensured unconditional stability of the chain.

#### Chain stability measurements

The operation of the entire chain at each stage of integration was observed for all combinations of input frequency, operating (RF) level, DC supply voltage, and termination VSWR by disabling the crystal oscillator

section of the solid-state source and injecting a signal from an external sweep generator. Any tendency to unstable behavior, such as sudden generation of spurious output frequencies, was considered unacceptable and resulted in removal of the offending assembly. Permanent X-Y recording of the tests provided a complete history of the performance of each Beacon LO chain and its components.

#### Frequency stability measurements

The LO short-term frequency stability was measured in the time and frequency domains. Initial measurements were made in the time domain, using a computing counter as shown in Figure 10. Two "identical" Beacon sources were mixed at 264 MHz to produce a difference frequency in the 100-kHz range. This signal, containing all of the noise characteristics of the higher frequency signals, was then amplified, filtered, and applied to

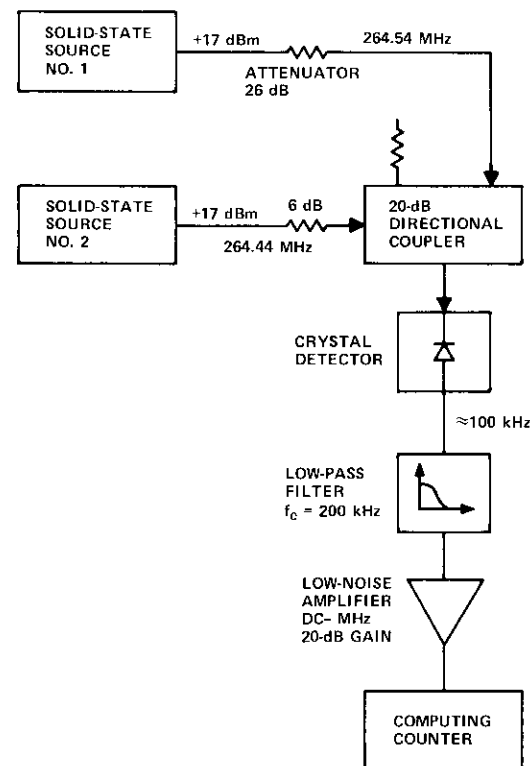


Figure 10. Measurement of Frequency Jitter in the Time Domain

the computing counter. The computer counter was programmed to make  $n$  separate frequency measurements over identical intervals  $\tau$  and to display the Allan variance [11], [12] defined as

$$\sigma(\tau) = \frac{1}{f_o} \sqrt{\frac{1}{2n} \sum_{i=1}^n (f_{2i} - f_{2i-1})^2} .$$

For  $n \geq 100$ , typical results are shown in Figure 11. Note that, for  $\tau \geq 0.1$  second, an rms frequency deviation of less than 0.03 Hz was observed for two sources operating at 264 MHz. For identical sources, this is equivalent to 1.5- and 2.1-Hz rms deviations at 19 GHz and 28 GHz, respectively. Although these time-domain data cannot be uniquely converted to the frequency domain and compared with the required specification of a 100-Hz line width at 19 GHz, the very low jitter was a good indication that the specification would be met with a wide margin.

Frequency-domain measurements were made by mixing two LO chain outputs at 2,380 MHz to produce a 100-kHz difference frequency, and then mixing this frequency with a second highly stable tunable oscillator to produce an output of approximately 10 Hz, as shown in Figure 12. It was found that this signal would pass through an active filter having a bandwidth of 1 Hz with essentially no loss, indicating that the equivalent signal line width was less than 0.7 Hz per LO at 2,380 MHz. With subsequent multiplication, this corresponds to line widths of less than 6 Hz at 19.04 GHz and 9 Hz at 28.56 GHz.

To confirm the assumption that subsequent frequency multiplication would not contribute to jitter, the test was later repeated using two 19.04-GHz signals from flight-qualified Beacons. The final double-heterodyned signal was passed through an active filter centered at 350 Hz with a 10-Hz bandwidth. The results confirmed the previous data.

#### Performance in vacuum

During thermal vacuum tests of the completed Beacon assembly, the frequency and output power (at 2,380 MHz) of the LO chain were monitored. The power level was constant within  $\pm 0.5$  dB from  $-10^\circ\text{C}$  to  $+35^\circ\text{C}$ , and decreased only 2 dB at  $-50^\circ\text{C}$ , where only a successful turn-on of the Beacon was required. Frequency stability was essentially as shown in Figure 5.

Since launch in March 1976, daily frequency excursions of the 19.04-GHz Beacon have been less than  $\pm 10$  kHz; successful operation of phase-lock receivers has been obtained with loop bandwidths as low as 1.0

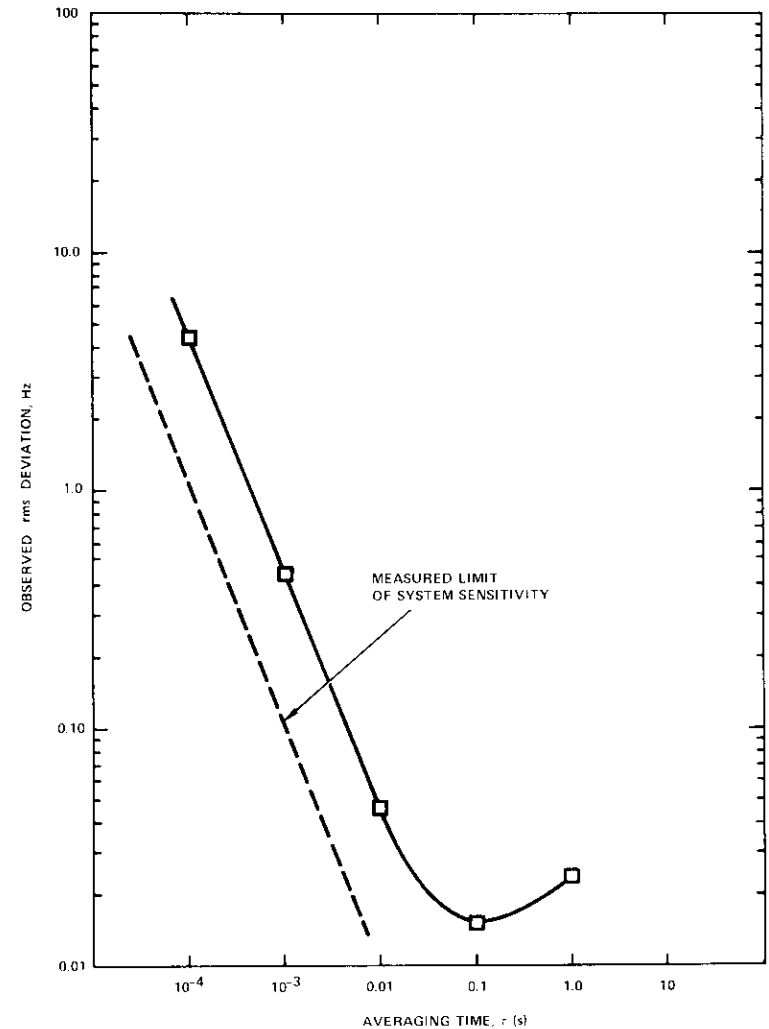


Figure 11. Observed Allan Variance for Two Solid-State Sources ( $\Delta f = 100$  kHz)

Hz [13]. This performance indicates that the actual in-orbit line width at 19.04 GHz must be considerably less than that measured in the laboratory.

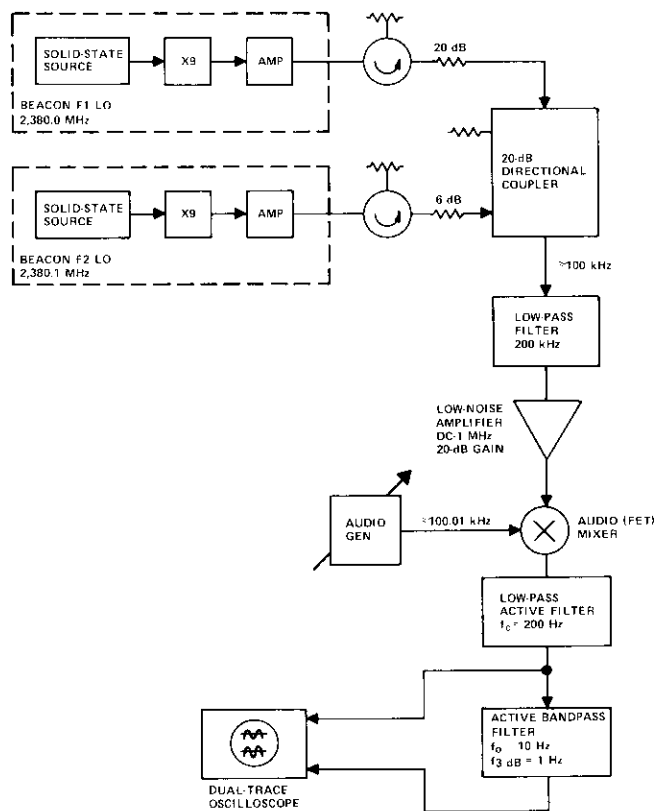
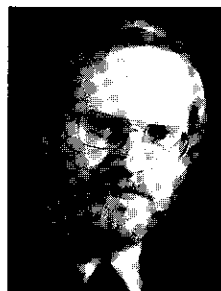


Figure 12. Equipment Configuration for Measurement of Signal Line Width in the Frequency Domain

## References

- [1] E. Haffner, "The Effects of Noise in Oscillators," *Proc. IEEE*, Vol. 54, No. 2, February 1966, pp. 179-198.
- [2] W. A. Edson, "Noise in Oscillators," *Proc. IEEE*, Vol. 48, No. 8, August 1960, pp. 1454-1466.
- [3] S. L. Johnson et al., "Noise Spectrum Characteristics of Low-Noise Microwave Tubes and Solid State Devices," *Proc. IEEE*, Vol. 54, No. 2, February 1966, pp. 258-265.

- [4] D. B. Leeson, "Short-Term Stable Microwave Sources," *Microwave Journal*, Vol. 13, No. 6, June 1970, pp. 59-69.
- [5] E. A. Gerber and R. A. Sykes, "State of the Art Quartz Crystal Units and Oscillators," *Proc. IEEE*, Vol. 54, No. 2, February 1966, pp. 103-116.
- [6] *Handbook of Semiconductor Electronics*, edited by L. P. Hunter, New York: McGraw-Hill, 1962, pp. 11-86.
- [7] W. H. Fonger, "A Determination of  $1/f$  Noise Sources in Semiconductor Diodes and Triodes," *Transistors I*, RCA Laboratories, Princeton, New Jersey, 1956.
- [8] J. L. Plumb and E. R. Chenette, "Flicker Noise in Transistors," *IEEE Transactions on Electron Devices*, ED-10, No. 9, September 1963, pp. 306-407.
- [9] R. C. Jaeger and A. J. Brodersen, "Low-Frequency Noise Sources in Bipolar Junction Transistors," *IEEE Transactions on Electron Devices*, ED-17, No. 2, February 1970, pp. 128-130.
- [10] H. E. Lee and R. Minton, "Designing Transistor Multipliers," *Microwaves*, November 1965, pp. 18-28.
- [11] D. W. Allan, "Statistics of Atomic Frequency Standards," *Proc. IEEE*, Vol. 54, February 1966, pp. 221-230.
- [12] Hewlett-Packard Corporation, *Computer Counter Applications Library*, Document 5952-0617.
- [13] C. Mahle, Private Communication.



Ronald E. Stegens received a B.S.E.E. degree from the Case Institute of Technology in 1964 and an M.S.E.E. from the State University of New York (Buffalo) in 1969. He participated in the design of electronically steerable antenna arrays at Sylvania Electronic Systems, Buffalo, New York. After joining COMSAT Laboratories in 1969, he developed microwave integrated circuit components for the ATS-6 experiment and the Beacon program. He is presently Assistant Manager of the Microwave Circuits Department of the Microwave Laboratory, responsible for development of FET amplifiers, oscillators, and mixers for use in future satellite communications systems.

## ***Thermal and structural design aspects of the Centimeter Wave Beacon***

N. L. HYMAN, D. PERLMUTTER, H. W. FLIEGER, AND P. R. SCHRANTZ

(Manuscript received November 12, 1976)

### ***Abstract***

The Centimeter Wave Beacon location on the spacecraft antenna mast was dictated by thermal and structural as well as electrical considerations. Numerous design problems had to be resolved. This paper presents the philosophy and some aspects of the designs. Thermal and structural testing is discussed and compared with telemetered flight results. Flight data have proven the temperature control integrity, and have allowed accurate determination of radiator absorptance degradation.

### ***Introduction***

The Centimeter Wave Beacon experiment presented a challenge in terms of thermal and structural design. Although communications equipment is usually placed within the spacecraft [1], [3], the Beacon was located on the COMSTAR spacecraft antenna mast [2], where it was subjected to severe launch vibration levels and then to the malevolent environment of space. Despite the environment at the mast location, the exacting RF requirements for the Beacon dictated a structural design of high integrity and a thermal design restricting temperature variations similar to those of the spacecraft interior.

Passive temperature control of the relatively constant power experiment is achieved by minimizing both solar heating and heat transfer between the Beacon and the spacecraft. The heat dissipated by the Beacon is rejected to space by radiators of a unique design. Appreciable weight is saved in the radiators by locally varying the thickness of the radiator face sheet in accordance with the nonuniform heat dissipation of the electronic components. Internal heaters are required when the Beacon is inactive.

Extensive use of honeycomb sandwich material in key areas provides a high ratio of stiffness to weight. Both packages are mounted to the antenna mast by titanium flanges which maintain the required rigidity and minimize launch load amplification at the sensitive internal components. Several electronic components utilize novel techniques to ensure electrical continuity in critical areas while allowing for vibrational and thermal movement. A complex multiple-step waveguide transition, electroformed to achieve close tolerances, is described herein.

Design verification is achieved by an extensive test program at the component and assembly levels as well as on a comprehensive thermal-structural test model. Telemetered temperatures from the first two flight Beacons demonstrate the effectiveness of the thermal design.

This paper discusses some of the history, philosophy, design techniques, and testing which resulted in the successful thermal and structural designs of the Centimeter Wave Beacon.

### **Spacecraft thermal-structural interface**

The Centimeter Wave Beacon experiment consists of two packages installed on either side of the COMSTAR antenna mast, with waveguide extending from the package output ports to three earth-viewing horn antennas. The packages were supplied by COMSAT Laboratories, while Hughes Aircraft Company furnished the waveguide and antennas.

To determine the best means of integrating the experiment into the spacecraft, a study was conducted to evaluate potential spacecraft/experiment interfaces. Two approaches were studied:

- a. Beacon packages located on the despun shelf (Figure 1),
- b. Beacon packages located on the antenna mast (Figure 2).

The study involved a joint effort between the thermal and structural engineers. A communications experiment located on the COMSTAR despun shelf had obvious appeal because of the stable temperature environment

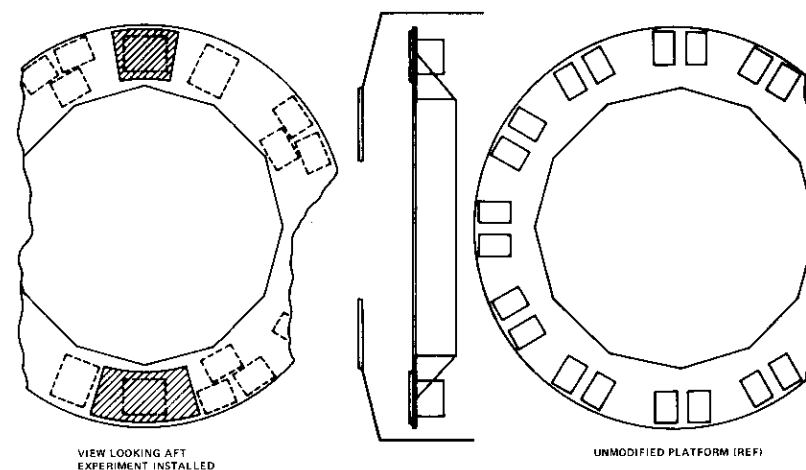


Figure 1. Millimeter Wave Experiment Despun Shelf Installation

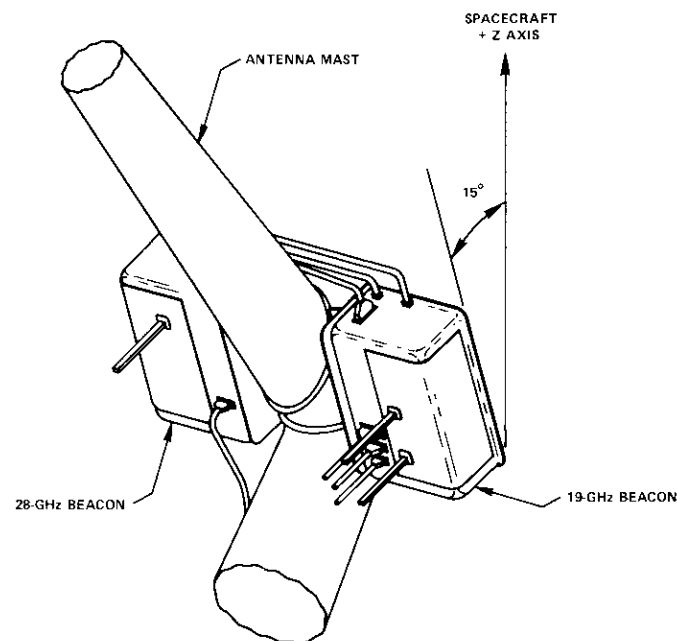


Figure 2. Millimeter Wave Experiment Mast Installation

and the potential for conventional integration into the antenna and other spacecraft systems. However, this location did not prove practical because the Beacon program began after the spacecraft design had been essentially completed. Extensive redesign of the despun platform, including physical modification and relocation of spacecraft components, would have been required to preserve the original temperature environment.

Platform temperature control would demand almost constant Beacon dissipation (full-time operation), in effect preventing the use of only excess beginning-of-life power. If the experiment were turned off when excess power were no longer available, the step change in shelf heat dissipation would cause significantly lower temperatures.

A logical solution to these dilemmas would be to select a Beacon location which provides maximum independence from the spacecraft and allows both spacecraft and Beacon designs to proceed smoothly with minimum interaction. Mounting on the antenna mast would certainly provide the maximum opportunity for physical independence. The next design step determined the optimum temperature control concept compatible with an exposed mast location and the degree of thermal interaction with the spacecraft. In a subsequent section, it will be seen that minimizing the thermal interface with the spacecraft (*i.e.*, conductive and radiative heat transfer between experiment and spacecraft) is a primary design criterion.

The concern for the increased overall bending moment at the COMSTAR despun clamp due to the Beacon's position on the mast was alleviated by results of structural analysis. The COMSTAR bearing and power transfer assembly (BAPTA) was identical to that of the INTELSAT IV-A satellite, having an antenna mast 1.5 m longer to accommodate a third receive antenna. It was possible, therefore, to permit additional weight on the COMSTAR mast. A COMSTAR dynamic model was prepared based on locating the Beacon at the mast elbow, and the resulting loads were shown to be somewhat less than those of INTELSAT IV-A. A concurrent thermal study determined the optimum attitude of the heat-rejecting radiators for minimum radiator size. The result, a minimized view of the spacecraft external surfaces, produced a 15° northward tilt, as shown in Figure 2.

Following these studies, the external mast location was recommended, based primarily on the following:

- a. the external location had little impact on the thermal environment of the spacecraft's primary communications components;
- b. the structural loads, although somewhat increased, were still moderate and within the design limit for the COMSTAR BAPTA;

- c. a thermal radiator directly viewing the space sink offered optimum mass utilization and therefore minimum weight;

- d. because the outer rim of the despun shelf provided a relatively severe vibration environment, the mast location offered an opportunity for an equivalent, if not improved, vibration environment;

- e. unlike the shelf location, the external mast location would permit removal and replacement of a Beacon package without any disassembly of the spacecraft main body.

After this approach was approved, a mutually acceptable structural and thermal interface specification was prepared.

### **Thermal design**

#### **Objectives**

The principal thermal design objective was to provide operating temperatures with a mean near room temperature and a tolerance range based on key component performance and reliability profiles. The operational Beacon temperature range was selected as 0°C to 40°C for component mounting surfaces. This was modified somewhat to account for a long-term, nonoperating storage with subsequent experiment turn-on. Also, because the IMPATT diodes have highly concentrated dissipation\* and thermophysical packaging limitations which inevitably lead to a junction temperature near 200°C, the "controlled mounting temperature" was carefully defined.

#### **Temperature control concept**

An externally mounted experiment package with a large constant heat dissipation is a good candidate for simple and reliable passive temperature control. A constant heat flux is maintained primarily through one well-defined path: from components to the space sink through the baseplate/radiator (a platform whose interior is a mounting surface and whose exterior is coated for maximum radiating effectiveness). Adequate conduction paths are needed between each component heat source and the baseplate and within the baseplate itself.

#### **Radiator orientation**

The optimum position of the Beacon radiator surface on the spacecraft is a function of both the direct insolation and infrared (IR) radiation from

\* For example, a 28-GHz IMPATT diode dissipates approximately 4 W in a volume of  $7 \times 10^{-6}$  cm<sup>3</sup>.

the external spacecraft surfaces. There are basic differences between these fluxes. For the most part, as one increases with changing radiator attitude, the other decreases. Solar flux absorption is a function of the optical property of solar absorptance ( $\alpha$ ), which should be minimized. While emittance ( $\epsilon$ ) determines IR flux absorption, another quantity to be minimized, it is also a basic measure of radiator effectiveness, with efflux radiation in direct proportion.

Another important consideration is prediction uncertainty. The solar flux vector as a function of time can be accurately determined. Prediction of IR flux from the external spacecraft surfaces, however, is relatively uncertain because of complex geometry and incompletely defined surface temperatures. IR inputs from the spacecraft forward sunshield are more predictable than those from the antenna complex, and are potentially much larger.

To evaluate the relative influence of solar and IR inputs, two radiator concepts were analyzed:

- a. a north-facing radiator which receives minimum sun exposure but views mast and antenna surfaces, and
- b. a radiator whose surface normal is anti-earth, receiving maximum solar flux (diurnally varying) and IR input only from the spacecraft conical sunshield.

If equal maximum temperatures are assumed for the two attitudes, the north-facing radiator requires twice the area and has a minimum temperature 30°C lower. The anti-earth orientation was chosen.

Spacecraft IR input was eliminated with a radiator plane viewing no spacecraft surfaces, far enough outboard, and with a slight northward tilt. Hence, radiator solar exposure is maximized and there will be an inherent diurnal temperature variation caused by solar flux absorption.

The most widely accepted surface treatment for minimizing solar absorption with high emittance and long-life stability is the silver-under-quartz optical solar reflector. The radiator design used a beginning-of-life  $\alpha$  of 0.10 with a 50-percent degradation allowance for the mission lifetime. The emittance of the radiator was 0.78. The average steady-state baseplate temperature with the sun at normal incidence would be approximately 30°C higher than the minimum temperature with no solar illumination.

#### **Antenna mast interface**

Because the temperature variation of the antenna mast was unknown at the start of Beacon design, maximum thermal resistance was the interface-

mounting thermal design objective. The interface specification had to define a maximum allowable heat flow from the Beacon while preventing heat flow into the experiment because mast temperature was not expected to rise above 20°C. This required a mounting with sufficient thermal resistance to limit the maximum efflux to 2 and 3 W from the 19- and 28-GHz packages, respectively, with both packages at a temperature of -10°C. Thermal vacuum testing proved that the thermal resistance across the interface was greater than anticipated. Thus, actual heat flow was at least an order of magnitude less than the specification limits.

#### **Baseplate/radiator design**

The components imposing the most severe thermal demand on the baseplate/radiator are the IMPATT diodes, with their small mounting surface and high dissipation rates exceeding 60 percent of total Beacon dissipation. For maximum radiator efficiency, component layout on the baseplate was adjusted for maximum separation between IMPATT diodes (and, with lower priority, between other dissipators) consistent with practical waveguide geometry.

Together with component placement, the radiator area must be considered. The thermal designer was initially presented with relatively new untested components (particularly the IMPATTs) whose dissipation had not been accurately defined. Since radiator sizing could not wait for the final definition of Beacon dissipation characteristics, two choices were presented:

- a. An oversized radiator based on most probable dissipations with added conservatism to allow for future dissipation increases. (The effective radiating area could be reduced by masking should dissipations decrease.)
- b. A radiator sized unconservatively for the thermal environment as determined in the initial design phase.

The second approach was chosen because of the strict weight budget; consequences of any future Beacon dissipation increases were understood and accepted for the electronic performance.

Radiator thermal design was based on a quasi-steady-state hot condition of maximum Beacon dissipation and insolation. An analytical thermal model of each Beacon package was developed with special emphasis on the radiator; *i.e.*, 102 of the total 131 nodes of the 28-GHz model were assigned to the radiator. Dissipation from each component was uniformly allotted to nodal areas within its footprint. Lateral conduction through

the honeycomb baseplate was based on the combined thicknesses of both face sheets. A sufficiently high core density guaranteed a negligible temperature difference between the face sheets.

Because the prime heat sources are few and concentrated, and their combined footprints are a small fraction of total radiator area, uniform face sheet thickness throughout does not represent the most efficient use of radiator mass. Maximum fin efficiency can be approached by increasing face sheet thickness in areas of greatest dissipation flux, as demonstrated in the classical analytical treatments of optimum radiating fin profile. The radiator is, in effect, an extended radiating fin for each mounted component. A computer program was written to generate radiator thickness profiles of minimum weight satisfying imposed maximum temperatures. As expected, the thickness contours generated by the program proved to be too complex for practical fabrication. Consequently, the skin thickness contours were slightly modified before being used in the large thermal model for temperature predictions. After several iterations, a final thickness distribution was achieved for the inner face sheet, as shown in Figure 3.

The Beacon project was the first application of this computer program to actual flight hardware, and as far as is known, the first use of variable-thickness, single-piece honeycomb face sheet in a spacecraft. The procedure resulted in a savings of approximately 30 percent in face sheet weight (270 g) as compared to face sheets of uniform thickness performing the same temperature control function.

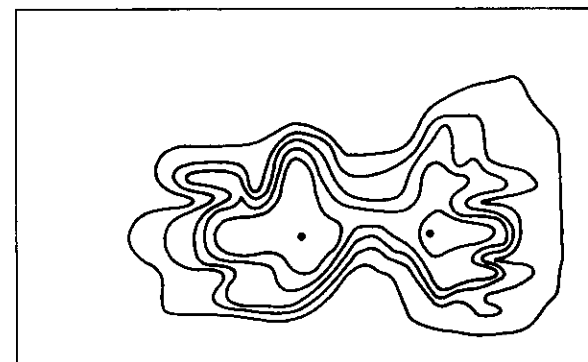
#### Insulation blanket

Very effective multilayer insulation blankets are applied over all other external surfaces to ensure that the radiator is the dominant heat transfer path. Multilayer insulation is a well-recognized, widely used thermal control material. Beginning at the inside layer, the materials are as follows:

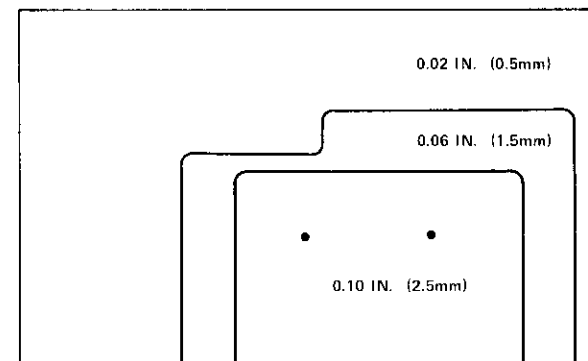
- a. one layer of 0.001-in. (0.025-mm) Mylar with an aluminized side facing inward to provide low emittance in addition to electrical conductivity;
- b. two layers of 8-mesh Dacron tulle;
- c. one layer of double-aluminized 0.00025-in. (0.006-mm) Mylar;
- d. 19 more layers of the same tulle-Mylar combination followed by a double layer of tulle;
- e. a 0.002-in. (0.051-mm) single-aluminized Kapton layer, with the non-metallized surface on the outside.

Appropriate venting slits are provided in all but the outer layer. The

• LOCATIONS OF CENTER OF IMPATT DIODE MOUNTS



CONSTANT-THICKNESS CONTOURS GENERATED BY PROGRAM, REPRESENTING MINIMUM WEIGHT



THICKNESS PROFILE OF FABRICATED BASEPLATE  
(OUTER FACE SHEET IS INCLUDED IN TOTAL THICKNESS)

Figure 3. Face Sheet Thickness Profiles of 19-GHz Baseplate/Radiator (results from analytical optimization program and final fabricated design shown in plan views)

exterior Kapton surface  $\alpha/\epsilon$  is assumed to be 0.4/0.76. Single-aluminized 0.005-in. (0.127-mm) Kapton forms a channel-shaped border around the mirrored radiator for a well-controlled and defined thermal boundary to blanket edges. The blanket is attached to its package with polyester hook-

and-loop fasteners, with the hook cemented to the Kapton border and the loop sewn onto corresponding blanket edges.

The many reported values of effective emittance and conductance were sufficiently accurate to estimate the heat flow through the Beacon blankets. Moreover, highly accurate predictions of heat flow were unnecessary since it should be at least an order of magnitude lower than the radiator heat flow. For temperature prediction, the effective emittance between innermost and outermost layers was taken as either 0.005 or 0.02, whichever value was more conservative for a particular analysis case. During cold storage thermal vacuum testing, with relatively low overall heat transfer, the 0.02 assumption was satisfactorily verified. Under the highest temperature conditions, heat flow through other paths is dominant.

#### **Nonoperating storage**

The potential for unacceptably low temperatures exists during post-launch and at other times when the Beacon is inoperative because the passive temperature control concept is based upon a relatively large and constant heat dissipation. The allowable lower temperature limits of Beacon components when inoperative could easily be exceeded unless a semi-active temperature control was introduced. This control was achieved by activating heaters of sufficient wattage to maintain acceptable minimum temperatures whenever the Beacon is turned off. The heaters were sized conservatively by considering a cold condition not quite achieved in orbit, *i.e.*, steady state with no external heat input. In a relatively straightforward manner, it was determined that 14 W of heater power in each package could maintain safe turn-on temperatures. Thin-film heaters, in 2- and 3-W sizes, were placed on the power conditioners and dual current regulators containing components most affected by the low temperature.

#### **Mechanical design**

##### **Objectives**

In terms of structural design, the most critical factors were the 30-lb (13.6-kg) weight limit and the need to minimize vibration response by isolating Beacon and spacecraft natural frequencies. To maintain positive and accurate control of the weight and center of gravity, a computer program was used during the design process. With periodic revisions of actual or predicted component weights as program input, a continuing

record of the weight margin and computed centers of gravity ensured that they were maintained within tolerance limits.

A 60-Hz minimum natural frequency for the Beacon was selected to provide proper separation from spacecraft natural frequencies. This design goal, although difficult to achieve because of the orientation of the radiators normal to the spacecraft mounting flange, was verified during the thermal-structural model vibration test program.

The use of aluminum for microwave components necessitated extensive silver electroplating to achieve acceptable microwave finishes. For several components, performance and ease of fabrication dictated the use of copper instead of aluminum alloy.

##### **Structure**

Honeycomb sandwich construction was used for baseplate/radiators because of its inherent stiffness-to-weight advantage. As discussed earlier, the inner face sheets were of varying thicknesses to permit optimum use of the thermally conductive aluminum, and a minimum baseplate weight. Additionally, to minimize weight and to allow the second-surface mirrors to be bonded to a flat undisturbed surface, all components were attached to the baseplate internal face with bonded blind inserts instead of through inserts.

The housings, which normally provide RF shielding and equipment protection, were an integral part of the structural design to carry baseplate loads onto the mounting flange. A concept which used a deep-drawn lightweight aluminum chassis augmented by internal stiffeners provided a rigid low-cost design solution.

The mounting flange acted as the mechanical interface to the spacecraft. It was constructed of titanium to achieve high stiffness and low thermal conductance. Similar to the housing, it was drawn to eliminate any fasteners or assembly joints. These design techniques achieved the structural and thermal requirements with a flange weighing only 0.8 lb (359 g).

The cumulative weight of the main structural components, namely, the housing, baseplate, and mounting flange shown in Figure 4, was less than 4 lb (1.8 kg) for each package.

##### **Components**

Several components utilize novel design features necessitated by the small dimensions required at higher microwave frequencies and the severe weight limitation. One such component was the multistep transformer used

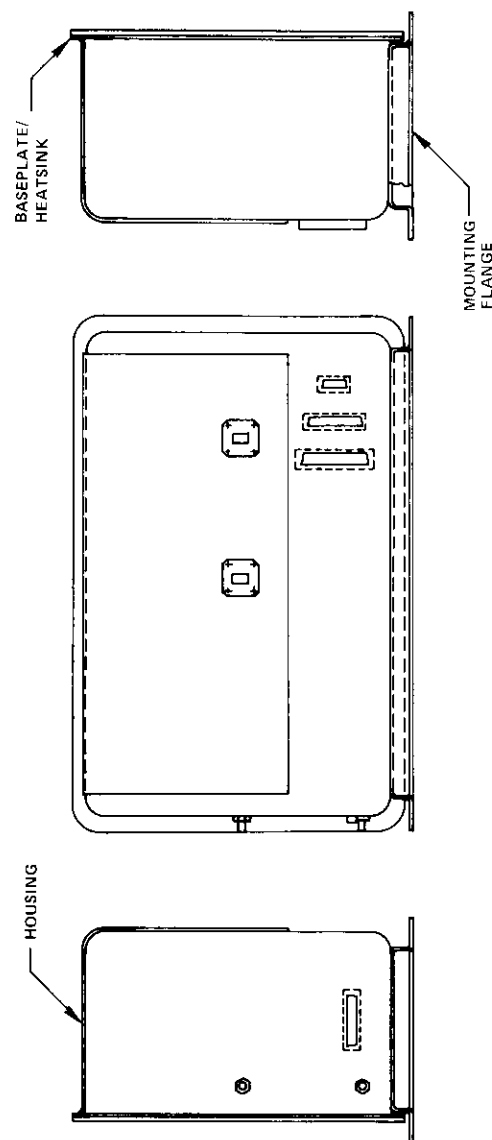


Figure 4. Centimeter Wave Beacon Typical Structural Components  
Showing 19-GHz Package

in the 19-GHz IMPATT amplifier module. The design required six steps with tolerances of  $\pm 0.001$  in. (0.025 mm) and a surface finish better than  $16 \mu\text{in.}$  ( $0.4 \mu\text{m}$ ). Fabrication using standard machining techniques was impractical due to the configuration and exacting tolerances; hence, electroformed copper was chosen to accomplish the stringent requirements. An aluminum mandrel was easy to fabricate and the electroformed part exactly duplicated the dimensions and finish of the mandrel. The finished transformer had a surface finish of better than  $8 \mu\text{in.}$  ( $0.2 \mu\text{m}$ ) and all tolerances were met. The weight penalty associated with the use of copper was minimal since the wall thicknesses were significantly less than those which would have been possible had aluminum been used.

Differences in thermal expansion presented another design challenge. For some components, consisting of several materials with differing coefficients of thermal expansion, the expected temperature variations coupled with the exacting tolerances made the problem quite severe. Several different solutions to this situation are presented.

The 28-GHz phase modulator, shown in Figure 5, was made with an aluminum body and a beryllium-copper center conductor. To compensate for differences in the thermal expansion of these two materials, the center conductor had an internal captivated spring ensuring contact with the diode. The spring had to be small and electrically conductive, and it had to deliver a predictable spring rate. The chosen spring, made of common steel wire, was 0.120 in. (3 mm) long, 0.086 in. (2 mm) in diameter, and had a 6.3-lb/in. (1,103-N/m) spring rate throughout its travel. To make it electrically conductive, it was gold plated prior to assembly.

A second solution to the thermal expansion problem is typified by the 19-GHz  $\times 2$  multiplier shown in Figure 6. The diode mount utilized a commercially available Fuzz Button\* loaded by a spring to ensure continuous contact at the base of the diode at all temperature extremes. The Fuzz Button is a cylindrical object consisting of intermeshed fine beryllium-copper wires which are gold plated. It offers a predictable diametrical expansion upon longitudinal compression by the spring and has a repeatable spring expansion rate.

As a final example, the center conductors of the  $\times 4$  and  $\times 6$  multipliers required another solution to thermal expansion problems. A multiplier is shown in Figure 7. Spring fingers fabricated at one end of the center conductor were closed slightly and heat treated to a predetermined spring

\* Registered trademark, Technical Wire Products Inc.

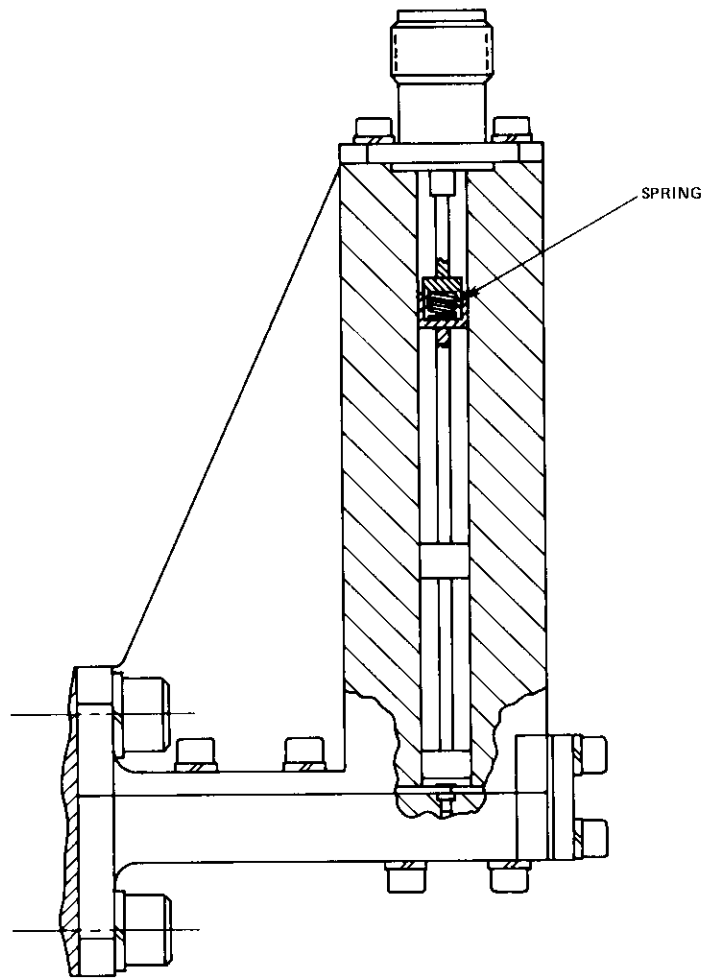


Figure 5. 28-GHz Phase Modulator

temper. The closed dimension, which was slightly smaller than the diameter of the diodes, also permitted longitudinal movement due to differing coefficients of thermal expansion and, additionally, assembly and manufacturing tolerances.

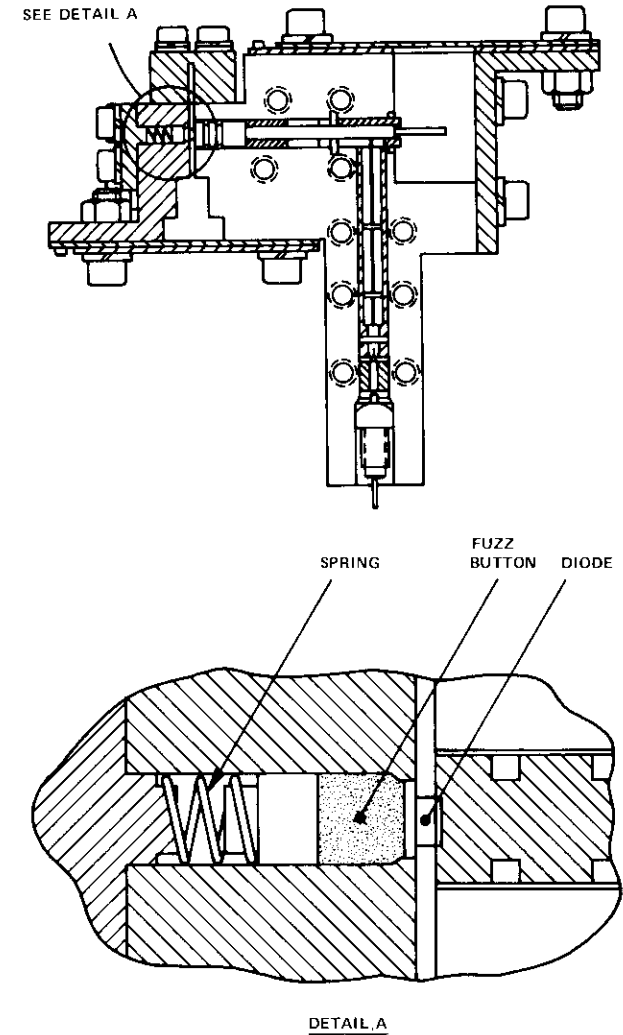


Figure 6. 19-GHz  $\times 2$  Multiplier

The solutions in these areas of concern, although not unique in concept, involve a novel approach to mechanical assembly of microwave parts, for which dimensions and tolerances are quite small. These techniques enabled the Beacon to be assembled with relative ease, while meeting the stringent weight and performance requirements.

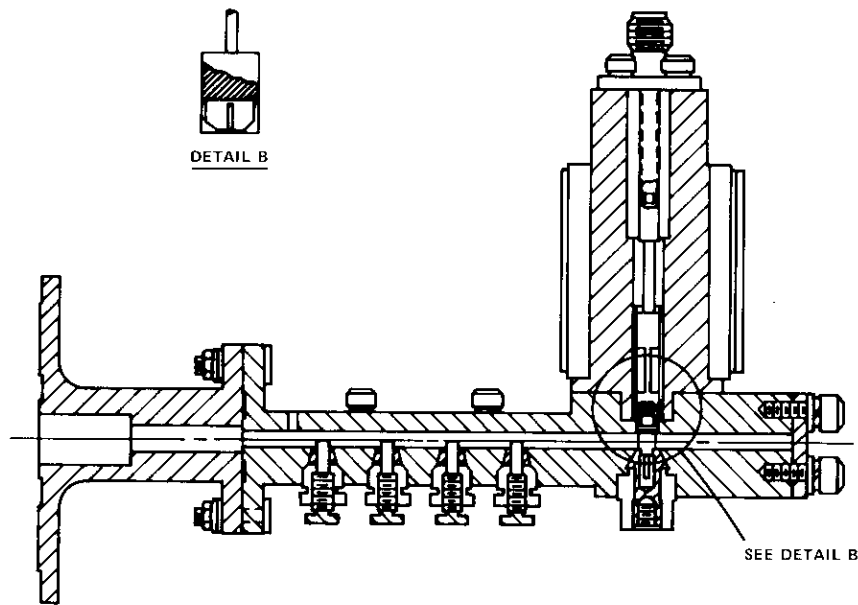


Figure 7.  $\times 4$  Multiplier

## Testing

### Thermal structural model

Thermal vacuum testing of a Beacon thermal structural model (TSM) is intended primarily to verify the thermal design through proper simulation of all thermal characteristics of the Beacon and the external thermal environment expected in orbit. The TSM's internal components are aluminum blocks, simulating actual component mass, heat capacities, and mounting areas. Appropriate resistive heaters represent each dissipative component. Insulation to the radiator is simulated with electrical dissipation in a thin-film heater bonded to the baseplate exterior beneath the optical-solar reflectors. The heater area is identical to the mirror coverage. Solar and IR radiation absorption by the insulation blanket surfaces is simulated with a number of similar rectangular, externally mounted, thin-film heaters. Heater emittance is identical to that of the blanket; hence, there is no change in exterior emittance. Less than full coverage of the blanket exterior by these heaters (thereby avoiding elaborate custom

heater designs) is permissible due to the relatively high resistance thermal path through the blanket. The diurnal variation of all external heater power has been achieved with individually preprogrammed power supplies.

The TSM was subjected to two thermal vacuum tests. The first, at COMSAT Laboratories, provided overall thermal design verification at the earliest possible stage in the program. In the second, which was conducted during the COMSTAR spacecraft solar simulation test, the TSM served as a surrogate for spacecraft integration purposes while receiving a second design verification test under a more realistic external thermal environment.

The TSM thermal vacuum test at COMSAT Labs had four phases, the first two simulating an inoperative Beacon, and the last two at full internal dissipation:

- a. a cool-down from launch with no heat input of any kind;
- b. steady-state storage, with 14 W of simulated storage heater dissipation in each package;
- c. cold phase, a 1-day winter solstice transient with radiator mirror surface  $\alpha = 0.08$ ;
- d. hot condition, with simulated solar input based on near summer solstice and mirror  $\alpha = 0.12$ .

Agreement between test results and analytical predictions was generally quite satisfactory, and no post-test thermal design modifications were deemed appropriate. As an example, Figure 8 shows the history of representative thermocouples in the 19-GHz TSM package during the hot case, together with a trace of the corresponding "baseplate average" temperature from an analytical model. Temperatures throughout the baseplate/radiator were examined using the larger analytical model and compared with those of the TSM thermocouples. Test temperatures were  $4^{\circ}\text{C}$  to  $6^{\circ}\text{C}$  lower than those predicted for both hot and cold conditions.

During COMSTAR testing, the TSM was subjected to a more realistic solar simulation using xenon lamps. Maximum temperatures from this test were slightly higher than those in the earlier test, and in fact, closer to the large model analytical predictions. The maximum temperatures occurred later for the 19-GHz and earlier for the 28-GHz package, about 1.5 hours out of phase. These differences can be explained as follows:

- a. The Beacon was in a partially uncollimated solar beam which produced approximately 1.15 solar constants at normal incidence on the radiators.
- b. The radiator absorptance assumed for the COMSAT test was 0.12; the actual absorptance under the xenon spectrum was probably higher.

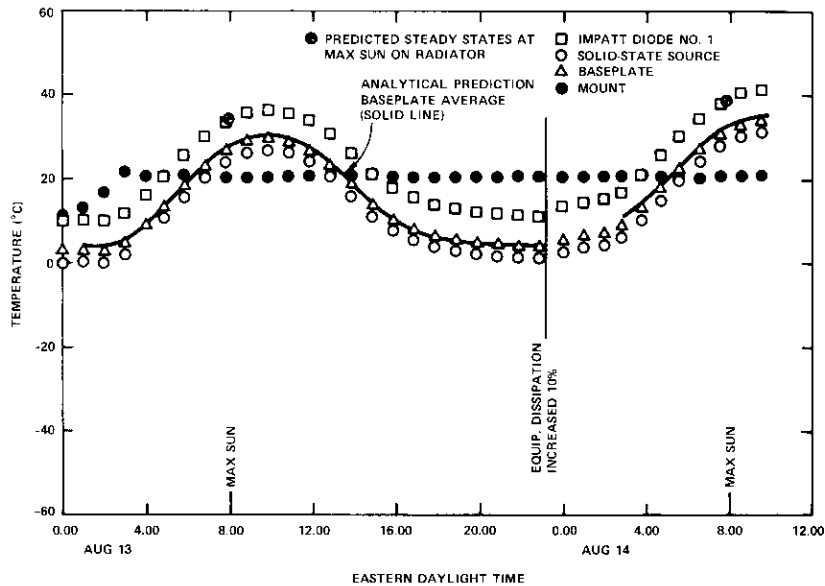


Figure 8. 19-GHz Beacon TSM Thermal Vacuum Test (hot case)

c. Heat flow into the packages through the insulation was probably greater during the solar simulation test because several blanket film heaters became detached during the COMSAT Laboratories test.

The TSM vibration tests qualified the structural design for flight. The baseplates were instrumented with accelerometers to determine natural frequencies and to evaluate the adequacy of the component qualification test specifications. Because the TSM packages were also scheduled to be qualified at the spacecraft level during the COMSTAR antenna qualification program, a protoflight qualification approach was used. The harness and heaters were checked for continuity after TSM vibration testing.

#### Flight model acceptance

After confidence in temperature predictions was reinforced by the results of the TSM test program, an acceptance testing procedure for all flight models was developed. The basic test philosophy was to duplicate in the flight models, with suitable acceptance level extensions, the expected in-orbit baseplate temperatures for all extreme conditions. Temperature

control within the liquid-nitrogen-shrouded chamber was achieved with fairly uniform heat flux input to the radiators from four voltage-controlled quartz-rod IR lamps (two for each radiator). Seven strategically placed thermocouples in each package gave a complete temperature profile of the experiment in addition to confirming the telemetry calibration of the three flight thermistor sensors. A baseplate-mounted thermocouple in each package (corresponding to a similarly located TSM sensor) served as the monitor for controlling the lamp voltage. The two packages of each flight Beacon were mounted to the same fixture (duplicating the spacecraft thermal and geometric interface) as the TSM, and fitted with their flight insulation blankets.

The test procedure can best be illustrated by data from the three thermistors over the complete 2.5-day test of the flight 3 model, as shown in Figure 9. The test phases were as follows:

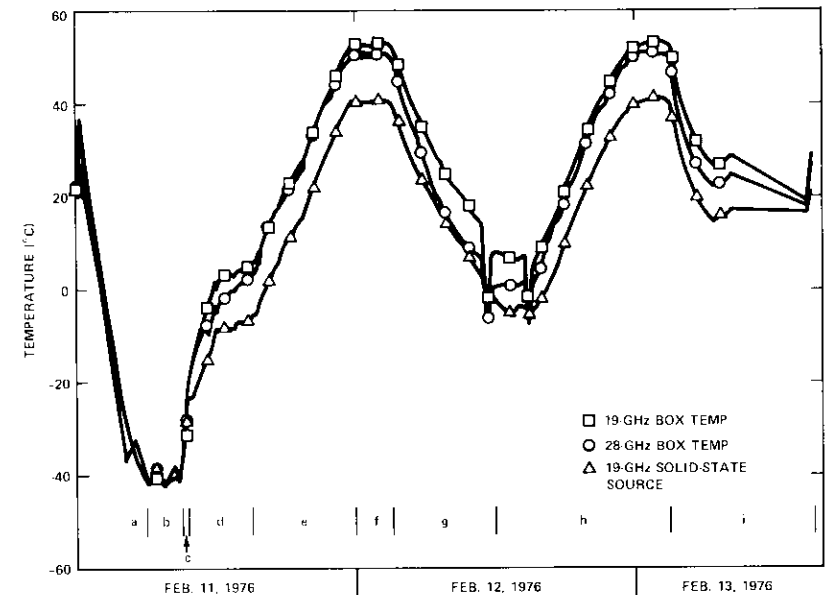


Figure 9. Beacon Flight Model 3 Thermal Vacuum Acceptance Test Temperature Telemetry

- a. post-launch cool-down from room temperature;
- b. 3-hour cold storage;

- c. warm-up to turn-on;
- d. turn-on and 3-hour cold soak;
- e. 9-hour (linear) transition to hot;
- f. 3-hour hot soak;
- g. 9-hour transition to cold;
- h. 15-hour total repetition of cold soak, transition, and hot soak;
- i. controlled return to room conditions.

Test levels were set to exceed expected in-orbit temperature limits by 5°C. Because power consumption varied somewhat among Beacons, exact temperature levels of hot and cold soaks were "customized" for each Beacon to account for differences in expected in-orbit temperatures.

The flight acceptance vibration test objective was to verify workmanship prior to shipping the Beacons for installation on the COMSTAR spacecraft. The Hughes Aircraft Company practice of deleting the component sinusoidal vibration test was adopted. However, the flight spare Beacons were qualified as protoflight units. Thus, each was exposed to both protoflight sinusoidal and random tests as shown in Table 1. The Beacon packages were vibrated separately with the non-vibrating unit intercon-

TABLE 1. PROTOFLIGHT VIBRATION TEST SPECIFICATION

a. Sinusoidal Vibration				
Spacecraft Axis	Frequency Range (Hz)	Acceleration Level*	Sweep Rate	
Longitudinal (Z)	5-15	0.6 i.d.a.	4 oct/min	
	15-30	6.9 g		
	30-60	11.5 g		
Lateral (X and Y)	60-2,000	5.0 g	4 oct/min	
	5-24.5	9.6 i.d.a.		
	24.5-30	18.4 g		
	30-2,000	5.0 g		
b. Random Vibration				
Spacecraft Axis	Frequency (Hz)	PSD Level (g <sup>2</sup> /Hz)	Overall Acceleration (g-rms)	Duration
Longitudinal (Z)	20-100	0.115	—	—
Lateral (X and Y)	100-210	-3 dB/oct	11	2 min/axis
	210-2,000	0.052	—	

\* i.d.a. is inches double amplitude, and g is gravitational acceleration, 0 to peak.

nected by semirigid coaxial cable and electrical interconnect harnesses. Tests run in the three orthogonal spacecraft axes anticipated the inputs which would occur during spacecraft vibration testing with a 15° reorientation of the vibration fixture for the Z and Y axes. The Beacon was operated during vibration testing and inspected after each test exposure.

#### Flight temperature data

Telemetered temperature data from each flight Beacon come from three thermistors, located at the 19-GHz solid-state source and the mounting bases of the second stage IMPATT diode assemblies of the 19- and 28-GHz packages. On-station data from the D-1 COMSTAR [Beacon flight spare (FS) model] have been studied since May 26, 1976, and data from the D-2 (Beacon flight-3 model) since August 23, 1976.

Figure 10 shows a 24-hour history of the temperature telemetry channels of the D-1 COMSTAR Beacon on June 6, 1976. Because this is very close to the maximum solar input, or hot design case, it is of interest to compare these data with earlier test and analysis data. Figure 11 shows

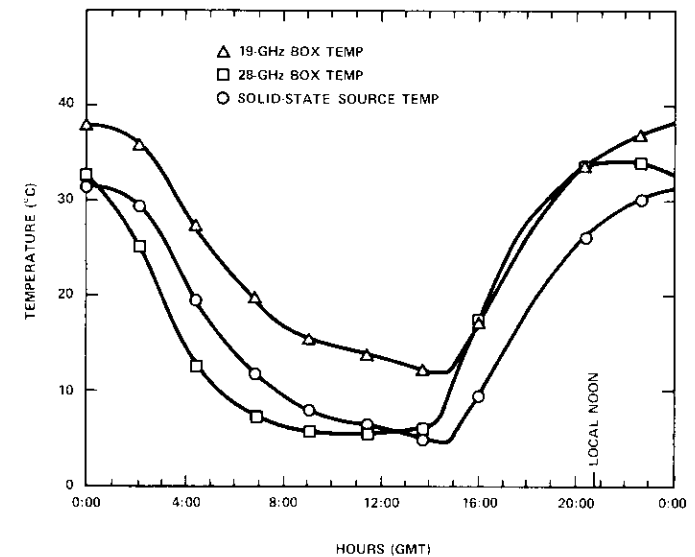


Figure 10. Typical 24-Hour History of Temperature Telemetry from Flight Spare Beacon on COMSTAR D-1 Spacecraft

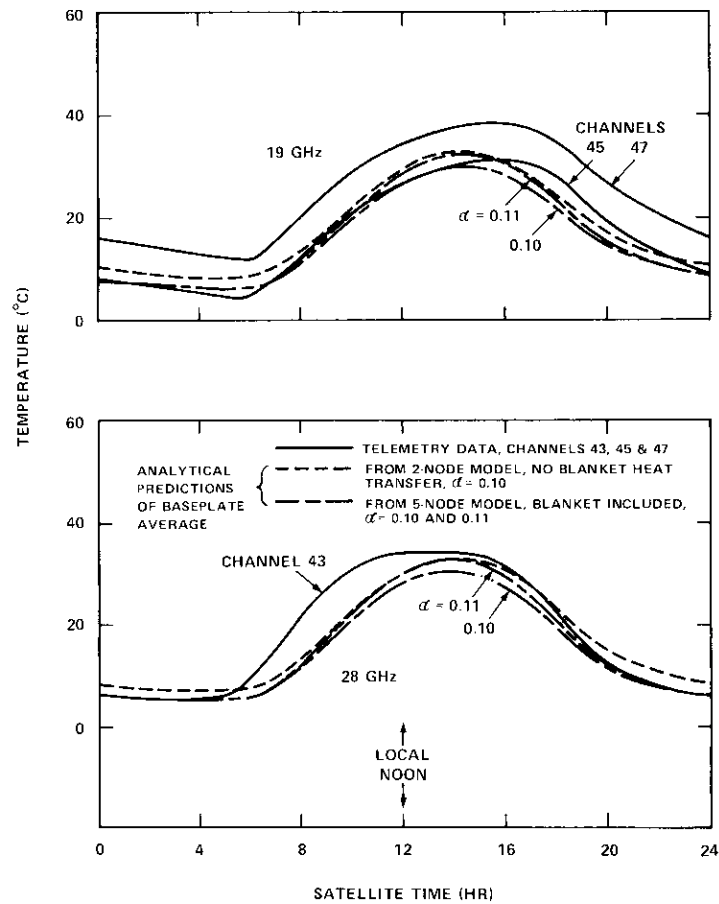


Figure 11. Comparison of Telemetered Temperature Data (from flight spare Beacon, June 6, 1976) with Analytical Predictions of Average Baseplate Temperature (maximum temperature conditions)

the flight data, together with predictions from two analytical models. The same flight data are compared with the results of the solar simulation test in Figure 12. Test temperatures were satisfactorily higher and of the same general shape as flight data, indicating good agreement. The slight difference between flight and predicted temperature profiles is ascribed

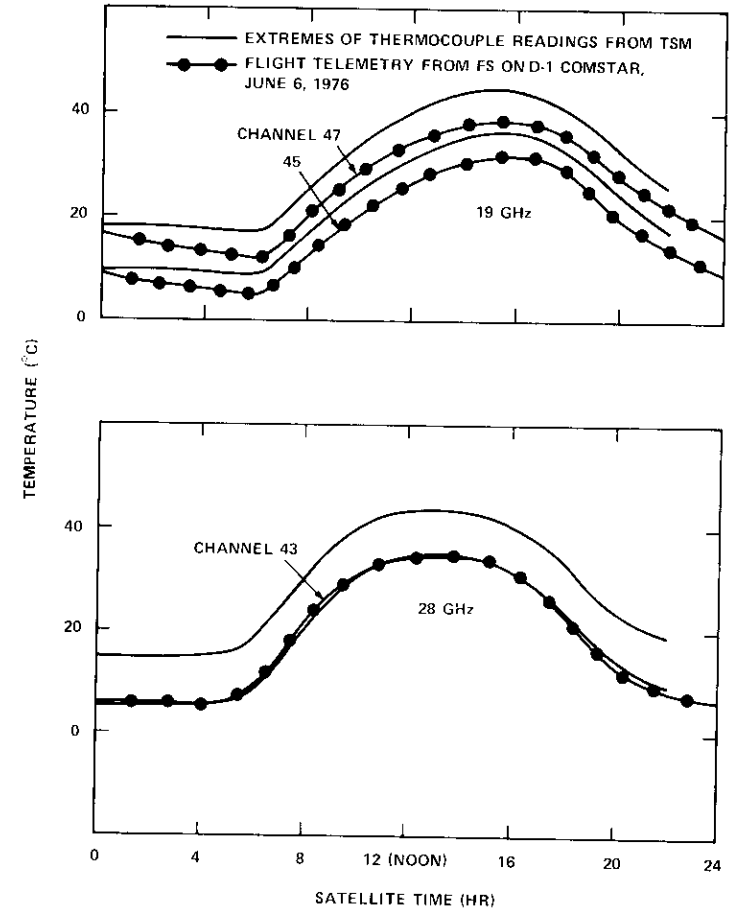


Figure 12. Comparison of TSM Temperatures During Hot Case of Spacecraft Solar Simulation Test of August 1975 with Flight Spare Telemetry of June 6, 1976

to a lack of detail in the analytical model in the area where the insulation blankets cover the mast.

The most significant conclusion from flight data investigation is that temperatures are indeed within the limits initially established, and that the individual Beacon flight models were subjected to acceptance test

temperatures with adequate margins beyond the flight conditions. Table 2 provides a direct comparison of flight and acceptance test temperature extremes for the flight spare (D-1 COMSTAR) and flight-3 (D-2 COMSTAR) Beacons.

TABLE 2. TEMPERATURE COMPARISON OF FLIGHT TELEMETRY AND ACCEPTANCE TEST EXTREMES

	Temperatures (°C)					
	D-1 COMSTAR Flight Spare Beacon			D-2 COMSTAR Flight-3 Beacon		
	19-GHz Box	19-GHz Solid- State Source	28-GHz Box	19-GHz Box	19-GHz Solid- State Source	28-GHz Box
Acceptance Test, Maximum	54	44	51	53	41	51
Flight Extremes,* Maximum	40	33	36	44	33	38
Minimum	12	4	5	6	11	11
Acceptance Test, Minimum	0	-10	-5	5	-5	0

\* Through August 1976 for D-1; through October 1976 for D-2.

Of considerable concern to long-term temperature stability are the degradation characteristics of the optical solar reflector covering on the radiators. While the precise source of mirror contamination or degradation cannot be discerned, and will not be conjectured herein, values of  $\alpha$  as a function of time have been extracted from the flight temperature data. The nearly constant power of the Beacon experiment and its negligible thermal interaction with the rest of the spacecraft provide an unprecedented opportunity to obtain accurate values for  $\alpha$ .

Results for the flight spare 28-GHz package through October 25, 1976, show  $\alpha$  increasing from 0.100 to 0.116 over 148 days; for flight-3,  $\alpha$  increases from 0.100 to 0.107 over 63 days, an approximately equal rate of increase. A disconcerting observation is that the  $\alpha$  increase shows no sign of leveling off, and that the change in  $\alpha$  is approximately constant at 40 percent/year. If  $\alpha$  increases at this same rate, the 1977 hot season temperatures would be 9°C above those at corresponding times in 1976. Mirror degradation is therefore an area of prime concern, and monitoring of mirror degradation will continue throughout the life of each Beacon.

## References

- [1] "The INTELSAT IV Spacecraft," edited by E. T. Jilg, *COMSAT Technical Review*, Vol. 2, No. 2, Fall 1972, pp. 271-389.
- [2] Gomaa E. A. Abutaleb et al., "The COMSTAR Satellite System," *COMSAT Technical Review*, Vol. 7, No. 1, Spring 1977, pp. 35-83.
- [3] A. J. Gopin and A. S. Friedman, "Thermal Analysis and Control of the Air Force Tactical Communications Satellite," *Communications Satellites for the 70's: Technology (AIAA Progress in Astronautics and Aeronautics, Vol. 25)*, edited by N. E. Feldman and C. M. Kelly, Cambridge, Massachusetts: M.I.T. Press, 1971.



Nelson Hyman received a B.M.E. degree from Georgia Institute of Technology in 1958 and a M.S.M.E. degree from the University of Maryland in 1959. Prior to joining COMSAT Laboratories in 1969, he was engaged in all aspects of spacecraft thermal design with NASA/Goddard Space Flight Center and Fairchild Industries. He is presently a member of the technical staff in the Thermal Control and Environmental Testing Department of the Spacecraft Laboratory. He has participated in the thermal performance analysis of the INTELSAT IV spacecraft and is the principal contributor to the thermal design of the Centimeter Wave Beacon.

David Perlmutter received a B.M.E. in 1967 and an M.M.E. in 1968 from Rensselaer Polytechnic Institute. In 1968 he began working at Raytheon's Space and Information Systems Division, where he assisted in the design of the Poseidon guidance computer. In 1969 he transferred to the Electromagnetic Systems Division, where he worked on the design of several airborne ECM systems. He joined COMSAT Laboratories in 1974 and has been involved in a variety of mechanical designs for spaceborne and earth-based systems. He is presently a member of the technical staff in the Mechanical Design Department of the Spacecraft Laboratory. He is a member of AIAA and ASME.





*Howard W. Flieger received B.S. (Chemistry) B.S.E. and Applied Science, and M.S.E. and Applied Science degrees from The George Washington University. Prior to joining COMSAT Laboratories, he was a research scientist with the National Bureau of Standards, specializing in low-temperature thermodynamics and high-temperature heat transport properties. In addition, he was responsible for the thermal design of experimental stabilized spacecraft at the Johns Hopkins University Applied Physics Laboratory. With COMSAT Laboratories since 1967, he is Manager of the Thermal Design and Environmental Testing Department of the Spacecraft Laboratory, concerned with spacecraft thermal research and development projects. He has participated in the thermal design, analysis, and testing of the INTELSAT III, IV, and V spacecraft programs. In addition, he was responsible for the thermal design and testing of the ATS-6 COMSAT Millimeter Wave Propagation Experiment and the Centimeter Wave Beacon. He is a member of AIAA, Sigma Tau, the AIAA Working Group on Space Simulation, and the AIAA 1977 Thermophysics Award Selection Committee.*

*Paul R. Schrantz received a B.M.E. from the University of Detroit in 1959 and an M.S. from Northwestern University in 1961. Prior to joining COMSAT Laboratories in 1968, he was employed as a structural analyst in the Space Department of the Applied Physics Laboratory/Johns Hopkins University. He has been involved in the evaluation of launch loads analysis and flight data, and has participated in the vibration qualification of INTELSAT IV-A and COMSTAR. In addition, he has directed the vibration testing of the ATS-6 transponder and Centimeter Wave Beacons. He has been responsible for the INTELSAT R&D projects in the spacecraft structures area, and is currently manager of the Stabilization and Structures Department of the Spacecraft Laboratory.*



*Paul R. Schrantz received a B.M.E. from the University of Detroit in 1959 and an M.S. from Northwestern University in 1961. Prior to joining COMSAT Laboratories in 1968, he was employed as a structural analyst in the Space Department of the Applied Physics Laboratory/Johns Hopkins University. He has been involved in the evaluation of launch loads analysis and flight data, and has participated in the vibration qualification of INTELSAT IV-A and COMSTAR. In addition, he has directed the vibration testing of the ATS-6 transponder and Centimeter Wave Beacons. He has been responsible for the INTELSAT R&D projects in the spacecraft structures area, and is currently manager of the Stabilization and Structures Department of the Spacecraft Laboratory.*

**Index: in-orbit testing, satellite, automatic control, measurement**

## ***In-orbit testing of communications satellites***

I. DOSTIS, C. MAHLE, V. RIGINOS, AND I. ATOHOUN

(Manuscript received October 19, 1976)

### ***Abstract***

This paper describes the techniques that have been developed and applied by the Communications Satellite Corporation to in-orbit testing of communications satellites. As the spacecraft complexity has increased over the years, the scope of the in-orbit tests has expanded significantly, and the present in-orbit test techniques have evolved from relatively simple evaluations to sophisticated measurements of satellite performance. The increased test requirements for the recent INTELSAT IV-A and COMSTAR spacecraft, with their complex antenna and transponder configurations, have led, in an effort to minimize satellite test time, to the development of the semiautomated test setup described in this paper. The specific measurements described are flux density for saturation, spacecraft e.i.r.p., antenna patterns, beam isolation, gain transfer characteristics, gain-to-noise temperature ratio, receiver local oscillator frequencies, traveling wave tube turn-on transients, in-band and out-of-band frequency response, and cross polarization.

### ***Introduction***

After a successful launch of a new communications satellite, it is desirable to test the communications subsystem while the spacecraft is in orbit. A comparison of the data obtained from in-orbit tests with the prelaunch data measured or derived from similar tests determines whether or not all

the communications subsystems of a spacecraft have successfully survived the launch into synchronous orbit. In addition, during in-orbit testing, highly accurate far-field antenna patterns of the satellite are obtained for the first time, since prelaunch antenna patterns are generally measured on non-ideal ranges.

Unlike usual laboratory measurements for which the object of the test is readily accessible, during in-orbit testing the spacecraft is in a geosynchronous orbit approximately 42,000 km away from the earth station from which the test is performed. Hence, the test setup calibration must take into account not only the earth station equipment and antenna, but also the RF path between the station and the spacecraft. The signal attenuation between these two antennas, however, is not constant but varies according to the atmospheric conditions. Consequently, testing procedures have been devised so that most of the measurements are relative and self-consistent.

Over the years, in-orbit testing at COMSAT has evolved in nature and scope from the testing of EARLY BIRD, the first commercial communications satellite—for which the main objective was to determine whether the spacecraft was operating satisfactorily—to the complete testing of present-day spacecraft such as the INTELSAT IV-A and COMSTAR. Continuous refinement of testing techniques has permitted both the measurement of more parameters with increased confidence, and the acquisition of greater amounts of data. While the scope and capabilities of in-orbit testing have been expanding, the capacity and complexity of communications satellites have greatly increased with the introduction of multifeed and dual-polarization antennas, a greater number of transponders, and a significantly greater number of switchable operating modes. As a result, the amount of data gathered during an in-orbit test has increased dramatically.

The technical objective of an in-orbit test has been to measure as completely and as accurately as possible the performance of the satellite under test. In addition to this objective there are two other very important considerations:

- a. the test should be performed in the shortest possible time so that the satellite can be placed in commercial operation as soon as possible after it has been launched,
- b. the test should be performed with the least expenditure of on-board fuel since the useful lifetime of the spacecraft is directly related to the amounts of fuel available.

Because these objectives could not have been met for INTELSAT IV-A and COMSTAR satellites if the manual testing procedures used prior to these spacecraft had been applied, a semiautomated testing system was de-

veloped. With this new system, the test time for the more complex INTELSAT IV-A is comparable to that required for INTELSAT IV despite the increased capacity and complexity of the former spacecraft.

### History of test development

The basic elements forming the link from an earth station to a spacecraft under test and back to an earth station are summarized in Figure 1. A test signal generated at the test site is amplified by a 6-GHz high-power amplifier (HPA) to a level typically ranging from a few watts to several kilowatts and then beamed through the earth station antenna toward the spacecraft under test. After attenuation of the order of 200 dB, this signal illuminates the spacecraft antenna and is amplified and translated by the spacecraft transponder, which typically consists of a 6-GHz low-noise amplifier (LNA) and a down-converter to 4 GHz followed by driver and transmitter amplifiers usually providing an RF power level of several watts. The test signal is then beamed to the earth station by the spacecraft transmit antenna and, after another free-space loss of about 196 dB, it reaches the earth station, where it is collected by the large-aperture antenna, amplified by the LNA, and processed in the receiver. To accurately measure the operating parameters of the spacecraft, the other elements of the link must be well known.

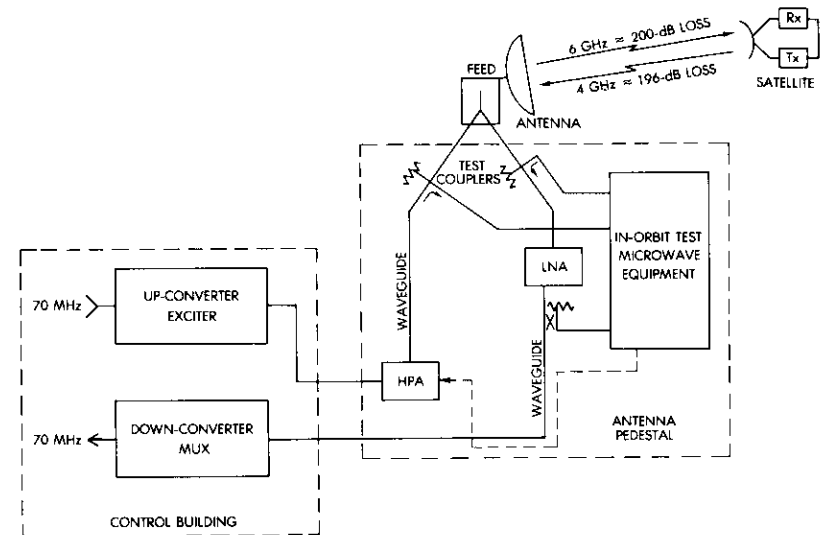


Figure 1. Link under Test

Many of the early satellite tests used the earth station operational communications equipment. This allowed easy access so that the transmission link could begin and end at 70 MHz, where measurements could readily be made with a minimal amount of test equipment. Unfortunately, this technique did not result in sufficient accuracy and repeatability, and over the years the measurement location was moved closer to the spacecraft. Consequently, starting with INTELSAT III all testing was conducted at the antenna feed using calibrated directional couplers and direct microwave measurements at 6 and 4 GHz.

In an effort to enhance accuracy, the absolute measurements necessary for an in-orbit test have been reduced to microwave power and frequency measurements; all other measurements are relative or can be derived from these measurements. For the up-link, the transmit power at 6 GHz is measured directly through a network of directional couplers. For the down-link, an injected carrier technique has proved to be the best solution. A locally generated 4-GHz signal, at a frequency slightly displaced from the received satellite carrier, is injected via directional couplers into the waveguide between the feed and LNA. The power level of this injected reference signal is precisely known through a 4-GHz power meter measurement and the use of coupler and attenuator calibration factors. After sufficient amplification by the LNA and additional amplifiers, both signals are displayed on a spectrum analyzer and made equal by adjusting a calibrated variable attenuator in the injected reference signal path. Hence, even noisy signals can be measured with an accuracy of a few tenths of a decibel, unaffected by any change in gain of the receive chain, while the calibration effort can be restricted to a few passive microwave components such as couplers and attenuators.

To achieve an acceptable measurement accuracy in an in-orbit test, experience gained over the years dictates careful calibration of the microwave power meters at 6 and 4 GHz, the passive microwave components such as couplers in up- and down-link setups, and the earth station antenna gain in both transmit and receive bands. Measurement of the earth station gain is a vital part of in-orbit testing because it can be a potential source of significant errors. Use of an earth station antenna dedicated to in-orbit testing has greatly enhanced accuracy and repeatability of the measurements. During the early years of satellite testing, a variety of earth station antennas with apertures ranging from 13 m (42 ft) to 30 m (97 ft) were used; today's level of precision was achieved only through the use of a dedicated antenna for which an excellent correlation between data obtained from star tracking, boresight measurements, and near-field tech-

niques was obtained after several years of effort.

In parallel with a steady improvement in measurement accuracy, the scope of spacecraft measurements has increased substantially. For instance, on EARLY BIRD equipment limitations constrained the testing to a small number of measurements. Starting with INTELSAT II satellites (Figure 2), transponder gain was evaluated by measuring the test carrier levels and, in addition, noting the level of a satellite Beacon signal which passed through the final traveling wave tube (TWT) and was suppressed as the test carrier level was increased.

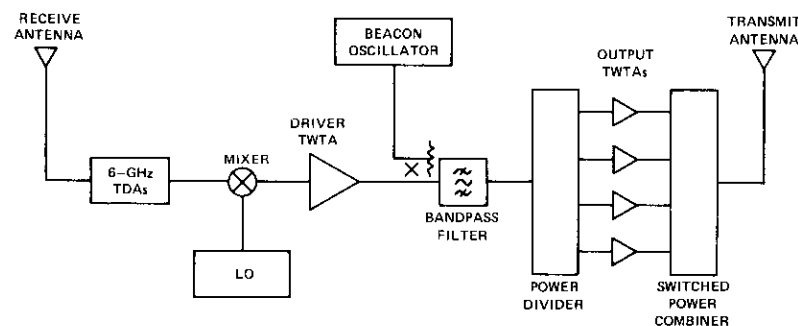


Figure 2. *INTELSAT II Communications Subsystem Simplified Block Diagram*

The advent of a despun spacecraft antenna on the INTELSAT III satellites, together with the use of a 30-m (97-ft) earth station antenna, resulted in the first spacecraft antenna pattern measurements as well as direct effective radiated power relative to isotropic (e.i.r.p.), gain, and satellite noise figure measurements. Frequency response was still a qualitative measurement, and spacecraft translation frequency was still measured to within an accuracy of no better than a few kHz by placing the injected reference carrier on top of the received signal and reading two frequency counters simultaneously. The amount and quality of data increased significantly compared to those obtained for previous satellites, primarily due to improved carrier-to-noise ratios, redundant tunnel diode amplifiers (TDAs), and TWTs in the spacecraft transponder.

On the INTELSAT IV series, antenna patterns of movable spacecraft antennas, the high-gain spot beams, and high-precision translation or local oscillator (LO) frequency measurements were added to the previous measurements. Swept techniques for measuring in-band and out-of-band frequency response were introduced using spectrum analyzer photographs

as a permanent record. Also, the first problems in correlating telemetry antenna pointing data with measured RF antenna patterns were encountered.

For INTELSAT IV-A and COMSTAR, the latest generation of COMSAT-tested satellites, measurement methods were developed to evaluate polarization and beam isolation performance, since both satellites provide frequency reuse via beam or polarization isolation. Figures 3 and 4 are simplified block diagrams of the RF sections of INTELSAT IV-A and COMSTAR spacecraft. The increased system complexity of INTELSAT IV-A and COMSTAR relative to previous satellites is readily observable. The transponder has significant amounts of redundancy to achieve reliable operation. The receivers are connected via redundant switching networks to the antennas. Diplexers enable the same antenna to be used for both receiving and transmitting at different frequencies and polarizations for COMSTAR, whereas separate receive and transmit antennas are used in INTELSAT IV-A. For each transponder all redundant paths must be evaluated during the in-orbit test. This increased complexity and the higher sensitivity necessary for beam isolation measurements in conjunction with stringent limitations on the allowable test time have led to development of the semiautomatic test system described in the following sections.

**Semiautomated test setup**

The semiautomated test setup allows rapid measurements at a number of discrete frequencies (the transponder band centers) without any major manual adjustments. As discussed previously, the down-link carrier from the spacecraft is compared with an injected reference carrier. Both of these signals are synchronized as the measurement frequency is shifted from one transponder to another, presenting a fixed spectrum display for evaluation by the test team. An AM nulling technique is used to accurately determine the spacecraft TWT amplifier (TWTA) saturation level. The setup can be operated in either a computer-controlled or a completely manual mode. The use of this setup has decreased the measuring time while providing significantly improved measurement repeatability.

The setup shown in Figure 5 consists of three racks of equipment which are controlled by an HP9830A programmable calculator. The system's basic functions are as follows:

- a. To generate a phase-locked signal of known power level at the up-link frequency. This signal, which is fed to the HPA at the earth station, is the up-link signal transmitted to the spacecraft.

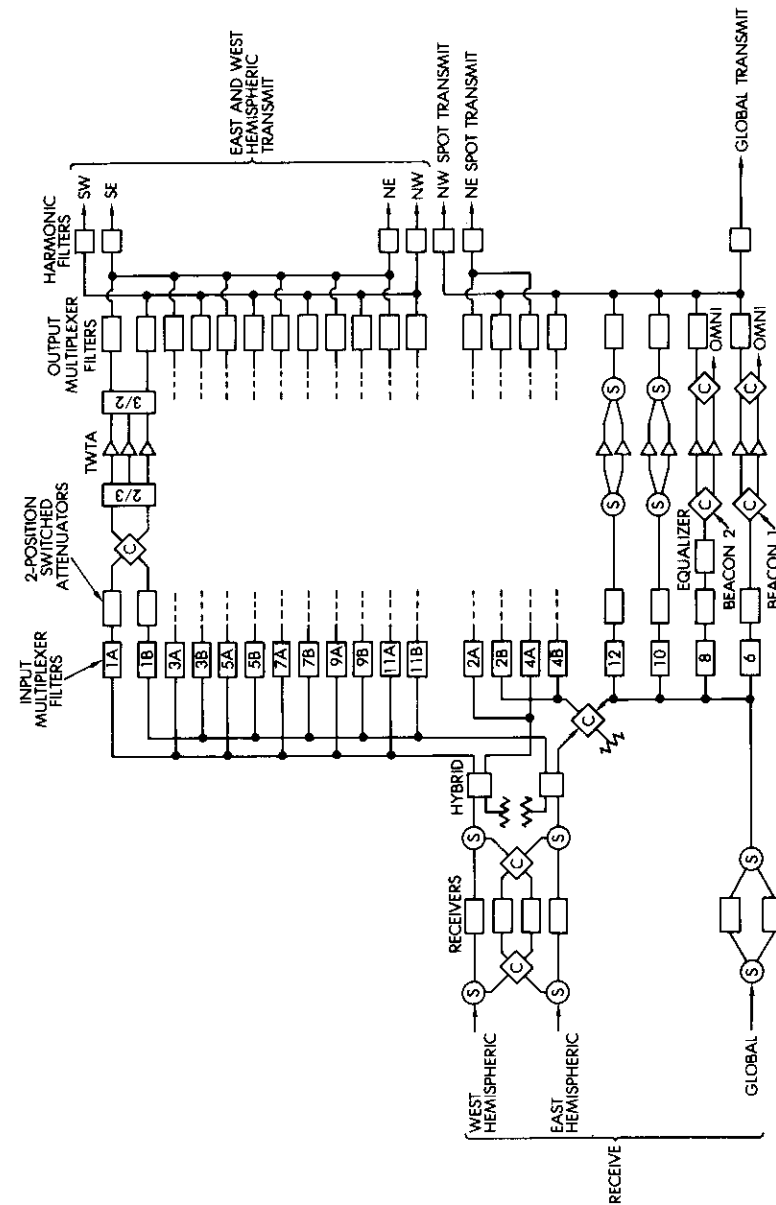


Figure 3. Simplified INTELSAT IV-A Block Diagram

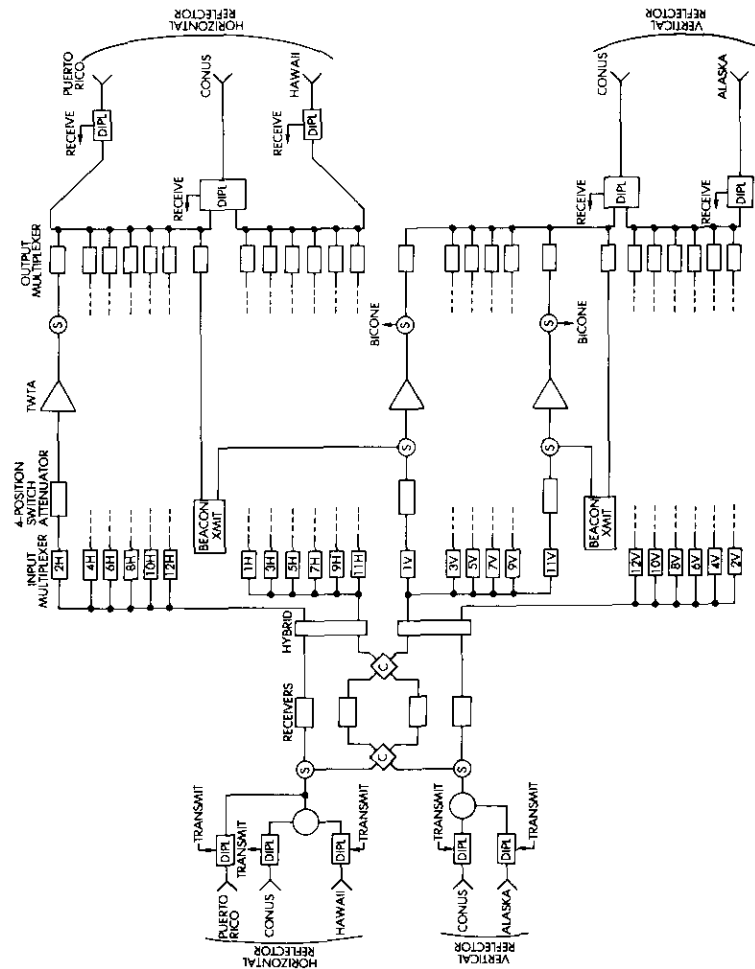


Figure 4. Simplified COMSTAR Block Diagram

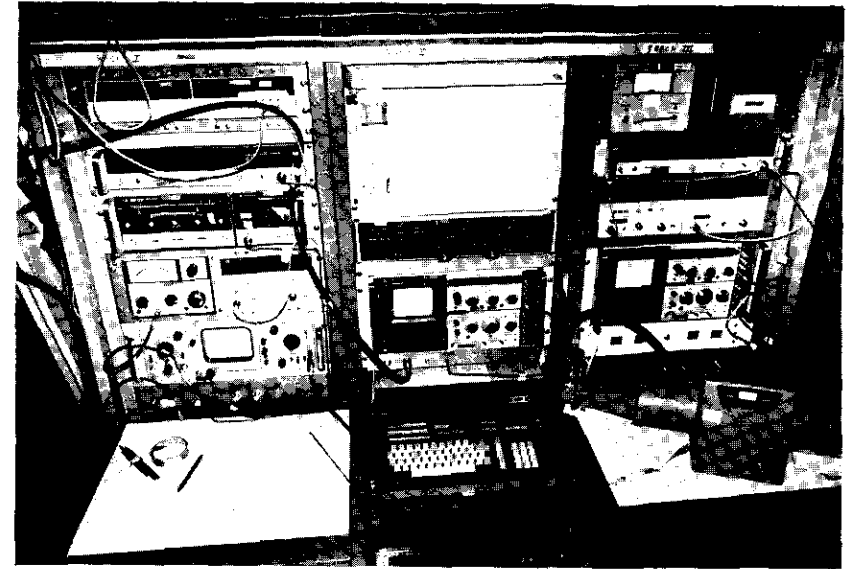


Figure 5. In-Orbit Test Setup

b. To generate a similar signal at the down-link frequency which is injected in front of the station's LNA.

c. To display and measure the LNA's output.

Figure 6 is a schematic diagram of the RF part of the system. The up-link signal is generated by a sweep oscillator which is phase-locked to synthesized signal generator #1. The phase-lock loop consists of a harmonic mixer, a synchronizer, a 10-MHz filter, and a coaxial switch, which is used to turn phase locking on and off. By means of an interface consisting of the ASCII (American standard code for information interchange) to parallel converter and a shift register, the HP9830A controller tunes the sweeper to the desired up-link frequency. The controller also adjusts the synthesizer frequency so that the fourth harmonic of this signal mixed with that of the sweeper is 20 MHz. The frequency synchronizer, which contains a 20-MHz reference oscillator, then locks the sweeper to the 20-MHz signal. The frequency of this phase-locked signal is monitored by frequency counter #1.

After being amplified by a TWTA, the up-link signal is channeled to the earth station's HPA and fed to the antenna. The signal is monitored by a crystal detector mounted on a cross-guide coupler. The output of the

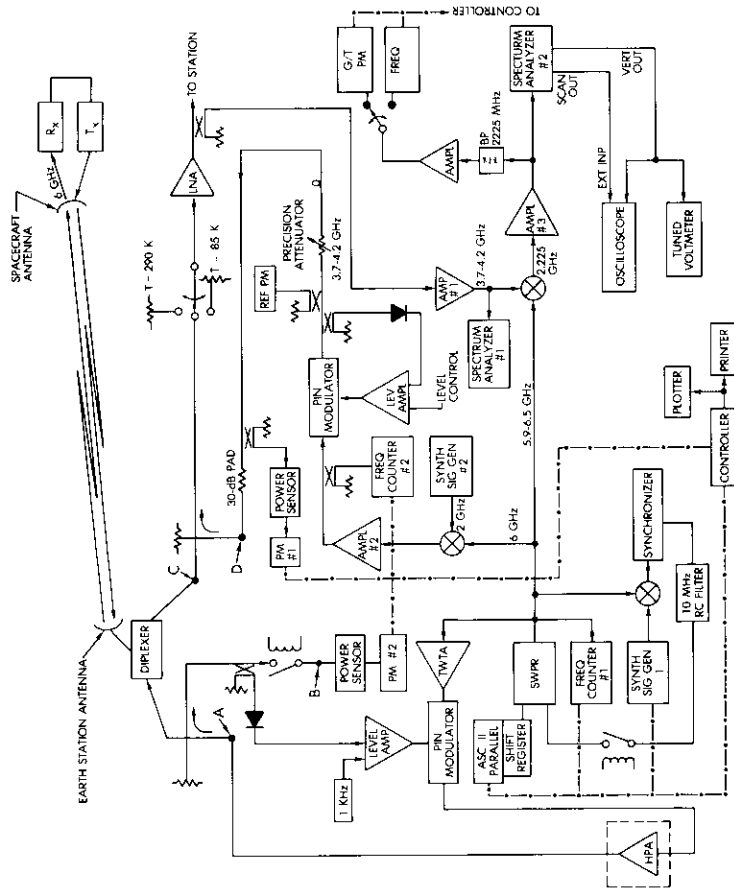


Figure 6. RF System Schematic Diagram

detector is amplified by a DC amplifier which drives a PIN modulator connected at the output of the TWT, thus providing a leveling loop. The up-link power level can be set by adjusting the DC offset of the leveling amplifier, and the signal's power level is monitored by a power head and meter at the cross-guide coupler. In addition, the up-link signal can be amplitude modulated by a 1-kHz sinusoidal wave through the leveling amplifier.

The down-link reference signal is generated by down-converting the up-link signal through a mixer. The LO frequency for this down-conversion is provided by synthesized signal generator #2, which is set at 2,225.1 MHz. After mixing, the reference signal is amplified and leveled to  $\pm 0.05$  dB across the 3.7- to 4.2-GHz band. This signal, whose frequency can be monitored by counter #2, is fed through a precision attenuator, which is used to adjust its power level, and is injected into the station's LNA through a cross-guide coupler. The level at the input of the precision attenuator is made frequency independent by means of a leveling loop and can be manually adjusted if necessary. It is monitored by the reference power meter to ensure proper stability.

After being amplified, the output signal from the station's LNA is displayed in spectrum analyzer #1. It is also mixed with the up-link signal to yield a product which is fixed in frequency and corresponds to the spacecraft's LO frequency. After being amplified, this signal is displayed in spectrum analyzer #2, which is used for comparing the received down-link signal with the injected reference signal. The display of the oscilloscope on rack 1 is slaved to the display of spectrum analyzer #2 so that it can be monitored by a second operator.

To determine the power required to saturate the spacecraft output TWTs,\* the following procedure is used. The up-link signal is amplitude modulated by a 1-kHz sine wave and spectrum analyzer #2 is set in the zero scan mode so that it acts as a narrowband receiver. Both displays show the 1-kHz sine waveform when the satellite is illuminated in the linear operating region. As the operator of rack 1 increases the up-link power, the amplitude of the sine wave decreases, goes to zero at saturation, and increases again past the saturation point. The exact power required for saturation is found when the tuned voltmeter, which is connected to the vertical output of spectrum analyzer #2, shows a minimum.

\*The output TWTAs of both INTELSAT and COMSTAR satellites saturate at a lower power level than their receivers.

The input signal to spectrum analyzer #2 is monitored through a coupler. After amplification, this signal can also be fed to a power meter for  $G/T$  measurements or to counter #2 for spacecraft LO frequency measurements.

The controller, in addition to setting the phase-locked up-link frequencies, provides automatic instrument calibration and power meter zeroing, and performs data acquisition from the power meters, frequency counters, and digital clock. These data are then properly formatted, printed, and recorded for plotting, if desired, at the completion of the measurements.

### Calibration

Calibration is performed at the beginning of each test of an individual satellite. All coupling constants are measured during this procedure.

#### Up-link calibration

The object of the up-link calibration is to determine the flux density at the spacecraft for a given power level transmitted from the earth station for each channel frequency. As shown in Figure 6, the flux density at the spacecraft is given by

$$\Psi_{U/L} = \text{e.i.r.p.}_{E/S} - 10 \log (4\pi D^2) \quad [\text{dBW/m}^2] \quad (1)$$

where  $\text{e.i.r.p.}_{E/S}$  is the earth station transmitted effective radiated power relative to isotropic in dBW,  $10 \log (4\pi D^2)$  is the spreading factor, and  $D$  is the distance between the earth station and the spacecraft in meters. The earth station e.i.r.p. is given by

$$\text{e.i.r.p.}_{E/S} = G_{E/S} + P_{Tx} \quad (2)$$

where  $G_{E/S}$  is the earth station's transmit antenna gain in dB, and  $P_{Tx}$  is the transmitted power in dBW:

$$P_{Tx} = C_1 + PM\#2 \quad (3)$$

where  $C_1$  is the setup calibration constant in dB between points  $A$  and  $B$  in Figure 6, and  $PM\#2$  is the reading of power meter #2 in dBm. Finally, combining equations (1)–(3) yields

$$\Psi_{U/L} = C_1 + G_{E/S} - 10 \log (4\pi D^2) + PM\#2$$

or

$$\Psi_{U/L} = PM\#2 + C_{U/L} \quad (4)$$

where

$$C_{U/L} = C_1 + G_{E/S} - 10 \log (4\pi D^2) \quad (5)$$

Constant  $C_{U/L}$  must be evaluated for each of the up-link channel center frequencies.

#### Down-link calibration

The object of the down-link calibration is to determine the correspondence between the spacecraft e.i.r.p. and the level of the injected signal at the test setup. From Figure 6,

$$P_{Rx} = \text{e.i.r.p.}_{S/C} - PL + G_{E/S} \quad [\text{dBW}] \quad (6)$$

where  $P_{Rx}$  is the power received at point  $C$ ,  $G_{E/S}$  is the earth station receive antenna gain in dB, and  $PL$  is the path loss in dB:

$$PL = 20 \log \left[ \frac{\lambda}{4\pi D} \right] \quad (7)$$

where  $\lambda$  is the wavelength and  $D$  is the distance between the spacecraft and the earth station, both in meters.

The injected signal is adjusted so that it equals the received signal  $P_{Rx}$ . Then, from Figure 6,

$$P_{Rx} = P_{inj} - C_{xguide} \quad (8)$$

where  $C_{xguide}$  is the cross-guide coupling coefficient in dB and  $P_{inj}$  is the injected signal in dBm at point  $D$ , which can be determined by using either the reference power meter and the down-link attenuator or the reading of power meter #1. That is,

$$P_{inj} = \text{Ref} - \text{Atten}_{D/L} - C_2 \quad (9)$$

or

$$P_{inj} = PM\#1 + C_3 \quad (10)$$

where  $\text{Ref}$  and  $PM\#1$  are the readings of the reference power meter and power meter #1 respectively, in dBm;  $\text{Atten}_{D/L}$  is the setting of the down-link attenuator in dB; and  $C_2$  is a constant that includes the coupling coefficient (in dB) of the reference power meter coupler, the 30-dB pad, and cable losses. Constant  $C_3$  is the coupling coefficient (in dB) for the coupler of power meter #1.

Combining equations (6), (8), and (9) yields

$$\text{e.i.r.p.}_{S/JC} = \text{Ref} - \text{Atten}_{D/JL} - C_A \quad (11)$$

where

$$C_A = G_{E/S} - C_2 - PL - C_{\text{guide}} \quad (12)$$

or combining equations (6), (8), and (10) yields

$$\text{e.i.r.p.}_{S/JC} = PM\#1 - C_B \quad (13)$$

where

$$C_B = G_{E/S} + C_3 - PL - C_{\text{guide}} \quad (14)$$

Constants  $C_A$  and  $C_B$  must be evaluated for each of the down-link channel center frequencies.

### Measurements

At the beginning of an in-orbit test, immediately after the calibration is completed, the antenna patterns are measured to determine the orientation of the spacecraft antennas. Subsequently, the antennas are reoriented at beam center for flux density and e.i.r.p. measurements.

### Antenna patterns

Antenna patterns are taken at fixed elevation and variable azimuth angles [1]. The spacecraft is oriented for the desired elevation cut, and the despun platform is oriented so that the antenna boresight points in the direction of the earth station. The up-link power required to saturate the spacecraft TWTA and the down-link power are measured, as described in subsequent subsections on flux density and e.i.r.p. These values are recorded and stored, and the process is repeated until both the up- and down-link levels at saturation for all the pertinent channels in this antenna orientation have been measured. The antenna pattern for each channel is plotted as it is measured to help determine the next orientation position for the antenna, and to provide a check on the consistency of the measured values. The antenna platform is then rotated to the new azimuth position relative to the earth station, and the sequence is repeated.

When enough azimuth points have been obtained, the stored values are plotted in their final form. For a given channel, the plot of the up-link power for saturation vs azimuth angle represents the receive antenna

pattern, while that of the down-link power or the down-link attenuator represents the transmit antenna pattern. This technique is successful because these antenna patterns can be obtained relative to the output TWTA saturation point, which is, of course, independent of the antenna orientation. Typical transmit and receive antenna patterns for the COMSTAR satellite are shown in Figures 7a and 7b, respectively, which include both the in-orbit measured points and the values predicted from prelaunch measurements.

### Beam isolation

Because of its high carrier-to-noise ratio, the semiautomated setup has made possible, for the first time, measurement of the isolation between two distinct beams originating from different antennas. In the case of transmit patterns, the isolation is measured by slewing the spacecraft across the desired coverage area and measuring the received power level as a function of platform orientation. The up-link power level is set at about 2-3 dB above the level required for saturation at the beam center to minimize the effect of the spacecraft receive pattern, over the specified coverage range, on the transmit patterns. Figure 8 shows a typical transmit beam isolation pattern for the INTELSAT IV-A spacecraft.

The receive isolation patterns are similarly obtained by slewing the platform across the desired azimuth range with an up-link signal level set within the linear operating region of the transponder under test. The down-link signal is then recorded as a function of the slewing angle. This swept plot is corrected by the shape of the down-link pattern and the amount of backoff from saturation.

The isolation patterns are not measured by using the point-by-point procedure because the rapid variation of the pattern as a function of angular position requires the measurement of a very large number of points to obtain meaningful data. Such a large number of points would require a great deal of testing time. The isolation patterns obtained by using the continuous slewing method are as good as or better than the prelaunch data, probably due to the absence of the antenna range effects which were present during prelaunch measurements.

### Flux density for saturation

An up-link signal is transmitted to determine the flux density necessary to saturate a spacecraft output TWTA. This signal is amplitude modulated using a 1-kHz sine wave. The received down-link signal is displayed on the down-link spectrum analyzer (#2 in Figure 6), which is set for a zero scan

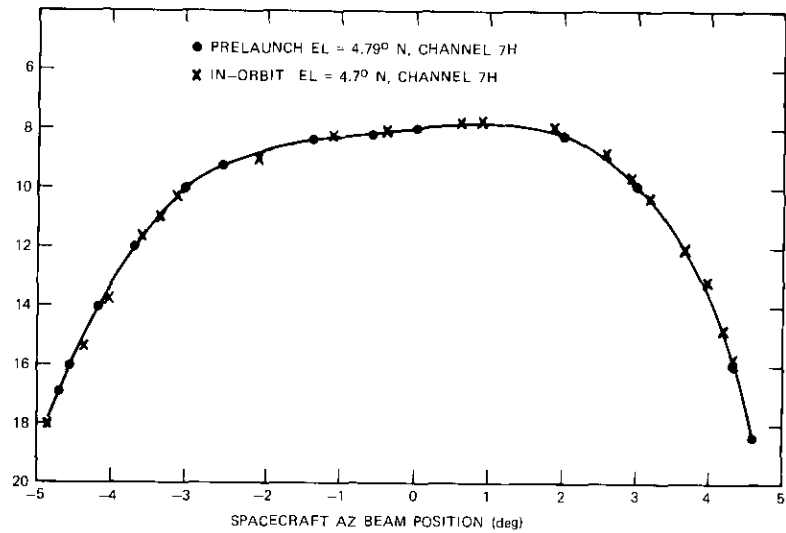


Figure 7a. Transmit Antenna Pattern for COMSTAR D-1

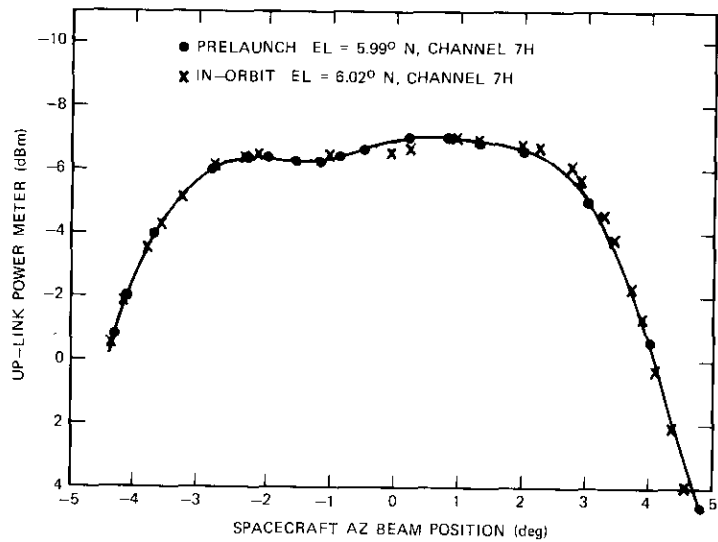


Figure 7b. Receive Antenna Pattern for COMSTAR D-1

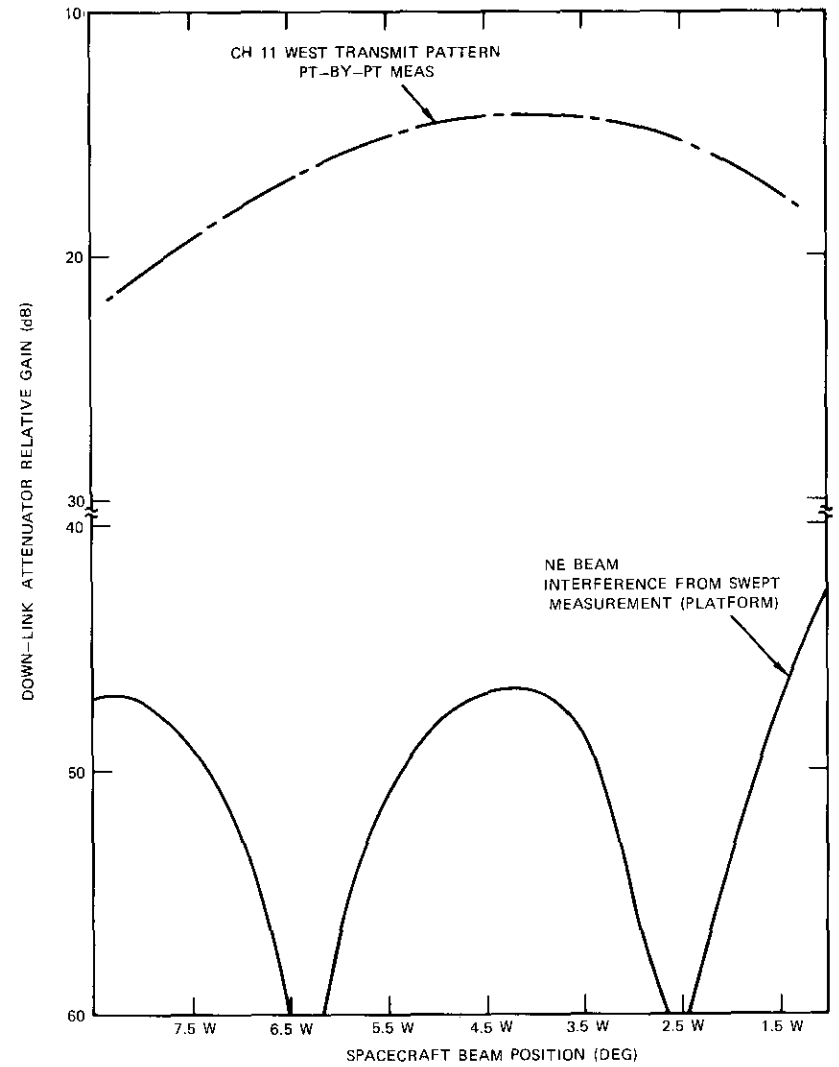


Figure 8. Typical INTELSAT IV-A Transmit Beam Isolation Pattern (elevation = 6°S)

mode linear display of 30-kHz bandwidth. The vertical output of this spectrum analyzer is connected to the tuned voltmeter. To determine the spacecraft illumination level which saturates the spacecraft output TWTA,

the transmitted power is then adjusted until a minimum is found on the voltmeter. The flux density corresponding to this level is computed from equations (4) and (5) by using the power measured by power meter #2.

The flux density required to saturate every output TWTA is measured at the center frequency corresponding to the appropriate channel after commanding the spacecraft to provide an RF path through the tube that is being measured. It should be noted that, since only one earth station is generally used for both transmission and reception from the satellite, the spacecraft must have an operating mode capable of this performance. In particular, satellites utilizing pattern isolation (such as INTELSAT IV-A) must provide up- and down-link capability in the same zone. Dual station testing has been performed for particular parameters with similar success; however, one test station is used whenever feasible. Typical results of these measurements together with prelaunch data for the INTELSAT IV-A and COMSTAR spacecraft are shown in Figure 9, which indicates that the maximum variation between the two measurements is less than 1 dB.

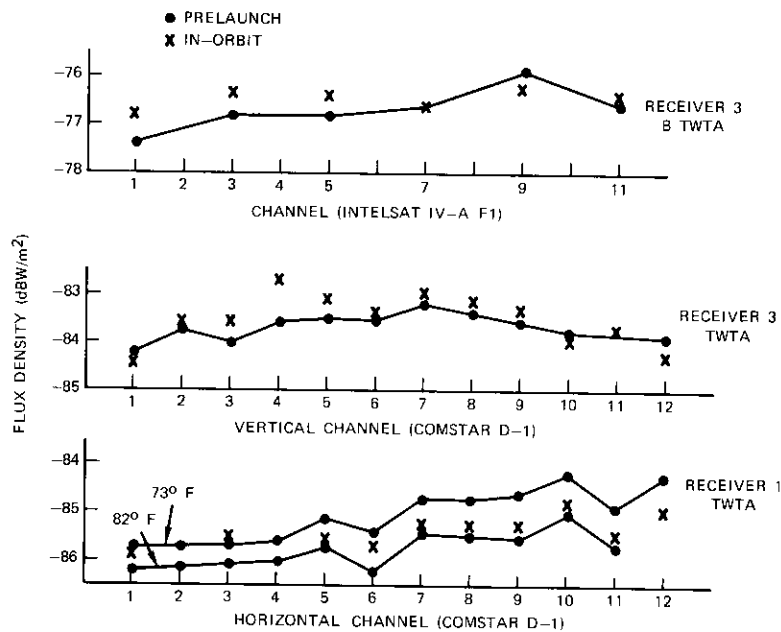


Figure 9. Flux Density for Saturation (INTELSAT IV-A F1 and COMSTAR D-1)

**Spacecraft e.i.r.p.**

The spacecraft e.i.r.p. is determined by saturating the output TWTA as described previously. The down-link spectrum analyzer is set for a linear display with a scan width that allows simultaneous viewing of both the down-link receiver carrier and the injected reference signal. The power level of the injected signal is then adjusted by means of the down-link attenuator so that it is equal to the received signal level.

The spacecraft e.i.r.p. is computed by using equations (11) and (12) or (13) and (14). Figure 10 shows both measured and predicted e.i.r.p. values for the INTELSAT IV-A and COMSTAR spacecraft, which, as can be seen, agree to within 0.8 dB. In actual practice, the flux density for saturation and the spacecraft e.i.r.p. for a given channel and TWTA are measured simultaneously.

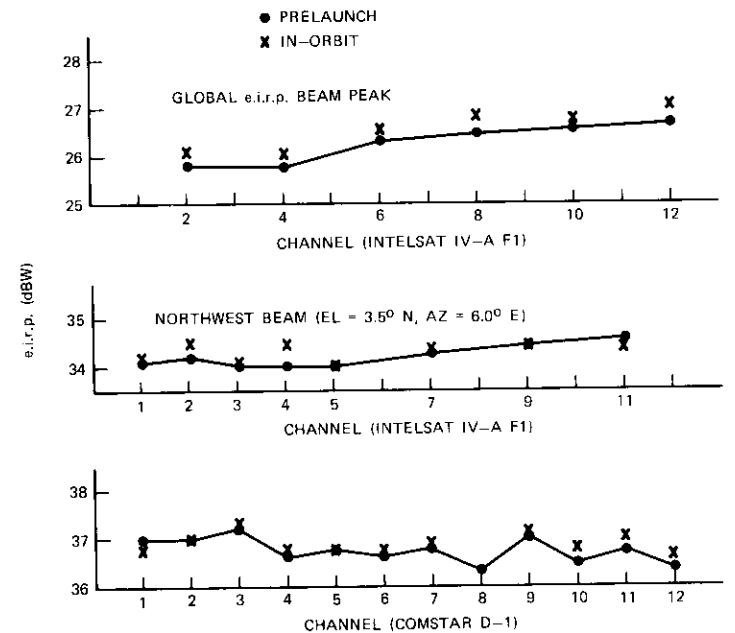


Figure 10. INTELSAT IV-A F1 and COMSTAR D-1 e.i.r.p.

**Spacecraft attenuators**

The up-link power level necessary to saturate the output TWTA whose attenuator is to be measured is determined and recorded. The attenuator

is then switched on and the new up-link saturation power level is found. The difference between these two levels is the attenuator value. Figure 11 shows typical measured attenuator values together with prelaunch data for the COMSTAR D-1 spacecraft.

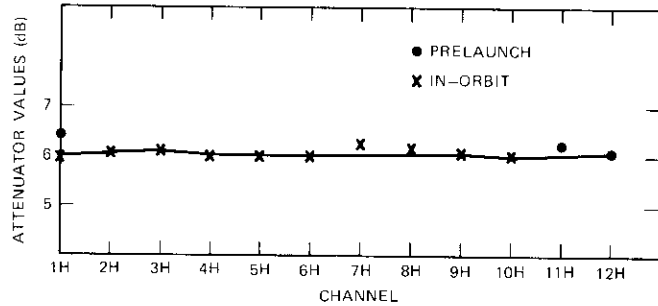


Figure 11. Attenuator Values (COMSTAR D-1)

**Gain transfer characteristic**

The gain transfer characteristic of a given spacecraft channel corresponding to a particular output TWTA is obtained by measuring and plotting the down-link signal level vs the up-link level. The results of such a measurement, together with prelaunch data for the COMSTAR D-1 satellite, are shown in Figure 12.

**Spacecraft receiver LO frequency**

The spacecraft receiver's LO frequency is determined by connecting a frequency counter instead of a power meter at point X and measuring the frequency while an up-link signal is transmitted. Since the frequency measured by the counter is the result of mixing the signal transmitted by the spacecraft and the up-link signal, it is equal to the spacecraft LO frequency which was used to down-convert the up-link signal. The accuracy of this measurement is generally limited by the resolution and stability of the counter and the additional error introduced by a possible Doppler shift. Characteristic results of these measurements together with prelaunch data are presented in Figure 13.

**Ratio of gain to noise temperature (G/T)**

To determine the spacecraft noise temperature, the received noise

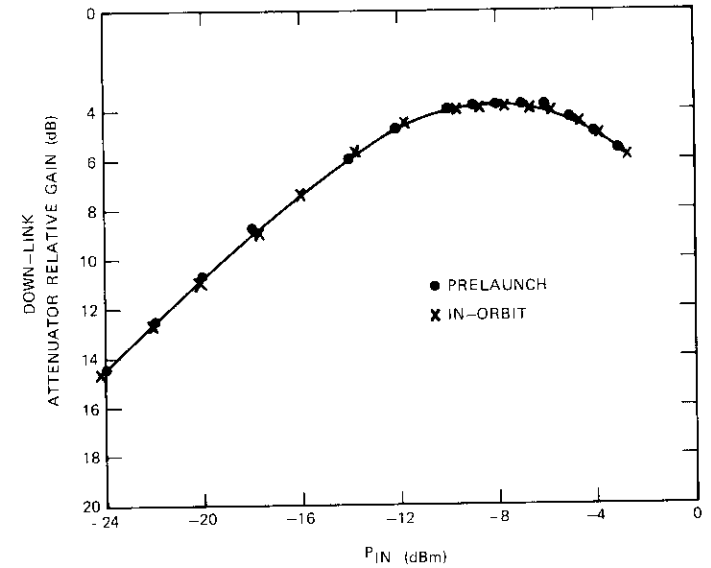


Figure 12. Channel 9 TWTA Transfer Characteristic

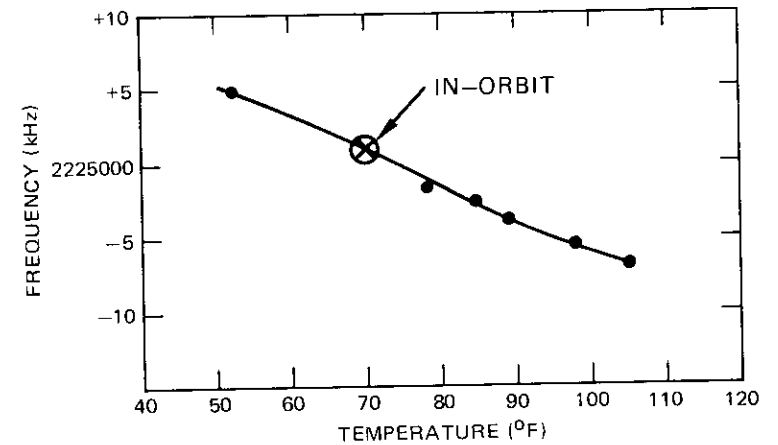


Figure 13. LO Frequency from 2,225 MHz

power level is measured at a given channel frequency during a period when no up-link signal is transmitted to the satellite. The received power, which

is due to noise originating from several sources, is given by

$$P_{meas} = P_{Rx} + P_{ant} + P_{sky} + P_{S/C} \quad (15)$$

where  $P_{Rx}$ ,  $P_{ant}$ ,  $P_{sky}$ , and  $P_{S/C}$  are the noise levels (in  $W$ ) originating from the earth station receiver, the earth station antenna, the sky, and the spacecraft, respectively.

The spacecraft noise temperature can be determined from equation (15) if  $P_{Rx}$ ,  $P_{ant}$ , and  $P_{sky}$  are known. To determine the noise level due to the earth station's receiver, two noise sources at known temperatures are connected to the input of the receiver by means of the RF switch in front of the earth station LNA. The measured noise levels are then

$$P_c = P_{cold\ load} + P_{Rx} = k[T_c + T_{Rx}]B \quad (16)$$

and

$$P_h = P_{hot\ load} + P_{Rx} = k[T_h + T_{Rx}]B \quad (17)$$

where  $T_c$ ,  $T_h$ , and  $T_{Rx}$  are the temperatures of the cold load, hot load, and receiver, respectively, in kelvin;  $k$  is Boltzmann's constant, and  $B$  is the bandwidth in Hz.

After  $P_c$  and  $P_h$  are measured, the station receiver is connected directly to the earth station antenna, which is pointed at the sky but away from the spacecraft. The received noise power is then

$$\begin{aligned} P_{e/s} &= P_{Rx} + P_{ant} + P_{sky} \\ &= k[T_{Rx} + T_{sky}]B = kT_{e/s}B \end{aligned} \quad (18)$$

where  $T_{Rx}$  is the equivalent noise temperature of the receiver,  $T_{sky}$  is the equivalent temperature of sky noise and noise generated at the station's antenna, and  $T_{e/s}$  is the overall equivalent system noise temperature, all in kelvin.

Combining equations (16), (17), and (18) gives

$$T_{e/s} = P_{e/s} \left( \frac{T_h - T_c}{P_h - P_c} \right) \quad (19)$$

and combining equations (15), (18), and (19) yields

$$T_{s/c} = T_{e/s} \left( \frac{P_{s/c}}{P_{e/s}} - 1 \right) \quad (20)$$

where  $T_{s/c}$  is the noise temperature in kelvin of the spacecraft at the frequency where the power levels were measured.

To obtain the  $G/T$  in dB, the spacecraft noise temperature is converted from kelvin to dB, referenced at 1 K, by using

$$T_{s/c} \Big|_{dB} = 10 \log T_{s/c}.$$

Then

$$G/T = G - T_{s/c} \Big|_{dB} \quad [dB] \quad (21)$$

where  $G$  is the spacecraft gain in dB which is measured as described previously in the gain transfer characteristics section. This method of obtaining the  $G/T$  is a point-by-point technique used during the in-orbit tests conducted by COMSAT until the test of the COMSTAR D-1 spacecraft.

A very promising swept technique has recently been developed. The swept measurement, which has been made feasible because of the high stability of the semiautomated test setup, allows a very rapid and accurate measurement of the  $G/T$  across all the channels of a spacecraft receiver. Typical results of swept  $G/T$  measurements are shown in Figure 14.

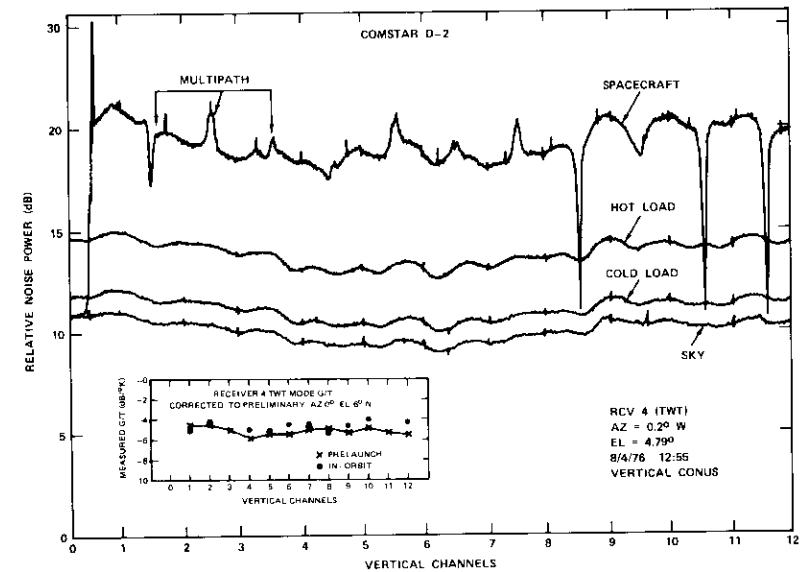


Figure 14. Typical Swept  $G/T$  Measurement Results

Further developments of this technique are presently being pursued, and additional information will be provided at a later date.

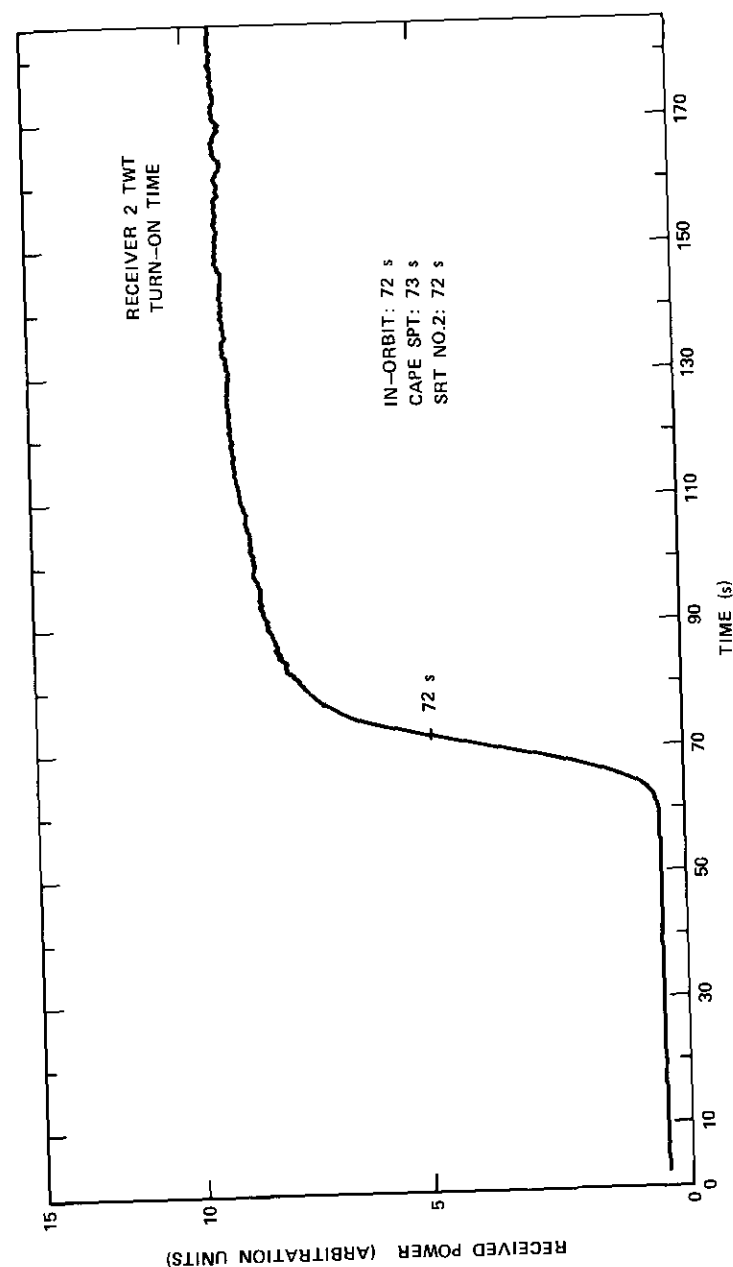
#### Spacecraft TWT turn-on transients

The turn-on transient characteristics of a given spacecraft TWTA are determined as follows. The tube to be measured is turned off and allowed to cool for at least four hours. One of the alternate tubes or microwave transistor amplifiers (MTAs) for this channel is turned on to provide satisfactory signal levels for the setup. The up-link signal level is then backed off by at least 14 dB from the tube's saturation to provide linear operation, and the down-link signal is displayed on spectrum analyzer #2 (Figure 6). The analyzer is set in the zero scan mode, and its vertical output is used to drive the vertical of an X-Y recorder, which is set for an extended time sweep. The spacecraft is then commanded to switch off the intermediary amplifier and to turn on the tube to be measured while the X-Y recorder is simultaneously triggered to scan. The resulting graph, Figure 15, shows the TWTA's transient characteristics.

#### In-band and out-of-band frequency response

The setup (Figure 6) is configured for non-digital operation and the phase-lock loop is disabled. To provide a swept up-link signal the swept frequency generator is set for an analog sweep of 70 MHz centered at the central frequency of the channel to be measured. On the down-link side, spectrum analyzer #2 (Figure 6) is set for linear display and its vertical output is connected to one of the vertical channels of the X-Y recorder. Spectrum analyzer #1 is fed the signal from the G/T port of the setup and set for a logarithmic display, and its vertical output is connected to the second vertical channel of the X-Y recorder. The horizontal channel of the recorder is driven by the sweep signal from the sweeper. The trace from the linear display will show at maximum resolution the in-band frequency response of the spacecraft filters, corresponding to the channel under test, while the logarithmic trace will provide the out-of-band rejection information for this channel.

To calibrate this setup, the frequency response of the earth station receiver must first be determined by turning the up-link signal off and the injected signal on. Both spectrum analyzers are tuned to the injected signal, phase locked to this signal, and set for a zero scan mode. Then the sweeper is set for a single sweep and the X-Y recorder is activated so that both logarithmic and linear graphs of the receiver frequency responses are obtained simultaneously. The graph paper on the recorder is calibrated



by means of the down-link attenuator. The event marker of the X-Y recorder is used during the sweep to write frequency intervals (as seen from down-link frequency counter #2) for the calibration of the horizontal axis of the graph.

After the graph is calibrated, the injected signal is turned off and the up-link signal is turned on. Both spectrum analyzers are tuned to the received down-link signal, and as before, are phase-locked and set to the zero scan mode. A new sweep is triggered and both channels are graphed. The corresponding difference between the trace for the earth station receiver and the trace obtained with the up-link signal on gives the frequency response of spacecraft filter. Typical results are shown in Figure 16.

#### Cross-polarization isolation

A swept frequency technique is used to measure cross-polarization isolation between the vertical and horizontal linear polarization on the COMSTAR spacecraft. An earth station with excellent polarization purity and independently adjustable polarization angles for up- and down-link bands is a prerequisite.

Since this is a relative measurement, precise calibration of both earth station antenna gain and up/down-link setup is not required. For this test, the swept up-link signal is leveled at the antenna feed and adjusted to drive the spacecraft TWTS to saturation. On the down-link side, spectrum analyzer photographs are taken with a swept injected leveled reference carrier, the down-link signal from the spacecraft with the link under test in a copolarization configuration, and the down-link signal from the spacecraft with the link under test in a cross-polarization configuration. For instance, for a measurement of down-link cross-polarization isolation between spacecraft transmit horizontal and earth station receive vertical, the following steps are performed:

- a. a calibration sweep is performed with an injected reference carrier;
- b. a spacecraft transmit horizontal/earth station receive horizontal copolarization calibration sweep is performed;
- c. the spectrum analyzer is connected to the vertical receive polarization, and successive sweeps are photographed while the earth station receive polarization is varied in steps over a  $2^\circ$  to  $3^\circ$  range centered about the ideal alignment;
- d. single-point measurements are usually taken at a few spots across the band to complement the photographs.

Since the earth station antenna and polarizers are significant contribu-

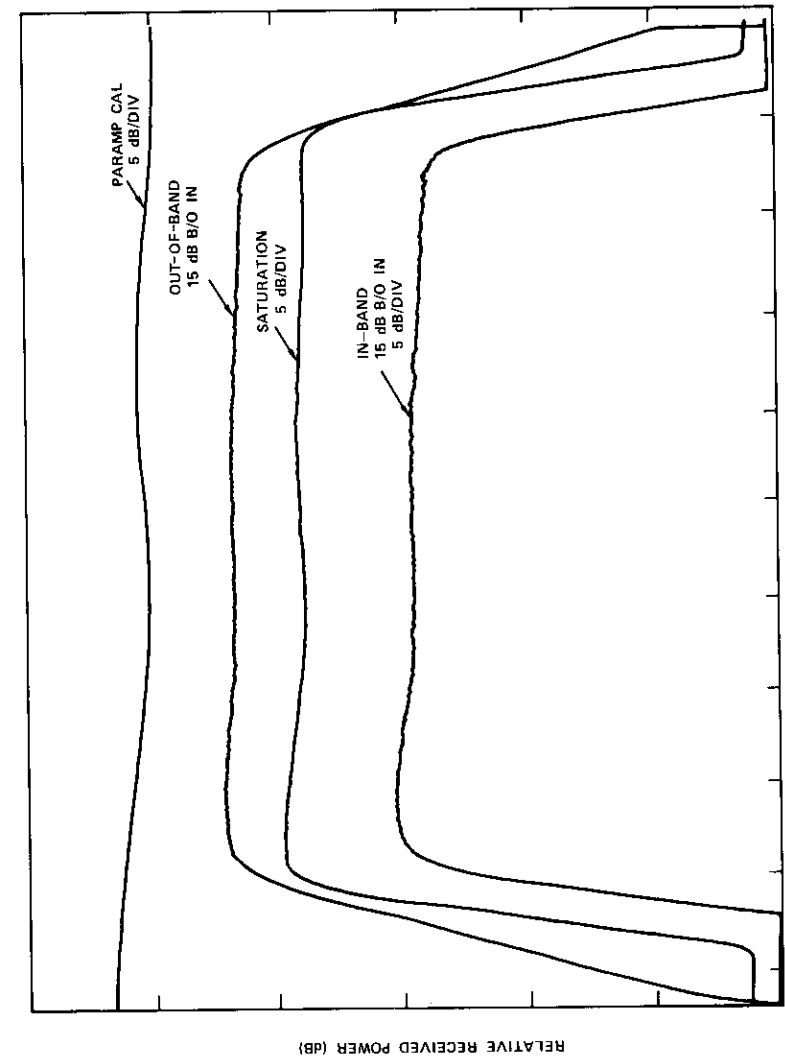


Figure 16. Spacecraft Filter Frequency Response

tors to the cross-polarization isolation of the link, exact knowledge of the earth station performance is essential and, by suitable manipulation, a bounded estimate of the satellite antenna performance can be obtained. Typical evaluated data are shown in Figure 17.

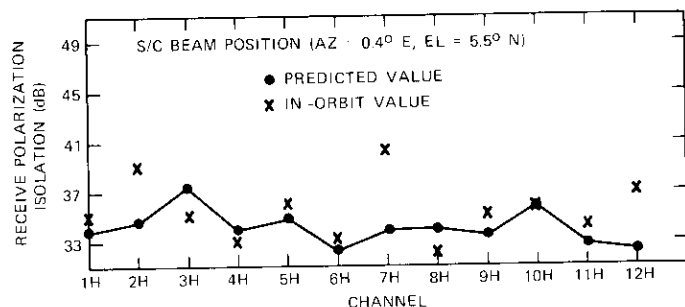


Figure 17. Cross-polarization Isolation

## Conclusions

The test setup used by the Communications Satellite Corporation for the in-orbit tests of the INTELSAT IV-A and COMSTAR spacecraft has been described. In addition, calibration procedures of this setup as a system, together with the earth station and the radiation path, have been presented. Based on these calibrations, the measurement of most of the RF characteristics of the spacecraft under test has been discussed, together with typical results. The procedures and techniques used for the successful measurement of these satellites are the result of continual evaluation and improvement during the testing of approximately 19 communications satellites.

## Acknowledgment

The authors wish to acknowledge the contribution of Mr. Simon Bennett, presently with INTELSAT, and Mr. Arnold Berman of COMSAT Laboratories, who contributed greatly to the early development of in-orbit testing. While many people have participated as members of in-orbit test teams and have contributed to the development of testing techniques and procedures, they are too numerous to acknowledge individually. The efforts of Mr. John Melville of COMSAT West, and Mr. Francois Assal and Dr. William Childs, both of COMSAT Laboratories, in implementing the semiautomated setup are acknowledged. Finally, the authors would like to thank Mr. Joseph

Jerome and Mr. Leonard Bonneau of COMSAT Laboratories who worked on the final implementation of the test system.

## Reference

- [1] "The INTELSAT IV Spacecraft," E. T. Jilg, editor, *COMSAT Technical Review*, Vol. 2, No. 2, Fall 1972, pp. 277-294.

I. Dostis received a B.E.E., *summa cum laude*, from the College of the City of New York in 1959, and an M.E.E. from New York University in 1961. Prior to joining COMSAT in 1961, he was employed by Western Electric Company, Bell Telephone Laboratories, and the College of the City of New York. Since joining COMSAT, he has worked primarily on the implementation, analysis, evaluation, and measurement of satellite communications systems. He is presently Director of Technical Planning and Operations in the INTELSAT Management Division. He is a member of Tau Beta Pi, Eta Kappa Nu, IEEE, and AAAS.



Dr. Christoph Mahle received Dipl. Ing. and Dr. S.C. Tech. degrees from the Swiss Federal Institute of Technology in 1961 and 1966, respectively. As Manager of the Transponders Department of the Microwave Laboratory at COMSAT Labs, he is responsible for directing research and development in such areas as analysis and laboratory verification of communications system performance applied to satellite transponders, and advancing the state-of-the-art of communications transponders. He has participated in systems design and evaluation of the communications transponders of the INTELSAT IV, IV-A, and V programs. In addition, he has been responsible for the design, development, and testing of the transponder orbited on ATS-6 as part of the COMSAT Millimeter Wave Propagation Experiment. He is a member of IEEE.



*Vasilis E. Riginos was born in Athens, Greece. He received B.E., M. Eng., and Ph.D. degrees in electrophysics from the Stevens Institute of Technology, Hoboken, N.J., in 1964, 1970, and 1973, respectively. He was NDEA Fellow at the Stevens Institute of Technology, where he worked on the transport properties of GaAs. He also helped with the development of the Physical Electronics Laboratory and taught physical electronics for several years. In 1974 he joined the Transponders Department of the Microwave Laboratory, where he has*

*been engaged in research on solid-state microwave devices and in the development of microwave measurement systems. In addition, he has been participating in the in-orbit testing of several communications satellites. He is a member of Sigma Xi, AAAS, IEEE, and the American Physical Society.*

*Ignace G. Atohoum was born in Ouidah (Bénin, West Africa). He received a B.S.E.E. from Colorado State University; an M.S.E.E. from Université Laval, Québec; and a Ph.D. in electrophysics from the Stevens Institute of Technology, Hoboken, N.J. From January 1968 to September 1969 he was a research and teaching assistant at the Université Laval and worked on semi-conductor integrated antennas. He joined the Stevens Institute of Technology in September 1970 as an assistant instructor.*



*A member of the technical staff of the Transponders Department of the Microwave Laboratory at COMSAT Laboratories since August 1974, he has been engaged in the modeling of Gunn effect devices and the communications characterization of Gunn effect amplifiers and multicollector traveling wave tube amplifiers operating in the 10- to 15-GMz band. In addition, he has been participating in the in-orbit testing of various communications satellites. He is a member of Sigma Xi and IEEE.*

**Index:** intermodulation, interference, mathematical model, coding theory, frequency allocation

## **Carrier frequency assignment for nonlinear repeaters**

R. J. F. FANG AND W. A. SANDRIN

(Manuscript received October 12, 1976)

### **Abstract**

Selective carrier frequency spacing is required in some space and mobile systems to reduce the effects of intermodulation interference due to the nonlinear characteristics of a common amplifier. This paper expresses the frequency assignment problem of avoiding or minimizing third-order intermodulation interference in terms of difference sets, thus permitting a definition of the concept of optimum frequency plans, an efficient assessment technique applicable to systems having constraints that preclude the use of ideal plans, and a connection with certain problems in coding and graph theory whose results are used to provide frequency plans superior to those previously published. The difference set concept is also extended to allow the generation of fifth-order intermodulation-free frequency assignments, and frequency planning examples are provided using plots of intermodulation spectra.

### **Introduction**

Intermodulation interference among carriers that share the same nonlinear repeater is of major concern in some space and mobile communications systems. In such applications, carrier frequencies are judiciously assigned to ensure minimum interference from intermodulation products. These systems, which are characteristically power limited, require the

more efficient nonlinear rather than linear amplifiers, and usually have a large although limited available bandwidth.

As an example, in the MARISAT system [1] several frequency-division multiple-access (FDMA) L-band signals are simultaneously amplified by the satellite's high-level traveling wave tube amplifier (TWTA). This amplifier is operated near saturation to maximize the output of the power-limited satellite-to-ship link.

Babcock [2] has provided channel assignment sequences which are free of third-order intermodulation products at the assigned carrier frequencies. Edwards et al. [3] have treated a similar problem with the added constraint that no two channel assignments may occupy adjacent frequency slots (a constraint necessary to prevent adjacent channel interference). This paper provides a formal description of the problem of evaluating frequency plans for third- and fifth-order intermodulation interference in terms of difference sets. This approach not only results in an easily applied and efficient evaluation method and a formal recognition of optimum frequency plans (in the sense of requiring the least channel slots or bandwidth), but also provides a connection with related problems in coding [4] and graph theory [5]. Results given in References 4 and 5 are recast in the form of frequency plans which are free of third-order intermodulation interference.

The following section treats the problem of finding a third-order intermodulation-free channel assignment plan. This problem is shown to be equivalent to that of searching for a single difference set triangle with distinct integer elements. If an optimum frequency plan is defined as that which requires the fewest consecutive channels to accommodate a given number of third-order intermodulation-free carriers, then the problem of finding such a frequency plan is shown to be equivalent to the mathematical problem of searching for a single difference set triangle with distinct integer elements and with the least largest element. Solutions [4], [5] to this mathematical problem are utilized to obtain optimum frequency assignments for cases in which there are no more than 11 carriers and suboptimum assignments for frequency plans having more than 11 carriers. Subsequently, the difference set concept is generalized to develop carrier arrangement conditions that will yield both third- and fifth-order intermodulation-free frequency assignments.

In some applications, carrier frequency plans may be constrained by requirements that certain channels must be assigned specific locations and that certain other channels must be unoccupied or by requirements for unequal carrier sizes. The use of difference sets to allow rapid evaluation

of such plans is discussed herein. In addition, examples indicating the nature of intermodulation products in various types of frequency plans are provided. Finally, related areas to which the results of this paper are applicable are discussed.

### ***Difference sets and channel frequency assignments***

A well-known technique for reducing intermodulation interference is the judicious selection of signal channel frequency assignments from a block of consecutive channels so that the significant intermodulation products fall on unused channel frequencies. The application of this technique requires ample bandwidth, since a significant number of the available channels must remain unoccupied. Babcock [2] has provided examples of channel frequency assignment plans that avoid third-order and, in some cases, both third- and fifth-order intermodulation products.

By examining the frequency difference matrix of a channel assignment plan, this section demonstrates an equivalence among the frequency assignment plans obtained by Babcock, the difference triangle sets treated in Reference 4 (in connection with error-correcting codes), and a graph theory problem described in Reference 5. The properties of these difference matrices or difference set triangles are discussed as they pertain to the channel assignment problem, and the results of References 4 and 5 are used to obtain a number of new third-order intermodulation-free channel assignment plans.

Consider, for example, a Babcock channel assignment plan with eight carriers, assigned to channels 1, 2, 5, 10, 16, 23, 33, and 35, respectively. It can be verified that none of the third-order intermodulation products fall onto any of these eight carriers as follows. The assigned channel mid-band frequencies are arranged according to channel numbers in ascending order, and the difference set triangle [4] for these eight assigned channel numbers is constructed as shown in Table 1. The entry for the  $i$ th row and  $j$ th column of the triangle, denoted as  $M_{ij}$  for  $j > i$ , represents the difference in channel frequency of the  $i$ th and  $j$ th carriers.

Observe that, since the elements of this difference triangle are distinct, no two pairs of carrier frequencies have the same frequency difference.\* That is,  $f_j - f_i \neq f_k - f_l$  for any two pairs of carriers  $(f_i, f_j)$  and  $(f_l, f_k)$  with  $j > i$  and  $k > l$ . This means that none of the third-order intermodulation products of the type  $f_j + f_l - f_i$  fall onto any other carrier  $f_k$  if

\* The same observation has been made by Edwards et al. [3].

$f_i, f_j, f_k$ , and  $f_l$  are distinct (i.e.,  $f_j + f_l - f_i \neq f_k$ ), and also that none of the third-order intermodulation products of the type  $2f_l - f_i$  fall onto any other carrier  $f_k$  if  $f_j = f_l$  or  $f_i = f_k$ . Since these are the only two types of third-order intermodulation products, it follows that no third-order intermodulation products fall onto any of these eight assigned channels.

TABLE 1. FREQUENCY DIFFERENCE TRIANGLE

$f_1$	$f_2$	$f$	$f_4$	$f_5$	$f_6$	$f_7$	$f_8$		
1	2	5	10	16	23	33	35		
	1	4	9	15	22	32	34	1	$f_1$
		3	8	14	21	31	33	2	$f_2$
			5	11	18	28	30	5	$f$
				6	13	23	25	10	$f_4$
					7	17	19	16	$f_5$
						10	12	23	$f_6$
							2	33	$f_7$
								35	$f_8$

To obtain a third-order intermodulation-free channel assignment, the corresponding frequency difference triangle must have distinct elements. Otherwise, there must exist some  $i, j, k$ , or  $l$  such that  $M_{i,j} = M_{k,l}$  for  $j > i$  and  $k > l$ , which means that  $f_j - f_i = f_k - f_l$  for some  $j > i$  and  $k > l$ . Thus,  $f_j + f_l - f_i = f_k$  for some  $j > i$  and  $k > l$ . In other words, there exist some  $j > i$  and  $k > l$  such that the third-order intermodulation products  $f_j + f_l - f_i$  will fall onto another assigned channel of frequency  $f_k$ . (When  $j = l$  or  $i = k$ , the third-order intermodulation product is of the type  $2f_l - f_i$ .) Therefore, the following theorem has been proved:

**Theorem 1:** Assume that there are  $L$  consecutive channels numbered  $1, 2, 3, \dots, L$ , respectively. Let  $N$  carriers at the input of a nonlinear repeater be assigned frequencies at the mid-bands of  $N$  channels ( $N < L$ ). Then the necessary and sufficient condition to preclude

third-order intermodulation products on the assigned channels is that the difference set triangle of these assigned carrier frequencies must have distinct elements.

**Corollary 1:** As stated previously, the problem of finding a third-order intermodulation-free channel assignment plan for a nonlinear repeater is equivalent to the mathematical problem of searching for a single difference set triangle with distinct elements.

In the literature the difference set triangle is usually represented by a difference set [4]. For example, in Table 1 the difference set triangle can be represented by the set  $(1, 3, 5, 6, 7, 10, 2)$ . From this set, the triangle can be constructed very easily. For instance, the entries  $M_{68}$ ,  $M_{57}$ , and  $M_{58}$  can be obtained as follows:

$$M_{68} \equiv f_8 - f_6 = (f_8 - f_7) + (f_7 - f_6) = 2 + 10 = 12$$

$$M_{57} \equiv f_7 - f_5 = (f_7 - f_6) + (f_6 - f_5) = 10 + 7 = 17$$

$$M_{58} \equiv f_8 - f_5 = (f_8 - f_7) + (f_7 - f_5) = 2 + 17 = 19$$

It is unnecessary to complete the triangle, however, because, once the difference set is known, the channel assignment can be obtained in two steps:

- a carrier is assigned to the first channel;
- the other carriers are assigned by adding the differences from the difference set to the assigned carrier one by one.

That is, for the example in Table 1,

$$\begin{aligned} f_1 &= 1 \\ f_2 &= f_1 + 1 = 2 \\ f_3 &= f_2 + 3 = 5 \\ f_4 &= f_3 + 5 = 10 \\ f_5 &= f_4 + 6 = 16 \\ f_6 &= f_5 + 7 = 23 \\ f_7 &= f_6 + 10 = 33 \\ f_8 &= f_7 + 2 = 35 \end{aligned}$$

If the differences are added in reverse order  $(2, 10, 7, 6, 5, 3, 1)$ , then channel assignment  $(1, 3, 13, 20, 26, 31, 34, 35)$  is obtained. This assignment is obviously equivalent to the original assignment  $(1, 2, 5, 10, 16, 23, 33, 35)$ , since it can be obtained by counting the channels backward.

For the example given in Table 1 and for any of the frequency plans

TABLE 2. OPTIMUM THIRD-ORDER INTERMODULATION-FREE FREQUENCY PLANS

No. of Third-Order Intermodulation-Free Carriers	Fewest Consecutive Channels Required		Babcock's Assignment	Optimum Assignment *
	Babcock's Assignment	Optimum Assignment		
2		2		1, 2 (unique)
3	4	4	1, 2, 4	1, 2, 4 (unique)
4	7	7	1, 2, 5, 7	1, 2, 5, 7 (unique)
5	12	12	1, 2, 5, 10, 12	1, 2, 5, 10, 12
				1, 3, 8, 9, 12
6	18	18	1, 2, 5, 11, 13, 18	1, 2, 5, 11, 13, 18
				1, 2, 5, 11, 16, 18
				1, 2, 9, 12, 14, 18
7	26	26	1, 2, 5, 11, 19, 24, 26	1, 2, 9, 13, 15, 18
				1, 2, 5, 11, 19, 24, 26
				1, 2, 9, 12, 21, 24, 26
				1, 2, 12, 17, 20, 24, 26
				1, 3, 4, 11, 17, 22, 26
				1, 3, 8, 14, 22, 23, 26
8	35	35	1, 2, 5, 10, 16, 23, 33, 35	1, 2, 5, 10, 16, 23, 33, 35 (unique)
9	46	45	1, 2, 5, 14, 25, 31, 39, 41, 46	1, 2, 6, 13, 26, 28, 36, 42, 45 (unique)
10	62	56	1, 2, 8, 12, 27, 40, 48, 57, 60, 62	1, 2, 7, 11, 24, 27, 35, 42, 54, 56 (unique)
11		73		1, 2, 5, 14, 29, 34, 48, 55, 65, 71, 73
				1, 2, 10, 20, 25, 32, 53, 57, 59, 70, 73

\*Based upon the results in Reference 5 and the construction procedure outlined in the text.

obtained by Babcock, the optimality or uniqueness of the assignment is not discussed. "Optimum" means that the channel assignment uses the fewest consecutive channel frequencies to accommodate a fixed number of carriers which are free of third-order intermodulation. This is a useful measure in practice. Channel assignments in which there is only one optimum plan (plus its reverse) are said to be "unique."

*Corollary 2:* The problem of finding an optimum channel assignment plan for a fixed number of carriers is equivalent to the mathematical problem of searching for a single difference set triangle that has the least largest element.

In general, the solution to the mathematical problem in corollary 2 is not available except in the special cases (which have been solved via exhaustive evaluation) in which the number of carriers is less than or equal to 11 [5]. On the basis of the results of Reference 5 and the construction procedure explained following corollary 1, the optimum third-order intermodulation-free channel assignment plans can be easily obtained and are listed in Table 2, in which Babcock's assignment is also given for comparison. It can be seen that some assignments are unique and that the 8-carrier Babcock plan (1, 2, 5, 10, 16, 23, 33, 35) is not only optimum but also unique.

Unfortunately, for more than 11 carriers, no optimum solution has yet been obtained. Some of the suboptimum plans which are given in Table 3 are constructed from the single difference sets generated by Robinson and Bernstein [4].

### Conditions for both third- and fifth-order intermodulation-free assignment

The difference set triangle concept can be extended to generate channel assignment plans that are free of both third- and fifth-order intermodulation interference. In this case, a frequency difference "pyramid" similar to the frequency difference triangle in Table 1 is required. This difference pyramid is constructed as follows. First, the  $N$  assigned channels are numbered in ascending order along  $X$ ,  $Y$ , and  $Z$  coordinates, respectively. Second, the  $M_{ijk}$  element is filled in with the double frequency difference  $f_i - f_j - f_k$  for all  $i > j \geq k$  and all  $k > i > j$ .

In the difference pyramid, if  $M_{ijk} = M_{lmn}$ , then

TABLE 3. SUBOPTIMUM THIRD-ORDER INTERMODULATION-FREE FREQUENCY PLANS FOR 11 OR MORE CARRIERS\*

No. of Third-Order Intermodulation-Free Carriers	Consecutive Channels Required	Assignment
12	86	1, 3, 7, 25, 30, 41, 44, 56, 69, 76, 77, 86
13	115	1, 24, 29, 30, 38, 54, 64, 76, 95, 97, 108, 112, 115
14	128	1, 6, 29, 39, 42, 50, 51, 69, 76, 93, 108, 122, 124, 128
15	156	1, 5, 6, 16, 34, 58, 60, 79, 106, 118, 126, 140, 143, 149, 156
16	180	1, 7, 20, 41, 59, 68, 79, 84, 110, 133, 134, 163, 166, 170, 179, 180
17	202	1, 19, 25, 47, 51, 68, 104, 113, 116, 127, 129, 160, 167, 168, 187, 197, 202
18	217	1, 3, 11, 23, 54, 57, 83, 84, 90, 99, 131, 149, 154, 168, 189, 193, 206, 217
19	247	1, 2, 7, 26, 33, 73, 101, 109, 121, 131, 154, 170, 188, 191, 205, 232, 234, 243, 247
20	284	1, 25, 31, 44, 56, 72, 76, 90, 105, 126, 128, 163, 168, 190, 207, 216, 273, 276, 283, 284
21	334	1, 5, 24, 38, 41, 49, 69, 79, 139, 148, 155, 190, 205, 239, 251, 252, 257, 278, 310, 332, 334
22	359	1, 4, 17, 46, 51, 52, 66, 105, 126, 143, 183, 207, 211, 219, 229, 238, 290, 301, 327, 334, 357, 359
23	373	1, 7, 23, 25, 44, 57, 96, 127, 138, 147, 173, 174, 202, 214, 259, 274, 282, 307, 312, 356, 366, 370, 373
24	426	1, 23, 42, 58, 73, 94, 100, 140, 148, 174, 218, 221, 235, 274, 284, 286, 297, 304, 329, 388, 389, 393, 417, 426

\* Based upon results in Reference 4 and the construction procedure outlined in the text.

$$f_i - f_j - f_k = f_l - f_m - f_n \quad (1)$$

$$f_i + f_m + f_n - f_j - f_k = f_l \quad (2)$$

and a fifth-order intermodulation product occurs at frequency  $f_l$ . Hence, each entry in the difference pyramid must be distinct to ensure a channel assignment plan that is free of fifth-, and as shown below, third-order intermodulation interference.

For the difference pyramid, the following conditions on  $i, j$ , and  $k$  are necessary to eliminate redundant and degenerate entries:

a.  $i > j$ . If all  $i$  and  $j$  are permitted, then

$$f_i - f_j - f_k = f_l - f_m - f_n \quad (3)$$

and

$$f_j - f_i - f_k = f_m - f_l - f_n \quad (4)$$

Hence, if  $i > j$ , half of the  $ijk$  "cube" is eliminated, since the  $i < j$  half contains only redundant information. This condition is similar to requiring  $i > j$  for the difference set triangle.

b.  $i \neq j$ . If  $i = j$ , then

$$f_i - f_i - f_k = -f_k \quad (5)$$

Thus,  $M_{iik}$  is a degenerate element.

c.  $k \neq i$ . If  $k = i$ , then

$$f_i - f_j - f_i = -f_j \quad (6)$$

Thus,  $M_{iji}$  is a degenerate element.

d.  $k < j$  and  $k > i$ . If all  $j$  and  $k$  less than  $i$  are permitted, then

$$f_i - f_j - f_k = f_i - f_k - f_j \quad (7)$$

and the equality  $M_{ijk} = M_{ikj}$  is degenerate. Hence,  $k$  must be restricted to  $k < j$  and  $k > i$ .

Conditions a through d define the  $M_{ijk}$  elements that form the difference pyramid, namely, all  $i > j \geq k$  and all  $k > i > j$ . With these conditions, equation (2) can be rewritten in one of the following forms:

$$f_l = f_i + f_m + f_n - f_j - f_k \quad (8)$$

$$f_l = 2f_i + f_n - f_j - f_k \quad (9)$$

$$f_l = 2f_i + f_n - 2f_j \quad (10)$$

$$f_l = 3f_i - f_j - f_k \quad (11)$$

$$f_l = 3f_i - 2f_j \quad (12)$$

Since the right-hand sides of equations (8)–(12) represent all of the generic types of fifth-order intermodulation products, it follows that, when all elements in the difference pyramid are distinct, no fifth-order intermodulation products are present in any of the assigned channels.

The first tier of the difference pyramid, defined as  $k = 1$ , is simply the difference set triangle with  $f_1$  subtracted from each element, as can be seen from equation (1). Since subtracting the same number from each element of a difference set triangle does not affect the distinctness of its elements, a frequency plan having a difference pyramid with distinct elements is free of third-order intermodulation products.

*Theorem 2:* The necessary and sufficient condition for a channel assignment to have neither third- nor fifth-order intermodulation products on the assigned channels is that the difference pyramid must have distinct elements.

*Proof:* The sufficient conditions for this theorem have been stated previously. These conditions are also necessary because, if the difference pyramid of a channel assignment plan which is free of both third- and fifth-order intermodulation does not have distinct elements, then for some  $i, j, k, l, m$ , and  $n$ , equation (1) will be true. Suppose that  $i = l$  (or  $j = m, k = n, j = n, k = m$  exclusively). Then,

$$f_j = f_m + f_n - f_k \quad (13)$$

Hence, a third-order intermodulation product will fall onto another assigned channel. This contradicts the hypothesis that the channel assignment plan is free of third-order intermodulation.

On the other hand, suppose that  $i \neq l, j \neq m, k \neq n, j \neq n$ , and  $k \neq m$ . Then equation (1) will not degenerate into equation (13). However, equation (1) can be put into any of the forms of equations (8)–(12). That is, some fifth-order intermodulation will fall onto another assigned channel. This also contradicts the hypothesis that the channel assignment is free of fifth-order intermodulation.

In the course of this investigation it has been found that Babcock's [2] channel assignment (1, 2, 8, 12, 27, 50, 78, 137) is not free of fifth-order

intermodulation since the double frequency differences  $27 - 12 - 12 = 3 = 12 - 8 - 1$  and consequently  $27 = 3 \times 12 - 8 - 1$ . That is, some of the fifth-order intermodulation among channels 1, 8, and 12 falls onto channel 27.

### Other considerations

In some applications, certain constraints may have to be imposed upon the difference set itself. For example [3], to avoid adjacent channel interference, consecutive channels may not be assigned. That is, no unity element is allowable in the difference set of the channel assignment plan.

In practice, the available bandwidth is not always sufficient to ensure a frequency assignment plan for a given number of channels that are free from third-order intermodulation interference. Also, in some systems certain channels must be constrained to specific frequencies for reasons not associated with avoiding intermodulation product interference. In such cases a channel assignment plan that minimizes (either on a uniform or a weighted basis) the amount of third-order intermodulation interference is desired. Since, to the authors' knowledge, there is no procedure for directly calculating such plans, trial and error techniques must be used. The difference set triangle makes the trial and error method a viable synthesis procedure since candidate plans can be evaluated very rapidly, and constraints and weighting factors can be easily specified. For example,  $f_j + f_i - f_i$  type products can be very easily distinguished from  $2f_j - f_i$  products. This is important since the former are 6 dB higher than the latter. Hence, the relative amount of third-order interference in each channel can be easily computed from the difference set triangle for plans having equal sized carriers.

The difference set triangle can also be used to obtain rapid computer assessment of frequency plans having unequal carrier sizes. If the carriers have unequal power, the intermodulation products falling on a particular frequency assignment (which are determined from the difference set triangle) can each be weighted by the product of the relative power levels of the carriers generating them. This procedure gives an accurate assessment of the relative intermodulation power falling on assigned carriers with unequal power, but carrier bandwidths are assumed to be small relative to the total available bandwidth.

Approximate relative assessments can be made for frequency plans having wideband carriers by modifying the preceding technique so that wideband carriers are represented by clusters of small contiguously spaced

carriers, and in the difference set triangle evaluation, not counting the intermodulation products generated among the components of a cluster. A crude method of handling wideband carriers is simply one in which a carrier is represented by one frequency location with a number of unassigned slots on either side of it.

A potential application for such an evaluation technique is an automated frequency planning scheme for FDMA/FM satellite systems (such as INTELSAT [6]) for which the effect of cochannel and adjacent channel interference on frequency planning may be equal to or greater than that of the intermodulation interference resulting from transponder operation in the quasi-linear mode. In such a planning scheme, in which the relative performance of many candidate plans is of interest, this technique provides a method of evaluation that requires much less computer time than the exact computation of intermodulation product levels, using for example, the techniques of Reference 7.

### Examples

Figures 1 through 3 comprise a sequence of frequency plans indicating the effects of carrier location on third-order intermodulation interference levels. Each figure shows the third-order intermodulation spectrum of a 10-carrier frequency plan. The three frequency plans, given in Table 4, represent uniformly, randomly, and optimally spaced (Table 2) carrier arrangements, respectively. The method described in Reference 7 has

TABLE 4. FREQUENCY PLANS FOR FIGURES 1-3

Carrier No.	Frequency Assignment		
	Figure 1 (uniform)	Figure 2 (random)	Figure 3 (optimum*)
1	1	1	1
2	7	3	2
3	13	14	7
4	19	17	11
5	25	21	24
6	31	26	27
7	37	30	35
8	43	39	42
9	49	50	54
10	55	56	56

\* Taken from Table 2.

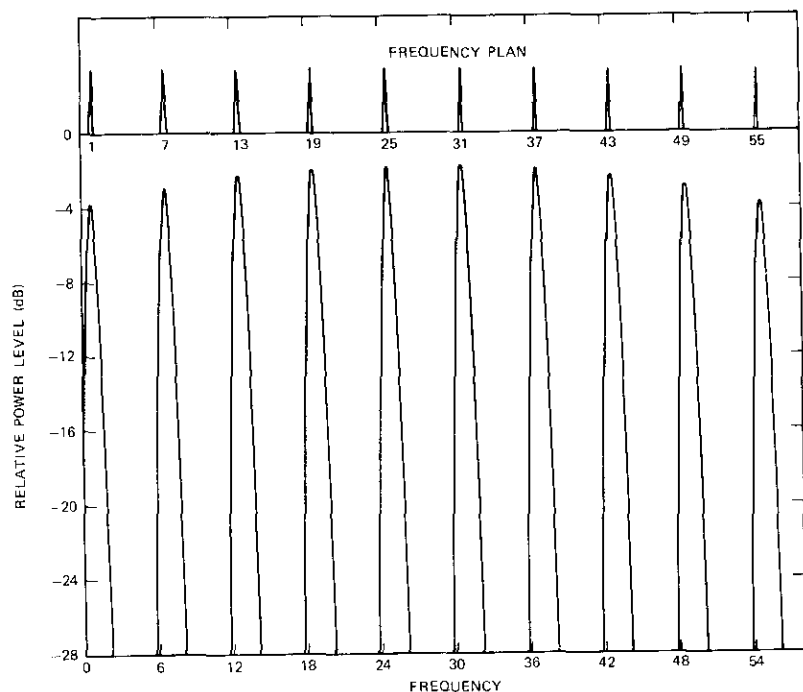


Figure 1. *Third-order Intermodulation Spectrum of a Uniformly Spaced 10-Carrier Plan*

been used to compute the spectra shown in these figures, with each carrier given equal power and assumed to have a Gaussian spectrum with an rms deviation of 0.2 times the basic frequency slot division.

The worst-case intermodulation interference condition is represented by the uniformly spaced case shown in Figure 1, whereas the best case is the optimum arrangement shown in Figure 3, where it can be seen that no intermodulation products fall on the assigned carrier frequencies. Figure 2, in which the carrier assignments have been selected at random, represents a condition between these extremes, for which the intermodulation occurs at various levels.

As a second example, difference set triangle evaluation techniques are applied to a constrained frequency plan. The constraints are intended to represent the bandwidth and assignment limitations that can exist in an

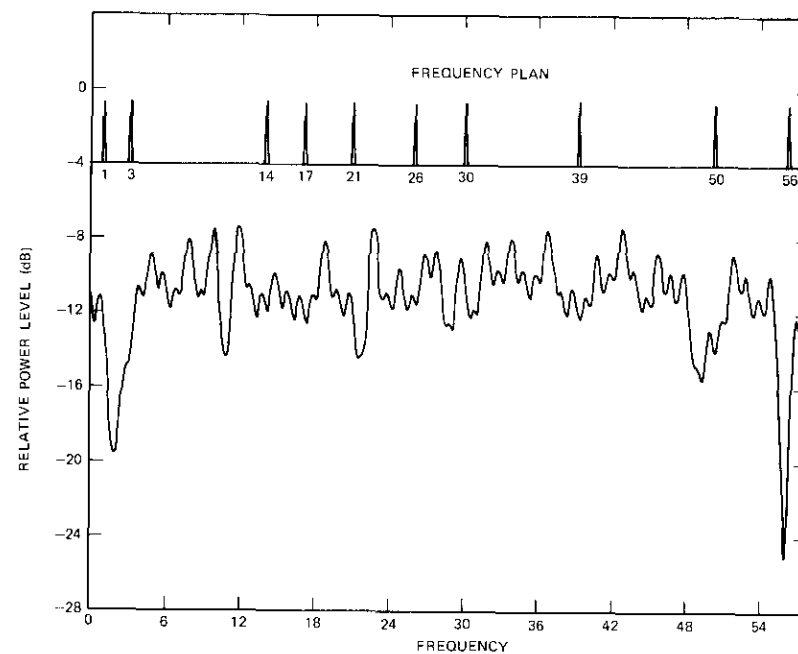


Figure 2. *Third-order Intermodulation Spectrum of a Randomly Spaced 10-Carrier Plan*

actual system. The objective of the exercise is to find a 16-carrier frequency plan which is as free from third-order intermodulation interference as possible, and which is subject to the following constraints:

- a. channel slots 21, 30, 59, and 180 must be occupied;
- b. contiguous channel slot assignments are not permitted;
- c. channel slots 1-5, 158-179, and 181 must not be occupied.

The best solution to this problem is carrier assignment plan (6, 11, 21, 24, 30, 42, 59, 81, 92, 103, 117, 125, 133, 137, 157, 180). Figure 4 shows the computed third-order intermodulation spectrum for this plan using equal sized carriers with spectra which are the same as those in Figures 1-3. It should be noted that the "gaps" in this spectrum occur at the assigned carrier frequencies.

In some applications it may be desirable to modify the preceding problem by having a mix of carrier sizes, as in the case of a system with both relatively narrowband voice (FM) traffic and digital data (PSK) carriers which occupy a wider bandwidth. For such a problem, the preceding

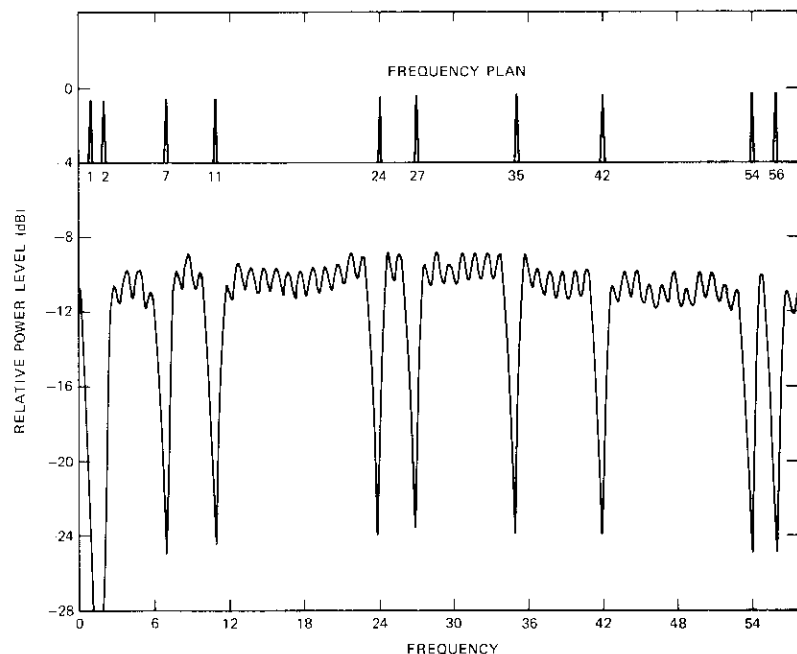


Figure 3. *Third-order Intermodulation Spectrum of an Optimally Spaced 10-Carrier Plan*

solution would be a good starting point, since it has some channel assignments, such as 157 and 59, with good isolation from neighboring channels. The techniques outlined in the previous section could then be used to achieve an improved solution.

#### **Application to related areas**

The problem discussed in this paper and modifications thereof have potential applications in related areas. For example, the concept of generating a constrained frequency plan may be extended to the generation of self-orthogonal forward-error-correcting codes with properties applicable to certain circumstances.

A phased array antenna having nonlinear amplifiers in each radiating element and transmitting signals at different frequencies in different directions will radiate intermodulation products in directions that are generally different from the main beam directions [8], thereby affording

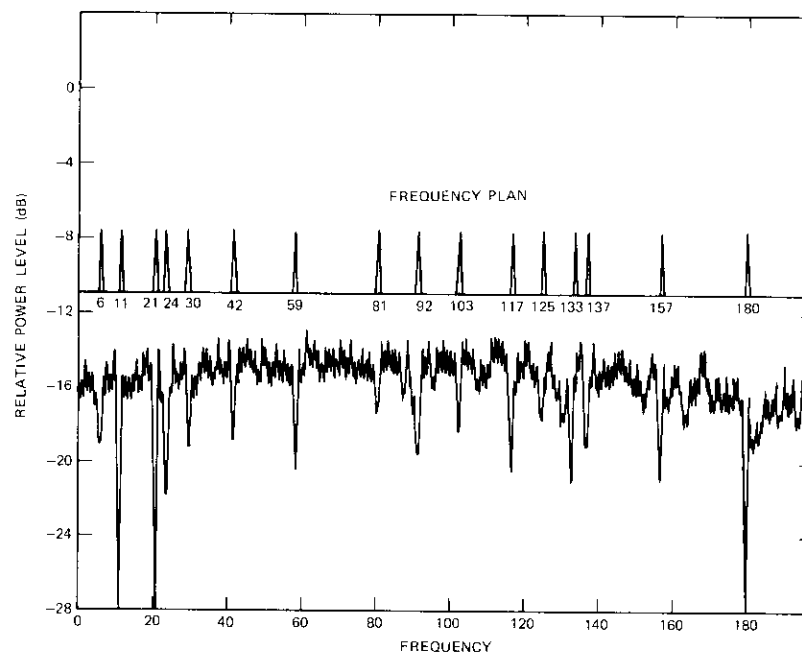


Figure 4. *Third-order Intermodulation Spectrum of a 16-Carrier Constrained Plan*

protection from intermodulation product interference. The relationships between the intermodulation beam directions and the main beam directions are essentially the same as those governing intermodulation product locations in the frequency domain. Hence, it is possible in multiple-beam phased array systems to exploit difference set sequences to suppress intermodulation interference in both the frequency and space domains.

Finally, the Butler matrix transponder (BMT) [9], [10] employs a "phase domain" to reduce intermodulation interference in systems employing contiguous frequency assignments. To ensure maximum intermodulation product protection in a BMT, difference sets are used to obtain the port assignment (*i.e.*, phase domain assignment) for each frequency.

#### **Acknowledgment**

*The authors are grateful for the contribution of G. R. Welti. The channel assignment material presented in this paper was stimulated by his develop-*

ment of a related difference set triangle in connection with the development of the Butler matrix transponder.

### References

- [1] D. W. Lipke and D. W. Swearingen, "Communications System Planning for MARISAT," IEEE International Conference on Communications, ICC 1974, Session 29, Minneapolis, Minnesota, *Conference Record*, pp. 29B-1-29B-5.
- [2] W. C. Babcock, "Intermodulation Interference in Radio Systems," *Bell System Technical Journal*, January 1953, pp. 63-73.
- [3] R. Edwards, J. Durkin, and D. H. Green, "Selection of Intermodulation-Free Frequencies for Multiple-Channel Mobile Radio Systems," *Proc. IEE*, Vol. 116, No. 8, August 1969.
- [4] J. P. Robinson and A. J. Bernstein, "A Class of Binary Recurrent Codes with Limited Error Propagation," *IEEE Transactions on Information Theory*, IT-13, No. 1, January 1967, pp. 106-113.
- [5] M. Gardner, "Mathematical Games," *Scientific American*, March 1972, pp. 108-112; June 1972, pp. 114-118.
- [6] "INTELSAT IV Communications System," edited by P. L. Bargellini, *COMSAT Technical Review*, Vol. 2, No. 2, Fall 1972, pp. 437-572.
- [7] J. C. Fuenzalida, O. Shimbo, and W. L. Cook, "Time-Domain Analysis of Intermodulation Effects Caused by Nonlinear Amplifiers," *COMSAT Technical Review*, Vol. 3, No. 1, Spring 1973, pp. 89-143.
- [8] W. A. Sandrin, "Spatial Distribution of Intermodulation Products in Active Phased Array Antennas," *IEEE Transactions on Antennas and Propagation*, November 1973, pp. 864-868.
- [9] G. R. Welti, "Butler Matrix Transponder Improvements," U.S. Patent Application, Serial No. 412399, November 2, 1972.
- [10] W. A. Sandrin, "The Butler Matrix Transponder," *COMSAT Technical Review*, Vol. 4, No. 2, Fall 1974, pp. 319-345.



Russell J. F. Fang is Manager of the Communications Systems Analysis Department of the Microwave Laboratory at COMSAT Laboratories. He is presently engaged in research and studies of advanced transmission systems for international and domestic satellite communications. Born in Chungking, China, he received a B.S. in electrical engineering from National Taiwan University (1962) and M.S. and Ph.D. in electrical engineering from Stanford University (1964 and 1968). Before joining COMSAT in 1968, he was employed by Stanford Electronics Laboratories (1965-1968), Stanford Research Institute (1964-1965), and the Chinese Air Force Electronics and Ordnance Division, Taiwan (1962-1963).

William A. Sandrin received a B.S.E.E. degree from the University of Vermont in 1963 and an M.E.E. degree from Rensselaer Polytechnic Institute in 1966. From 1966 to 1971 he worked for the Boeing Company, Aerospace Group, where he was involved in space communications system design and in the development of phased array antennas. In 1971 he joined COMSAT Laboratories, where he has been engaged in multibeam antenna studies, transponder linearizer development, and systems analysis. He is presently a member of the Communications Systems Analysis Group of the Transmission Systems Laboratory. He is a member of IEEE, Tau Beta Pi, and Eta Kappa Nu.



**Index:** rain, adaptive control, polarization, frequency reuse

## ***A dual-polarized 4/6-GHz adaptive polarization control network***

A. E. WILLIAMS

(Manuscript received November 1, 1976)

### ***Abstract***

Rain can cause significant degradation in the polarization isolation of a satellite dual frequency reuse communications system. This paper describes the design of a suboptimal 4-GHz adaptive correction circuit employing independently rotatable  $90^\circ$  and  $180^\circ$  polarizers. Experimental results indicate that the adaptive network operated successfully in the COMSAT unattended earth terminal in the presence of rain.

### ***Introduction***

A dual-polarized frequency reuse communications satellite system can suffer significant depolarization and hence channel degradation due to cross polarization in the presence of rain. Since the interference varies with time, some form of adaptive correction may be employed to correct the depolarization. Solutions to this problem have been considered by Chu [1], [2], DiFonzo [3], Kreutel [4], and Barton [5], and summarized by DiFonzo, Trachtman, and Williams [6].

---

This paper is based upon work performed in COMSAT Laboratories under the sponsorship of the International Telecommunications Satellite Organization (INTELSAT). Views expressed in this paper are not necessarily those of INTELSAT.

It has been shown that four degrees of freedom are generally required for complete polarization control; therefore, a polarization adaptive circuit must contain four variable parameters. However, at 4 and 6 GHz the principal rain depolarization effect is due to differential phase; the effect of differential attenuation is negligible except for extremely heavy rain rates. Under these conditions the number of degrees of freedom required for polarization control is reduced to two, and the adaptive network becomes a suboptimal circuit having two variable parameters. This paper addresses this particular case and presents the design of a simple adaptive circuit consisting of cascaded 90° and 180° polarizers which act as a differential phase corrective network. Justification for this design and design details are described, together with results obtained from the laboratory and the unattended earth terminal (UET) at Clarksburg.

**Differential phase shift network, justification and design**

The effect of rain on the electromagnetic transmission medium is modeled by assuming that the nonspherical raindrops provide differential attenuation and differential phase [7], [8]. Isolation degradation can be computed on the basis of the values of differential phase shift and attenuation as a function of rain rate [9]. Since cross-polarization interference can be treated as an additional noise component, the resultant carrier-to-noise ratio (which determines the ultimate communications capacity of a system) can then be computed from the initial carrier-to-thermal-noise ratio.

These results are shown in Figures 1 and 2 for circularly polarized fields\* at 4 and 6 GHz and an average rain cell depth of 5 km. At these frequencies the effect of differential attenuation is clearly small. This property provides ample justification (from a system point of view) for providing only differential phase correction in a 4/6-GHz dual-polarized communications system. This assumption makes it possible to eliminate two degrees of freedom from the depolarization correction problem and results in a suboptimal adaptive network with only two variable parameters.

\* For linear polarization, the isolation degradation is a function of canting angle. At 45° the isolation degradation is equal to circular polarization, but at other angles it is less.

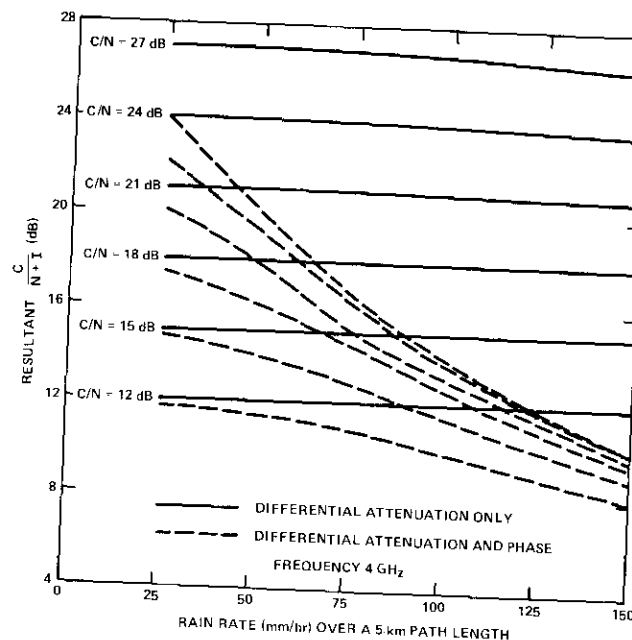


Figure 1. Resultant Carrier-to-Noise Ratio Due to Rain at 4 GHz

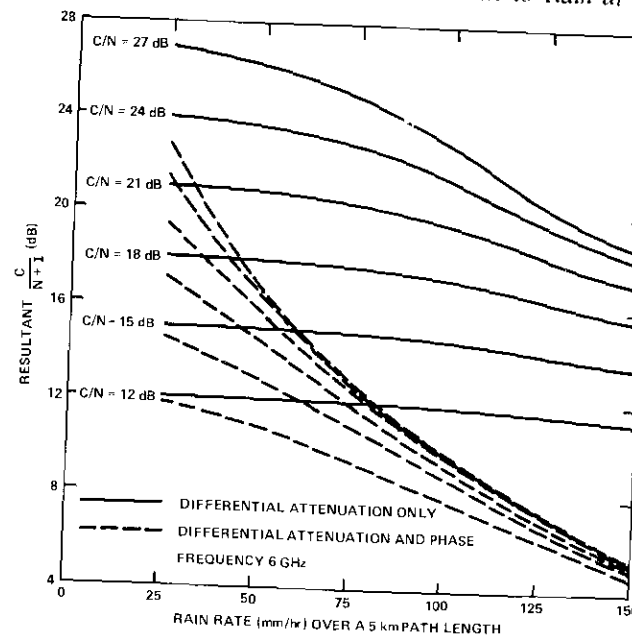


Figure 2. Resultant Carrier-to-Noise Ratio Due to Rain at 6 GHz

The simplest microwave network which achieves this objective consists of independently rotatable  $90^\circ$  and  $180^\circ$  polarizers followed by an orthomode transition, as shown in Figure 3. Reference 6 has shown that a cascaded set of independently rotatable  $90^\circ$  and  $180^\circ$  polarizers can convert dual orthogonal elliptical polarization to either dual linear or dual circular polarization. Alternatively, this polarizer set can convert any orthogonal polarization state to any other orthogonal polarization state. That is, the cascaded polarizer set operates as a phase shift aligned at some angle to the transverse plane.

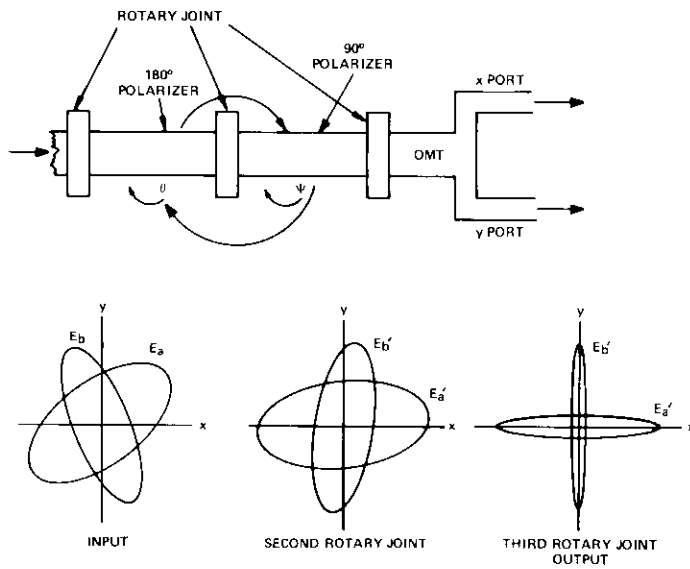


Figure 3. Microwave Polarizer Circuit

Consider the polarizer network placed in the receive port of an earth station. The satellite will transmit a dual linearly or a dual circularly polarized 4-GHz field which will generally be depolarized by the propagation medium so that a dual elliptically polarized set of fields is received at the earth station. The angular position of the polarizers is then adjusted to convert the input dual elliptically polarized fields to dual linearly polarized fields at the output orthomode transducer (OMT).

Figures 4 and 5 show the domain of polarizer angular positions in terms of propagation medium differential phase shift for both transmitted dual linear and dual circular polarization. Note that the solution domains depend on the relative positions of the  $90^\circ$  and  $180^\circ$  polarizers with respect

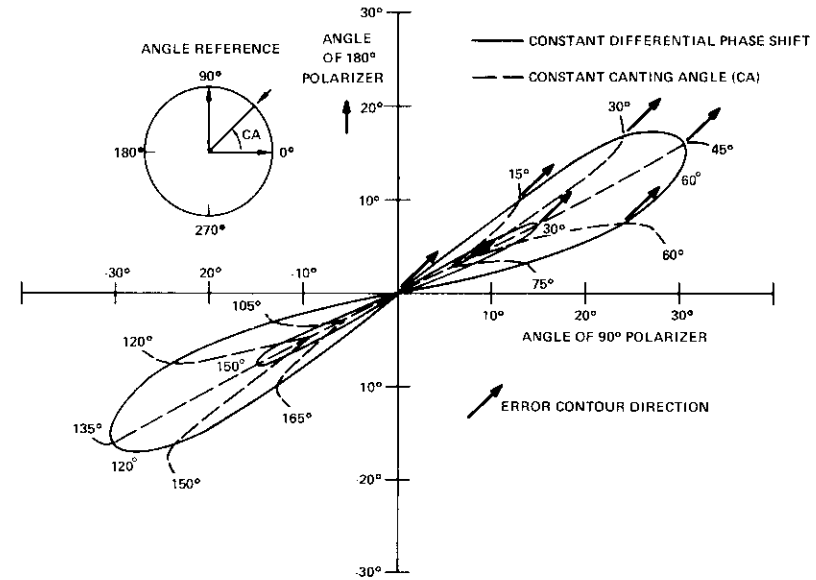


Figure 4a. Solution Contours for Transmitted Linear Polarization  $90^\circ$ ,  $180^\circ$  Polarizer Set

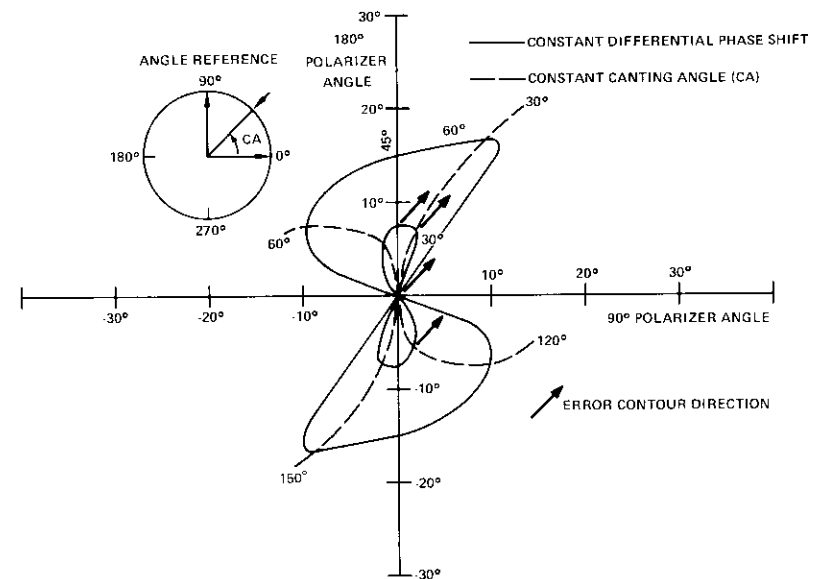


Figure 4b. Solution Contours for Transmitted Linear Polarization  $180^\circ$ ,  $90^\circ$  Polarizer Set

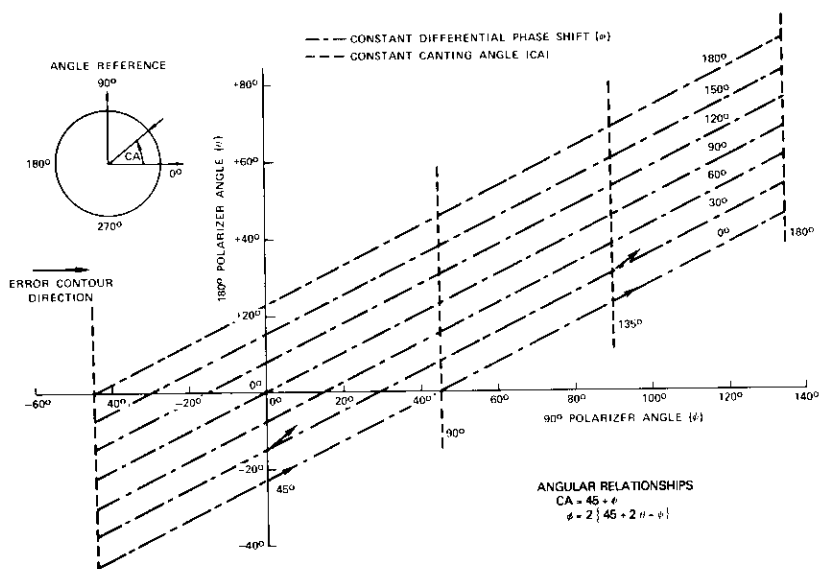


Figure 5a. Solution Contours for Transmitted Circular Polarization  
90°, 180° Polarizer Set

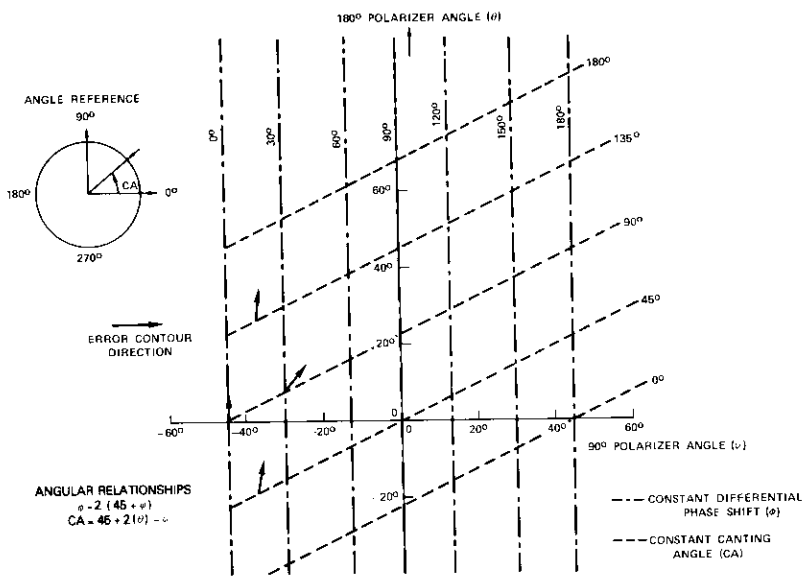


Figure 5b. Solution Contours for Transmitted Circular Polarization  
180°, 90° Polarizer Set

to the feed horn and output OMT. For example, for a dual circularly polarized system, the 180° polarizer should be placed closest to the feed horn to minimize the possible range of polarizer angular movement.

The 90° and 180° polarizer set is ideally suited for use in adaptive correction circuits for the following reasons:

a. The polarizers can be constructed in circular waveguide with axial ratios less than 0.17 dB (or isolations greater than 40 dB) over the full satellite 500-MHz bandwidths. The circuit is therefore a wideband circuit.

b. The polarizers have very low loss (<0.03 dB) so that the circuit can be placed in the receive waveguide antenna feed without any significant noise temperature degradation.

c. The low loss of the polarizers combined with their high-power breakdown characteristic makes the circuit directly applicable to the high-power transmit portion of the antenna feed.

d. Recent results by Taur [10] have shown that the rate of change of rain depolarization has a cutoff frequency of 0.2 Hz with a 20-dB fall-off to at least 100 Hz. Therefore, a correction system using mechanical polarizers can be designed to have an adequate response time.

### Adaptive correction circuit

For the microwave polarizer circuit to operate as a dual-polarized receive adaptive circuit, two cw beacons, one for each polarization, at different frequencies are transmitted from the satellite and received via the two orthogonal ports of an orthomode junction. For polarization restoration, the reception of one beacon in the other polarization and vice versa results in errors which must be minimized to ensure that nearly dual linear polarization is received at the OMT ports.

An analysis presented in Reference 6 shows that the two errors are not directly related to the polarizer angular position, but rather that each is related to a transcendental combination of both positions. Consequently, direct feedback control cannot be achieved by employing simple amplitude receiver concepts. However, it may be obtained by using a microprocessor unit to control the polarizer angular positions so that the polarizer error power levels (voltages squared) are continuously minimized. Figure 6 is a schematic of this adaptive circuit which includes a diagram of the error processing and control from receivers to polarizer angular positions. To achieve precise polarizer position control com-

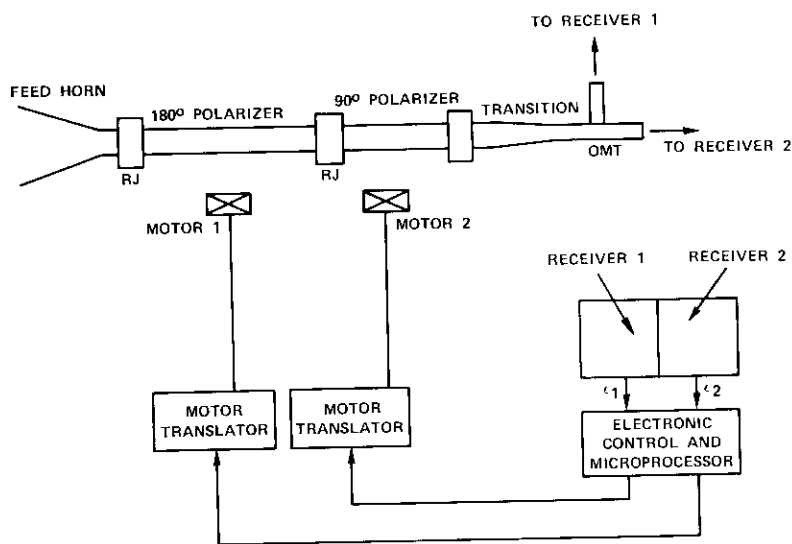


Figure 6a. Adaptive Correction Circuit

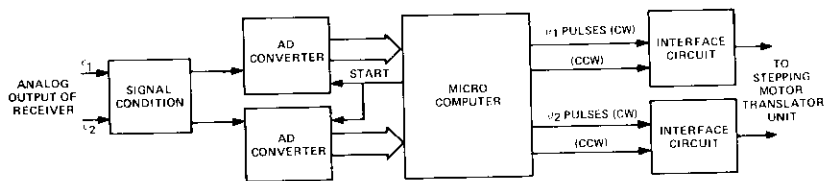


Figure 6b. Electronic Control Unit

patible with the microprocessor circuitry, digital stepping motors have been used to drive the polarizers in steps of  $0.18^\circ$  at a rate of 100 steps per second.\*

This control system was modeled on a digital computer by using the sum of the error power levels ( $\epsilon_1^2 + \epsilon_2^2$ ) as the total error,  $\epsilon^2$ , and by minimizing this error with incremental  $0.18^\circ$  polarizer steps until each polarizer in turn had achieved a minimum. To realize adequate receiver sensitivity, a cross-polarization error of  $-20$  dB relative to the copolarization level

\* Environmental test results described in the next section indicate that this performance specification is satisfactory.

was set equal to the full 256 levels of the analog-to-digital converter.\* Figure 7 is typical computer printout showing the digital error voltage levels and the successive rotation of the polarizers.

### Experimental results

A wideband 4-GHz receive adaptive circuit consisting of independently rotatable  $90^\circ$  and  $180^\circ$  polarizers, together with microprocessor, stepping motor units, and optical encoders for angular measure, was assembled and tested in the laboratory under simulated earth station carrier-to-noise ratio conditions. Testing was performed using transmitted circular polarization and a differential phase shifter to simulate the propagation medium. The microwave circuit was configured with the  $90^\circ$  polarizer closest to the OMT, since in a circularly polarized system the total polarized movement is minimized (see Figure 5).

Experimental results in the laboratory showed that copolarization-to-noise ratios of 50 dB had to be maintained to obtain a satisfactory nulling response. Alternatively, at a cross-polarization level of  $-30$  dB relative to the copolarization, a cross-polarization-to-thermal noise ratio of 20 dB was required to achieve adequate nulling. Results in the laboratory indicated that adaptive correction for both single and dual channels yielded nearly identical results. Therefore, it was decided that a single polarization channel would be used for earth station measurements. While this would not represent a true dual-polarized adaptive test, it would permit a simpler experimental system. Further, successful polarization linearity at the OMT would still answer the critical question of whether the circuit could follow the rate of change of rain.

The 4-GHz adaptive polarizer circuit, corrugated feed horn, and OMT shown in Figure 8 were installed in the COMSAT UET at Clarksburg, together with the receivers, motor amplifier drivers, and a printer for recording the polarizer angular positions. To simulate a single satellite beacon, a cw signal at 6,162.5 GHz was transmitted from the 42-ft Andover telemetry, tracking, and command antenna to the INTELSAT IV-A F2 spacecraft, which translated the frequency to 3,937.5 GHz and retransmitted the signal as a circularly polarized field to the feed in the UET.

Data taken during the summer of 1976 indicated that the adaptive

\* To safeguard against power supply failure, for example, the microprocessor was programmed to execute a slow minimizing search if the cross-polarization error exceeded  $-20$  dB.

```

INITIAL CHOICE FOR PHI 1, PHI 2
?
-25.0, -12.4
INPUT FOR ANGLE INCREMENT
?
0.18°
TYPE 1 FOR SUM, TYPE>1 FOR NO SUM
?
2
NO OF CYCLES FOR SUM OF SQUARES
?
3
EV1      EV2
252      255
ROTATE 180°PLATE
250      258
252      255
255      252
252      255
ROTATE 90°PLATE
269      269
252      255
235      241
220      228
204      216
190      204
176      193
163      182
150      172
138      162
127      153
116      145
106      137
97       130
88       123
79       117
72       112
65       107
58       102
52       99
47       95
42       93
38       90
35       89
32       87
30       87
28       87
26       87
26       88
26       87

ROTATE 180°PLATE
31      96
26      87
23      79
19      71
16      63
13      56
11      50
10      44
9       38
8       33
8       28
8       24
9       20
10      17
12      14
14      12
12      14
ROTATE 90°PLATE
16      16
12      14
8       13
5       12
3       12
1       12
0       13
1       12
ROTATE 180°PLATE
1       16
1       12
3       9
4       7
6       4
9       3
6       4
ROTATE 90°PLATE
9       5
6       4
5       5
6       4

LB/4 = 90°  LB/2 = 180°  XPOLA  XPOLB
-30.40    -15.28    36.99944  35.58321
NO OF LB/4 MOVES  NO OF LB/2 MOVES
0          42          0          28
TYPE 1 FOR PLOT - TYPE>1 FOR NO PLOT
?

WHERE EV = DIGITAL ERROR LEVEL
256 = CO-CROSSPOLARIZATION = 20 dB

```

Figure 7. Computer Simulation of Nulling Algorithm

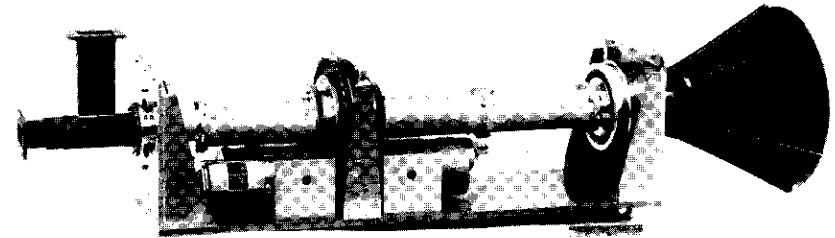


Figure 8. Photograph of Adaptive Circuit

circuit could indeed follow the fluctuations of the propagation medium and in particular the rate of change of rain rates. Two very good examples of the circuit's operation have been reduced to graphical form and are presented in Figures 9 and 10. Data recorded during these rainstorms consisted of the rain rate obtained from a single tipping bucket rain gauge located 50 meters from the antenna, the angular positions of the 90° and 180° polarizers, and the copolarization and cross-polarization levels after correction. The angular positions of the polarizers were printed as a function of time (at a rate of three readings per second) and converted (using the relationship shown in Figure 5) to show cross-polarization levels which would have occurred if the adaptive circuit had not been working. Peak depolarization levels of 7.5 and 12.0 dB are indicated, with depolarization levels less than 15 dB lasting more than 15 minutes. However, polarization correction to an average value of better than 30 dB was maintained throughout the two rainstorms.

While any correlation between rain rate and depolarization level should be treated with a certain amount of caution, a number of interesting observations can be made concerning the data shown in Figures 9 and 10. First, for both rain events, a few minutes elapsed between the occurrence of the peak rain rate and the time when the peak depolarization was recorded. This discrepancy was due to the storm's approaching from the north and moving past the rain gauge and into the microwave beam, which was pointing in a southeasterly direction.

Secondly, the rain cell for the Sunday event appears to be greater in time scale (and hence distance) than the Saturday storm. This observation is confirmed by the fact that the peak rain rate on Saturday does not produce the greatest depolarization. The intercept rain cell depth, *i.e.*, the rain cell width which intercepts the microwave beam, can be approximately estimated from the peak rain rate and the depolarization level.

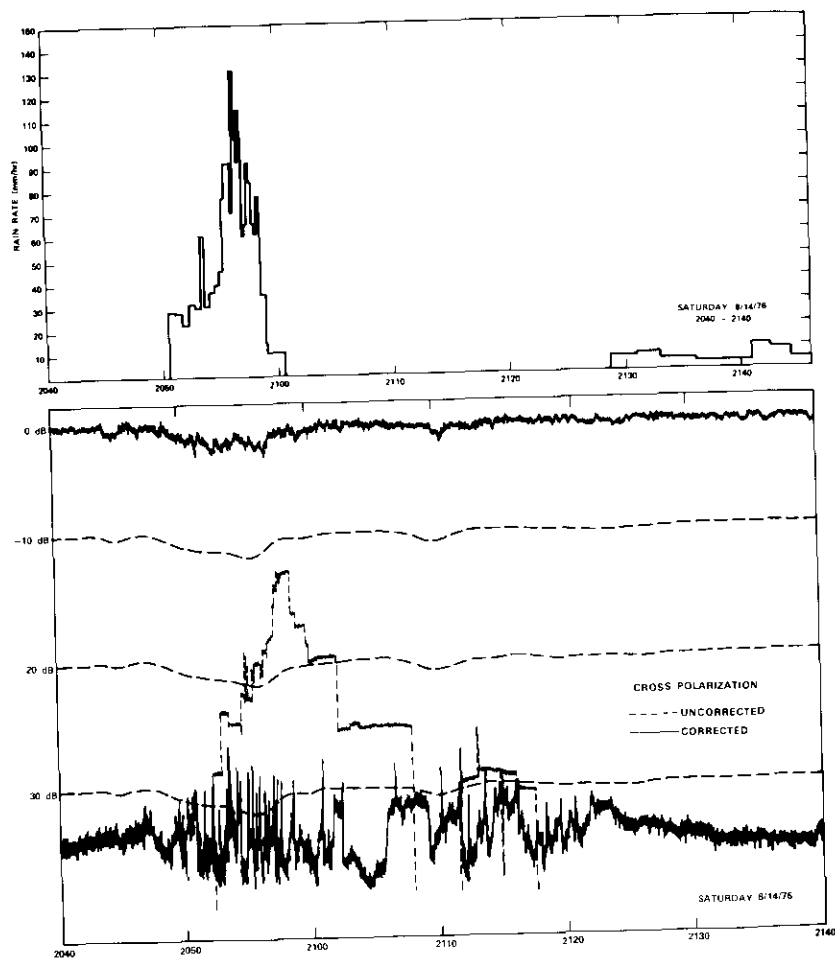


Figure 9. Corrected and Uncorrected Cross-polarization Levels and Rain Rate for Saturday, 14 August 1976

Rain cell intercept depths of 5 and 9 km are indicated for the Saturday and Sunday rainstorms, respectively. These figures are entirely consistent with the maximum possible depolarization propagation path of 12.8 km, which is computed from a beam elevation angle of  $23^\circ$ \* and a generally assumed rain ceiling of 5 km.

\* UET elevation angle to INTELSAT IV-A F2 is  $23^\circ$ .

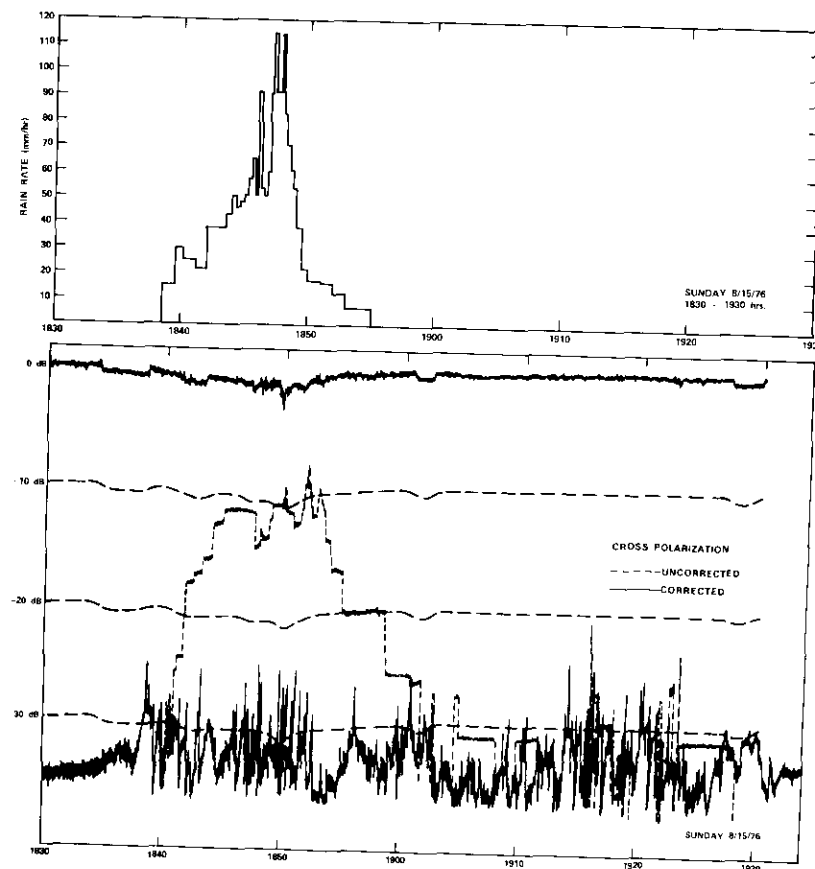


Figure 10. Corrected and Uncorrected Cross-polarization Levels and Rain Rate for Sunday, 15 August 1976

One further interesting result which can be evaluated from the polarizer angle readings (using the relationship shown in Figure 5) is the canting angle or alternatively the average orientation of the raindrops. Figures 11 and 12 summarize these data as a function of time and show that during both rainstorms the average orientation of the raindrops is horizontal to within  $\pm 5^\circ$ . For small depolarization the sensitivity of the  $180^\circ$  polarizer angular position is low and consequently the canting angle error is high. This explains why at the edges of the rainstorms the canting angle departs significantly from a horizontal position.

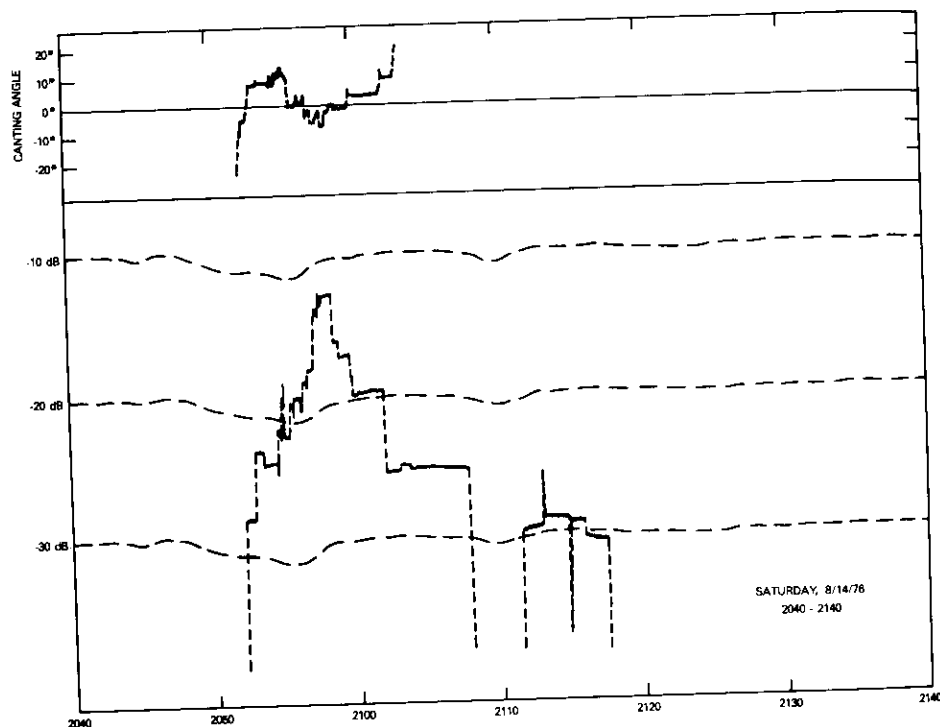


Figure 11. Canting Angles and Corrected Cross-polarization Levels for Saturday, 14 August 1976

### Conclusions

This paper has described both the justification for correcting only differential phase in a dual-polarized 4- and 6-GHz satellite communications link and the design of an adaptive circuit which employs independently rotatable  $90^\circ$  and  $180^\circ$  polarizers as a wideband 500-MHz differential phase shifter. Experimental results at 4 GHz show that the adaptive network provides polarization correction in the presence of rain with depolarization levels in excess of 10 dB kept at an average of 30 dB below the copolarization level.

### Acknowledgments

The author would like to acknowledge the assistance of Messrs. R. W. Kreutel, D. F. DiFonzo, and W. S. Trachtman, who contributed significantly

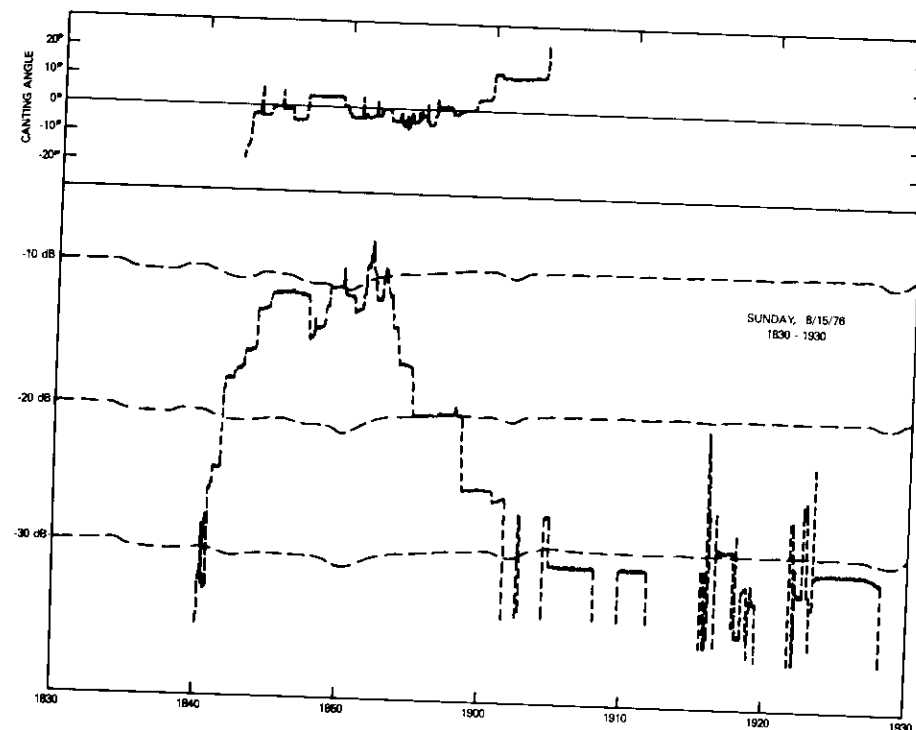


Figure 12. Canting Angles and Corrected Cross-polarization Levels for Sunday, 15 August 1976

to the design phases of this project. He would also like to acknowledge the assistance of Messrs. J. Bleiweis, who constructed the microprocessor; R. W. Gruner, who constructed the OMT and polarizers; and F. L. Frey, who assembled the adaptive network and was responsible for the smooth running of the UET experiments. Special thanks are also due to Dr. R. Taur, who assisted with the interpretation of the rain and the depolarization data.

### References

- [1] T. S. Chu, "Restoring the Orthogonality of Two Polarizations in Radio Communication Systems, I," *Bell System Technical Journal*, Vol. 50, No. 9, November 1971, pp. 3063-3069.
- [2] T. S. Chu, "Restoring the Orthogonality of Two Polarizations in Radio Communication Systems, II," *Bell System Technical Journal*, Vol. 52, No. 3, March 1973, pp. 319-327.

- [3] D. DiFonzo, Private Communication.
- [4] R. W. Kreutel, "The Orthogonalization of Polarized Fields in Dual Polarized Radio Transmission Systems," *COMSAT Technical Review*, Vol. 3, No. 2, Fall 1973, pp. 375-386.
- [5] S. K. Barton, "Methods of Adaptive Cancellation for Dual Polarization Satellite Systems," *The Marconi Review*, Vol. XXXIX, No. 200, First Quarter 1976.
- [6] D. DiFonzo, W. Trachtman, and A. E. Williams, "Adaptive Polarization Control for Satellite Frequency Reuse Systems," *COMSAT Technical Review*, Vol. 6, No. 2, Fall 1976, pp. 253-282.
- [7] T. Oguchi, "Attenuation of Electromagnetic Waves Due to Rain with Distorted Rain Drops, Part I," *Journal of Radio Research Labs (Japan)*, No. 33, September 1960, pp. 467-485.
- [8] T. Oguchi, "Attenuation of Electromagnetic Waves Due to Rain with Distorted Rain Drops, Part II," *Journal of Radio Research Labs (Japan)*, No. 53, January 1965, pp. 19-44.
- [9] R. Taur, "Rain Depolarization: Theory and Experiment," *COMSAT Technical Review*, Vol. 4, No. 1, Spring 1974, pp. 187-190.
- [10] R. Taur, Private Communication.

Albert E. Williams was born in Albany, Australia. He received a B.E. in electrical engineering from the University of Western Australia, Perth, in 1962, and a Ph.D. from University College, London, England, in 1966. From 1966 to 1968 he was a lecturer in the Department of Electrical Engineering, University of Western Australia. Currently, he is a technical staff member of the Antennas Department of the Microwave Laboratory at COMSAT Laboratories, where he is working on antenna and filter theory applicable to future communications satellites. Dr. Williams was a joint recipient of the Institute of Electrical Engineers (London) Sylvanus P. Thompson Premium award in 1966.



Index: ALOHA system, satellite, communications networks

## ***A dynamic model for satellite nonsynchronous ALOHA systems***

A. K. KAUL

### ***Abstract***

The so-called ALOHA systems are random multiple-access packet-switched broadcast networks with retransmission as the error recovery protocol. The synchronous or "slotted" ALOHA system and its derivatives have been extensively investigated in recent years for both terrestrial and satellite packet transmissions. The dynamic characteristics and stability of nonsynchronous ALOHA systems have recently been investigated for terrestrial packet systems with negligible propagation delay. This paper presents a model for satellite ALOHA systems characterized by large propagation delays and examines its use in predicting the dynamic characteristics and steady-state stability and performance of such systems. This is followed by a discussion of the considerations required for "optimal" design of a satellite ALOHA system.

### ***Introduction***

The application of random multiple-access (RMA) techniques over a broadcast radio communications channel has been the subject of significant work in recent years. This technique is of great interest in terms of geostationary communications satellites because of the relative ease with which these satellites can provide broadcast coverage over geographically dispersed areas.

A random-access satellite communications system is characterized by a population of earth stations which have direct and immediate access to a shared broadcast satellite communications channel. Each user accesses the channel, without any established protocols, every time it must transmit a block of data. The term "random access" arises from the assumption that the occurrence of transmittable data at each station, and hence the station's access to the channel, is a random bursty process. In a computer communications environment it has been found that data generation processes are indeed bursty and that they can be described as random processes [1].

It is clear that, since a population of users contends for the channel, there will be occasions when transmissions from more than one user overlap in time, creating signal distortion and hence transmission errors. Because computer communications systems cannot tolerate significant amounts of data transmission errors, a correction or recovery procedure must be implemented in such systems. While transmission errors due to signal impairments within the channel can be reduced by proper design of the communications facilities, errors caused by overlapping transmissions are dependent on the user and data traffic configurations. Most recovery schemes which have been implemented or proposed utilize error detection and packet retransmission, but the use of error-correcting RMA codes has also been proposed [2].

Historically, the ALOHA random-access system was proposed and implemented as a UHF radio broadcast system at the University of Hawaii [3] using retransmissions for error recovery. Since then, a number of derivatives, including slotted ALOHA [4], reservation [5], [6], and multidestination TDMA [7] systems, have been proposed. Systems operating in dynamically adjustable mixed modes (e.g., mixed reservation-slotted ALOHA systems) have also been suggested. These schemes are intended to increase the maximum channel efficiency beyond the 18.4-percent limit for ALOHA systems, but this improvement is achieved by introducing additional complexity or controls in the random-access systems.

While synchronous ALOHA systems are more efficient than nonsynchronous systems, this increase in efficiency requires additional control to be introduced into the system. In an actual satellite system design, tradeoffs must be made between system efficiency and complexity or cost. Thus, the nonsynchronous ALOHA systems may be a viable option for a number of configurations, and their operational characteristics should be investigated despite their relative overall transmission inefficiency.

The pioneering work in ALOHA systems was performed by Abramson

[3], who showed that, for an ALOHA system, under equilibrium conditions, the relationship between the average number of new packets transmitted into the channel per second ( $r$ ), and the average number of total transmissions per second ( $R$ ) is

$$r = R e^{-2R\tau} \quad (1)$$

where  $\tau$  is the packet transmission time.

The main assumption in the derivation of this equation is that the total transmission, composed of new and retransmitted packets of identical size, constitutes a Poisson process. Based on this assumption, the probability that a packet will interfere in time (collide) with other transmitted packets has been shown to be

$$P_c = 1 - e^{-2R\tau} \quad (2)$$

Hence, equation (1) indicates that, under steady-state conditions, the average number of successful transmissions per second (represented by the right-hand side) is equal to the average rate of generation of new packets. With the normalized channel utilization (or throughput),  $S$ , and channel traffic,  $G$ , defined as

$$S = r\tau$$

and

$$G = R\tau$$

the steady-state ALOHA equation [equation (1)] is written in a more elegant form as

$$S = G e^{-2G} \quad (3)$$

indicating that the maximum possible utilization is about 18.4 percent ( $1/2e$ ) and occurs when the channel traffic is 0.5.

The main disadvantage of this steady-state formulation is its inability to predict the stability of a steady state or the dynamic behavior of a system. Steady-state stability is an important consideration, since it is expected that departures from steady-state operation will be caused by stochastic fluctuations in system parameters in an operational system.

Most of the ensuing work has evolved as a result of attempts to improve the maximum utilization by using time slotting [4] and dynamic slot reservation techniques [5]-[7]. The University of Hawaii ALOHA project

has been the source of several reports dealing with specific aspects of radio ALOHA system performance (e.g., mix of packet sizes) using simulation techniques. On the other hand, while formulations for the dynamic behavior and stability of slotted ALOHA systems have been presented by several authors (see, for example, References 8-10), the only significant effort in formulating a dynamic theory for unslotted ALOHA has been presented recently by Carleial and Hellman [11]. This is probably due to the dwindling interest in the less efficient ALOHA systems, and to the greater difficulty associated with a formulation for nonsynchronous systems in which, unlike slotted systems, packet transmissions do not occur at discrete times.

Carleial and Hellman, by assuming negligible propagation delays, have been able to formulate a dynamic theory for terrestrial radio ALOHA systems. However, this formulation is incompatible with satellite ALOHA systems in which the propagation delays are large relative to packet transmission times and random retransmission delays. Specifically, two of their main assumptions for a radio packet environment (i.e., that the overall retransmission delay is essentially a random variable, and that a system immediately senses a collision) break down in a satellite environment where the retransmission delay has a large deterministic component (the fixed propagation delay), and a user cannot determine the need for retransmission immediately after a packet collision, but only after a certain time lag.

This paper proposes a technique for defining time in discrete epochs which is applicable to satellite systems, and which allows the dynamic behavior of an ALOHA system to be characterized. This is followed by an investigation of the usefulness of the model in predicting dynamic behavior and steady-state performance characteristics of satellite systems, along with a discussion of some of the criteria leading to the design of an optimal satellite ALOHA system.

### Characterization of satellite ALOHA systems

In a satellite ALOHA system the earth stations with access to the channel can be defined as users. An earth station may serve as a collection point for packets generated by one or more "terminals", with the packet generation process either uncontrolled or controlled by the earth station through suitable earth-station-to-terminal protocols. The maximum average rate at which a station or user can transmit traffic into the channel is determined by both the channel operating characteristics and the buffering capability available at the station.

It is convenient to establish the theory for satellite ALOHA systems in terms of users with a single-packet buffering capability, and to examine the consequences of larger buffer sizes at a later stage. First, it will be assumed that a basic satellite ALOHA system is characterized by a number of single-packet buffered users. A packet transmitted by a user is stored in the buffer for a minimum holding time,  $\tau_h^m$ , which is expressed in terms of the packet transmission time,  $\tau$ , and propagation delay,  $\tau_s$ , as

$$\tau_h^m = \tau + \tau_s \quad (4)$$

The satellite delay,  $\tau_s$ , is either a 1-hop (0.27-s) or a 2-hop (0.54-s) propagation delay, depending on whether the user senses the need to retransmit by listening in on his own transmission, or by receiving a suitable acknowledgment message from the destination. The minimum holding time is thus the minimum time that a station is "disabled" and consequently cannot transmit more than one packet of any type per interval  $\tau_h^m$ .

In addition, if a user senses that a retransmission is required, an additional random delay,  $\tau_d$ , which is generally of the order of a few  $\tau$ , is introduced prior to packet retransmission to prevent packets from colliding again on retransmission. Hence, the overall retransmission delay,  $\tau_r$ , between successive retransmissions is

$$\tau_r = \tau_h^m + \tau_d = \tau + \tau_s + \tau_d \quad (5)$$

Retransmission delay  $\tau_r$  clearly consists of a fixed deterministic component,  $\tau_h^m$ , and a random component,  $\tau_d$ . The value of  $\tau_d$  is selected at random from some bounded distribution (e.g., a "uniform" distribution), for which the upper bound ( $k\tau$ ) is determined by constraining the probability of simultaneous user retransmissions so that it is acceptably small.

In the design of satellite systems, unlike some terrestrial facilities, it is relatively easier to tailor the satellite channel data transmission rate to user requirements without being constrained *a priori* to select a given channel capacity. Hence, it can generally be expected that

$$\tau_d \ll \tau_s \quad (6)$$

since it is possible to choose systems having packet transmission times,  $\tau$ , which are negligible compared to the satellite delay,  $\tau_s$ . Hence, the retransmission delay is

$$\tau_r \approx \tau_h^m \approx \tau_s \quad .$$

From the preceding discussion, it is clear that, if an average retransmission delay,  $\tau_r$ , is redefined as

$$\tau_r = \tau + \tau_s + \bar{\tau}_d \quad (7)$$

then the variations of true delay from this quantity are essentially the variations of  $\tau_d$  about the mean  $\bar{\tau}_d$ , and are negligible in satellite systems satisfying equation (6). This suggests that in satellite systems time can be defined in successive "epochs" of duration  $\tau_r$  given by equation (7) and that in any epoch the following processes should be observed:

a. The average number of retransmissions in an epoch will be determined by the number of packet collisions in the preceding epoch. That is, on the average, for every packet undergoing a collision in the previous epoch, the user will retransmit only one packet in the current epoch at approximately the same time location (Figure 1) at which the collision occurred.

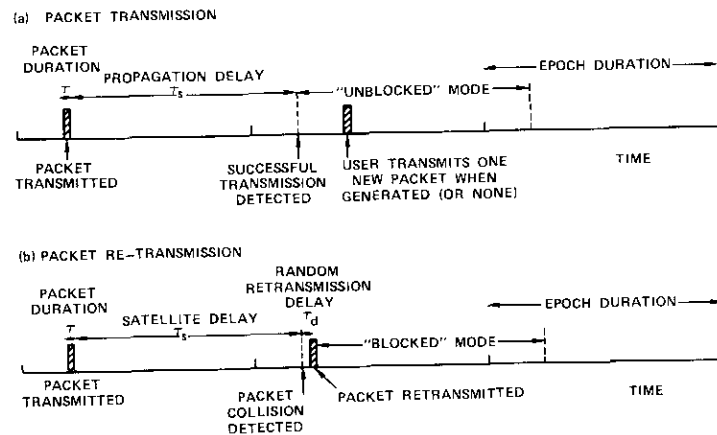


Figure 1. Packet Transmission and Retransmission within Epochs

b. Every user in an "unblocked" mode, i.e., each user who finds that his packet has not collided in the preceding epoch, will transmit an average of  $\lambda_o$  packets in the current epoch. Because of the practical constraints imposed by single-packet buffering, the unblocked user must transmit only one packet or no packets at all in this epoch. Hence,  $\lambda_o$  can be redefined as the probability that an unblocked user will

transmit a packet in an epoch of duration  $\tau_r$ , because of the requirements

$$\lambda_o \leq 1 \quad (8)$$

### Model for homogeneous satellite ALOHA systems

To develop a model for the dynamic behavior of a homogeneous (identical user) satellite ALOHA system, the following initial assumptions are employed:

a. Time is defined in epochs of constant duration  $\tau_r$  given by equation (7).

b. The system consists of  $N$  active and identical single-packet buffered users sharing a common broadcast satellite channel, and characterized by the probability  $\lambda_o$  that any unblocked\* user will transmit a packet in a given epoch. Also, from the previous discussion, a user cannot transmit more than one packet of any type in any epoch.

c. Packets have a constant length and a duration  $\tau$ . The channel capacity is sufficiently large that  $\tau$  is negligible in comparison with the satellite propagation delay.

d. In a given epoch, the transmission of new and retransmitted packets from the population of  $N$  users is randomly distributed, and  $N$  is large enough so that these packet arrivals in the channel can be approximated by a Poisson process.

e. Transmission errors due to channel noise are negligible.

f. Packets are accepted from the terminals only when a station becomes unblocked by using appropriate protocols.

g. Retransmissions, when required, have the highest priority.

One of the first consequences of the model and the previous discussions is that, when a packet transmitted by a user undergoes a collision in a given epoch, the user will retransmit the packet (and only that packet) in the next epoch (with probability equal to one) and is blocked from transmitting a new packet. On the other hand, an unblocked user can transmit only one new packet in a given epoch with probability  $\lambda_o$ , or remain idle with probability  $1 - \lambda_o$ .

It is clear that the state of the system during an epoch  $k$  can be com-

\*A user who is not blocked from transmitting a new packet by the requirement of retransmitting in the current epoch.

pletely specified by the scalar  $R^k$  representing the number of retransmitted packets in that epoch. That is, if  $R^k$  is known, the average number of new packets,  $A^k$ , transmitted in epoch  $k$  is simply

$$A^k = (N - R^k) \lambda_o \quad (9)$$

the total average number of packet transmissions,  $T^k$ , is

$$T^k = A^k + R^k = (N - R^k) \lambda_o + R^k \quad (10)$$

and under the Poisson assumption, the packet collision probability during epoch  $k$  is

$$P_c^k = 1 - \exp \left\{ -2 \frac{T^k}{\tau_r} \right\} \quad (11)$$

Equations (9), (10), and (11) fully describe all the processes of interest occurring in epoch  $k$  if  $R^k$  is specified for a given system.

Once the system state in epoch  $k$  has been established on the basis of  $R^k$ , it can be seen that the average state  $R^{k+1}$  of the system in the next epoch ( $k + 1$ ) is simply determined by the average number of packet collisions which occur in epoch  $k$ . Thus, for a given state  $R^k$ , the "average" expected state,  $R^{k+1}$ , is given by

$$R^{k+1} = T^k P_c^k$$

or, from equations (10) and (11),

$$R^{k+1} = \left\{ (N - R^k) \lambda_o + R^k \right\} \cdot \left\{ 1 - \exp \left[ -2 \frac{\tau}{\tau_r} \left\{ (N - R^k) \lambda_o + R^k \right\} \right] \right\} \quad (12)$$

Hence, the average time evolution of the state of the system is described by equation (12).

Alternatively, the average growth in an epoch for a system in state  $R^k$  can be expressed as

$$\delta(R^k) = R^{k+1} - R^k \quad (13a)$$

or

$$\delta(R^k) = (N - R^k) \lambda_o - T^k \exp \left\{ -2T^k \frac{\tau}{\tau_r} \right\} \quad (13b)$$

where  $T^k$  is defined by equation (10). Further, if the system state is defined by the fraction of users which retransmit in epoch  $k$ , as  $r^k$ , then

$$N\delta(r^k) = (1 - r^k) N\lambda_o - T^k \exp \left\{ -2T^k \frac{\tau}{\tau_r} \right\} \quad (14)$$

where

$$T^k = (1 - r^k) N\lambda_o + r^k N \quad (15)$$

Since this is valid for any epoch  $k$  and a given state  $r^k$ , the superscript can be omitted, and

$$\delta(r) = \frac{1}{N} \left[ (1 - r) N\lambda_o - T \exp \left\{ -2T \frac{\tau}{\tau_r} \right\} \right] \quad (16)$$

where

$$T(r) = (1 - r) N\lambda_o + rN \quad (17)$$

Equation (16) characterizes the average growth per epoch in the state of the system specified by  $r$ , the fraction of users which are retransmitting. To put equation (16) in a more elegant form, the following quantities are defined:

$$\text{transmission factor, } \alpha = \frac{\tau}{\tau_r} \quad (18)$$

$$\text{maximum channel input from the users, } S_o = \alpha N\lambda_o \quad (19)$$

$$\text{channel traffic, } G(r) = \alpha T \quad (20)$$

where  $\tau$  is the packet duration. The dynamic ALOHA equation can then be written as

$$\Delta(r) = (1 - r) S_o - G(r) e^{-2G(r)} \quad (21)$$

where

$$G(r) = (1 - r) S_o + rU \quad (22)$$

and the normalized average growth rate,  $\Delta(r)$ , is

$$\Delta(r) = \alpha N\delta(r) \quad (23)$$

where  $N\delta(r)$  is the actual growth per epoch. The parameter  $U$  (which can be called the normalized population) is given by

$$U = \alpha N \quad (24)$$

It is interesting to observe that dynamic equation (21) indicates that, when the system is in a given state, the average growth rate during an epoch is simply the difference between actual channel input and channel throughput during the epoch, corresponding to the first and second terms on the right-hand side of equation (21). It can also be seen that the average dynamic behavior of a system in state  $r$  is completely specified by equation (16) when the parameters  $\alpha$ ,  $N$ , and  $\lambda_o$  are specified. This set is the necessary and complete set of descriptive parameters for a homogeneous satellite ALOHA system of identical single-packet buffered users. "Normalized" equation (21) allows the system description to be specified in terms of only two parameters,  $S_o$  and  $U$ . To distinguish between the two, the set  $(\alpha, N, \lambda_o)$  will be called "real system parameters" and the set  $(S_o, U)$  "theoretical system parameters." However, it should be noted that a conversion to real parameters from the set  $S_o$  and  $U$  is possible only if the transmission parameter  $\alpha$  is known. Thus, although a given  $S_o$  and  $U$  uniquely define equation (21), translation to real system parameters requires knowledge of  $\alpha$ , which then allows  $N$  and  $\lambda_o$  to be determined as follows:

$$N = \frac{U}{\alpha} \quad (25a)$$

and

$$\lambda_o = \frac{S_o}{U} \quad (25b)$$

Since  $S_o$  and  $U$  completely specify the normalized average growth rate, the behavior of  $\Delta(r)$  as a function of system state  $r$  for given values of  $S_o$  and  $U$  can be examined, subject to the constraints that

$$U > 0$$

$$S_o > 0$$

and

$$\frac{S_o}{U} = \lambda_o \leq 1 \quad (26a)$$

or

$$S_o \leq U \quad (26b)$$

For a homogeneous single-packet buffered system characterized by  $S_o$  and  $U$ , the normalized average growth rate per epoch  $\Delta(r)$  in state  $r$  ( $0 \leq r \leq 1$ ) can be calculated by using equation (21). Figures 2 and 3

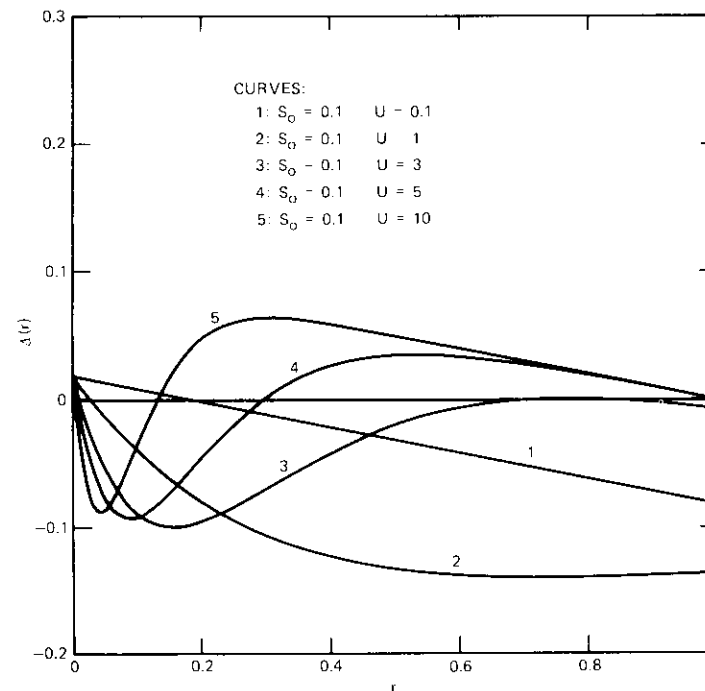


Figure 2. Normalized Average Growth Rate per Epoch,  $\Delta$ , for Initial System States  $r$  and Systems with the Same  $S_o$  and Different  $U$

show  $\Delta(r)$  as a function of  $r$  for several sets of  $S_o$  and  $U$ . For a given system in state  $r$ , the normalized growth rate is either positive or negative, and the average change in  $r$  expected in one epoch can be obtained from  $\Delta(r)$  by using

$$\delta(r) = \frac{\Delta(r)}{U} \quad (27)$$

Thus, on the average the state of a system will drift to state  $[r + \delta(r)]$  in an epoch, and the drift in the next epoch will be determined by  $\Delta(r)$  corresponding to the new state. To interpret these curves, it should be

noted that they represent average behavior, and that in a real system stochastic fluctuations will exist.

The zeros of the function  $\Delta(r)$  correspond to the steady states of a system.

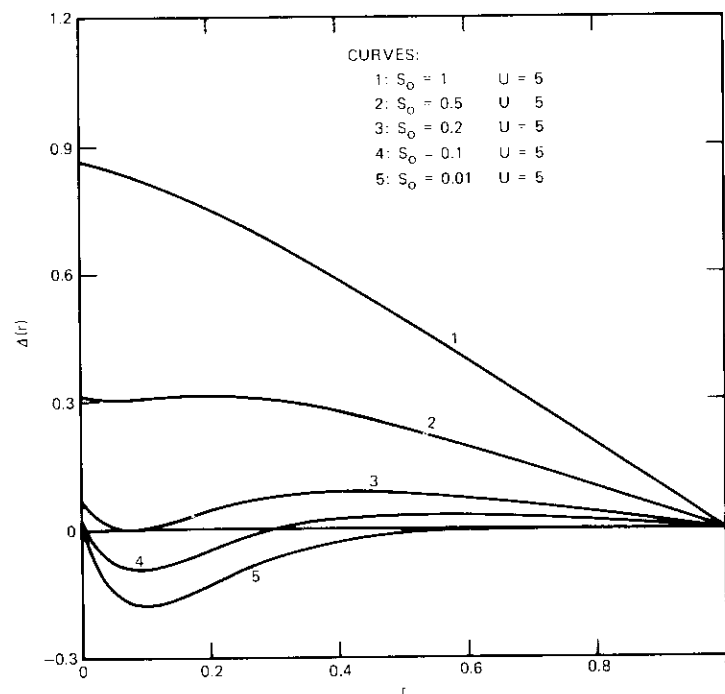


Figure 3. Normalized Average Growth Rate per Epoch,  $\Delta$ , for Initial System States  $r$  and Systems with the Same  $U$  and Different  $S_0$ .

The stability of a steady state can be determined by an evaluation of system behavior when the system undergoes small excursions from the steady state due to fluctuations. For example, in curve 2 of Figure 4, which has three steady states, state B is unstable because recovery from variations in the state at point B is impossible. The other two states are partially stable, *i.e.*, totally stable in one direction and partially stable in the other. Thus, while state A is totally stable against variations tending to decrease  $r$ , it is stable against increases in  $r$  only as long as they do not send the state beyond point B. Similarly, state C is totally stable against an increase in  $r$ , but only partially stable against decreases. Hence, systems with three

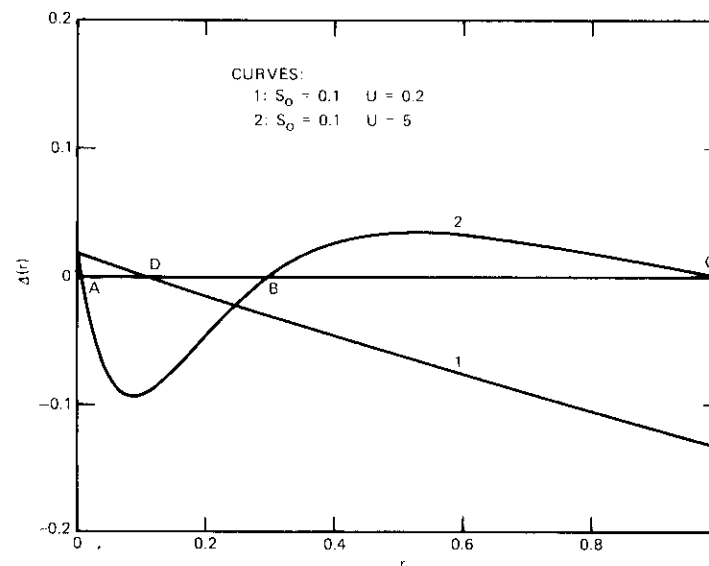


Figure 4. Typical Monostable and Bistable Systems

steady states will always exhibit this bistable (2-stable-state) behavior. On the other hand, the single steady state D in curve 1 is totally stable.

### Steady-state properties

The steady-state behavior and properties of satellite ALOHA systems will be investigated in some detail by first examining the existence of steady states and then evaluating the performance parameters of the system under stable steady-state conditions.

#### Existence of steady states

Equation (21) shows that, for a given system ( $S_0$  and  $U$ ) subject to the constraints that

$$S_0 > 0 \quad (28a)$$

$$U > 0 \quad (28b)$$

$$S_0 \leq U \quad (28c)$$

steady states will exist if there are solutions  $r_0$  ( $0 \leq r_0 \leq 1$ ) to the equation

$$(1 - r_o) S_o - G(r_o) e^{-2G(r_o)} = 0 \tag{29}$$

where  $G(r_o) = (1 - r_o) S_o + r_o U$  . (30)

It is clear that the  $r_o$ 's are the points of intersection of the straight line

$$y = (1 - r) S_o \tag{31}$$

with the curve

$$y = G(r) e^{-2G(r)} . \tag{32}$$

The following conclusions can be drawn by examining these curves:

- a. For any given system a single steady state (monostable system) or a triplet of steady states (bistable system) will always exist.
- b. The existence of a bistable system is governed by the following conditions. For  $S_o < 1/2e$ , bistable systems can always be found for sufficiently large  $U$ , while for  $S_o > 0.5$ , only monostable systems can exist. For  $1/2e \leq S_o \leq 0.5$ , no general conclusions concerning the existence of bistable systems can be drawn, and equation (21) must be used to determine whether a system is monostable or bistable.

**Stability of steady states**

As discussed earlier, monostable systems are totally stable, while bistable systems are only partially stable and transitions between the two partially stable states are possible. Figure 5 shows a series of systems for which the relative stability of the lower stable state decreases, while that of the upper stable state increases as the population is increased and the total maximum channel input remains constant.

It should be noted that, in homogeneous single-buffered ALOHA systems, there is no "runaway" effect in the channel (i.e., the channel traffic cannot build up indefinitely) because of the existence of a steady state\* which is stable against all further increase in  $r$  (e.g., C or D in Figure 4). Physically, this is because the possible number of retransmissions per epoch is bounded by the number of users,  $N$ , and the number of new packet transmissions decreases linearly with the number of retransmissions. From the nature of monostable and bistable systems and the certainty that all systems are of one of these two types, it can also be observed that a system will always

\*However, this steady state may be undesirable because of the large number of blocked users.

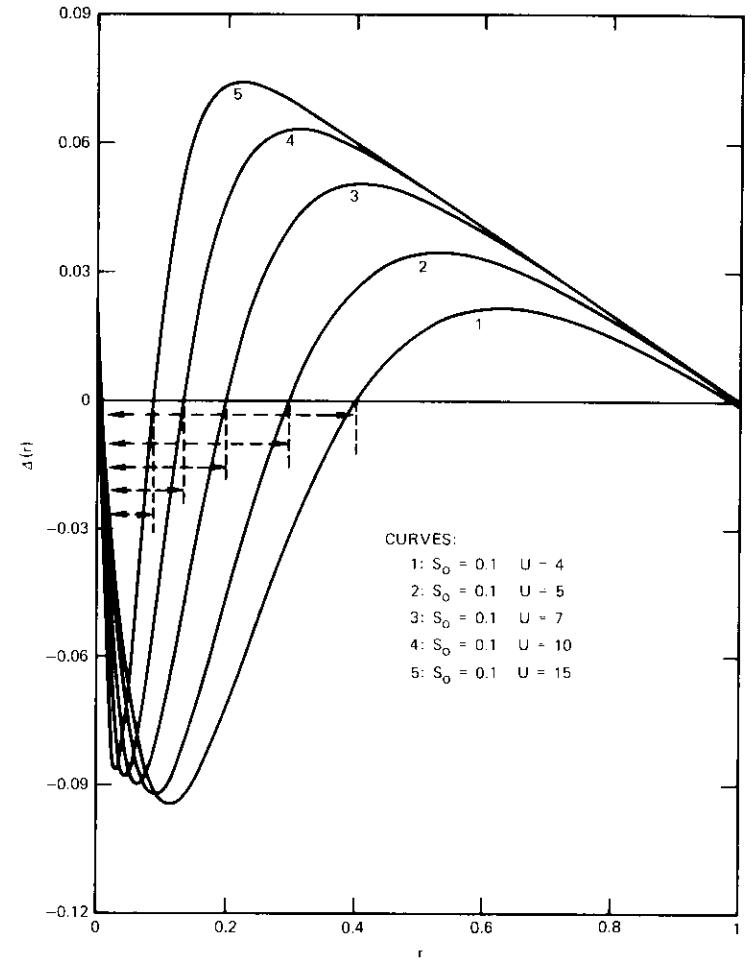


Figure 5. Bistable Systems with Different Degrees of Stability at the Two Partially Stable Steady States (A and C)

tend toward a stable steady state no matter what its initial state. The implication is that, for such systems, the stable steady-state characteristics and performance are of prime importance, while the transient behavior is significant only when changes occur in the system structure (i.e.,  $S_o$  and/or  $U$ ).

**Channel throughput**

The channel throughput,  $T_o$ , under steady-state conditions is given by

$$T_o = S_o(1 - r_o) = G(r_o) e^{-2G(r_o)} \quad (33)$$

where the steady-state channel traffic  $G(r_o)$  is given by

$$G(r_o) = S_o(1 - r_o) + Ur_o = T_o + Ur_o \quad (34)$$

From the right-hand side of equation (33), it is clear that the maximum possible throughput or utilization,

$$T_o^{\max} = \frac{1}{2e} \quad (35)$$

occurs if steady state  $r_o$  is such that

$$G(r_o) = 0.5 \quad (36)$$

**Packet delays**

To avoid confusion in evaluating the effects of packet delay, two parameters for measuring this aspect of system performance, each with a different implication in terms of the usefulness of a system, are defined:

*a. Mean packet delay ( $\bar{d}_p$ ):* The average delay experienced by a packet in the system under steady-state conditions between the point of transmission and the point of reception. This is the performance measure needed by the end users of the systems. From this point of view, the ALOHA system introduces an average path delay  $\bar{d}_p$  into the path of a packet between two terminals.

*b. Mean packet holding time ( $\bar{d}_h$ ):* The average time which a packet spends in an earth station buffer and hence the average time a single packet buffer is disabled once a new packet is loaded.

To derive expressions for these quantities under equilibrium conditions,  $p_i$  is defined as the probability that a packet will require  $i$  ( $i = 0, 1, \dots, \infty$ ) retransmissions; hence,

$$p_i = P_c^i(1 - P_c), \quad i = 0, 1, \dots, \infty \quad (37)$$

where the equilibrium collision probability,  $P_c$ , under the Poisson approximation, is

$$P_c = 1 - e^{-2G(r_o)} \quad (38)$$

For a packet requiring  $i$  retransmissions, the packet delay and holding time can be written as

$$d_{p,i} = \tau_f + i\tau_r \quad (39)$$

and

$$d_{h,i} = (i + 1) \tau_r \quad (40)$$

respectively, where

$$\tau_f = \tau + \tau_{sf}$$

and  $\tau_r$  is the average retransmission delay defined by equation (7).

It should be noted that  $\tau_{sf}$  is the 1-hop satellite propagation delay, while  $\tau_r$  is approximately equal to the 1- or 2-hop propagation delay, depending on whether the user listens in on his own transmission or uses a message from the destination to determine the need for retransmissions. In the former case,

$$\tau_f \approx \tau_r \quad (41)$$

while if acknowledgment messages are used,

$$\tau_f \approx \frac{1}{2} \tau_r \quad (42)$$

The averaged parameters are thus

$$\bar{d}_p = \sum_{i=0}^{\infty} d_{p,i} p_i = \sum_{i=0}^{\infty} (\tau_f + i\tau_r) P_c^i(1 - P_c) \quad (43)$$

and

$$\bar{d}_h = \sum_{i=0}^{\infty} d_{h,i} p_i = \sum_{i=0}^{\infty} (i + 1) \tau_r P_c^i(1 - P_c) \quad (44)$$

yielding the expressions

$$\bar{d}_p = \tau_r e^{2G(r_o)} - (\tau_r - \tau_f) \quad (45)$$

and

$$\bar{d}_h = \tau_r e^{2G(r_o)} \quad (46)$$

Thus, in systems where  $\tau_r$  is a 1-hop delay,

$$\bar{d}_p = \tau_r e^{2G(r_o)} = \bar{d}_h \quad (47)$$

while in 2-hop systems using acknowledgment messages (when the effect of errors in the transmission of acknowledgments is ignored),

$$\bar{d}_p = \left[ e^{2G(r_o)} - \frac{1}{2} \right] \tau_r \quad (48)$$

and

$$\bar{d}_h = e^{2G(r_o)} \tau_r \quad (49)$$

Although the values of  $\bar{d}_h$  in equations (47) and (49) are identical, the value of  $\tau_r$  is different for the two types of systems.

From the preceding expressions, it is clear that the mean delays increase exponentially with  $G(r_o)$ . Thus, in a given system, each stable operating point is associated with a unique value of equilibrium channel traffic  $G(r_o)$ , which in turn uniquely determines the associated delays and a channel throughput,  $T_o$ . Figure 6 shows the relationship between the delays and the equilibrium throughput as a function of  $G(r_o)$ . Since it is desirable to operate systems with high throughputs and low delays, systems with  $G(r_o) > 0.5$  are undesirable. In addition,  $G(r_o) \leq 0.5$  involves a tradeoff between throughput and delay. These tradeoffs, which will be discussed later, are important in the design of a system. Systems operating at maximum throughput ( $1/2e$ ) have delays

$$\bar{d}_p = \bar{d}_h \simeq e\tau_r \simeq 0.73 \text{ s} \quad (50)$$

for 1-hop systems, and

$$\bar{d}_p \simeq \left( e - \frac{1}{2} \right) \tau_r \simeq 1.2 \text{ s} \quad (51a)$$

and

$$\bar{d}_h \simeq e\tau_r \simeq 1.47 \text{ s} \quad (51b)$$

for 2-hop systems.

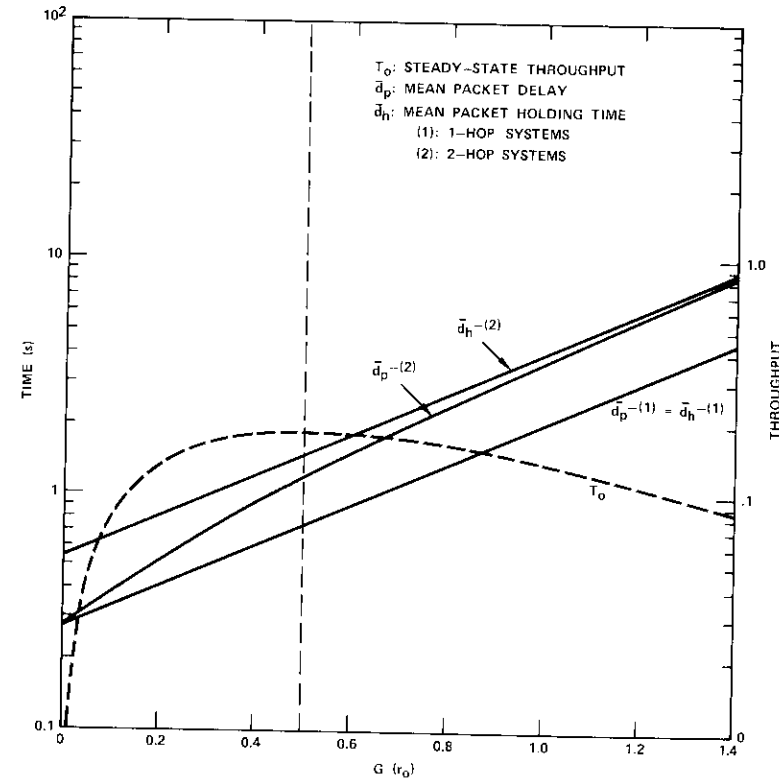


Figure 6. Throughput and Mean Packet Delays as Functions of Equilibrium Channel Traffic

**Maximum throughput systems**

It has been shown that the maximum possible steady-state throughput or utilization achievable is  $1/2e$ . The systems which can be operated in stable steady-state conditions corresponding to maximum throughput are determined by first noting that, if a steady state  $r_o$  corresponds to maximum throughput, it must satisfy

$$S_o(1 - r_o) = G(r_o) e^{-2G(r_o)} = T_o = \frac{1}{2e} \quad (52)$$

so that

$$r_o = 1 - \frac{1}{2eS_o} \tag{53}$$

and

$$G(r_o) = S_o(1 - r_o) + r_oU = 0.5 \tag{54}$$

It can be shown that this is possible only if a system satisfies the condition

$$U = \frac{S_o(e - 1)}{2eS_o - 1} \tag{55}$$

If the requirements of equation (28) are imposed, the condition for a maximum throughput system is given by

$$\frac{1}{2e} < S_o < 0.5 \tag{56}$$

and for  $S_o$  in this range  $U$  satisfies equation (55). If equation (55) is re-written as

$$S_o = \frac{U}{1 + e(2U - 1)} \tag{57}$$

and the constraints of equation (28) are imposed again, the alternative condition for a maximum throughput system is

$$U > 0.5$$

and  $S_o$  for a given  $U$  in this range must satisfy equation (57). This relationship is expressed in Figure 7, which shows the "feasible domain" in  $(S_o, U)$  space and the maximum throughput system curve. It should be noted that, in a maximum throughput system,  $G(r_o)$  is always 0.5,  $r_o$  is given by equation (53), and the delays are given by equation (50) or (51).

**System design considerations**

The system design problem is generally\* that of achieving, under stable

\*Earth station cost vs expected traffic is also an important consideration, but this is a problem of optimal earth station configurations.

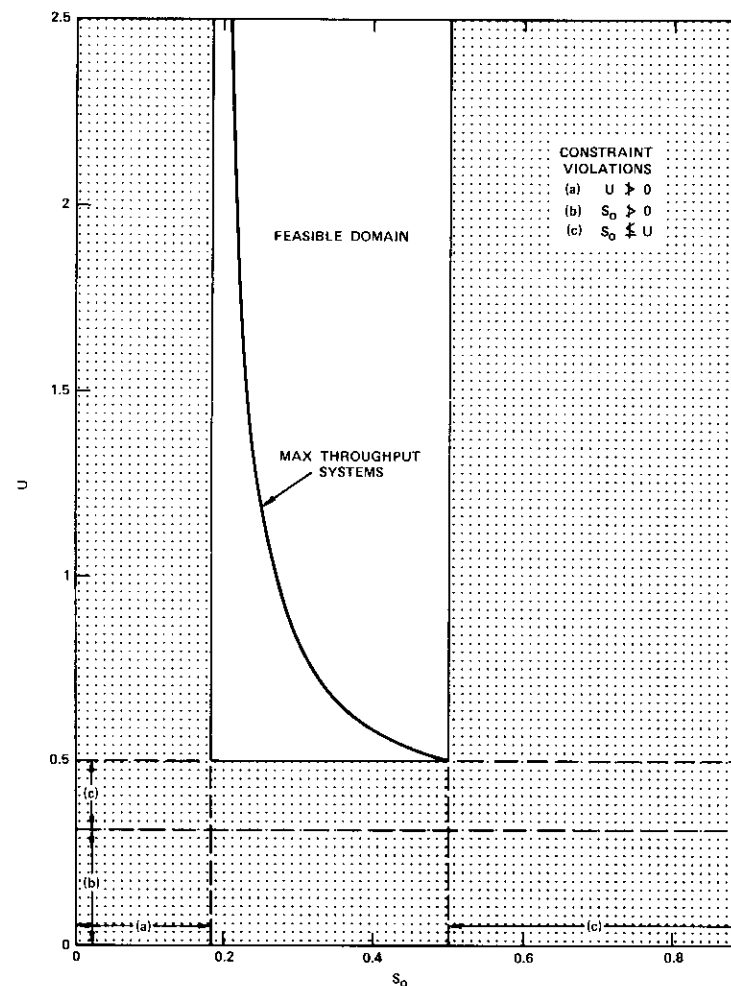


Figure 7. System Parameters for Maximum Throughput Systems

steady-state operation, the maximum possible channel utilization compatible with a mean packet delay which is lower than thresholds established by the end users of the system. No satellite ALOHA system design can accommodate users whose threshold for acceptable mean packet delay,  $d_p$ , does not satisfy the precondition

$$d_p^o > \tau_{sf} = 0.27 s \quad (58)$$

If the threshold delay is larger than the mean packet delay corresponding to maximum throughput (see Figure 6), then the design of a maximum efficiency system is limited only by the maximum throughput value (1/2e) possible for an ALOHA system; such a configuration is called a "throughput-limited system." If, on the other hand, the user delay threshold is below the mean delay at maximum throughput [but satisfies equation (58)], then a maximum throughput system will be incompatible with user requirements. In this case the system must sacrifice throughput to achieve mean delays acceptable to the user. Such systems, which are limited by user delay requirements, are called "delay-limited systems."

A design exercise normally starts with a user profile specified by  $\lambda_o$ , which is determined by the number of active terminals\* (and their characteristics) associated with each earth station. The system design is then completed by choosing transmission system characteristics (packet size and channel capacity) yielding a transmission parameter  $\alpha$ , and the number of users,  $N$ , to be accommodated in the system. If the user delay constraint  $d_p^o$  were not a consideration, then for a given  $\lambda_o$  and  $\alpha$ , the number of stations to be incorporated in the design could be selected to yield maximum utilization. However, consideration of  $d_p^o$  leads to the possibility that the optimal system design may be either a throughput-limited or a delay-limited system.

To determine the conditions under which each type of system is an optimal design, it should be noted that a throughput-limited system is feasible only if the mean packet delay associated with it is less than  $d_p^o$ . For 1-hop systems with  $G(r_o) = 0.5$ , from equation (47) the condition for which throughput-limited systems are the optimal design is

$$d_p^o > e\tau_r \quad (59)$$

Similarly, for 2-hop systems, the condition for which throughput-limited systems are the optimal design is

$$d_p^o > \left(e - \frac{1}{2}\right)\tau_r \quad (60)$$

\*Terminals are assumed to be prohibited from originating packets unless the station is unblocked.

When this condition is satisfied, a maximum throughput system design will satisfy user delay requirements; the design of such systems has been discussed in the preceding section. Alternatively, for a given user profile  $\lambda_o$ , and a choice of  $\alpha$ , the number of users,  $N_m^T$ , required for a throughput-limited system can be computed from equation (57) or (55) as

$$N_m^T = \frac{1}{2e\alpha} \left[ \frac{1}{\lambda_o} + e - 1 \right] \quad (61)$$

For  $d_p$  satisfying equation (58) but not satisfying equation (59) [or equation (60) for 2-hop systems], the optimal design is a delay-limited system. The parameters for the design of such a system can be obtained as follows. For a 1-hop system,  $d_p$  in units of  $\tau_r$  is

$$d_p^o = e^{2G(r_o)}$$

so that the delay-limited system must have channel traffic

$$G^{th}(r_o) = \frac{1}{2} \ln_e d_p^o < 0.5 \quad (62)$$

In addition,

$$T_o = S_o(1 - r_o) = G^{th} e^{-2G^{th}} \quad (63)$$

and

$$G^{th} = T_o + r_o U \quad (64)$$

which yield the relationship

$$S_o \left\{ \left[ 1 - \frac{1}{U} (G^{th} - T_o) \right] \right\} = T_o \quad (65)$$

Thus, converting to real system parameters for a given  $\lambda_o$  and choice of  $\alpha$  yields the number of users,  $N_m^d$ , associated with a delay-limited system:

$$N_m^d = \frac{G^{th}}{\alpha\lambda_o} [(1 - \lambda_o) e^{-2G^{th}} + \lambda_o] \quad (66)$$

where  $G^{th}$  is given by equation (62). Since  $G^{th} < 0.5$ , the delay-limited

system always corresponds to the lower stable state in a potentially bistable system with the state  $r_o$  given by

$$r_o^d = \frac{G^{th}}{\alpha N_m^d} (1 - e^{-2G^{th}}) \quad (67)$$

Figure 8 shows the populations  $U_{max} = \alpha N_m^d$  or  $\alpha N_m^T$  for optimally efficient systems compatible with specified delay requirements  $d_p^o$  and the channel utilization,  $T_o$ , for these values.

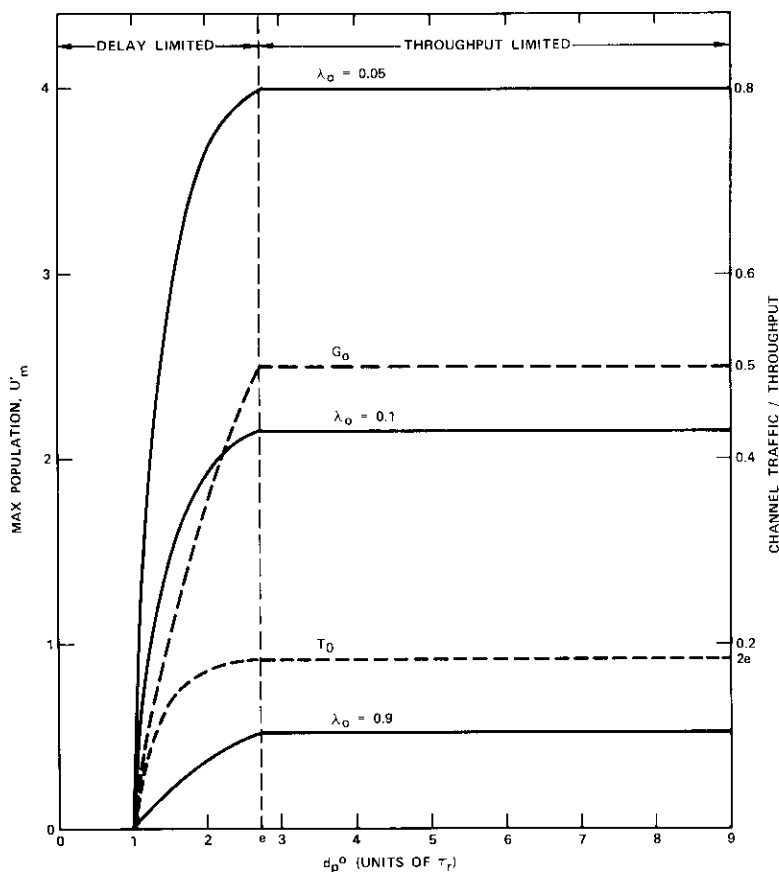


Figure 8. Maximum Efficiency Systems as Functions of User Delay Threshold,  $d_p^o$

The equations for 2-hop delay-limited systems are the same as equations (66) and (67) except that  $d_p^o$  in units of  $\tau_r$  is

$$d_p^o < (e - 0.5) \quad (68)$$

and

$$G^{th} = \frac{1}{2} \ln_e \left( d_p^o + \frac{1}{2} \right) < 0.5 \quad (69)$$

with throughput-limited systems still specified by equation (61).

When all of these theoretical results are translated to a real satellite system, it becomes clear that a system of identical single-packet buffered users, operating in a stable equilibrium state  $r_o$ , yields an average transmission rate  $\lambda_a$  per user per epoch  $\tau_r$ :

$$\lambda_a = \lambda_o(1 - r_o) \quad (70)$$

where

$$0 \leq \lambda_o \leq 1$$

and

$$0 \leq r_o \leq 1$$

Hence,

$$\lambda_a \leq 1 \quad (71)$$

This implies that, on the average, a single-packet buffered earth station will transmit less than one packet per interval  $\tau_r$ . For  $\tau_r$  corresponding to 1- or 2-hop satellite systems, this is equivalent to an average transmission rate of at most four packets per second or two packets per second, respectively. However, earth station equipment is currently relatively high in cost, and it is not desirable to design earth stations yielding such low data transmission rates. This design problem can be overcome by using multipacket buffered earth stations.

As long as the mean delay between packet transmissions at an earth station is much larger than the packet duration  $\tau$ , a system of  $M$  users, each with an  $m$ -packet buffer, is approximately equivalent to a system of  $M \times m$  single-packet buffered users in which each group of  $m$  users shares common RF facilities. Hence, this theory for single-packet buffered users can be used directly, but the average earth station packet transmission rate,  $\Lambda_a$ , is

$$\Lambda_a = m\lambda_o(1 - r_o) \quad (72)$$

With a suitable choice of  $m$ ,  $\Lambda$  can have as large a value as desired subject to the limitation that

$$\frac{1}{\Lambda_n e^{2G(\tau_o)}} > \frac{\tau}{\tau_r} = \alpha \quad (73)$$

Hence, in practical satellite systems, cost considerations may necessitate the use of multi-packet buffered stations. The system performance can still be predicted by using the techniques for single-packet buffered systems developed in this paper over an equivalent number of single-packet buffered users.

Finally, although in a finite user population a system failure caused by an unbounded increase in packet delay is impossible, an optimal configuration may be a bistable system designed to operate at the lower stable point. Such a system can undergo transitions in the undesirable upper stable point (e.g., Figure 4, curve 2), and a backward transition may not occur for a long time without active intervention or control. Hence, some method of system monitoring and control is necessary in an operational satellite ALOHA system so that undesirable system states are detected and action is taken to revert the system back to the desirable operating point.

### Conclusions

It has been shown that, as long as the random retransmission delay introduced at the earth stations associated with a satellite ALOHA system is negligible compared to the satellite propagation delay, a dynamic theory for satellite ALOHA system performance can be formulated by considering time in epochs whose duration is approximately equal to the propagation delay. Such a formulation makes it possible to predict the average dynamic behavior of a system composed of earth stations with single-packet buffers. Such a system may not be a cost-effective satellite system, but the same formulation can be applied to multi-packet buffered systems by using an equivalent single-packet buffered system.

It has also been observed that the theory predicts the existence of either monostable or bistable systems depending on the real system parameters ( $\alpha$ ,  $N$ ,  $\lambda_o$ ) or the theoretical parameters ( $S_o$ ,  $U$ ). In a bistable system, transitions between the two partially stable states can be caused by stochastic variations in the system parameters. Such systems should operate at the lower stable state associated with low delays.

The average system performance under stable steady-state operation has been examined, and it has been shown that there is a feasible domain in  $S_o$ ,  $U$  space (Figure 7) in which an ALOHA system with the maximum possible utilization ( $1/2e$ ) can be designed. In general, as indicated by Figure 6, the throughput-delay tradeoff is such that the optimally efficient system design can be either throughput limited or delay limited depending on the delay requirements of the end users of the system.

### References

- [1] E. Fuchs and P. E. Jackson, "Estimates of Distributions of Random Variables for Certain Computer Communications Traffic Models," *Communication of the Association of Computing Machinery*, Vol. 13, No. 12, December 1970, pp. 752-757.
- [2] W. W. Wu, "Random Multiple Access Codes," International Symposium on Information Theory, University of Notre Dame, Notre Dame, Indiana, October 28-31, 1974, *Proc.*, pp. 78-79.
- [3] N. Abramson, "The ALOHA System—Another Alternative for Computer Communications," 1970 Fall Joint Computer Conference, *AFIPS Conference Proc.*, Vol. 37, pp. 281-285.
- [4] L. Kleinrock and S. S. Lam, "Packet Switching in a Slotted Satellite Channel," 1973 National Computer Conference, *AFIPS Conference Proc.*, Vol. 42, pp. 703-710.
- [5] L. G. Roberts, "Dynamic Allocation of Satellite Capacity Through Packet Reservation," 1973 National Computer Conference, *AFIPS Conference Proc.*, Vol. 42, pp. 711-716.
- [6] W. Crowther et al., "A System for Broadcast Communication: Reservation-ALOHA," 6th Hawaii International Conference on System Science, Honolulu, Hawaii, 1973, *Proc.*, pp. 371-374.
- [7] R. Binder, "A Dynamic Packet-Switching System for Satellite Broadcast Channels," IEEE International Conference on Communications, June 1975, Vol. III, pp. 41-1-41-9.
- [8] L. Kleinrock and S. S. Lam, "On Stability of Packet Switching in a Random Multi-Access Broadcast Channel," 7th Hawaii International Conference on System Science, Honolulu, Hawaii, January 1974; *Proc. of the Special Subconference on Computer Networks*, pp. 73-77.
- [9] G. Foyolle et al., "The Stability Problem of Broadcast Packet Switching Computer Networks," International Workshop on Computer Architecture and Networks—Modelling and Evaluation, Institut de Recherche d'Informatique et d'Automatique, August 1974, *Proc.*, pp. 135-140.

- [10] S. S. Lam and L. Kleinrock, "Packet Switching in a Multi-access Broadcast Channel: Performance Evaluation," *IEEE Transactions on Communications*, COM-23, No. 4, April 1975, pp. 410-422.
- [11] A. B. Carleial and M. E. Hellman, "Bistable Behavior of ALOHA-type Systems," *IEEE Transactions on Communications*, COM-23, No. 4, April 1975, pp. 401-410.



*Ashok K. Kaul received a B.Sc (1963) and an M.Sc (1966) in physics from the University of Jammu and Kashmir, India, and a Ph.D. in physics from the University of Maryland (1972). As a member of the technical staff of Computer Sciences Corporation (1970-1973), he was involved with several radio astronomy projects for NASA aimed at the analysis and interpretation of data from the RAE and IMP satellites. He joined COMSAT Laboratories in 1973 as a member of the technical staff of the Transmissions Systems Laboratory.*

*He is currently involved in investigations of satellite networks for computer communications.*

## CTR Notes

### SCPC satellite telephony with 4-dimensionally-coded quadrature amplitude modulation

G. R. WELTI

Manuscript received July 1, 1976

#### Introduction

This note shows that quadrature amplitude modulation (QAM) with 4-dimensional (4D) coding can be combined with pulse code modulation (PCM) or adaptive delta modulation (ADM) to increase the capacity of a single-channel-per-carrier (SCPC) satellite transponder. Calculations show that the capacity of a typical 36-MHz INTELSAT transponder ranges from 587 to 1,565 voice channels for 64-kbps PCM and from 1,174 to 3,130 voice channels for 32-kbps ADM, depending on the type of satellite beam and the size of the earth station. With voice activation, the shortest code ( $M = 8$ ) requires an average C/N of about 6 dB, and the longest practical code ( $M = 256$ ) requires a C/N of 15 dB.

#### Signal constellations

This note discusses the application of 4D-QAM, as described in Reference 1, to SCPC telephony via satellite. For this application, 4D-QAM can be

---

This note is based on work performed at COMSAT Laboratories under the sponsorship of the International Telecommunications Satellite Organization (INTELSAT). Views expressed in this paper are not necessarily those of INTELSAT.

---

*Mr. Welti is Senior Staff Scientist, COMSAT Laboratories.*

combined with ADM and speech activation to conserve bandwidth as well as power. For practical reasons, only the six signal constellations shown in Figure 1, in which the code length  $M = 2^k$  where  $k$  is an integer will be considered.

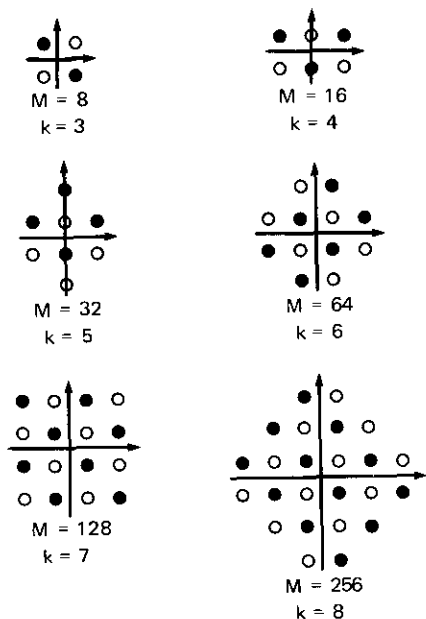


Figure 1. 4D-QAM Signal Constellations

4D coding is applied to these constellations as follows. Pulses are transmitted in related pairs. The first pulse in each pair is selected from the points in the constellation in Figure 1. The second pulse is selected from the subset of points having the same (black or white) color as the point chosen for the first pulse.

For even values of  $k$ , the constellations in Figure 1 contain  $3i$  points of each color, where  $i$  is a power of 2. The corresponding codes with  $M = 2(3i)^2$  are expurgated to yield codes with  $M = 16i^2 = 2^k$ . To minimize average power, the codewords with the greatest energy are eliminated.

#### Bandwidth and power requirements

PCM telephone voice channels are sampled at 8,000 samples/second, and each sample is converted to an 8-bit word, using either  $A$ -law or  $\mu$ -law compression, to yield a bit rate of 64 kbps.

Adaptive delta modulation (ADM) can be implemented in several ways [2], [3]. Basically, the voice channel is sampled at a rate much greater than the Nyquist rate. Differences between the actual and predicted samples are then encoded using one bit per sample. Various adaptive schemes can be used for the prediction to achieve good fidelity at a bit rate of 32 kbps.

As explained in the preceding section, for a code with  $2^k$  codewords, 4D-QAM transmits  $k/2$  bits per pulse. For the codes in Figure 1,  $k$  varies from 3 to 8. The required RF bandwidth, including guardbands, for 4D-QAM is  $2(1 + \rho)/k$  cycles/bit, where  $\rho$  is the roll-off factor associated with the shaping filters in the modulator and the matched filters in the demodulator. A reasonable value for  $\rho$  is 0.15.

In SCPC applications, additional guard space may be needed to allow for oscillator drift. This additional bandwidth can be specified in terms of a fixed number of hertz per carrier. The required amount of additional guard space is governed by equipment cost considerations, and is typically less than 10 kHz per carrier.

The bandwidth requirements discussed above are summarized in Table 1.

TABLE 1. REQUIRED BANDWIDTH/CARRIER (kHz)

Transmission Method	Channel Bit Rate (kbps)	Bits per Pulse Pair, $k$					
		3	4	5	6	7	8
PCM	64	49.1	36.8	29.4	24.5	21.0	18.4
ADM	32	24.5	18.4	14.7	12.3	10.5	9.2

This table assumes a filter roll-off factor of 0.15 and includes no guard space for oscillator drift.

It has been shown [1] that, ideally, the number of decision errors per source bit committed by the maximum likelihood decoder is

$$P_B = \frac{N}{k\sqrt{2\pi}} \int_{\sqrt{\gamma/2E}}^{\infty} \exp\left(\frac{-t^2}{2}\right) dt$$

where  $N$  is the average number of adjacent codewords in the 4D signal constellation,  $k$  is twice the number of bits per pulse,  $\gamma$  is the average carrier-to-noise power ratio at the decoder input, and  $E$  is the normalized average energy per pulse. Table 2 lists the code properties and ideal  $\gamma$  values for  $P_B = 10^{-4}$ .

TABLE 2. IDEAL CODE CHARACTERISTICS

Code Length, $M$	Number of Adjacent Codewords, $N$	Average Energy, $E_2$	Ideal $\gamma$ for $P_B = 10^{-4}$ (dB)
8	6.000	0.250	8.80
16	8.375	0.439	11.26
32	10.063	0.625	12.78
64	12.250	0.875	14.24
128	13.500	1.250	15.76
256	15.500	1.750	17.23

A detailed analysis of 4D-QAM impairments has been conducted. The six contributors to implementation loss are as follows:

- quantization loss in the demodulator,  $L_Q$ ;
- loss due to offset control error,  $L_O$ ;
- loss due to automatic level control error,  $L_A$ ;
- loss due to carrier phase error,  $L_P$ ;
- loss due to timing error,  $L_T$ ;
- loss due to intersymbol interference,  $L_I$ .

Based on this analysis, estimates of reasonable values for these losses are given in Table 3, where the losses and ideal  $\gamma$  values are combined to give

TABLE 3. REQUIRED C/N FOR  $P_B = 10^{-4}$ 

Code Length, $M$	Losses (dB)						Ideal $\gamma$ (dB)	$(C/N)_{req}$ (dB)
	$L_Q$	$L_O$	$L_A$	$L_P$	$L_T$	$L_I$		
8	0.1	0.2	0.1	0.1	0.1	0.2	8.8	9.6
16	0.2	0.2	0.1	0.1	0.1	0.2	11.3	12.2
32	0.2	0.2	0.1	0.1	0.1	0.3	12.8	13.8
64	0.2	0.2	0.2	0.2	0.1	0.3	14.2	15.4
128	0.1	0.2	0.2	0.2	0.1	0.4	15.8	17.0
256	0.1	0.2	0.3	0.3	0.2	0.4	17.2	18.7

the resulting values of required C/N. These estimates are based on the following assumptions:

- Number of analog-to-digital converter bits = 4 for  $M = 8$ ; 5 for  $M = 16, 32$ , and 64; and 6 for  $M = 128$  and 256.

- Offset error = 4 percent of distance between signal points.
- Automatic level control voltage error = 2 percent.
- Phase error =  $2^\circ$ .
- Timing error = 2 percent of pulse period.
- Signal-to-intersymbol-interference ratio = 28 dB.

In SCPC applications (as demonstrated in the SPADE system), the average power requirements can be further reduced by exciting the carrier only in the presence of speech activity [4]. The amount of average power reduction provided by voice activation is 4 dB. The total C/N requirements for  $P_B = 10^{-4}$  with voice activation are summarized in Table 4.

TABLE 4. REQUIRED C/N FOR SCPC

Bits per Pulse Pair, $k$	3	4	5	6	7	8
C/N (dB)	5.6	8.2	9.8	11.4	13.0	14.7

#### SCPC transponder capacity with 4D-QAM

The bandwidth-limited transponder capacities for two SCPC transmission methods and six 4D-QAM codes are listed in Table 5, which is

TABLE 5. 36-MHZ TRANSPONDER CAPACITIES (SCPC VOICE CHANNELS)

Transmission Method	Channel Bit Rate (kbps)	Bits per Pulse Pair, $k$					
		4	4	5	6	7	8
SCPC/PCM	64	587	782	980	1,176	1,371	1,565
SCPC/ADM	32	1,176	1,565	1,959	2,341	2,743	3,130

derived from Table 1. These values are obtained by dividing the 36-MHz transponder bandwidth by the per-channel bandwidth requirements from Table 1, and by further reducing the resulting capacities by a factor of 4/5 to provide a 25-percent guardband for local oscillator drift.

The transponder capacity vs required C/N is plotted in Figure 2 using the information provided in Tables 4 and 5.

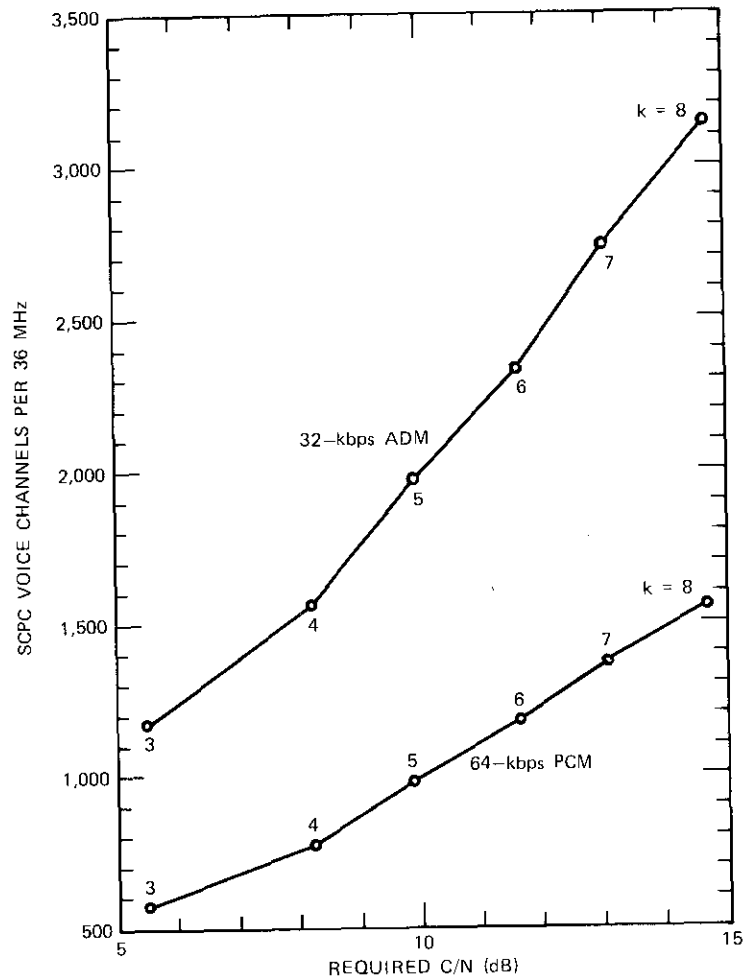


Figure 2. Transponder Capacities

Tables 6 and 7 show how 4D-QAM can be applied to an actual satellite. The satellite link parameters in these tables correspond to those of an INTELSAT IV-A [5], while the down-link C/N values correspond to those of Standard A and B earth stations with G/T values of 40.7 and 31.7 dB/K, respectively. It can be seen that, for the indicated number of SCPC channels per transponder, the rain margin is more than 2 dB, which is considered adequate for 6/4-GHz transmission. The indicated PCM capacities could be doubled by employing 32-kbps ADM.

TABLE 6. INTELSAT IV-A SCPC TRANSMISSION TO STANDARD A EARTH STATION

Parameter	Beam		
	Spot	Hemi	Global
e.i.r.p., Beam Edge (dBW)	29.0	26.0	22.0
Output Backoff (dB)	-7.0	-6.0	-4.2
Usable Bandwidth (MHz)	25.0	25.0	25.0
(dB-Hz)	74.0	74.0	74.0
Saturation Flux Density (dBW/m <sup>2</sup> )	-67.5	-67.5	-67.5
Satellite G/T (dB/K)	-11.6	-11.6	-17.6
Up-Link C/N (dB)	26.0	27.0	22.0
Carrier-to-Intermodulation Ratio (dB)	23.5	21.8	18.9
Down-Link C/N (dB)	21.2	19.2	17.0
Total C/N (dB)	18.4	16.9	14.1
Cochannel Interference Loss (dB)	1.0	0.8	0
Available C/N (dB)	17.4	16.1	14.1
Required C/N (dB)	14.7	13.0	11.4
Rain Margin	2.7	3.1	2.7
Bits/Pulse Pair, <i>k</i>	8	7	6
Maximum Number of 64-kbps Channels/Transponder	1,565	1,371	1,176

TABLE 7. INTELSAT IV-A SCPC TRANSMISSION  
TO STANDARD B EARTH STATION

Parameter	Beam		
	Spot	Hemi	Global
e.i.r.p., Beam Edge (dBW)	29.0	26.0	22.0
Output Backoff (dB)	-4.5	-3.5	-2.0
Usable Bandwidth			
(MHz)	25.0	25.0	25.0
(dB-Hz)	74.0	74.0	74.0
Saturation Flux Density (dBW/m <sup>2</sup> )	-67.5	-67.5	-67.5
Satellite G/T (dB/K)	-11.6	-11.6	-17.6
Up-Link C/N (dB)	28.5	29.5	24.2
Carrier-to-Intermodulation Ratio (dB)	18.5	16.8	14.5
Down-Link C/N (dB)	14.7	12.7	10.2
Total C/N (dB)	13.1	11.2	8.7
Cochannel Interference Loss (dB)	0.3	0.2	0
Available C/N (dB)	12.8	11.0	8.7
Required C/N for $P_B = 10^{-4}$ (dB)	9.8	8.2	5.6
Rain Margin	3.0	2.8	3.1
Bits/Pulse Pair, $k$	5	4	3
Maximum Number of 64-kbps Channels/ Transponder	980	782	587

#### Acknowledgment

The author wishes to thank M. Sugiyama for analyzing the implementation losses due to tracking errors.

#### References

- [1] G. R. Welti, "PCM/FDMA Satellite Telephony with 4-Dimensionally Coded Quadrature Amplitude Modulation," *COMSAT Technical Review*, Vol. 6, No. 2, Fall 1976, pp. 323-338.
- [2] J. C. Su, H. G. Suyderhoud, and S. J. Campanella, "A Strategy for Delta Modulation in Speech Reconstruction," *COMSAT Technical Review*, Vol. 6, No. 2, Fall 1976, pp. 339-355.
- [3] H. R. Schindler, "Delta Modulation," *IEEE Spectrum*, October 1970, pp. 69-78.
- [4] A. M. Werth, "SPADE: A PCM/FDMA Demand Assignment System for Satellite Communications," 1969 INTELSAT/IEEE International Conference on Digital Satellite Communications, London, England, November 25-27, 1969.
- [5] J. Dicks and M. Brown, Jr., "INTELSAT IV-A Transmission System Design," *COMSAT Technical Review*, Vol. 5, No. 1, Spring 1975, pp. 73-104.

### Field tests of 120-channel hybrid modems via satellite

D. CHAKRABORTY, M. SUGIYAMA, AND T. MURATANI

(Manuscript received December 16, 1977)

#### Introduction

There is still a large gap between the Shannon bound [1] and the communications capacity achieved in practice by using conventional modulation methods. In satellite communications, FM was a logical choice for matching the widely used FM terrestrial links with the satellite links. On the other hand, digital modulation (PCM/PSK/TDMA) is economical and practical when a full transponder is available. For light and intermediate traffic, different modulation methods, possibly advantageous in terms of power and bandwidth conservation, merit attention.

Mixed modulation schemes such as combined pulse amplitude and phase modulation have been described in the literature [1]-[6]. For example, mixed modulation schemes for satellite communications have been proposed by Welti [7]-[9]. Welti's 2-pulse amplitude and phase modulation scheme (hereafter referred to as hybrid modulation) has been adopted in the design of two 120-FDM-channel hybrid modems for satellite circuits [10].

In these modems the input (a 120-channel FDM signal) is sampled at 1,088 kHz and each sample is resolved into 21 quantized levels and a quantization residue. The descriptors of each sample are transmitted with two amplitude and phase modulated pulses at a 2,176-kbaud rate. Seven coarse levels modulate the first pulse, while three fine levels and the

This note is based upon work performed at COMSAT Laboratories under the sponsorship of the International Telecommunications Satellite Organization (INTELSAT). Views expressed herein are not necessarily those of INTELSAT.

*Dr. Chakraborty is a member of the technical staff, Communications Processing Laboratory, COMSAT Laboratories.*

*Messrs. Sugiyama and Muratani, formerly INTELSAT nominees assigned to COMSAT Laboratories, have returned to Nippon Electric Company and Kokusai Denshin Denwa Laboratories, respectively.*

quantization residue modulate the second pulse. The processing gain that can be obtained from hybrid modulation is approximately 21 dB for a carrier-to-noise ratio (C/N) above the threshold C/N ratio of 14 dB, while the bandwidth is half that required with FM.

A field test was organized jointly by COMSAT Laboratories and KDD Laboratories to investigate the characteristics of experimental hybrid modems using an INTELSAT IV satellite in the Pacific Ocean region and earth station facilities located at Paumalu, Hawaii, and Ibaraki, Japan. The following experiments were performed:

- a. 2-way measurements of signal quality between Japan and the U.S. using the operational INTELSAT IV F-8 satellite, east spot-beam transponder 5, and west spot-beam transponder 4;
- b. measurements of the effect of the cochannel and adjacent channel interference on the hybrid modulated carrier;
- c. 2-way speech tests and demonstrations using a pair of telephone channels in one of the two supergroups of the hybrid modulated carrier, with the remaining supergroup traffic simulated by white noise loading.

**Two-way measurements of signal quality**

Test signals were transmitted from the Paumalu I system via INTELSAT IV F-8 satellite, with transponder 5 connected to the west spot beam covering the Ibaraki earth station. From Paumalu to Ibaraki, the entire transponder (transponder 5) was available for test purposes. The test signals consisted of multicarrier loading typical of that currently in use in the INTELSAT IV frequency plan. The frequency plan and the transmission parameters of the multicarrier test signals are shown in Figure 1. The transmission parameters and the relative levels of the carriers indicate that the power and bandwidth allocations of the 60-channel FDM/FM carrier are the same as those of the 120-channel hybrid modulated carrier. The frequency multiplexing arrangement is shown in Figure 2.

Test signals from Ibaraki were transmitted via INTELSAT IV F-8 transponder 4, which was connected to the east spot beam covering the Paumalu earth station. Transponder 4 handled commercial traffic using two FM carriers: a 432-channel carrier in a 15-MHz slot with 1.48-MHz rms deviation, and a 252-channel carrier in a 10-MHz slot with 1.01-MHz rms deviation. The test signal from Ibaraki to Paumalu consisted of a hybrid modulated carrier occupying an RF slot of 2.5-MHz bandwidth.

The multicarrier C/N measured at Ibaraki over the hybrid modulated carrier receive bandwidth of 2.18 MHz and the top channel (534-kHz

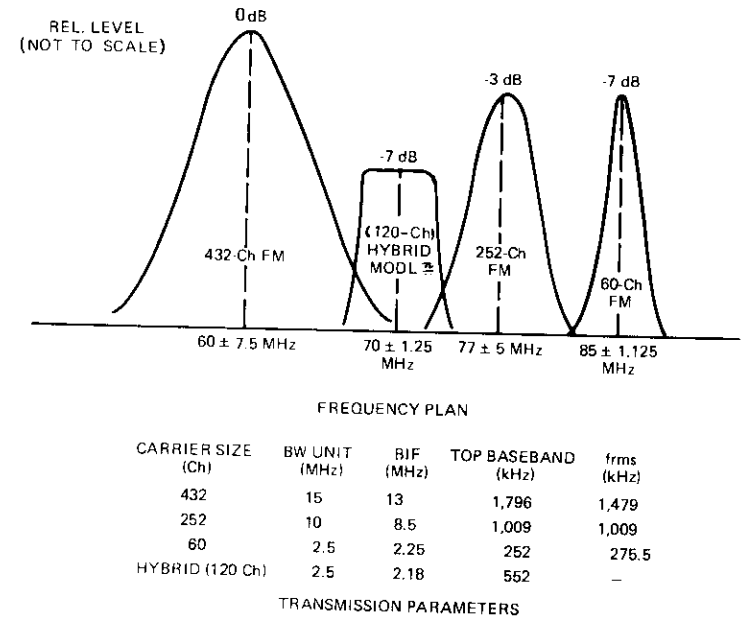


Figure 1. Frequency Plan and Transmission Parameters

slot) noise power ratio (NPR) are shown in Figure 3 as functions of the transponder input backoff. It can be seen that the multicarrier C/N decreases as the transponder operating point approaches saturation. This is due to intermodulation noise falling on the hybrid modulated carrier slot. As expected, a similar trend is shown in the NPR curve. The NPR is defined as the ratio of noise power in a test channel when all channels are loaded with white noise to noise power in the test channel when all channels except the test channel are fully noise loaded. The resulting weighted signal-to-noise (S/N) ratio is

$$(S/N)_w = NPR (dB) + 10 \log_{10} \left[ \frac{(SG \text{ bandwidth}) \times 2}{b} \right] - L + I$$

where SG bandwidth = 312-552 kHz

$$L = \text{load factor} = -1 + 4 \log 120$$

$$I = \text{C.C.I.R. psophometric weighting} = 2.5 \text{ dB}$$

$$b = \text{telephone channel effective bandwidth} = 3.1 \text{ kHz.}$$

Thus,

$$(S/N)_w = \text{NPR (dB)} + 17.1 \text{ (dB)}.$$

The weighted S/N ratios measured at Ibaraki and Paumalu as functions of the earth station e.i.r.p. are shown in Figure 4, where the test channel

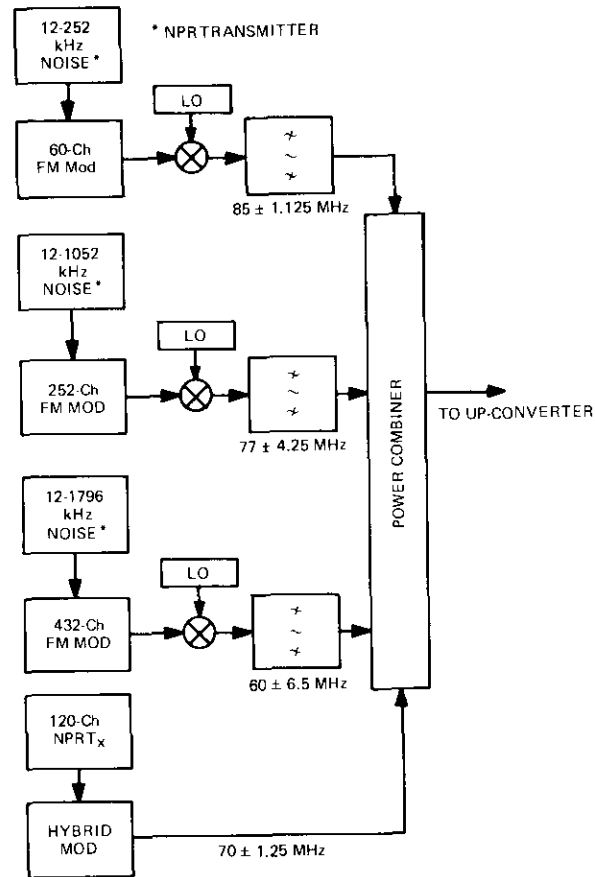


Figure 2. Frequency Multiplexing Plan

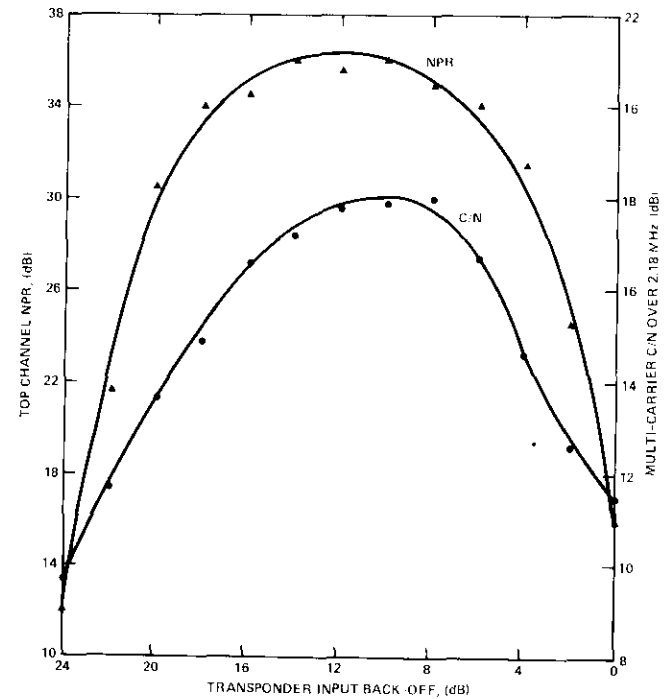


Figure 3. Top Channel NPR and Multicarrier C/N vs  $(BO)_{Tn}$

was centered at 360 kHz. The space link weighted S/N requirement is 51 dBm0p (50 dBm0p overall, including terrestrial noise).

**Cochannel and adjacent channel interference**

The effect of cochannel interference (64-Mbps, 4-phase PSK interference) on the hybrid modulated carrier was measured at Ibaraki in a multicarrier environment with the test signal transmitted from Paumalu. The degradation of the hybrid modulated carrier top channel NPR (relative to the value at a carrier-to-interference [C/I] ratio of  $\infty$ ) is shown in Figure 5 as a function of C/I ratio for various values of the transponder input backoff. The multicarrier C/N values measured over the hybrid modulated carrier receive noise bandwidth are also shown in Figure 5 for the corresponding transponder input backoff curves. For a high input backoff operating condition (e.g., 18 dB), the system C/N is closer to the threshold point (C/N = 14 dB for an ideal channel) and hence the deg-

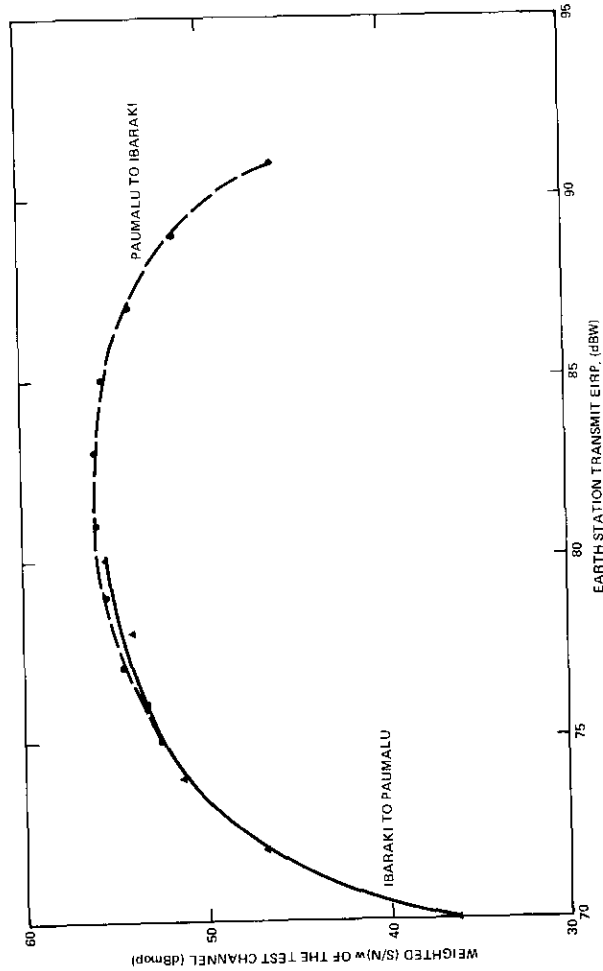


Figure 4. Test Channel Signal-to-Noise Ratio vs Earth Station e.i.r.p.

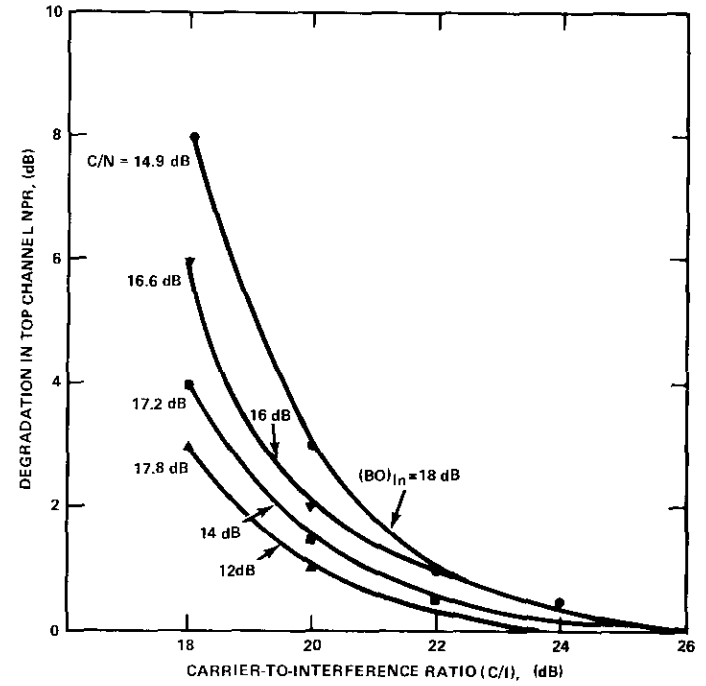


Figure 5. Degradation in Top Channel Due to Cochannel Interference

radiation due to cochannel interference is excessive. As the transponder operating point approaches the normal working region (10-14 dB), the receive C/N improves and hence the degradation in top channel NPR is reduced.

The effect of adjacent channel interference was studied by progressively reducing the center-to-center frequency separation of two hybrid modulated carriers and noting the degradation in the top channel NPR of the desired carrier. To eliminate the effect of intermodulation distortion, the FM carriers used in this test were removed and the transponder loading was achieved by using a single strong (unmodulated) cw carrier which was judiciously allocated to prevent any intermodulation product from falling on the desired channel. In this test the transponder was loaded with the equivalent power of fourteen 2.5-MHz-bandwidth hybrid modulated carriers to represent full loading. However, 12-carrier loading was repre-

sented by the cw (unmodulated) carrier and hence the relative level of this carrier was +11 dB above that of each hybrid modulated carrier.

The top channel NPR was measured at Ibaraki for different values of  $\Delta F$ , the center-to-center frequency separation of the adjacent hybrid carriers, at different backoff points. No measurable channel degradation was observed until  $\Delta F$  was reduced below 2.4 MHz.

**Speech tests and demonstrations**

The signal processing technique (e.g., mapping and analog-to-digital and digital-to-analog conversions) used in hybrid modulation has not been used in commercial telephony. Therefore, the actual speech quality through the hybrid modem was investigated. Two telephone channels were used as send-receive channels in group A (channel 12) of supergroup 2, while supergroup 1 was noise loaded. The schematic arrangements of the speech tests are shown in Figure 6.

Speech signals (8 dB below the test tone) were transmitted from Paumalu through west spot-beam transponder 5 in a multicarrier environment. Return speech signals were transmitted from Ibaraki using east spot-beam transponder 4 handling live traffic as well as the hybrid modulated carrier. The operating e.i.r.p. values were 83 dBW from Paumalu to Ibaraki and 80 dBW from Ibaraki to Paumalu. Under these conditions a number of two-way speech tests were conducted over a period of six days as follows:

- a. Recorded test speech from a source tape was transmitted to Ibaraki and looped back to Paumalu where it was recorded.
- b. The conversations of Paumalu earth station operators were recorded by Ibaraki and then retransmitted to Paumalu for recording.
- c. A facility similar to that described in a was provided to Ibaraki for recording its own loopback signal.
- d. A speech test demonstration facility between Japan and the U.S. was extended to COMSAT Laboratories, Clarksburg, Maryland, using the order-wire terminal connecting Paumalu to Clarksburg via the Jamesburg earth station and terrestrial links.
- e. A prolonged speech demonstration extending over a period of four hours was provided between Ibaraki and Paumalu for the benefit of the KDD, NEC, and COMSAT staffs.
- f. Recorded test speech transmitted to Ibaraki with variable e.i.r.p. from Paumalu was looped back to Paumalu at a constant e.i.r.p. (80 dBW) from Ibaraki. This enabled Paumalu to record the test speech at different  $(S/N)_w$  ratios ranging from 43-55 dBm<sub>0p</sub> from

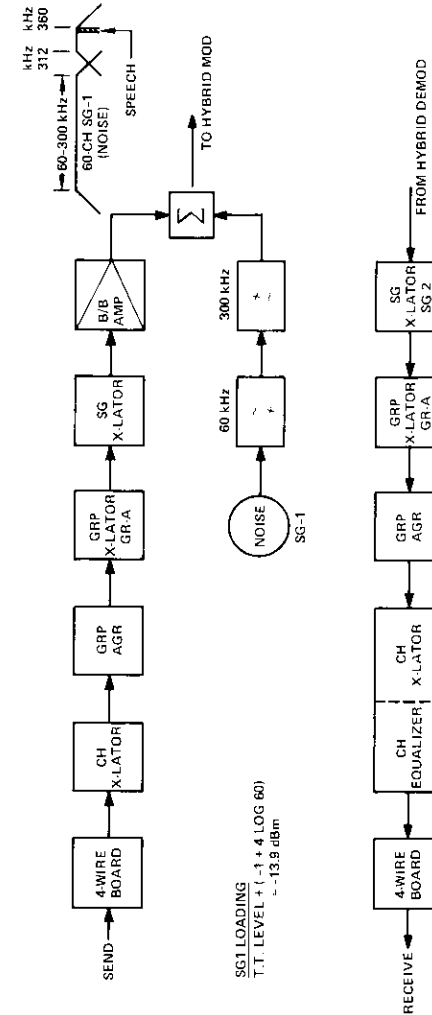


Figure 6. Basic Schematic Arrangement for Speech Tests Using 120-Channel Hybrid Modem

Paumalu to Ibaraki and at a constant 54.5 dBm0p from Ibaraki to Paumalu.

Observations of more than 20 engineers, scientists, and technicians from COMSAT, KDD, and NEC indicate that the quality of the test speech obtained through the hybrid modem satellite channel operating in an FDMA mode of operation utilizing an RF slot of 2.5 MHz for 120 FDM telephone channels is entirely acceptable. The resulting  $(S/N)_w$  is approximately 55–56 dBm0p for a C/N ratio of about 18 dB in a receive bandwidth of 2.18 MHz through a spot-beam transponder operating in conjunction with a standard INTELSAT earth station. The recorded speech will undergo further evaluation by Laboratory methods.

### Conclusions

The results of the 120-channel FDMA HYBRID modem field tests suggest the following conclusions:

a. The measured weighted S/N on the top telephone channel is in the range of 55–56 dBm0p for a C/N of about 18 dB in an RF bandwidth of 2.2 MHz (55 dBm0p from Japan to the U.S. and 56 dBm0p from the U.S. to Japan).

b. The system can tolerate cochannel broadband interference with about 0.5-dB degradation in channel performance (S/N ratio) for a C/I ratio of 22 dB (measured over the hybrid modulated carrier receive bandwidth of about 2.2 MHz).

c. Two hybrid modulated carriers can be transmitted with center-to-center frequency separation of 2.4 MHz with no degradation in channel performance (specification value = 2.5 MHz).

d. The new technique used in the signal processing causes no objectional effects.

The field tests have confirmed the evidence previously gathered from the laboratory simulation tests. It can therefore be concluded that the hybrid modulation techniques used meet C.C.I.R.-quality channel requirements and can improve the FDMA channel capacity of spot/zonal-beam-type transponders by at least a factor of two.

### Acknowledgment

Thanks are due to S. J. Campanella and C. J. Wolejsza for many useful discussions.

### References

- [1] C. E. Shannon, "A Mathematical Theory of Communication," *The Bell System Technical Journal*, Part I, Vol. 27, No. 3, July 1948, pp. 379–423; Part, II Vol. 27, No. 4, October 1948, pp. 623–656.
- [2] C. R. Cahn, "Combined Digital Phase and Amplitude Modulation Communication Systems," *IRE Transactions on Communications Systems*, Vol. CS-8, September 1960, pp. 150–155.
- [3] J. C. Hancock and R. W. Lucky, "Performance of Combined Amplitude and Phase-Modulated Communications Systems," *IRE Transactions on Communication Systems*, Vol. CS-8, December 1960, pp. 232–237.
- [4] C. N. Campopiano and B. G. Glazer, "A Coherent Digital Amplitude and Phase Modulation Scheme," *IRE Transactions on Communications Systems*, March 1962, pp. 90–95.
- [5] J. M. Wozencraft and I. M. Jacobs, *Principles of Communications Engineering*, New York: John Wiley & Sons, Inc., 1965, pp. 611–614.
- [6] D. D. McRae, "Performance Evaluation of a New Modulation Technique," *IEEE Transactions on Communications Technology*, August 1971, COM-19, No. 4/pp. 431–445.
- [7] G. R. Welfi, "Pulse-Amplitude-and-Phase Modulation," COM-19, No. 4, Second INTELSAT International Conference on Digital Satellite Communications, Paris, France, November 1972, *Proc.*, pp. 208–217.
- [8] G. R. Welfi, "Application of Hybrid Modulation to FDMA Telephony via Satellite," *COMSAT Technical Review*, Vol. 3, No. 2, Fall 1973, pp. 419–430.
- [9] C. M. Thomas, C. L. May, and G. R. Welfi, "Hybrid Amplitude-and-Phase Modulation for Analog Data Transmission," *IEEE Transactions on Communications*, COM-23, No. 6, June 1975, pp. 634–645.
- [10] T. Furuya et al., "Hybrid Modem for 120 Channels FDM Telephony Signal Transmission," Third International Conference on Digital Satellite Communications, Kyoto, Japan, November 1975, *Proc.*, pp. 91–98.

# **Summary of the INTELSAT V communications performance specifications**

J. C. FUENZALIDA, P. RIVALAN, and H. J. WEISS

(Manuscript received January 13, 1977)

## **Introduction**

On September 21, 1976, COMSAT, acting as the Management Services Contractor for INTELSAT, signed a contract with the Aeronutronic Ford Corporation (now the Ford Aerospace and Communications Corporation) for the design and construction of seven INTELSAT V spacecraft, the first of which is to be delivered by July 21, 1979. The specifications for this new spacecraft, resulting from several years of intensive studies, represent a significant advance in terms of communications capabilities and technical sophistication of spacecraft used to carry commercial communications traffic.

This note, which describes some of the more significant technical parameters specified for the INTELSAT V spacecraft, concentrates on the characteristics relating to the potential utilization of the payload. Thus, most of the information presented herein concerns the spacecraft communications subsystem, *i.e.*, the transponders and antennas. Other spacecraft features are briefly described in order to present the payload characteristics in a more general context.

## **General characteristics of the INTELSAT V spacecraft**

The INTELSAT V spacecraft is an active repeater communications satellite intended for use in a geosynchronous equatorial orbit. It is to be

This note is based upon work performed at COMSAT under the sponsorship of the International Telecommunications Satellite Organization (INTELSAT). Views expressed in this paper are not necessarily those of INTELSAT.

---

*Jorge C. Fuenzalida is Manager of Communication Systems Studies, COMSAT.*

*Patrick Rivalan is Senior Staff Scientist, Communication System Studies, COMSAT.*

*Hans J. Weiss is Director of Systems studies, COMSAT.*

compatible with placement into transfer orbit by either the Atlas-Centaur launch vehicle or the Space Transportation System (STS).

This requirement imposes limits on the maximum spacecraft mass at launch, which, including the apogee motor and spacecraft adapter assembly, must be less than 1,869 kg (4,121 lb) for the Atlas-Centaur with DI-A fairing and 1,897 kg (4,181 lb) for the STS. The spacecraft is to be designed to meet all specification requirements without interruption for seven years in orbit. Accordingly, there is a requirement for batteries to permit full operation during eclipse and for onboard fuel to perform east-west and north-south stationkeeping maneuvers during the full 7-year life.

INTELSAT V is to be body stabilized with sun-oriented solar arrays, representing a significant departure from previous INTELSAT spacecraft, which were all spin stabilized. Figure 1 shows the overall configuration of

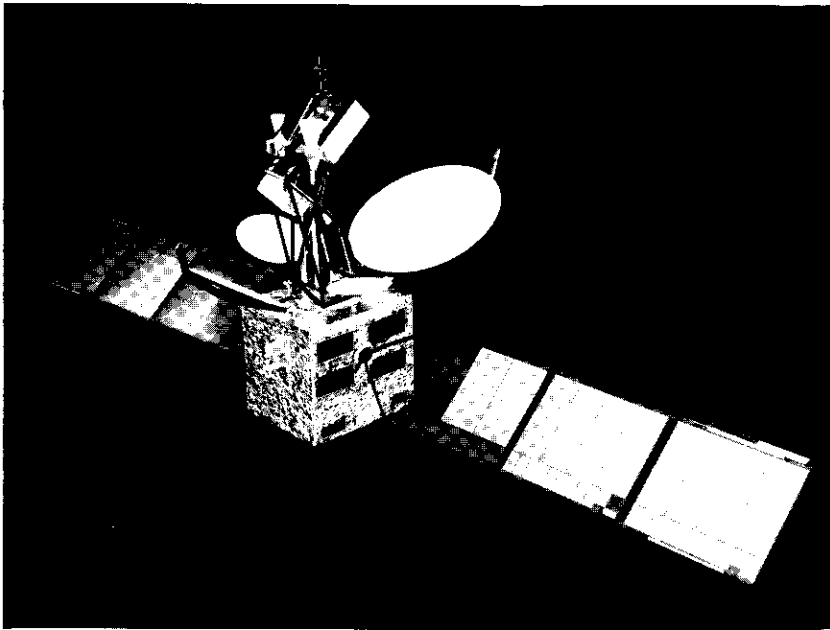


Figure 1. Overall Spacecraft Configuration

the spacecraft. It is expected that orbit control maneuvers will be performed to keep the spacecraft longitude within  $\pm 0.1^\circ$  of its assigned station and the plane of its orbit within  $\pm 0.1^\circ$  of the equatorial plane.

The pointing accuracy required from the spacecraft is not explicitly specified in the contract. However, all specification requirements must be met under the worst-case pointing error expected from the spacecraft, or when the spacecraft is subject to combined pointing errors of  $\pm 0.2^\circ$  in pitch,  $\pm 0.2^\circ$  in roll, and  $\pm 0.4^\circ$  in yaw, whichever is worse.

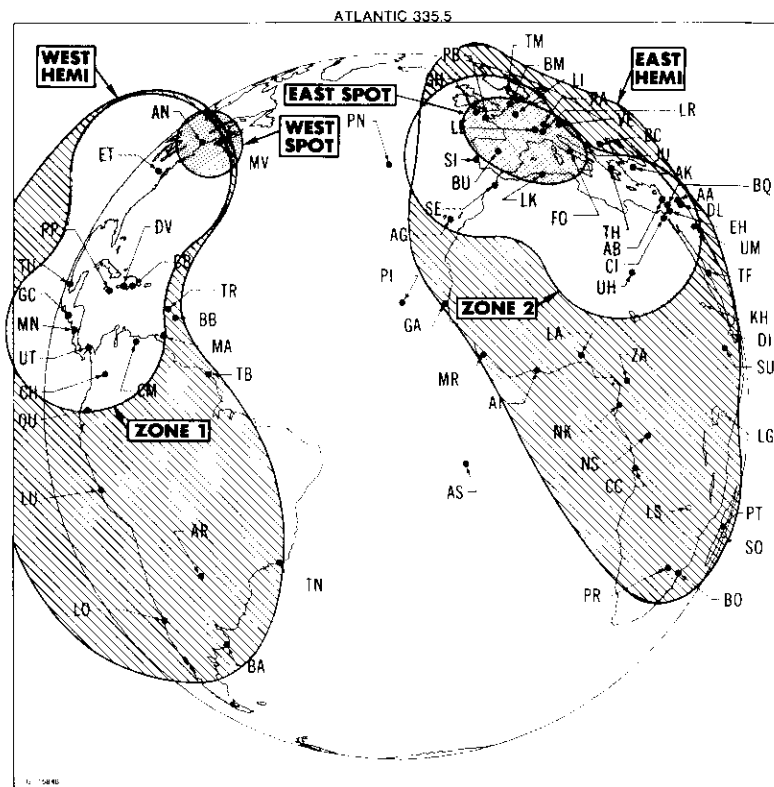
Stringent reliability requirements have been imposed on the spacecraft to ensure its continuous availability during its lifetime. Specifications call for a probability of survival for the complete spacecraft (with more than 65 percent of the RF channels operational in each coverage area) of at least 0.99 after two months. After seven years in orbit, the probability of survival must be higher than 0.75, including eclipse operation. Further, any single piece part, subassembly, or assembly (except the apogee motor) whose failure can cause the loss of 65 percent or more of the channels in any coverage area must have an estimated survival probability of 0.99 or more for the full seven years in orbit. Finally, any items which are subject to known wear-out or deterioration mechanisms must have a design life of at least 10 years.

#### Coverages, channelization, and connectivity requirements

The beam coverage, transponder channelization, and transponder interconnectivity specifications comprise the broadest definition of the required payload capabilities. These factors are in most cases sufficient to define a spacecraft concept and to allow a preliminary evaluation of its potential applications and utility.

#### FREQUENCY BANDS AND BEAM COVERAGES

The INTELSAT V communications subsystem operates in two frequency band pairs: the 6/4-GHz bands (5,925–6,425 MHz up-link and 3,700–4,200 MHz down-link) and the 14/11-GHz bands (the 14,000- to 14,500-MHz band for the up-links and the split 10,950- to 11,200-MHz and 11,450- to 11,700-MHz bands for the down-links). The spacecraft utilizes these bands in seven distinct coverage areas, five at 6/4 GHz and two at 14/11 GHz. Reuse of the frequency bands between coverage areas is accomplished by means of spatial and/or polarization isolation. Table I summarizes the coverages and their associated polarizations, and Figures 2a–2c show the coverage areas for each of the three ocean regions. These coverages are specified in terms of a set of earth station locations at which the various performance characteristics must be met. The specifications require that, once in orbit, each spacecraft must be reconfigurable via ground command to satisfy the coverage requirements of each of the three

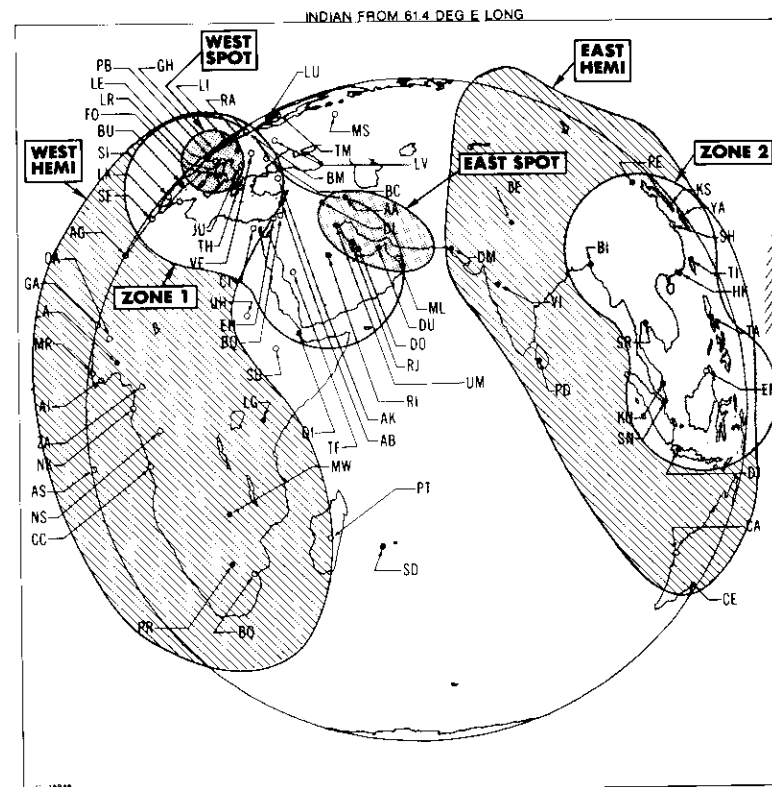


a. Atlantic Ocean Region  
Figure 2. INTELSAT V Coverages

TABLE 1. INTELSAT V COVERAGE BEAMS\*

Band	Coverage	Polarization	
		Up-Link	Down-Link
6/4 GHz	Earth	Left-Hand Circular	Right-Hand Circular
	West Hemispheric	Left-Hand Circular	Right-Hand Circular
	East Hemispheric	Left-Hand Circular	Right-Hand Circular
	Zone 1	Right-Hand Circular	Left-Hand Circular
14/11 GHz	Zone 2	Right-Hand Circular	Left-Hand Circular
	East Spot	Linear	Linear
	West Spot	Linear	Linear

\* The polarization of the east spot coverage shall be orthogonal to that of the west spot coverage.

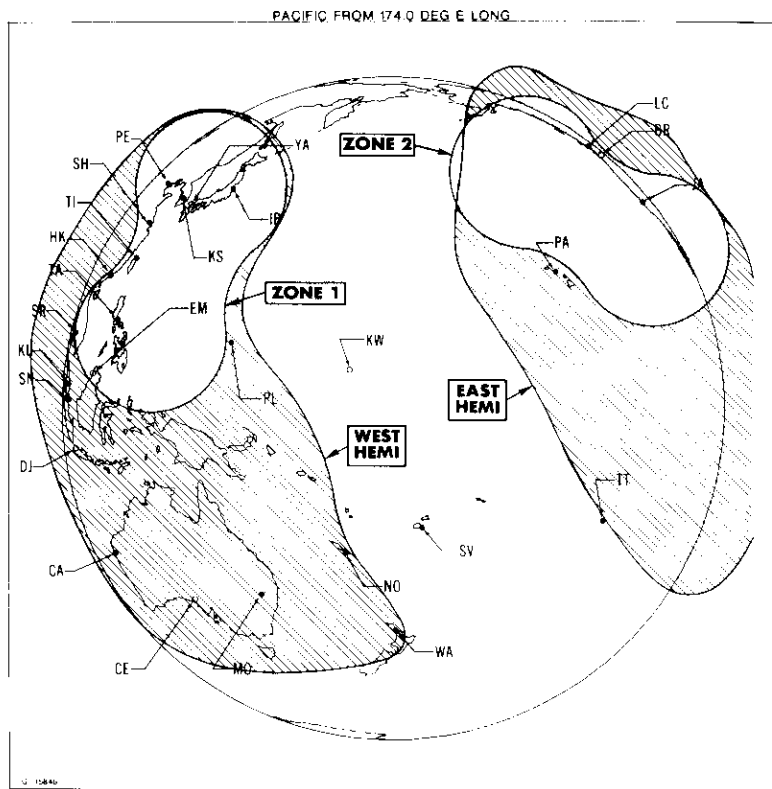


b. Indian Ocean Region  
Figure 2. INTELSAT V Coverages

ocean regions. The 14/11-GHz spot coverages are to be steerable over the portions of the earth's disk shown in Figure 2d.

TRANSPONDER CHANNELIZATION PLAN

The interconnection of the receive coverages with the transmit coverages necessary to establish the desired signal paths is accomplished at the transmission channel level. The necessary signal paths can be established independently for each of the various segments (transmission channels) of each frequency band. The frequency band segments defining the transmission channels are indicated in the transponder channelization plan shown in Figure 3. Each frequency band is subdivided into 12 nominal 40-MHz increments identified by a number from 1 to 12. When a channel extends over more than one of these increments, it is identified by a multi-

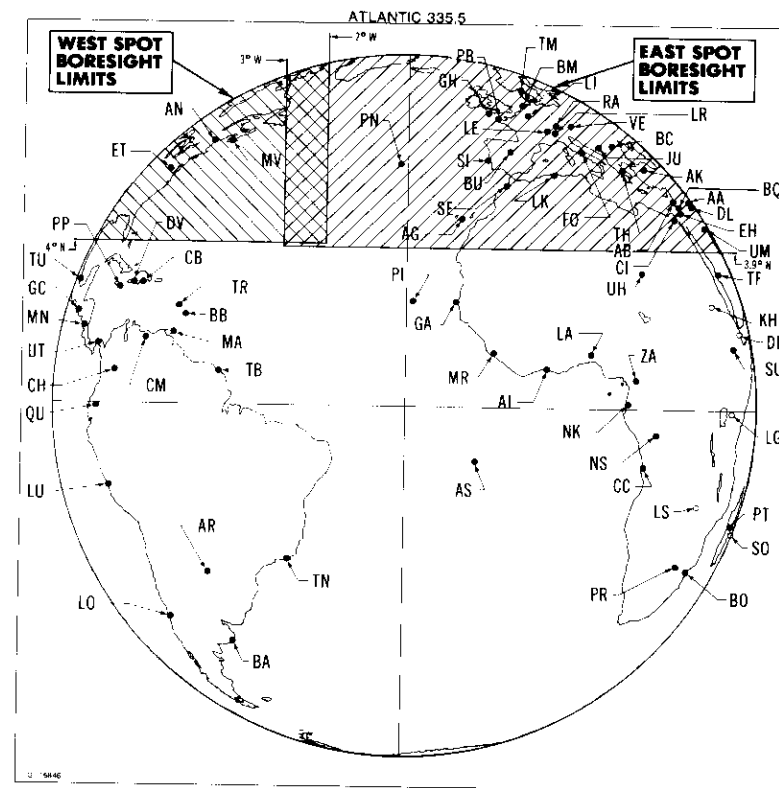


c. Pacific Ocean Region  
Figure 2. INTELSAT V Coverages

ple channel number, e.g., channel (1-2) or channel (7-12). In the case of channel (7-8), the dotted line in the channelization plan indicates that on the up-link the channelization consists of two independent channels, 7 and 8, while on the down-link these channels are combined to form a single channel, (7-8).

**TRANSPONDER SWITCHING CAPABILITIES**

The communications subsystem will incorporate a number of channel routing switches so that any of the possible interconnections defined in Table 2 can be established through ground commands. Each interconnec-



d. Spot-Beam Steering Capabilities  
Figure 2. INTELSAT V Coverages

tion can be realized independently for each channel, although a channel can interconnect only one receive coverage to one transmit coverage. Figure 4 is a representative block diagram showing the signal flow through the spacecraft transponder.

**Overall communications performance specifications**

The performance requirements summarized in this section apply to each overall transmission channel, including antennas, receivers, channelizing filters, and transmitters. These specifications, which permit the use of FDMA/FM, FDMA/PSK, or TDMA/PSK transmission, are grouped into four



TABLE 2. INTELSAT V TRANSPONDER INTERCONNECTION CAPABILITIES

From	To	West Spot	East Spot	West Hemi	East Hemi	Zone 1	Zone 2	Global
West Spot		(1-2)	(1-2)	(1-2)	(1-2)	(7-8)	(7-8)	
		(5-6)	(5-6)	(5-6)	(5-6)			
		(7-12)	(7-12)					
East Spot		(1-2)	(1-2)	(1-2)	(1-2)	(7-8)	(7-8)	
		(5-6)	(5-6)	(5-6)	(5-6)			
		(7-12)	(7-12)					
West Hemi		(1-2)	(1-2)	(1-2)	(1-2)	(3-4)	(3-4)	
		(5-6)	(5-6)	(3-4)	(3-4)	(5-6)	(5-6)	
				(5-6)	(5-6)	(7) (8) (9)	(7) (8) (9)	
East Hemi		(1-2)	(1-2)	(1-2)	(1-2)	(3-4)	(3-4)	
		(5-6)	(5-6)	(3-4)	(3-4)	(5-6)	(5-6)	
				(5-6)	(5-6)	(7) (8) (9)	(7) (8) (9)	
Zone 1		(7-8)	(7-8)	(3-4)	(3-4)	(1-2)	(1-2)	
				(5-6)	(5-6)	(3-4)	(3-4)	
						(5-6)	(5-6)	
Zone 2		(7-8)	(7-8)	(3-4)	(3-4)	(1-2)	(1-2)	
				(5-6)	(5-6)	(3-4)	(3-4)	
						(5-6)	(5-6)	
Global						(7-8)	(7-8)	
						(9)	(9)	
						(10)	(10)	
						(11)	(11)	
					(12)	(12)		

categories: link performance, linearity, filter characteristics, and other miscellaneous specifications.

LINK PERFORMANCE PARAMETERS

The primary performance parameters of the communications subsystem are given in Tables 3 and 4. These parameters determine the link power budgets and the associated communications capacities for the various operational modes.

TABLE 3. BEAM ISOLATION, RECEIVE G/T, AND TRANSMIT e.i.r.p.

Polarization Performance (voltage axial ratio for transmit and receive beams)		
Global		1.09
Hemispheric		1.09
Zone		1.09
Antenna Isolation (dB) (minimum beam isolation for transmit and receive beams)		
Hemi to Hemi		27
Hemi to Zone		27
Zone to Zone		27
Spot to Spot		
8° E-W Separation		33
6.5° E-W Separation		27
Receive System G/T (dB/K)		
6-GHz Global		-18.6
6-GHz Hemispheric		-11.6
6-GHz Zone		-8.6
14-GHz East Spot		0.0
14-GHz West Spot		3.3
e.i.r.p. (dBW)		
4-GHz Global		
Channels (7-8)		26.5
Channels 9, 10, 11, 12		23.5
4-GHz Hemi or Zone		
Channels (1-2), (3-4), (5-6), (7-8)		29.0
Channel 9		26.0
11-GHz East Spot		
Channels (1-2), (5-6), (7-12)		41.1
11-GHz West Spot		
Channels (1-2), (5-6), (7-12)		44.4

TABLE 4. SATURATION FLUX DENSITY

Up-Link Beam	Saturation Flux Density (dBW/m²)	
	High Gain	Low Gain
6-GHz, All Beams		
Channels (1-2), (3-4), (5-6), 7, 8, (7-8)	-72.0 ± 2	7.5 dB higher
Channels 9, 10, 11, 12	-75.0 ± 2	7.5 dB higher
14-GHz East Spot		
Channels (1-2), (5-6), (7-8), (7-12)	-77.0 ± 2	5 dB higher
14-GHz West Spot		
Channels (1-2), (5-6), (7-8), (7-12)	-80.3 ± 2	5 dB higher

NONLINEAR CHANNEL PERFORMANCE SPECIFICATIONS

The specifications applying to the input sections common to more than one transmission channel are summarized in Table 5, while those applicable to the overall transmission channel are summarized in Table 6.

TABLE 5. NONLINEAR PERFORMANCE SPECIFICATIONS APPLICABLE TO INPUT SECTIONS COMMON TO MORE THAN ONE TRANSMISSION CHANNEL

a. Single-carrier performance			
Flux Density Illuminating the Spacecraft (dBW/m <sup>2</sup> )		Total Phase Shift (deg)	Intelligible Crosstalk Ratio (dB)
6 GHz	14 GHz		
-60	-67.5	1.5	-175 + 20 log $f_m$ (Hz)
-69	-76.5	0.2	-193 + 20 log $f_m$ (Hz)

b. 2-carrier performance			
Flux Density Illuminating the Spacecraft for Each of Two Carriers (dBW/m <sup>2</sup> )		C/I (dB)	
6 GHz	14 GHz		
-63	-70.5	26	
-68	-75.5	36	
-73	-80.5	46	

In both cases the maximum total phase shift, minimum intelligible crosstalk ratio, and minimum carrier-to-intermodulation (C/I) ratio have been specified as functions of the illumination flux density. In addition, the maximum allowable AM-to-PM (AM/PM) transfer coefficient has been specified for each transmission channel.

FILTER REQUIREMENTS

Filtering specifications include in-band group delay and gain slope, and out-of-band response specifications. The INTELSAT V group-delay requirements are summarized in Figure 5, in which the product of the maximum group delay and transmission channel bandwidth is expressed as a function of the frequency from band center, normalized to the transmission channel bandwidth. In addition, the group delay must be higher than 2 ns at any frequency within the usable bandwidth.

TABLE 6. NONLINEAR PERFORMANCE SPECIFICATIONS APPLICABLE TO EACH TRANSMISSION CHANNEL

a. Phase Linearity of Each Transmission Channel			
Relative Flux Density <sup>a</sup> (dB)	Output Transmission Phase Shift (deg)	AM/PM Transfer Coefficient (deg/dB)	
-0	46	8.0	
-3	38	9.0	
-6	28	9.0	
-9	18	8.0	
-12	12	5.0	
-14	9	3.0	
> -14	—	3.0	

b. Intelligible Crosstalk Ratio			
Relative Flux Density <sup>a</sup> (dB)	Channel Bandwidth (MHz)	Location of Modulated Carrier Center Frequency <sup>b</sup>	
		Within the Center 70% of the Usable Bandwidth	Over 100% of the Usable Bandwidth
0 to -14	34, 36, 41	-171 + 20 log $f_m$	-149 + 20 log $f_m$
> -14		-177 + 20 log $f_m$	-155 + 20 log $f_m$
0 to -14	72, 77	-173 + 20 log $f_m$	-151 + 20 log $f_m$
> -14		-179 + 20 log $f_m$	-157 + 20 log $f_m$

c. Amplitude Linearity	
Relative Flux Density <sup>a</sup> per Carrier (dB)	Maximum Intermodulation-to-Carrier Ratio <sup>d</sup> (dB)
-3.0	-10
-10.0	-15
-17.0	-26

<sup>a</sup> Flux density illuminating the spacecraft related to the flux density which produces single-carrier saturation.

<sup>b</sup> The modulation frequency,  $f_m$ , is expressed in Hz.

<sup>c</sup> Flux density illuminating the spacecraft for each of two equal-amplitude carriers below the flux density which produces single-carrier saturation.

<sup>d</sup> Maximum level of third-order intermodulation product relative to the level of each of the RF carriers, measured at the output of each transmission channel.

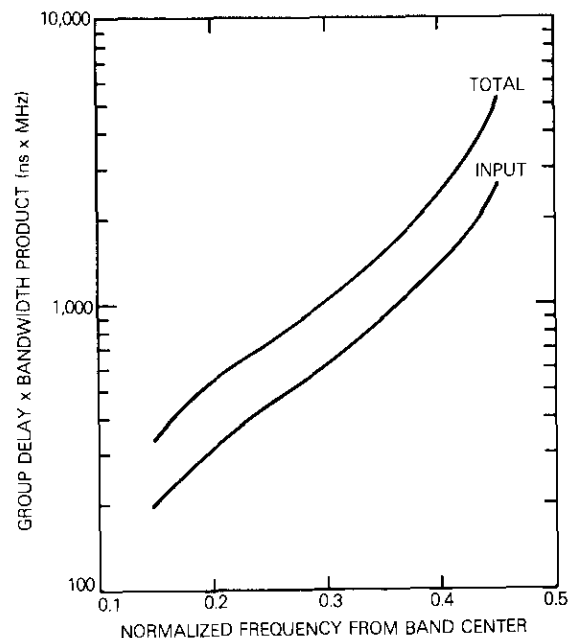


Figure 5. *Input and Total Group-Delay Performance Requirements*

The gain slope requirements and typical out-of-band response specifications are summarized in Tables 7 and 8, respectively. The narrowband response specifications have been chosen so that they can be met by 8-pole input filters and 6-pole output filters.

#### ADDITIONAL MISCELLANEOUS SPECIFICATIONS

In addition to the communications parameters included in these three categories, several other transponder performance characteristics have been specified in the contract. Although the performance characteristics summarized in Table 9 are perhaps of less general interest, they are essential to the proper operation of the INTELSAT V communications payload.

TABLE 7. GAIN SLOPE REQUIREMENTS

Channel Usable Bandwidth (MHz)	Percent of Usable Bandwidth Centered on Channel Frequency	Input <sup>a</sup> Maximum Gain Slope (dB/MHz)	Total <sup>b</sup> Maximum Gain Slope (dB/MHz)
34, <sup>c</sup> 36, 41	70	0.05	—
	80	0.07	0.12
	90	0.20	0.30
	100	0.70	0.90
72, 77	70	0.04	—
	80	0.05	0.07
	90	0.10	0.15
	100	0.35	0.45
241	70	0.03	—
	80	0.04	0.05
	90	0.04	0.05
	100	0.12	0.15

<sup>a</sup> Input gain slope is that gain slope measured between the input to the transmission channel (including receive antenna) and the input to the final power amplifier.

<sup>b</sup> Total gain slope is that gain slope measured over the total transmission channel, including receive and transmit antennas.

<sup>c</sup> 34 MHz for input gain slope only.

TABLE 8. TYPICAL OUT-OF-BAND RESPONSE SPECIFICATIONS

Out-of-Band Response Parameter	Frequency from Band Center Normalized to Usable Bandwidth	Maximum Out-of-Band Response (dB)
Narrowband Receive	0.69	-30
	0.83	-40
Narrowband Transmit	0.69	-25
	0.83	-30
Narrowband Total	0.69	Sum of narrowband receive and transmit
	0.83	
Wideband Receive	0.30	-20
	0.40	-30

TABLE 9. ADDITIONAL COMMUNICATIONS PARAMETER SPECIFICATIONS

Spurious Outputs (in the transmit bands at the input of any transmit antenna)	
In any 1.0-MHz band	-55 dBW
In any 4-kHz band	-60 dBW
Repeater Isolation	50 dB
Long-Term Frequency Stability	
Over lifetime including initial tolerances and eclipse effects	
6-4 GHz	$\pm 10$ parts in $10^6$
6-11 GHz	$\pm 4$ parts in $10^6$
14-4 GHz	$\pm 2$ parts in $10^6$
14-11 GHz	$\pm 7$ parts in $10^6$
Over one month excluding eclipse effects	
6-4 GHz	$\pm 10$ parts in $10^7$
6-11 GHz	$\pm 4$ parts in $10^7$
14-4 GHz	$\pm 2$ parts in $10^7$
14-11 GHz	$\pm 7$ parts in $10^7$
Gain Stability (over any day, at the center of each transmission channel)	1 dB peak-to-peak
Overdrive Capability (without subsequent degradation of performance or lifetime)	20 dB
Switching Outage	<25 ms
11-GHz Beacons	
Frequency	
First Beacon	between 11,196 and 11,200 MHz
Second Beacon	between 11,450 and 11,454 MHz
Frequency Stability	3 parts in $10^6$
e.i.r.p.	6 dBW over earth coverage
Power Stability	
Over any operating day	1 dB peak-to-peak
Over operating lifetime	2 dB peak-to-peak

## Translations of Abstracts in this issue

### Le programme COMSTAR

R. D. BRISKMAN

#### Sommaire

L'article décrit le programme COMSTAR, sa genèse et l'élaboration des études techniques de base le concernant. Il définit les caractéristiques principales du programme et se penche sur les questions de mise en oeuvre; il donne également un aperçu des résultats obtenus en exploitation. En outre, il étudie certains aspects techniques touchant le service de télécommunication, les satellites, lanceurs et stations terriennes, ainsi que le système de poursuite, télémétrie et télécommande.

### Le système à satellites COMSTAR

G. E. ABU TALEB, M. C. KIM, K. F. MANNING, J. F. PHIEL, JR.,  
ET L. H. WESTERLUND

#### Sommaire

L'article brosse un tableau du système à satellites de télécommunication de COMSAT GENERAL qui, en liaison avec le secteur terrien AT&T-GSAT, constitue le système national à satellites COMSTAR. Après avoir décrit le satellite et ses divers sous-ensembles, l'article s'attarde sur le détail du sous-ensemble de télécommunications et se termine par un examen des caractéristiques des stations terriennes, de façon à donner au lecteur une vue d'ensemble du système.

Les études relatives au système à satellites COMSTAR sont fondées sur l'emploi du mode de transmission analogique MRF-MF et une capacité de 1.200 voies téléphoniques unidirectionnelles par répéteur. Mais en régime d'exploitation réelle, il est prévu que la capacité dépassera 1.500 voies par répéteur. Le système peut également assurer la transmission de données (bande étroite ou large bande), de signaux de télévision et de porteuses numériques à grande vitesse; il peut fonctionner en AMRF ou AMRT, ou encore combiner ces deux modes d'accès multiple. Les ingénieurs du système

síncrono ("slotted") y sus derivados han sido investigados a fondo en los últimos años en relación con las transmisiones de servicios integrados por líneas terrestres y vía satélite. Recientemente se llevaron a cabo investigaciones de las características dinámicas y la estabilidad de los sistemas ALOHA no síncronos para la transmisión de servicios integrados por líneas terrestres que tienen un insignificante tiempo de propagación. Se presenta un modelo de los sistemas ALOHA para satélites, caracterizado por largas demoras de propagación, y se examina su empleo para predecir las características dinámicas, la estabilidad de régimen permanente y el desempeño de dichos sistemas. A esto sigue un análisis de las consideraciones requeridas para concebir el diseño "óptimo" de un sistema ALOHA para satélites.

### INDEX TO 1976 CTR AUTHORS

- ALLISON, J. F., see Revesz, A. G. [CTR76/096].  
 ASSAL, F., see Chen, M. H. [CTR76/107].  
 ASSAL, F., Mahle, C. & Berman, A., "Network Topologies to Enhance the Reliability of Communications Satellites," Fall, pp. 309-322 [CTR76/108].  
 BERMAN, A., see Assal, F. [CTR76/108].  
 CAMPANELLA, S. J., "Digital Speech Interpolation," Spring, pp. 127-158 [CTR76/100].  
 CAMPANELLA, S. J., see Su, J. S. [CTR76/110].  
 CHEN, M. H., Assal, F. & Mahle, C., "A Contiguous Band Multiplexer," Fall, pp. 285-307 [CTR76/107].  
 CHOU, S. M., Koskos, P. & Getsinger, W. J., "The Unattended Earth Terminal Low-Noise Amplifier," Spring, pp. 89-105 [CTR76/098].  
 DIFONZO, D. F., Trachtman, W. S. & Williams, A. E., "Adaptive Polarization Control for Satellite Frequency Reuse Systems," Fall, pp. 253-283 [CTR76/106].  
 FANG, D. J. & Jih, J., "A Model for Microwave Propagation Along an Earth-Satellite Path," Fall, pp. 379-411 [CTR76/112].  
 GATFIELD, A. G., "Error Control on Satellite Channels Using ARQ Techniques," Spring, pp. 179-188 [CTR76/102].  
 GETSINGER, W. J., see Chou, S. M. [CTR76/098].  
 GORDON, G. D. & DeRocher, W. L.\*, "Repairing a Communications Satellite on Orbit," Spring, pp. 25-56 [CTR76/095].  
 HSING, J., "Pitch Axis Adaptive Control," Fall, pp. 425-433 [CTR76/114].  
 JANKOWSKI, J. A., "A New Digital Voice-Activated Switch," Spring, pp. 159-178 [CTR76/101].  
 JIH, J., see Fang, D. J. [CTR76/112].  
 KAPLAN, M. H.† & Patterson, T. C., "Attitude Acquisition Maneuver for Bias Momentum Satellites," Spring, pp. 1-23 [CTR76/094].  
 KOSKOS, P., see Chou, S. M. [CTR76/098].  
 KREUTEL, R. W., "Wide-Angle Sidelobe Envelopes of a Cassegrain Antenna," Spring, pp. 71-88 [CTR76/097].  
 KURJAN, D. & Wachs, M., "TV Cochannel Interference on a PCM-PSK SCPC System," Fall, pp. 413-424 [CTR76/113].  
 MAHLE, C., see Chen, M. H. [CTR76/107] and Assal, F. [CTR76/108].

\*Non-COMSAT author.

†INTELSAT.

‡COMSAT consultant.

- MEULENBERG, A., "Electrical Discharges on Spacecraft at Synchronous Altitude," Spring, pp. 189-193 [CTR76/103].
- MORGAN, W. L., "Satellite Utilization of the Geosynchronous Orbit," Spring, pp. 195-205 [CTR76/104].
- PATTERSON, T. C., see Kaplan, M. H. [CTR76/094].
- REVESZ, A. G., Allison, J. F. & Reynolds, J. H., "Tantalum Oxide and Niobium Oxide Antireflection Films in Silicon Solar Cells," Spring, pp. 57-59 [CTR76/096].
- REYNOLDS, J. H., see Revesz, A. G. [CTR76/096].
- SINHA, A. K., "A Model for TDMA Burst Assignment and Scheduling," Fall, pp. 219-251 [CTR76/105].
- SU, J. S., Suyderhoud, & Campanella, S. J., "A Strategy for Delta Modulation in Speech Reconstruction," Fall, pp. 339-355 [CTR76/110].
- SUYDERHOUD, H. G., see Su, J. S. [CTR76/110].
- TRACHTMAN, W. S., see DiFonzo, D. F. [CTR76/106].
- TSUJI, Y.†, "Phase Ambiguity Resolution in a 4-Phase PSK Modulation System with Forward-Error-Correcting Convolution Codes," Fall, pp. 357-377 [CTR76/111].
- WACHS, M., see Kurjan, D. [CTR76/113].
- WELTI, G. R., "PCM/FDMA Satellite Telephony with 4-Dimensionally-Coded Quadrature Amplitude Modulation," Fall, pp. 323-338 [CTR76/109].
- WILLIAMS, A. E., see DiFonzo, D. F. [CTR76/106].
- WOLEJSZA, C. J., "Effects of Oscillator Phase Noise on PSK Demodulation." Spring, pp. 107-125 [CTR76/099].

†INTELSAT.

### COMSAT AUTHORS PRESENTATION AND PUBLICATION INDEX—1976

The following is a cross-referenced index of technical publications and presentations by COMSAT authors outside of *COMSAT Technical Review*. The code number at the end of an entry is the reprint code number by which copies may be ordered from Lab Records at COMSAT Laboratories, P.O. Box 115, Clarksburg, MD 20734.

- AGRAWAL, B. N., "Mode Synthesis Technique for Dynamic Analysis of Structures," *J. of Acoustical Soc. of Amer.*, June 76, pp. 1329-1338 [76CLR25].
- ALLISON, J. F., see Revesz, A. [76CLR19] and Revesz, A. [76CLR12].
- ALLISON, J. F. & Crabb, R. L.\*, "What is Simulated AMO?," Pres. at IEEE 12th Photovoltaic Spec. Conf., Baton Rouge, La., Nov. 76.
- ARNDT, R. A., see Rittner, E. S. [76CLR24].
- ASSAL, F. T., see Rozec, X.\* [76CLR16].
- ATIA, A. E. & Williams, A. E., "General TE011-Mode Waveguide Bandpass Filters," *IEEE MTT-24*, Oct. 76, pp. 640-648 [76CLR30].
- ATIA, A. E. & Williams, A. E., "Temperature Compensation of TE011-Mode Circuit Cavities," *IEEE MTT-24*, Oct. 76, pp. 668-669 [76CLR31].
- ATIA, A. E. & Williams, A. E., "Waveguide Filters for Space—Smaller, Lighter—and Fewer Cavities," *Microwave Systems News*, Aug.-Sep. 76, pp. 75-78 [76CLR40].
- ATIA, A. E. & Williams, A. E., "Synthesis, Realization and Measurement Techniques of Narrow Bandpass Multiple Coupled Cavity Filters," *IEEE PROC. Int. Soc. Circuits & Syst.*, Apr. 76, pp. 544-547 [76CLR47].
- ATOHOON, I. E., see Riginos, V. [76CLR02].
- BARGELLINI, P. L., "Satellite Communications, Fundamental Concepts and Recent Developments," *Atti dei Convegni Lincei*, Vol. 42, 1976, pp. 337-361 [74CLR56].
- BARGELLINI, P. L., see Edelson, B. I. [76CLR09].
- BENEDICT, R. N. & Kolsrud, J. E., "Digital Service in the INTELSAT Network," *IEEE EASCON '76 Record*, pp. 102A-102G [76CLR34].
- BETZ, F.\*, Stockel, J. R. & Gaudet, A.\*, "Nickel-Hydrogen Storage Battery for Use on Navigation Technology Satellite-2," *Int. Energy Conv. Eng. Conf. PROC.*, Vol. 1, Sep. 76, pp. 510-516 [76CLR38].
- BILLERBECK, W. J., see Esch, F. [76CLR36].

\*Non-COMSAT author.

†INTELSAT.

- BLEIWEIS, J. J., see Tammes, J.\* [76CLR39].
- BRISKMAN, R. D., "System Considerations for Advanced North American Domestic Satellites," Pres. at 6th AIAA Comm. Sat. Syst. Conf., Montreal, Apr. 76, AIAA Paper No. 76-222.
- BROWN, M. P., "The International Telecommunications Satellite Organization (INTELSAT)," *Communications Satellite Systems: An Overview of the Technology*, R. Gould & Y. Lum, ed., N.Y.: IEEE Press, 1976, pp. 23-28 [76CLR28].
- BROWN, M. P., "The USSR Domestic System (Molniya/Orbita)," *Communications Satellite Systems: An Overview of the Technology*, R. Gould & Y. Lum, ed., N.Y.: IEEE Press, 1976, pp. 29-32 [76CLR29].
- CAMPANELLA, S. J., see McClure, R.\* [76CLR03] and Suyderhoud, H. [76CLR51].
- CHAKRABORTY, D., see Wolejsza, C. [76CLR14].
- CHARYK, J. V., "Satellite Communications," *The Impact of Space Science on Mankind*, T. Greve, F. Leid, and E. Tandberg, ed., N.Y.: Plenum Press, 1976.
- CHILDS, W. H., "Design Techniques for Bandpass Filters Using Edge-Coupled Microstrip Lines on Fused Silica," *IEEE MTT-S*, June 76, pp. 194-196 [76CLR23].
- COOL, R., see Meulenberg, A.
- CURTIN, D. J., see Esch, F. [76CLR36].
- CURTIN, D. J., see Meulenberg, A.
- DEAL, J. H. & Buegler, J.\*, "A Demand-Assignment Time-Division Multiple Access System for Military Tactical Application," Pres. at 6th AIAA Comm. Sat. Syst. Conf., Montreal, Apr. 76, AIAA Paper No. 76-270 [76CLR06].
- DICKS, J. L., see Schultze, P.† [76CLR11].
- DICKS, J. L., "INTELSAT Earth Station Standards and Their Impact on Orbit Efficiency," Pres. at IEEE EASCON Sep. 76 [UPO50CL].
- DIFONZO, D. F., English, W. J. & Trachtman, W. S., "Antenna Depolarization Measurements Using Satellite Signals," *IEEE AP-S Int. Symp. Oct. 76 PROC.*, pp. 282-285 [76CLR41].
- DIFONZO, D. F., see English, W. J. [76CLR42].
- DILL, G. D., Tsuji, Y.† & Muratani, T.†, "Application of SS-TDMA in a Channelized Satellite," *IEEE ICC June 76 CONF REC*, pp. 51-1-51-5 [76CLR17].
- DUNLOP, J. D., Van Ommering, G. & Earl, M. W., "Ni-H<sub>2</sub> Battery Flight Experiment," Pres. at 10th Int. Power Sources Symp., England, Sep. 76 [UPO52CL].
- EARL, M. W., see Dunlop, J. D. [UPO52CL].

\*Non-COMSAT author.

†INTELSAT.

- EARLY, L. B., "Economics of Communications Satellites—1976," Pres. at 27th IAF Cong., Anaheim, CA, Oct. 76, Paper No. IAF 76-130 [76CLR35].
- EDELSON, B. I. & Bargellini, P. L., "Technology Development for Global Satellite Communications," Pres. at 6th AIAA Comm. Sat. Syst. Conf., Montreal, Apr. 76, AIAA Paper No. 76-234 [76CLR09].
- EDELSON, B. I., Wood, H. W. & Reber, C. J., "Cost Effectiveness in Global Satellite Communications," *Raumfahrtforschung*, Mar./Apr. 76, pp. 83-92 [76CLR20].
- EDELSON, B. I., "Satellite Communications Technology," *J. of Astron. Sci.*, July-Sep. 76, pp. 193-219 [76CLR45].
- ENGLISH, W. J., see DiFonzo, D. F. [76CLR41].
- ENGLISH, W. J., DiFonzo, D. F. & Trachtman, W. S., "Polarization Diagrams for CP Antenna Analysis," *IEEE AP-S Int. Symp. Oct. 76 PROC.*, pp. 286-289 [76CLR42].
- ESCH, F. H., Billerbeck, W. J. & Curtin, D. J., "Electric Power Systems for Future Communications Satellites," Pres. at 27th IAF Cong., Anaheim, CA, Oct. 76, Paper No. IAF 76-237 [76CLR36].
- FANG, D. J. & Harris, J. M., "A New Method of Estimating Microwave Attenuation over Slant Propagation Path Based on Rain Gauge Data," *IEEE AP-24*, May 76, pp. 381-384 [76CLR13].
- FREY, F. see Williams, A. E. [76CLR50].
- GALANTE, F. M.†, "The Impact of Western European Climate on the Design of SATCOM Systems at 11/14 GHz," *IEEE ICC June 76 CONF REC*, pp. 12-9-12-13 [76CLR21].
- HAMMOND, J. L.\*, Schaefer, D. J. & Leon, B. J.\*, "Methods of Monitoring and Fault Isolation for Digital Communication Links," *Natl. Telecom. Conf.*, Nov. 76, *PROC.*, Vol. II, pp. 22.3-1-22.3-5 [76CLR52].
- HARRIS, J. M. & Steinhorn, J. P., "Effects of Rain on Communications Satellite Systems Tradeoffs," *IEEE ICC June 76 CONF REC*, pp. 12-14-12-18 [76CLR15].
- HARRIS, J. M., see Fang, D. [76CLR13].
- HIRVONEN, J.\*, Revesz, A. G. & Kirkendall, T. D., "Rutherford Backscattering Investigation of Thermally Oxidized Tantalum on Silicon," *Thin Solid Films*, Apr. 76, pp. 315-322 [76CLR22].
- JONES, M. & Wachs, M., "Measured 60 Mbps 4-Phase PSK Signal Impairments Through Earth Station HPA and Satellite Transponder," *Natl. Telecom. Conf. Nov. 76 PROC.*, Vol. II, pp. 21.2-1-21.2-5 [76CLR48].
- KIM, M. C., "COMSAT General's Domestic Satellite System (COMSTAR)," Pres. at Conf. on Near Term Satellite Communications Systems, NASA/Goddard Spaceflight Center, Greenbelt, Md.

\*Non-COMSAT author.

†INTELSAT.

- KIRKENDALL, T., see Hirvonen, J.\* [76CLR22] and Revesz, A. [76CLR32].
- KOLSRUD, J. E., see Benedict, N. [76CLR34].
- KREUTEL, R. W., "A Multiple-Beam Torus Reflector Antenna for 20/30 GHz Satellite Communications Systems," Pres. at 6th AIAA Comm. Sat. Syst. Conf., Montreal, Apr. 76, AIAA Paper No. 76-302 [76CLR10].
- LEBOWITZ, S., "High Rate Error Correction Codes, The Correlation Decoding Approach," *Natl. Telecom. Conf. Nov. 76, PROC*, Vol. I, pp. 13.1-1-13.1-5 [76CLR49].
- LIPKE, D. W., see Swearingen, D. W.
- LUKSCH, W., see Martin, E. J.
- MARTIN, E. J., "MARISAT—A New Commercial Application of Communications Satellite Technology," Pres. at Canaveral Council of Tech. Societies 13th Space Congress, Apr. 1976.
- MARTIN, E. J. & Luksch, W.\*, "Cooperation Between U.S. and Europe in Telecommunications Programs for Mobile Applications," Pres. at 27th IAF Congress, Anaheim, CA, Oct. 1976, Paper 76-221.
- MASS, J.†, see Taur, R. R. [UPO47CL].
- McCLURE, R. B.\*, Tsuji, Y.† & Campanella, S. J., "Digital Communications Channel Architecture," Pres. at 6th AIAA Comm. Sat. Syst. Conf., Montreal, Apr. 76, AIAA Paper No. 76-228 [76CLR03].
- MEADOWS, G., "Spacecraft Contamination by Ion Thrusters with Two and Three Electrode Extraction Systems," Pres. at 12th AIAA Elec. Prop. Conf., Key Biscayne, FL, Nov. 76, AIAA Paper No. 76-1055 [76CLR60].
- MEULENBERG, A., "Evidence for a New Discharge Mechanism for Dielectrics in a Plasma," *Spacecraft Charging by Magnetospheric Plasmas*, A. Rosen, ed., Cambridge: MIT Press, 1976, pp. 237-246 [76CLR46].
- MEULENBERG, A., "A Novel Coverslide for Solar Cells," *CNES Int. Conf. on Solar Electricity* [France], Mar. 76, pp. 199-208 [76CLR56].
- MEULENBERG, A., "Proton Damage to Silicon from Laboratory and Space Sources," Pres. at 12th IEEE Photovoltaic Spec. Conf., Baton Rouge, LA, Nov. 76.
- MEULENBERG, A., Curtin, D. & Cool, R., "Comparison of Several Types of High Efficiency Solar Cells," Pres. at 12th IEEE Photovoltaic Spec. Conf., Baton Rouge, LA, Nov. 76.
- MOTT, R. C., see Sicotte, R.\* [76CLR26].
- ONUFYRY, M., see Suyderhoud, H. [76CLR51].
- ONUFYRY, M. & Litster, J. F.\*, "Digital Multi-Channel Echo Suppressor," *IEEE ICC Jun 76 CONF REC*, pp. 36-13-36-17 [76CLR53].
- PENTLICKI, C. J. & Poubeau, P.\*, "Magnetic Bearing Momentum Wheel," Pres. at 6th AIAA Comm. Sat. Syst. Conf., Montreal, Apr. 76, AIAA Paper No. 76-239 [76CLR05].
- REBER, C. J., see Edelson, B. I. [76CLR20].

\*Non-COMSAT author.

†INTELSAT.

- REDMAN, P. C., "A Microprocessor-Based Computer Developmental System for Satellite Application," *Int. Tel. Conf. Sep. 76, PROC*, pp. 71-76 [76CLR54].
- REISENWEBER, J. H., JR., "High Performance Thermal Louver Development," Pres. at 11th AIAA Thermophysics Conf., San Diego, July 76, AIAA Paper No. 76-460 [76CLR58].
- REVESZ, A. & Allison, J., "Electronic Properties of the Silicon-Thermally Grown Tantalum Oxide Interface," *IEEE ED-23*, May 76, pp. 527-529 [76CLR12].
- REVESZ, A., Reynolds, J. H. & Allison, J. F., "Optical Properties of Tantalum Oxide Films on Silicon," *J. of the Electrochem. Soc.*, June 76, pp. 889-894 [76CLR19].
- REVESZ, A., see Hirvonen, J.\* [76CLR22].
- REVESZ, A. & Kirkendall, T. D., "Film-Substrate Interaction in Si/Ta and Si/Ta<sub>2</sub>O<sub>5</sub> Structures," *J. of Electrochem Soc.*, Oct. 76, pp. 1514-1519 [76CLR32].
- REYNOLDS, J. H. see Revesz, A. [76CLR19].
- RIGINOS, V. E., Bohn, P.\* & Atohou, I. G., "A 3-Dimensional Computer Simulation of the Trapped-Domain Mode in Gunn Devices," *IEEE PROC*, Mar 76, pp. 385-386 [76CLR02].
- RITTNER, E. S. & Arndt, R. A., "Comparison of Silicon Solar Cell Efficiency for Space and Terrestrial Use," *J. of App. Phys.*, July 76, pp. 2999-3002 [76CLR24].
- RITTNER, E. S., "Recent Advances in Silicon Solar Cells for Space Use," *Advances in Electronics and Electron Physics*, Vol. 42, N.Y.: Academic Press, 1976, pp. 41-54 [76CLR57].
- RITTNER, E. S., "An Improved Theory of the Silicon p-n Junction Solar Cell," Pres. at IEEE Int. Elec. Dev. Meeting, Wash., D.C., Dec. 76, Paper No. 4.3.
- ROBERTSON, E. A., "Communications Requirements for the INTELSAT V Spacecraft," *IEEE EASCON '76 RECORD*, pp. 40A-40H [76CLR33].
- ROZEC, X.\* & Assal, F. T., "Microwave Switch Matrix for Communications Satellites," *IEEE ICC June 76 CONF REC*, pp. 35-13-35-17 [76CLR16].
- SCHAEFER, D. J., see Hammond, J. L.\* [76CLR52].
- SCHULTZE, P. H.†, Itohara, S.† & Dicks, J. L., "Use of the INTELSAT Space Segment for Domestic Systems," Pres. at 6th AIAA Comm. Sat. Syst. Conf., Montreal, Apr. 76, AIAA Paper No. 305 [76CLR11].
- SICOTTE, R. L.\* & Mott, R. C., "Design Space Qualified Millimeter Wave Doublers," *Microwaves*, July 76, pp. 46-58 [76CLR26].
- STEINHORN, J. P., see Harris, J. [76CLR15].

\*Non-COMSAT author.

†INTELSAT.

- STOCKEL, J. F., see Betz, F.\* [76CLR38] and Van Ommering, G. [76CLR43].
- STRAUSS, R., "The State-of-the-Art of High Power Amplifiers for Satellite Communications Above 10 GHz," Pres. at 6th AIAA Comm. Sat. Syst. Conf., Montreal, Apr. 76, AIAA Paper No. 76-300 [76CLR08].
- STRAUSS, R., "Development of Product Assurance Requirements for the INTELSAT Satellite Series," *Product Assurance*; PROC, Eur. Space Agency, SP-116, Sep. 76, pp. 217-237 [76CLR44].
- SUYDERHOUD, H., Onufry, M. & Campanella, S. J., "Echo Control in Telephone Communications," *Natl. Telecom. Conf., Nov. 76 PROC*, Vol. I, pp. 8.1-1-8.1-5 [76CLR51].
- SWEARINGEN, D. W., "MARISAT Program," *IEEE EASCON '76 RECORD*, pp. 39-A-39-B, Sep. 1976.
- SWEARINGEN, D. W. & Lipke, D. W., "MARISAT Multiple Access Capabilities," *IEEE ICC June 76 CONF REC*, pp. 51-10-51-13.
- TAMMES, J. B.\* & Bleiweis, J. L., "An RF Monopulse Attitude Sensing System," *Int. Tel. Conf, Sep. 76 PROC*, pp. 46-55 [76CLR39].
- TAUR, R. R. & Mass, J.†, "Rain Depolarization and its Effects Upon Satellite Communications Systems," Pres. at IEEE ICC June 76 [UPO47CL].
- TAUR, R. R., "Simultaneous 1.5 and 4 GHz Ionospheric Scintillation Measurement," *Radio Science*, Dec. 76, pp. 1029-1036 [76CLR55].
- TRACHTMAN, W. S., see Di Fonzo, D. [76CLR41] & English, W. J. [76CLR42].
- TSUJI, Y.†, see McClure, R. B.\* [76CLR03] & Dill, G. D. [76CLR17].
- UZUNOGLU, V., see Wolejsza, C. [76CLR14].
- VAN OMMERING, G. & Stockel, J. F., "Characteristics of Nickel-Hydrogen Flight Cells," *Power Sources Symp. June 76 PROC*, pp. 124-128 [76CLR43].
- VAN OMMERING, G., see Dunlop, J. D. [UPO52CL].
- VAN TREES, H. L., "Future INTELSAT System (1986-1993) Planning," Pres. at 6th AIAA Comm. Sat. Syst. Conf., Montreal, Apr. 76, AIAA Paper No. 76-233 [76CLR04].
- WEISS, H. J., "Coordination Between Satellite Networks in the Geostationary at 27th IAF Cong., Anaheim, CA, Oct. 76. Paper No. IAF 76-200 [76CLR37].
- WACHS, M. R., see Jones, M. [76CLR48] and Weinreich, D. [76CLR18].
- WEINREICH, D. E. & Wachs, M. R., "A Laboratory Simulation of Multiple Unmodulated Interference Sources on Digital Satellite Channels," *IEEE ICC June 76 CONF REC*, pp. 51-20-51-25 [76CLR18].

\*Non-COMSAT author.

†INTELSAT.

- WEISS, H. J., "Coordination Between Satellite Networks in the Geostationary Satellite Orbit," Pres. at IEEE EASCON Sep. 76 [UPO51CL].
- WILLIAMS, A. E., see Atia, A. E. [76CLR30], [76CLR31], [76CLR40], [76CLR47].
- WILLIAMS, A. E. & Frey, F., "A Dual Polarized 5-Frequency Feed," *Natl. Telecom. Conf. Nov. 76 PROC*, Vol. III, pp. 49.4-1-49.4-2 [76CLR50].
- WOLEJSZA, C., Chakraborty, D. & Uzunoglu, V., "A Universal Modem Design for Digital Satellite Communications," *IEEE ICC June 76 CONF REC*, pp. 3-12-3-18 [76CLR14].
- WOOD, H. W., see Edelson, B. I. [76CLR20].
- WU, W. W., "New Convolutional Codes—Part II," *IEEE COM-24*, Jan. 76, pp. 19-33 [76CLR01].
- WU, W. W., "New Convolutional Codes—Part III," *IEEE COM-24*, Sep. 76, pp. 946-955 [76CLR27].